# Characterising Tumour Volume and Growth Dynamics in Non-Small Cell Lung Cancer

by

Boyue Ding

A Doctoral Thesis

Department of Medical Physics and Biomedical Engineering

Submitted in the fulfilment of the requirements for the award of Doctor of Philosophy of University College London

December 2024

# Declaration

I, Boyue Ding, confirm that the work presented in this thesis is my own. Where information has been derived from other sources, I confirm that this has been indicated in the thesis.

# Acknowledgements

I am particularly grateful to my supervisor, Professor Gary Royle, at University College London, for all his support, guidance, and confidence in me. I would also like to express my appreciation for the suggestions and help from Professor Maria Hawkins and Dr Crispin Hiley, who were there initially. I would also like to thank Catarina Isabel Correia Veloso Da Veiga, Dr John Fenwick, and Dr Douglas Brand, who provided me with valuable advice.

I want to thank the members of the Department of Medical Physics and Biomedical Engineering, including James Vallerine, Hyothaek Lee, Ying Zhang, Huei-Tyng Huang, Zhuoyan Shen, and all the staff.

I would also like to thank Professor Mariam Jamal-Hanjani**,** Wing Kin Liu, Sonya Hessey and Olivia Lucas. I would like to thank Professor Allan Hackshaw for helping me with statistical analysis questions.

Additionally, I would like to express my gratitude to my father, my mother, my partner and all my family members, as well as those who have supported me in my country and the UK. Without their support, I would not have been able to complete my Ph.D. studies.

Finally, I want to thank all the patients involved in this study, as well as the TRACERx Consortium, PEACE Consortium, and Darwin Consortium.

# Abstract

**Background:** This study aims to investigate the factors influencing recurrence and survival in non-small cell lung cancer (NSCLC) from the TRACERx cohort study, optimise surveillance and refine management to enhance patient prognosis using imaging.

**Method:** 200 stage I–III NSCLCs diagnosed between 2013 and 2020 from 13 hospitals in the UK were analysed. Univariable and multivariable Cox models were used to assess associations between clinical characteristics and outcomes. Segmented lesions analysis evaluated metastasis patterns. Surveillance intensity was categorised based on the time from surgery to the first post-operative scan. RECIST criteria were used to evaluate progression-free survival (PFS) and volume changes pre-treatment and post-treatment. ROC curves were used to determine the optimal volume for predicting relapse and progression.

**Results:** Manually contoured primary tumour volume (HR=2.68) was a stronger predictor of relapse site, tumour dynamics and prognosis than diameter-based volume estimates, pT stage or pTNM staging. Larger primary tumours were associated with early relapse, extrathoracic relapse, higher recurrence burden and worse prognosis. Similarly, higher relapse rates were associated with high heterogeneity, larger tumour burden, faster progression, extrathoracic involvement, and poorer survival, highlighting volume and growth rate as better prognostic predictors than lesion count. Pre-treatment growth rate showed a weak correlation with post-treatment growth rate. In pT2N0M0 tumours, exploratory thresholds for high-risk volume (>17,010 $mm^3$) and growth rate (>58 $mm^3$/day) were identified. A tumour volume reduction of more than 65% during initial therapy was associated with improved progression-free survival (AUC=0.81). These thresholds are exploratory and derived from a limited cohort; larger, prospective studies are needed to confirm them before integrating them into clinical practice.

Gender, Age and Smoking status were not significantly associated with DFS overall, but current smokers showed higher relapse risk after 2.5 years. Recurrence patterns varied by histology and tumour location. LUSC had larger tumours and peaked at 9–12 and 15–18 months, while LUAD peaked at 12–15 months, with late relapse (>1.5 years) more

common in larger LUAD. Intrathoracic relapses, primarily in the lung, correlated with better prognosis, whereas extrathoracic relapses were linked to worse outcomes, particularly in cases with brain involvement. Intrathoracic relapses were likely to progress with new lesions. Conversely, those with extrathoracic relapses often experienced the simultaneous appearance of new lesions and localised expansions, leading to more complex and aggressive progression modes. Relapse rates did not differ in terms of the number of progression events.

Surveillance frequency based solely on the TNM stage was insufficient. High-frequency did not improve overall survival, as seen in previous findings, nor did it reduce relapse volume. Site-specific relapse patterns may help to tailor follow-up intensity in the future.

**Conclusions:** Tumour volume and growth rate outperform lesion count and traditional staging in predicting relapse dynamics, patterns and survival. Intrathoracic relapses, primarily in the lungs, are associated with better outcomes, whereas extrathoracic relapses, especially in the brain and multiple organs, indicate faster relapse speed and poorer prognoses. Standard TNM-based follow-up protocols are insufficient; incorporating tumour volume, growth rate, and relapse site could support more personalised follow-up strategies.

# Impact Statement

## Introduction

Lung cancer remains the leading cause of cancer-related deaths worldwide, with non-small cell lung cancer (NSCLC) accounting for approximately 85% of all lung cancer cases. Despite advancements in surgical techniques and therapies, 30% of NSCLC patients go through recurrence with various relapse periods, and outcomes are diverse, necessitating improved strategies for prediction, surveillance, and treatment management.

## Research Objectives

This study investigates relapse patterns and scrutinises current guidelines and practices in NSCLC, focusing on anatomical locations, volume changes, surveillance frequency and the impact of tumour heterogeneity on prognosis and treatment strategies. The research aims to develop a non-invasive method for predicting prognosis and tailoring surveillance protocols by using tumour volume and morphology. This approach integrates clinical data with imaging findings to offer a comprehensive framework for disease management and personalised treatment strategies.

## Methods and Novel Contributions

Using the TRACERx dataset, the largest and most comprehensive imaging-clinical dataset on NSCLC relapse, this research includes detailed data on tumour volumes, locations, follow-ups, and progressions. A contouring guideline was established for all time points. A keyword-based extraction system was established to support natural language processing (NLP)-based automation in radiology reports. These tools align with UKRI and NHS digital innovation strategies and could help future AI platforms to streamline imaging workflows, enhance diagnostic precision, and support personalised cancer care. Diagnostic, follow-up, relapse/progression, and final pre-mortem scans were longitudinally contoured for 200 patients. In total, over 2,400 scans and more than 3,200 individual lesions were manually contoured. Precise tumour volume measurements at individual lesion levels were established to capture chronological and anatomical changes, providing a detailed characterisation of tumour growth dynamics, including relapse, progression and prognosis, which informs personalised surveillance suggestions for better clinical management. No other study to date has achieved this level of detail. Select the

unique relapsed patients, and these will also be used at the UCL Cancer Institute in the future. The study will combine genomic and ctDNA data to elucidate tumour evolution, construct a metastatic gene phylogenetic tree, and explore treatment resistance mechanisms. By analysing this extensive dataset, the study seeks to uncover variability in relapse characteristics, potentially leading to more personalised and effective management strategies for NSCLC patients.

## Impact and Significance

This research addresses critical gaps in understanding and managing NSCLC relapse by integrating advanced imaging techniques, particularly tumour volume and growth rate, with clinical data. It proposes a novel methodology for predicting relapse and understanding tumour heterogeneity. Additionally, it provides insights into personalised surveillance and treatment approaches, improving survival rates and quality of life for NSCLC patients. The comprehensive dataset and innovative analysis pave the way for future research and clinical applications, establishing a foundation for more effective and cost-efficient clinical guidelines.

## Statement of Contributions by the Authors

This project is a collaboration between Professor Gary Rolye's and Professor Mariam Jamal-Hanjani's teams. All non-small cell lung cancer patients are from the TRACERx Consortium, PEACE Consortium, and Darwin Consortium.

Wing Kin Liu and the Imaging Manager from Mariam Jamal-Hanjani's team requested a consecutive series of Computed Tomography (CT), Positron Emission Tomography (PET-CT), Magnetic Resonance Imaging (MRI), and bone scans and reports from CTC among 14 hospitals. Staff from the 14 hospitals labelled all scans and reports with the hospital IDs, time points, and imaging types. Each scan was sent on a single disc from MACRO to RDS, not multiple scans on a single disc. Each scan report was also saved as a PDF corresponding to the scan date and each patient's essential clinical characteristics. All the datasets were then transferred to Royle's server by Catarina Isabel Correia Veloso Da Veiga, a member of Royle's team.

Hyothaek Lee from Royle's team created and ran a sorting code to check the metadata of the DICOM files against several criteria before sorting them into scan-by-scan folders. Each date folder from CTC contains all DICOM files from the day of the scan, representing different scans in one folder, making it indistinguishable. The sorting process results in DICOM files representing each scan within a single folder. After sorting, the DICOM files within the individual scan folder are converted into a single NIfTI file format. As DICOM files require several hundred individual files to represent a single image scan, converting to a single NIfTI file is more convenient for image processing and keeping track of the files. After Hyothaek Lee successfully converted it to the NIfTI format, the corresponding DICOM files were compressed to lower the file count.

Once NIfTI files were uploaded, I manually verified the accuracy of each imaging file's patient ID and date on the Royle team's server. I was trained and worked as a radiation oncologist for 6 years. I segmented all the patients' imaging scans using ITK-snap, including baseline, follow-up, recurrence, progression, and the last scan before death, as indicated in the CT reports. Additionally, I selected certain imaging scans to verify

through Eclipse. Wing Kin Liu would provide the tissue biopsy ± autopsy information to me as well. I used all this information to contour each lesion in a distinctive label name and colour. I developed a contouring guideline for all timepoints. I set up a keyword-based extraction system from radiology reports to support natural language processing (NLP)-based automation. Additionally, I extracted the tumour volume and other imaging factors. If I have any questions about the segmentation, I would seek help from a clinical consultant, Dr Crispin Hiley. Finally, I sent all the volumes of lesions and the corresponding label names of individual patients at each time point to Wing Kin Liu. Sonya Hessey from Mariam Jamal-Hanjani's team helped me create a foundation code to plot the tumour growth rate curve through the whole processing, treatment and imaging information added to the plot. Professor Allan Hackshaw helped me with statistical analysis questions.

# Research Paper Declaration Form

Characterizing the evolutionary dynamics of cancer proliferation in single-cell clones with SPRINTER. Nature Genetics (2024). Olivia Lucas, Sophia Ward, Rija Zaidi, Abigail Bunkum, Alexander M. Frankell, David A. Moore, Mark S.Hill, Wing Kin Liu, Daniele Marinelli, Emilia L. Lim, Sonya Hessey, Cristina Naceur-Lombardelli, Andrew Rowan, Sukhveer Purewal, Haoran Zhai, Michelle Dietzen, ***Boyue Ding***, Gary Royle, TRACERx Consortium, PEACE Consortium, Nicholas McGranahan, Mariam Jamal-Hanjani, Nnennaya Kanu, Charles Swanton, Simone Zaccaria.

W. Liu, ***Boyue Ding***, H. Sonya, et al. Tracking Metastatic Dissemination and Tumour Growth using Longitudinal Imaging and ctDNA. American Association for Cancer Research (2024).

Wing Kun Liu, ***Boyue Ding***. et al. Mapping the pattern and pace of tumour dissemination using longitudinal imaging and ctDNA in the TRACERx lung study. Annals of Oncology (2022).

Evolutionary characterisation of lung cancer metastasis. Submitted

# List of Figures

Fig. 1.1 Overview of study workflow across the disease trajectory in NSCLC patients ····· 36
Fig. 2.1 Timing and labelling of imaging scans used in this study ····· 44
Fig. 2.2 Schematic diagrams illustrating the contouring procedures using ITK-SNAP ····· 48
Fig. 2.3 Example of repeated tumour contouring on baseline CT scans for patient LTX0103 ····· 51
Fig. 2.4 Example of tumour segmentation using Eclipse and ITK-SNAP for comparison ····· 52
Fig. 2.5 Comparison of primary tumour volumes in 64 patients across two studies ·· 54
Fig. 2.6 Comparison between Volume-RECIST and standard RECIST Criteria for tumour progression detection ····· 63
Fig. 2.7 Correlation between diameter-based and manually contoured tumour volumes ····· 64
Fig. 2.8 Comparison of primary tumour volume (log-transformed) using diameter-based calculation and manual contour method····· 65
Fig. 2.9 Comparison of manual contouring and diameter-based tumour volume calculations across three agreement subgroups ····· 68
Fig. 2.10 Overview of scan inclusion and contouring in the study cohort····· 70
Fig. 2.11 Tumour volume changes over time fitted with the Gompertz model ····· 73
Fig. 2.12 Line plot showing tumour volume progression using linear interpolation between scans····· 74
Fig. 2.13 Illustration of the method used to calculate tumour growth rate in this study based on segmented tumour volumes and the time interval between two relevant scans ····· 75
Fig. 3.1 Overview of contoured patients in the TRACERx longitudinal Imaging cohort ····· 84
Fig. 3.2 Each year recurrence proportion post-surgery····· 87
Fig. 3.3 Distribution of manually contoured and diameter-based primary tumour volumes in patients stratified by 2-year relapse status ····· 89
Fig. 3.4 Relationship between primary tumour volumes and relapse characteristics · 92

Fig. 3.5 Overall survival post-surgery across pT, pTNM and primary volume risk groups ……94
Fig. 3.6 Annual recurrence ratios after surgery across clinical and demographic subgroups ……98
Fig. 3.7 Distribution of relapse timing (in months) stratified by histological subtypes ……99
Fig. 3.8 Distribution of relapse timing (in months) stratified by pathological TNM stage ……100
Fig. 3.9 Yearly recurrence ratios by primary tumour volume subgroups and ROC curves for manually contoured primary tumour volume, diameter-based volume, pT stage, and pTNM stage ……102
Fig. 3.10 Relationship between primary tumour growth rates and primary tumour volumes across histological subtypes ……104
Fig. 3.11 Relationship of relapse tumour growth rate and volume in different histologies ……105
Fig. 3.12 Annual recurrence hazard ratios across primary tumour volume groups (small, median, and large), stratified by clinical and demographic subgroups ……106
Fig. 3.13 Comparison of baseline tumour volume and growth rate across TNM stages ……109
Fig. 3.14 Relationship of relapse tumour volume and growth rate in different TNM stages ……109
Fig. 3.15 Relationship between primary tumour volume and growth rate across distinct primary tumour locations ……110
Fig. 3.16 Relationship between primary tumour volume, relapse volume, relapse speed and DFS ……112
Fig. 3.17 Receiver Operating Characteristic (ROC) curve illustrating the predictive performance of tumour volume and growth rate for relapse in pT2N0M0 NSCLCs ……116
Fig. 4.1 Distribution of disease-free survival (DFS) times among relapsed patients following surgery ……134
Fig. 4.2 Scatter plot of relapse timing by anatomical organ and subsite ……136
Fig. 4.3 Difference of DFS among Intrathoracic, Extrathoracic and Both relapse sites ……138
Fig. 4.4 DFS distributions among relapse sites and tumour burden categories ……139
Fig. 4.5 Relapse probability among tumour burdens and relapse site ……140

Fig. 4.6 Patterns of relapse growth and its association with tumour burden, site, and survival ····· 141
Fig. 4.7 Scatter plot of overall relapse timing and last scan before death by anatomical organ and subsite ····· 144
Fig. 4.8 Kaplan–Meier survival curves comparing overall survival post-recurrence according to the presence or absence of initial relapse and final scan in the lung, bone, brain, liver, pleura, intrathoracic and extrathoracic lymph node, extrathoracic soft tissue, liver and adrenal glands ····· 146
Fig. 4.9 Survival curves illustrating the impact of lung and brain relapse on post-recurrence overall survival ····· 149
Fig. 4.10 Progression trajectories of patients with initial relapse within the lung ····· 151
Fig. 4.11 Progression trajectories of patients with initial relapse within the intrathoracic lymph node ····· 153
Fig. 4.12 Progression trajectories of patients with initial relapse within the brain ···· 154
Fig. 4.13 Overall survival post-recurrence stratified by relapse site: lung, intrathoracic lymph node, brain, and multiple-organ relapse ····· 156
Fig. 4.14 Overall survival post-recurrence stratified by initial metastatic status and lesion count ····· 157
Fig. 4.15 Tumour number and increased number at relapse and progressions across different relapse growth rate categories ····· 159
Fig. 4.16 Relationship between volume and speed across progression events ····· 160
Fig. 4.17 Relationship between relapse growth rates, progression volumes and lesion numbers at the first relapse, first progression, second progression and third progression ····· 161
Fig. 4.18 Progression trajectories ····· 164
Fig. 4.19 Overall survival post-recurrence stratified by progression trajectories ····· 165
Fig. 4.20 Relationship between the relapse site, relapse speed, and progression mode at the first, second, and third progressions ····· 166
Fig. 5.1 Illustration of the method of total tumour volume calculation ····· 183
Fig. 5.2 Definition of the post-operation year in this study ····· 185
Fig. 5.3 Flow chart of surveillance strategy analysis across different phases ····· 186
Fig. 5.4 Surveillance timing following surgery ····· 188
Fig. 5.5 Time from surgery to first surveillance imaging by surveillance intensity group ····· 190

Fig. 5.6 Comparison of overall survival post-surgery across surveillance intensity groups ····· 194
Fig. 5.7 Overall survival post-surgery stratified by three surveillance intensity groups in early-stage tumours ····· 195
Fig. 5.8 Median surveillance duration across different primary tumour volume groups stratified by surveillance intensity ····· 196
Fig. 5.9 Overall survival post-surgery in small tumours and across different primary tumour growth rates among three intensity surveillance groups ····· 197
Fig. 5.10 Proportion of dominant relapse organs across surveillance intensity groups ····· 199
Fig. 5.11 Distribution of surveillance periods and post-recurrence survival (PRS) by dominant relapse site and surveillance intensity ····· 200
Fig. 5.12 Comparison of relapse tumour volumes across surveillance intensity groups ····· 204
Fig. 5.13 Progression-free survival stratified by relapse location ····· 205
Fig. 5.14 Overall survival post-recurrence in 130 relapsed patients, categorised by length of progression-free survival ····· 206
Fig. 5.15 Overall survival post-recurrence stratified by best treatment response after first-line therapy ····· 207
Fig. 5.16 Relationship between tumour volume, growth rate at first progression, and best response status to initial therapy ····· 208
Fig. 5.17 Relationship between tumour volume and growth rate at first progression and their association with overall survival ····· 209
Fig. 5.18 The Receiver Operating Characteristic (ROC) curve assessing volume change in the dominant lesion after first-line therapy post-recurrence ····· 211
Fig. 5.19 Conceptual models illustrating two tumour growth patterns ····· 212
Fig. 5.20 Distribution of total tumour volume based on timing of peak tumour burden ····· 212
Fig. 5.21 Overall survival post-recurrence based on early versus late growth patterns ····· 213
Fig. 5.22 Lesion status in relation to tumour growth timing among 97 dead patients ····· 215
Fig. 5.23 Examples of patients with late-peaking tumour volume showing intrapatient and interpatient heterogeneity and resistance to immunotherapy ····· 215

# List of Tables

Table 2.1 Comparison of tumour response assessment criteria: WHO, RECIST 1.0, and RECIST 1.1 ····· 59
Table 2.2 Response Evaluation Criteria 1.1 ····· 62
Table 3.1 Clinical and demographic characteristics of 200 patients included in this study ····· 85
Table 3.2 200 patients' primary tumour volume and tumour growth rate ····· 88
Table 3.3 Univariate and multivariate Cox regression analyses of clinical and tumour-related factors associated with recurrence ····· 91
Table 3.4 Univariate and multivariate Cox regression analyses identifying factors associated with recurrence in patients with stage pT2N0M0 NSCLC ····· 114
Table 4.1 Clinical characteristics of 130 patients included in the relapse analysis cohort ····· 131
Table 4.2 Clinical and tumour characteristics associated with single-lung relapse ··· 152
Table 4.3 Clinical and tumour characteristics associated with single-intrathoracic lymph node relapse ····· 153
Table 4.4 Clinical and tumour characteristics associated with single-brain relapse··· 155
Table 5.1 Treatment characteristics of patients following relapse ····· 184
Table 5.2 Patient demographics for the 3 surveillance groupings, presented as n (%) for categorical variables and median for continuous variables ····· 191
Table 5.3 Multivariable analysis of surveillance intensity overall survival post-surgery ····· 194
Table 5.4 Summary of first-line post-relapse treatment strategies among relapsed patients ····· 207

# Abbreviations

| Abbreviation | Meaning |
|---|---|
| NSCLC | Non-small cell lung cancer |
| LUAD | Lung adenocarcinoma |
| LUSC | Lung squamous cell carcinoma |
| LCC | Large Cell Carcinoma |
| OS | Overall survival |
| DFS | Disease-free survival |
| PFS | Progression-free survival |
| PRS | Post recurrence-free survival |
| Benjamini–Hochberg FDR | Benjamini–Hochberg False Discovery Rate |
| AUC | Area Under the Curve |
| ROC | Receiver Operating Characteristic |
| FRRN | Full resolution residual network |
| MRRN | Multi resolution residual network |
| PDEs | Partial Differential Equations |
| SCNA | Subclonal Copy Number Alterations |
| GLCM | Grey-level cooccurrence matrix |
| HU | Hounsfield Units |
| RECIST | Response Evaluation Criteria in Solid Tumours |
| ctDNA | Circulating tumour DNA |
| CT | Computed Tomography |
| PET | Positron Emission Tomography |
| MRI | Magnetic Resonance Imaging |
| HRCT | high-resolution computed tomography |
| CTPA | CT Pulmonary Angiogram |
| LDCT | Low-dose Computed Tomography |
| CTC | Central Tumour Registry |
| RDS | Radiology Data Storage System |
| TRACERx | Tracking Cancer Evolution through Therapy |

| | |
|---|---|
| PEACE | Posthumous Evaluation of Advanced Cancer Environment |
| EMT | Epithelial-to-mesenchymal transition |
| EGF | Epidermal growth factor |
| EGF | Epidermal growth factor receptor |
| WHO | World Health Organization |
| NCCN | National Comprehensive Cancer Network |
| ESMO | European Society for Medical Oncology |
| AACP | American Academy of Chest Physicians |
| SEER | Surveillance, Epidemiology, and End Results |
| PR | Partial Response |
| PD | Progressive Disease |
| SD | Stable Disease |
| CR | Complete Response |
| NC | No Change |
| RANO | Response Assessment Neuro-Oncology |
| irRECIST | Response Evaluation Criteria in Solid Tumours |
| SPRG | Spherical Region-Growing Method |
| HLA | Human Leukocyte Antigen |
| HLA LOH | HLA loss of heterozygosity |
| SCNA | Subclonal Copy Number Alterations |
| ITH | Intratumour heterogeneity |
| TNM | Tumour-nodes-metastasis |
| CV | Coefficient of Variation |
| DWI | Diffusion-weighted Imaging |
| IQR | Interquartile Range |
| ODE | Ordinary Differential Equations |
| PDE | Partial Differential Equations |
| BTGR | Baseline tumour growth rate |
| LACE | Lung Adjuvant Cisplatin Evaluation |
| TMB | Tumour Mutation Burden |
| PD1 | Programmed Cell Death Protein 1 |
| C-index | Concordance index |

# Contents

**Declaration** ····· **2**

**Acknowledgements** ····· **3**

**Abstract** ····· **4**

**Impact statement** ····· **6**

**Statement of Contributions by the Authors** ····· **8**

**Research Paper Declaration Form** ····· **10**

**List of Figures** ····· **11**

**List of Tables** ····· **15**

**Abbreviations** ····· **16**

**1 Introduction** ····· **20**

**2 Chapter One: Literature Review, Background, Objectives, and Novel Contributions** ····· **21**

**3 Chapter Two: Methodology** ····· **39**

**4 Chapter Three: Analysing Recurrence Rates and Using Clinical and Imaging Factors to Predict Disease-free Survival in Non-Small Cell Lung Cancer** ····· **80**

**4.1 Highlights** ····· **80**

**4.2 Introduction** ····· **82**

**4.3 Results** ····· **84**

**4.4 Results Summary** ····· **117**

**4.5 Discussion** ····· **118**

**4.6 Conclusions** ····· **125**

**5 Chapter Four: Patterns and Outcomes of Recurrence and Progression: Tumour Dynamics, Timing, and Location in Non-Small Cell Lung Cancer** ····· **126**

**5.1 Highlights** ····· **126**

**5.2 Introduction** ····· **129**
**5.3 Results** ····· **131**
**5.4 Results Summary** ····· **168**
**5.5 Discussion** ····· **170**
**5.6 Conclusions** ····· **176**
**6 Chapter Five: Recommendations for NSCLC Surveillance and Optimal Tumour Reduction Post-Treatment for Improved Prognosis** ····· **177**
**6.1 Highlights** ····· **177**
**6.2 Introduction** ····· **179**
**6.3 Patients and Methods** ····· **181**
**6.4 Results** ····· **187**
**6.5 Results Summary** ····· **218**
**6.6 Discussion** ····· **219**
**6.7 Conclusions** ····· **224**
**7 Chapter Six: Summary and Future Work** ····· **225**
**8 Appendices** ····· **229**
**9 Bibliography** ····· **245**

# Introduction

Prostate, breast, colorectal and lung cancers are the most prevalent malignancies among the diverse types of cancers. Despite a gradual decline in mortality rates over the past two decades, lung cancer remains the leading cause of cancer-related deaths, particularly among patients over the age of 50 [1]. The 3-year relative survival rate is only 40% [1]. Among the various histological types, non-small cell lung cancer (NSCLC) is the most common type of lung cancer, accounting for approximately 85% [2].

Tumour heterogeneity is crucial in evolution and can be evaluated through genomics or imaging data. Molecular technologies represent the gold standard for diagnosing in personalised medical treatments [3,4]. However, these approaches have several limitations. Histologic assessments may fail to capture intratumour heterogeneity due to spatial resolution limits of tissue samples, and obtaining samples from specific lesion locations can be challenging. Consequently, reliance on limited biopsy techniques could lead to misleading clinical decision-making [5].

On the other hand, imaging provides a noninvasive alternative to present comprehensive tumour information. While numerous qualitative studies have explored imaging evaluation heterogeneity, there is a notable lack of quantitative analyses, like volumetric assessments. This gap is primarily due to the need for a universal agreement on quantitative methodology and the unclear relationship between imaging findings and underlying tumour evolution. A previous study shows that the number of circulating tumour cells may be associated with primary tumour volume, especially in LUADs with extrathoracic metastasis [6]. Using imaging alongside genomics can address questions about metastasis seeding procedures and predict prognosis, as imaging complements the lack of anatomical, functional, and volumetric information in genomic data.

Due to the variability in the timing and locations of relapse, the optimal timing for post-operative surveillance remains to be determined. NCCN guidelines recommend evaluations every 6 to 12 months for the first two years, followed by annual evaluations [7]. Despite the recommendations, adherence in the real world is inconsistent. Therefore, it is urgent to develop precise, individualised screening protocols.

# Chapter One

# Literature Review, Background, Objectives, and Novel Contributions

## 1. Literature Review

## Tumour Burden, Imaging Characteristics, and Clinical Outcomes in Non-Small Cell Lung Cancer

Non-small cell lung cancer is still a challenging target in public health. With the promotion of cancer diagnosis and the progression of surgery, chemotherapy, radiation therapy, immunotherapy, and targeted therapy, lung cancer mortality is decreasing. However, the treatment bottleneck is still common, resulting in tumour relapse. Lung cancer with limited metastases may have a distinct clinical outcome. Understanding the mechanisms and choosing the proper treatment method still need to be discussed.

Gene sequencing can dynamically detect and monitor tumour evolution, but obvious disadvantages exist. A biopsy can only extract information about part of the tumour lesions instead of reflecting all the tumour's characteristics. The cost burden is unaffordable to specific patients, and biopsy is also an invasive operation with a risk of bleeding and infection. Imaging can act as a surrogate.

### 1.1 Non-Small Cell Lung Cancer

Cancer remains a significant global public health concern. Among the most common types are prostate, breast, colorectal, and lung cancers. While overall cancer mortality has gradually declined over the past two decades, lung cancer continues to be the leading cause of cancer-related deaths. Each day, approximately 340 people die from lung cancer, nearly 2.5 times more than from colorectal cancer, particularly among patients over the age of 50. Notably, the mortality rate among women is higher than that of men [1]. The treatment of advanced NSCLC has been revolutionised by the introduction of chemoradiotherapy, targeted therapy, and immunotherapy in clinical practice, especially radiation, which can improve local-regional control and overall survival, making it the gold standard. However, many cancers inevitably develop. The 3-year relative survival

rate is only 40% [1]. Approximately 60% of NSCLCs will develop brain metastases during the disease, which is the most common metastatic site, followed by contralateral lung, lymph nodes, liver, and adrenal glands [8]. It's an urgent task to find the mechanisms of tumour progression. With the rapid advancement of imaging technology, including computed tomography (CT), 18F-FDG positron-emission tomography (PET), and magnetic resonance imaging (MRI), it is now easier and more convenient to detect early metastases, thereby providing appropriate clinical management for all types of metastases.

**1.2 Oligometastatic Disease and Genomics for Non-Small Cell Lung Cancer**

Oligometastatic disease is recognised as a limited metastatic burden and was first mentioned by Hellman and Weichselbaum in 1995 [9]. The precise definition is diversified in related research. Most researchers define oligometastatic disease as an intermediate stage between localised and widely spread disease. Some researchers have confirmed that this stage involves no more than three organs, and all distant metastases add up to 5 or fewer [10].

Some lesions progress quickly to widespread metastases, while others remain stable in a limited number of organs. Diversity mechanisms can cause tumour evolution. One of them is gene alteration. Mutations and chromosomal instability can characterise gene alteration. Different pathologies may be correlated with different types of gene mutations; most mutations in adenocarcinoma lung cancer are tumour suppressor mutations, nearly half of them are TP53 and oncogene mutations, only one third is KRAS, while distinguishing from squamous cell carcinoma, tumour suppressors mutations, almost all are TP53 and only 16% PIK3CA of oncogene mutations [11–12]. Rearrangement is the most commonly detected in adenocarcinoma, and ALK gene rearrangements are the most common type that can predispose to liver metastasis [11–12]. EML4–ALK1 rearrangement is associated with pleural metastases [13,14]. EGFR is associated with brain metastases [15,16]. Li and Vignot [17–18] demonstrated that copy number changes, such as MET (the most frequent one), can be detected in brain metastases and are correlated with early cerebral metastasis events [19]. 7q36, 8p12 and 10q22 gain in squamous lung cancer, deletions at 4q in lymph nodes metastases [20]. Molecular phenotypes are inconsistent and can change due to tumour evolution. Various routes of tumour seeding contribute to tumour heterogeneity, which can result in varied responses to treatment [21–27].

Different organ metastases in non-small cell lung cancer have distinct mortality rates. The clinical outcome showed that the mortality rates associated with bone, brain, liver, lung, and multiorgan metastases were 73.2%, 72.7%, 78.3%, 65.4%, and 77.5%, respectively. Liver metastases and multiorgan metastases had the worst survival [28]. The late phase of liver regeneration may promote metastasis (particularly in the lung) in colorectal cancer and stimulate tumour growth in gastrointestinal tumours [29,30]. These findings reveal different organ metastases that may harbour a diverse tumour growth rate.

### 1.3 Imaging Factors

Molecular technologies, including genomic and proteomic sequencing, are widely regarded as the gold standard for diagnosing and individualised medical treatment [3,4]. However, gene sequencing has notable limitations, including high costs, lengthy processing times, and technical complexity. Moreover, due to cancer heterogeneity, a single tissue sample may not fully reflect the anatomic and functional features of a whole solid tumour. As a result, limited biopsy techniques may misguide the choice of clinical practice [4]. Regarding the limitations of molecular diagnosis, medical imaging offers a noninvasive analysis of cancer, containing anatomic, physiological, and morphological characteristics at multiple time points, which can assist clinicians in making informed decisions for precision medicine.

Radiomics comprises a variety of features extracted from medical images. Specific imaging types can assist in diagnosing molecular markers [31], and clinicians can use radiomics as a surrogate for predictive biomarkers. Those high-throughput quantitative data can be classified into two subtypes: semantic and agnostic. Semantic features [32–34] are clinician-interpretable indicators, typically annotated by radiologists. These features are familiar to clinicians and have been shown to correlate with clinical outcomes. Semantic features are qualitative or semi-quantitative features and often describe the tumour morphological characteristics, including size, location (e.g., right vs left, upper vs lower, central vs peripheral), margin (e.g., smooth or irregular borders), cavitation (the presence of an air- or fluid-filled space within a tumour is often associated with necrosis or rapid tumour growth), multifocal lesions (the presence of two or more distinct tumour foci within the lung that are not connected by continuous tumour tissue), air space (presence of air-filled bronchi that remain visible within or adjacent to the tumour, indicating that the bronchi are not completely obstructed), and density (the degree of

radiographic attenuation on CT, typically measured in Hounsfield Units, which can differentiate between solid, subsolid or necrosis). Agnostic features [35] are automatically extracted using computational algorithms without predefined clinical interpretation. These features quantify tumour characteristics from voxel-level image data and are grouped into three-level statistical outputs: 1. First-order statistics: describe the distribution of individual voxel intensities (e.g., mean, standard deviation, skewness); 2. Second-order statistics: capture spatial relationships between voxels (e.g., grey-level cooccurrence matrix, GLCM); 3. Higher-order statistics: apply mathematical methods to highlight more complex patterns, often related to texture or heterogeneity, which are associated with survival outcomes in lung cancer [36].

### 1.3.1 Radiomics Signatures Related to Gene Mutations

Lee found that tumours with an SUV value over 5.0 on PET/CT scans were related to EGFR mutations in lung cancers [37]. Tumours with EGFR mutation tend to be smaller, have a more regular shape, have more ground-glass opacities and air bronchograms, show pleural retraction, have more calcifications, and show less fibrosis [38,39]. Zhou [40] indicated that distinguishing between EGFR+ and EGFR– tumours based on morphological features from CT is challenging. Conversely, Liu [41] found that CT attenuation, tumour main direction, and texture can moderately predict EGFR status. This study was limited to 298 peripheral lung adenocarcinomas, commonly associated with fewer atelectasis events. Therefore, a large cohort might be required. Among EGFR mutation subtypes, tumours with exon 21 mutations were larger and had a higher proportion of ground glass, which exhibited fewer air bronchograms [42,43]. EGFR also correlates with specific metastasis patterns, including diffuse lung and lytic bone and brain metastases [43].

ALK rearrangement lung cancers typically present as large, round, solid, peripheral lesions, often located in the lower lobes [39,44–46]. They are associated with lymphangitic carcinomatosis, pleural and pericardial metastases, lymphadenopathy in non-tumour lobes, and sclerotic bone and brain metastases [39,45]. Similar findings were reported for ROS1 rearrangements [34], though extrathoracic metastases occur less frequently than in EGFR mutations and ALK rearrangements (ROS1, 49%; ALK, 75%; EGFR, 72%). Peripheral, solid tumours with spiculation are commonly detected in ROS1+ primary tumours, with cavitation, air bronchograms or calcifications being less common [47].

KRAS mutations are exclusively associated with adenocarcinoma and can predict poor recurrence-free survival [48,49]. In summary, gene alterations occur in over half of extrathoracic metastases, with ALK rearrangement being the most common, occurring in 75% of cases.

Beyond gene mutations, few articles have explored the application of radiomics in predicting PD-L1 expression. Clinical trials, such as CheckMate-017 and CheckMate-057, have demonstrated that PD-1/PD-L1 inhibitors can benefit patients with advanced NSCLC [50] more effectively than chemotherapy alone. KEYNOTE-010 demonstrated that NSCLCs with a TPS≥50% who failed front-line chemotherapy achieved longer PFS with Pembrolizumab [51,52]. Durvalumab can be used as consolidation therapy for NSCLCs following concurrent chemotherapy, and survival can be prolonged by nearly 20 months [53]. Given the vital role of immunotherapy in cancer treatment, Jiang used radiomics to analyse the relationship between imaging characteristics and PD-L1 expression in a retrospective study involving 399 NSCLC patients. The study found that CT, PET, and PET/CT features showed AUC values of 0.97, 0.61 and 0.97, respectively. In contrast, the prediction of PD-L1 expression over 50% resulted in AUC values of 0.91, 0.75 and 0.88 [54].

Radiomics can also be applied to identify breast cancer receptors [55–58]. The application of radiomics extends beyond oncology, aiding in the detection of dementia, mental illness, and glioblastoma [59–61].

### 1.3.2 Radiomics Signatures Related to Clinical Outcomes

Despite TNM staging being widely used in postoperative lung cancer prognosis, variations in prognosis among patients of the same stage indicate that no single marker fully explains tumour complexity. A previous study demonstrated that clinical characteristics, including age, gender, surgical procedure, adjuvant chemotherapy, tumour size, TNM stage, histology, smoking status, metastasis location, number and size, were associated with clinical outcomes [62–67]. Radiomics, an innovative imaging biomarker that incorporates quantitative image features such as location, volume, shape, and texture, provides insights into tumour heterogeneity, a primary cause of treatment failure [4,68]. Thus, radiographic parameters and clinical characteristics can be used to

predict overall survival and allow pre-treatment risk stratification, helping to make an optimal, personalised treatment regimen.

Imaging alone, in conjunction with tumour size, a prevalent imaging phenotype in recent precision clinical practices, has shown predictive value for survival [69,70]. However, tumour volume alone provides only moderately prognostic value for distant metastasis [71]. Additionally, previous studies have primarily focused on the volume of the primary tumour, with limited attention given to the volume of relapsed lesions [69,71]. Tumour volume can also be a predictor of treatment response. Nishino [72] enrolled 44 EGFR-positive NSCLCs undergoing first-line targeted treatment and observed that a reduction in tumour volume by the eighth week markedly improved overall survival. That research was limited by a small sample size and lacked accurate tumour volume contouring, relying on semi-automated segmentation based on the longest diameter. Other imaging factors, including satellite nodules in the primary tumour lobe, lobulated margin, pleural attachment, blurry edges, lesion major axis and minor axis, were indicators of poorer clinical outcomes [49].

Models incorporating clinical and radio features showed more accurate predictions [73,74]. Studies [75–76] further underscored this by identifying factors such as current smoking status, primary malignancy, tumour size, location, adenocarcinoma histology, visceral pleural invasion and angiolymphatic invasion as being associated with a shorter disease-free survival (DFS). Advanced studies have explored radiomics' potential in various cancers, demonstrating its ability to predict treatment response and clinical outcomes effectively, from assessing pathologic responses in NSCLCs treated with neoadjuvant chemoradiotherapy [77,78] to evaluating rectal cancers' response to treatment [79] and distinguishing radiation-induced fibrosis from tumour recurrence [71].

Moreover, low-dose computed tomography (LDCT) has proven instrumental in the early detection of lung cancer, significantly reducing mortality rates [80]. Comparative studies of radiologists' detection accuracy and radiomic prediction models have shown that diagnostic and predictive models substantially increase accuracy and specificity [81–82]. Radiomics presents a promising approach for early cancer detection and personalised treatment strategies, underscoring its value in precision medicine and the ongoing pursuit of enhancing patient care.

### 1.3.3 Radiomics Signatures with Signal Pathway

Remarkably, models based on computational image features achieved an 85% accuracy rate, with performance primarily associated with tumour size, edge shape, and sharpness. Specifically, air bronchograms on CT scans correlated significantly with down-regulated genes in the hypoxia pathway and up-regulated genes in the Ras pathway [49]. Genes linked to larger tumours were up-regulated in pathways related to extracellular matrix remodelling [83] and epithelial-to-mesenchymal transition (EMT) [84], both critical predictors of tumour invasion and metastasis. Zhou [85] found that the active EMT and EGF pathways were associated with indistinct margins and a ground-glass texture. In contrast, inactive pathways corresponded with smooth margins and solid lesions, predominantly in the upper right lung lobe.

In conclusion, radiographic features correlate with distinct signalling pathways, providing an invasive method for highlighting the biological mechanisms of cancer, illustrating the potential of radiogenomics to enhance our understanding of cancer's genetic landscape and inform tailored treatment strategies.

# 2 Background: Evaluation of Tumour Progression, Tumour Auto-segmentations, Growth Model and Surveillance

## 2.1 Tumour Progression Evolution

In 1981, the World Health Organisation (WHO) established the first version to evaluate the treatment effectiveness [86]. However, this version had ambiguous aspects. For example, a Partial Response (PR) can be defined in two ways: one method involves calculating the change in the longest diameter multiplied by the greatest perpendicular diameter. In contrast, the other method depended on linear tumour measurement. This ambiguity led to various response criteria, resulting in differing assessments of treatment efficacy [87]. The Response Evaluation Criteria in Solid Tumours (RECIST) was published in 2000 to address the need for standardised criteria. This version defined target lesions as up to 5 per organ and up to 10 in total, setting the threshold for response at an increase of more than 20% or a decrease of more than 30%, rather than 50%. This criterion was validated as a practical guideline for predicting survival in a 10-year study [88]. However, this version is also limited; it does not define the lymph node status.

With the widespread application of new imaging technologies, such as PET-CT [77], the need for clear, standard criteria for lymph nodes has become evident. Researchers also questioned whether the number of target lesions could be reduced without affecting accuracy, making the criteria more practical and effective for clinical practice. To address these issues, an updated version of the RECIST 1.1 criteria was published in 2009 [89]. In the latest version, the number of target lesions was reduced to 2 per organ, with a total of up to 5. Additionally, a lymph node's short axis had to be greater than 15mm to confirm malignancy. As more researchers confirmed that tumour shapes are often irregular rather than round, using diameter to represent total tumour information was considered unfair. Volume measurement could provide a more accurate reflection of precise details. However, no standard rule exists for evaluating the progression using tumour volume. Some researchers have shown that a 20% increase in the diameter of a spherical tumour results in a 72.8% increase in its volume. In comparison, a 30% decrease in diameter corresponds to a 65.7% reduction in volume [90].

There are other less standard criteria for evaluating tumour response. The RANO (Response Assessment Neuro-Oncology) criteria are specifically designed for glioblastomas and incorporate MRI results. The International Working Group (Cheson) Criteria are tailored for lymphoma, while the Revised Choi Criteria are intended for metastatic renal cell carcinoma treated with sunitinib. Additionally, the Immune-related Response Evaluation Criteria in Solid Tumours (irRECIST) are recommended for assessing the effects of immunotherapy [91].

### 2.2 Tumour Volume Segmentation

Manual tumour contouring is time-consuming, prompting numerous researchers to develop algorithms for segmenting primary tumours using CT-based semi-automatic methods. Here is a comparison of common semi-automatic segmentation methods:

1. Seeded Region Growing [92,93]: is widely used in medical imaging research, and starts with seed pixels and expands regions by adding neighbouring pixels within the target region. However, inaccuracies may arise if seeds are not correctly selected, and the method might not fully correspond to the target. The Spherical Region-Growing Method (SPRG) [94] aims to enhance existing methods by utilising spheres instead of pixels. However, the irregular shape of tumours and noisy images can lead to segmentation inaccuracy.

2. Level-Set Based Active Contour Model [95,96]: starts with an initial contour around the object; the contour then moves based on the edges. This model can handle complex shapes but struggles with fuzzy and discontinuous boundaries.
3. Localised Region-Based Active Contour Model [97]: Like the level-set-based contour method, this method focuses on a local region instead of the entire image. This method highly relies on a pleasing reference contour. It utilises foreground and background parameters to describe small local regions, but it fails to trace regions with deep concavity and handle varying densities accurately.
4. Clustering-Based Segmentation [97]: K-means and fuzzy C-means are widely used. However, they are required to predefine the number of clusters. They failed to handle mixed imaging intensities and did not account for spatial information, leading to anatomically inaccurate results.
5. CT-Based Dense U-networks, V-networks and ResNet [98–101]: These innovative neural networks aim to achieve automatic segmentation and require extensive training data. Their segmentation accuracy heavily depends on the similarity between reference and target images, and the unpredictable tumour shape and small nodules challenge the inclusion of all potential patterns in templates.
6. Full resolution residual network (FRRN) and Multi-resolution residual network (MRRN) [102,103]: These advanced deep learning methods were built based on ResNet. However, they are still impacted by the variabilities of the reference images.

There is also research about PET/CT auto-segmentation; however, due to the standard guidelines of oncology diagnosis, there are limitations to using PET/CT as a widely adopted tool. Furthermore, PET/CT lacks precise anatomical detail when contouring metabolic regions on PET scans. Comparing semi-automatic to manual contouring reveals a high correlation. However, the studies often face limitations due to small patient cohorts, diverse lesion morphologies, individual variability, precise image registration challenges, specific lesion locations, and a focus on certain primary or relapse types, such as peripherally located primary tumours only [92,104]. Given the timing, anatomy, and morphology heterogeneity, expecting a single algorithm to segment all cancer types effectively is unrealistic.

### 2.3 Tumour Growth Mathematical Models

Various methods [105] for calculating tumour growth rates have been reported in the literature, many of which model growth using exponential or logistic growth. This thesis focuses exclusively on the Gompertz growth model due to its relevance to tumour behaviour. The Gompertz model [106] describes tumour growth as a sigmoidal (S-shaped) curve, where tumours proliferate in the early phase and then slow down as they approach a plateau. This feature reflects the biological reality, known as the carrying capacity, where cell proliferation is restricted by limited nutrients, reduced oxygen supply, and physical space, resulting in a deceleration in growth rate over time. However, this model fails to account for several critical factors: 1. Impact of diversity treatments [26]: treatment shapes metastatic diversity by applying selective pressure. Treated metastases frequently harboured private monoclonal driver mutations absent from the primary tumour, indicating treatment-driven evolution of resistant clones. Untreated metastases remain polyclonal, like primary tumours; 2. Heterogeneous growth patterns [107–110]: Tumour growth is not uniform; different lesions within the tumour may harbour diverse subclones; 3. Immune microenvironment and selection pressure [107,111,112]: The immune system plays a critical role in shaping tumour evolution. Lung tumours undergo dynamic selection by immune cells, leading to clonal sweeps and immune escape. Notably, LUAD tends to experience early (truncal) immune selection, while LUSC shows more subclonal selection, suggesting differences in the timing of immune selection pressures between LUAD and LUSC. Mechanisms of immune escape include neoantigen editing, loss of HLA expression (which impairs antigen presentation), and PD-L1 upregulation, all of which suppress T-cell activity and lead to immune evasion. These factors highlight the limitations of the exponential and Gompertz models.

A linear model is used in early research to analyse tumour growth dynamics. It considers that tumour growth initially follows an exponential pattern but later transitions to a constant growth rate over time. In many cases, linear growth calculations provide a more straightforward and practical approach to estimating tumour progression. Additionally, numerous studies use mathematical modelling, but they also face limitations, such as restricted data access, issues with dataset representativeness, high computational demands, and poor interpretability of complex models in clinical practice [113]. These challenges make it difficult to generalise and apply models effectively in real-world scenarios.

### 2.4 Tumour Growth Dynamics and Evolution in Lung Cancer: Insights and Gaps

Lung cancer progression is heterogeneous and affected by genetic evolution, immune pressure, anatomical factors, smoking exposure, histological subtype and treatment effects. Large-scale studies, including the National Lung Matrix Trial and TRACERx, have significantly improved our understanding of the evolutionary and immunogenomic landscape in non-small cell lung cancer (NSCLC). However, none of these studies have explored how tumour growth rate influences relapse timing, relapse sites, or TNM staging despite its potential relevance to tumour behaviour and clinical outcomes.

1. Histology and immune pressure: The histological subtype plays a significant role in tumour evolution. Lung adenocarcinomas (LUAD) often undergo truncal selection, where early driver mutations, such as EGFR, KRAS, and STK11, dominate the tumour's phylogeny. Squamous cell carcinomas (LUSC) undergo subclonal selection, indicating more dynamic genomic changes throughout progression [107]. Immune microenvironments differ markedly between subtypes: LUADs tend to have lower CD8+ T-cell infiltration, with dispersed immune cells and small localised clusters, while LUSCs exhibit structured, immune-rich regions, suggesting different patterns of cancer evolution [114]. Morphological subtypes also correlate with relapse sites—tumours with micropapillary features or air bronchograms tend to relapse intrathoracically, whereas solid tumours with necrosis are more likely to recur extrathoracically. Despite these findings, no study has systematically analysed how growth rate dynamics vary between histologies or how these differences contribute to TNM stage progression and site-specific relapse.

2. Smoking Status and Tumour Biology: 75% of ever-smoker LUADs show strong evidence of smoking-related mutation. These mutations tend to localise in the right lung and upper or middle lobes of the lung, supporting a biological basis for tumour localisation patterns. However, 8% of LUAD cases lacked tobacco-induced mutagenesis but showed mutation patterns similar to those of never-smokers, enriched in EGFR, RET, ROS1, ALK, and MET mutations, suggesting a distinct lung cancer biology in some smokers, independent of direct tobacco mutagenesis [107]. Smoking is associated with mutational diversity and early metastatic dissemination (often occurring at <8 mm tumour size) [115], yet its impact on tumour growth rate and how this might influence relapse risk has not been explored.

3. Genetic Evolution and Subclonal Diversity: Genetic heterogeneity plays a critical role in tumour evolution and relapse. Polyclonal seeding and Subclonal Copy Number

Alterations (SCNA–ITH) are associated with extrathoracic metastasis; however, neither subclonal whole gene doubling nor subclonal expansion score independently predicted DFS or relapse sites [107,115]. These studies largely overlook tumour volume and growth rates, which may interact with genomic instability to drive progression. Moreover, the absence of preoperative ctDNA is associated with a better prognosis, and longitudinal surveillance can detect relapse before it becomes radiologically apparent in ~20% of cases [116]. However, factors such as tumour size and volume thresholds for ctDNA detection (e.g., >10 $cm^3$) are inconsistently accounted for.

4. Anatomical Patterns of Relapse: Initial recurrence sites significantly impact survival. Brain, bone, pleural and multi-site involvement had a worse prognosis, whereas isolated lung involvement may have a better outcome. Predictors such as tumour size, SUV, and lymph node status are associated with higher relapse risk [117]. However, newer data shows that less than 20% of metastatic relapses originated from primary lymph node involvement, indicating that the lymph node is a predictor of relapse rather than a direct route to distant metastases [115]. Importantly, these studies have not dissected single-organ relapse routes or explored how tumour growth rate and lesion number influence the progression routes**.**

**2.5 CT Surveillances Post-surgery**

Until 2007, there were no large clinical trials to evaluate the impact of CT imaging schedules on patient prognosis. A Japanese study reviewed 1,398 resected NSCLCs and found that patients in stages II–III who received chest CT scans during follow-up had significantly longer overall survival rates than those monitored through physical examinations and chest X-rays [92,118]. However, this study was criticised for imbalanced baseline characteristics between the two groups, which led to selection bias. Additionally, other studies have highlighted that the risk of developing new primary lung cancers is approximately 2% annually. While the benefit of intensive imaging for detecting secondary tumours remains unclear, regular follow-up imaging may still be beneficial for patients at lower risk [119,120].

A recent inquiry from a cohort of 140 patients receiving annual chest CT scans revealed that 30 out of 168 scans showed equivocal lesions, and only 14, less than half, represented recurrent disease [121]. This finding underscores the critical role of radiologists and physicians in diagnosis and decision-making. A comparison between forty trial patients

with locally advanced NSCLC undergoing routine CT imaging and thirty-five non-trial control patients receiving less intensive radiologic follow-up showed no survival rate differences [122]. Early relapse detection via CT surveillance may benefit Stage I patients; however, it has no observable impact on survival [123]. Moreover, a large study involving 2442 stage I patients with various imaging follow-up intensities – 3 months (60–150 days), 6 months (151–300 days), and 12 months (301–450 days) – found no association between surveillance intensity and 5-year overall survival [124]. The limitations of this study include a potential bias towards not treating recurrences in patients under less intensive surveillance, which may be attributed to clinicians who conduct less aggressive surveys. This bias could lead to worse survival outcomes and a propensity for healthier patients to undergo more frequent surveillance over time. Additionally, the patient's enrollment time can span more than 10 years, during which time imaging techniques have undergone significant improvements. A larger study reviewed more than 4,000 NSCLCs and found that more frequent CT imaging checks don't improve survival [125]. However, the inclusion of a significant number of stage III NSCLCs and a higher proportion of such patients in the high-intensity imaging group may lead to bias. Defining the optimal method to assess surveillance intensity in research is challenging.

Frequent follow-ups may increase cost and patient anxiety. A balanced, cost-effective, and patient-centred surveillance approach should be informed by an understanding of tumour biology and clinical characteristics, aiming for timely curative treatments to improve clinical outcomes.

# 3 Aims and Objectives

Workflow is illustrated in Figure 1.1. Imaging scans were systematically collected across multiple phases. Manual segmentation of malignant lesions at each time point can help in a detailed analysis of tumour dynamics across a diverse patient cohort. This research aims to build the most extensive global imaging dataset to track tumour evolution from diagnosis to death by contouring individual malignant lesions and recording imaging factors. Furthermore, it aims to develop a non-invasive method for predicting prognosis, exploring tumour evolution heterogeneity, and customising disease management

protocols by using tumour volume, growth speed, and morphology from imaging and clinical characteristics.

### 3.1 Aim One:

Create the largest global imaging dataset to track tumour evolution from diagnosis to death by contouring individual malignant lesions and recording imaging factors. The goal is to better understand how recurrence rates vary across different subgroups of non-small cell lung cancer (NSCLC) patients, with particular emphasis on evaluating primary tumour volumes and growth rates as predictors of relapse.

### Objective One:

Manually review and contour the baseline, recurrence and follow-up scans to establish a volumetric dataset of anatomic malignant and equivocal lesions. Use the Kaplan–Meier method to calculate annual tumour recurrence rates, including subgroup analyses based on age, gender, smoking status, pathology, TNM stage, and tumour volume. Explore factors influencing tumour recurrence and identify recurrence patterns across various clinical and imaging characteristics using Cox regression analysis. Specifically, investigate the relationship between tumour volume and growth speed, assess their impact on recurrence, and propose criteria for adjuvant therapy in pT2N0M0 tumours.

### 3.2 Aim Two:

This study aims to explore and characterise the heterogeneity of relapse, progression, and prognosis across different tumour sites and growth patterns in non-small cell lung cancer. Specifically, it seeks to:

1. Investigate the temporal and spatial diversity of tumour relapse.
2. Examine the patterns of progression with an emphasis on tumour burden, anatomical location, and growth rate.
3. Assess the prognostic impact of site-specific recurrences on patient outcomes.

### Objective Two:

1. Exploring the Heterogeneity of Relapse:
    - Analyse timing and common sites of relapse, with an emphasis on intrathoracic and extrathoracic tumour burden.

- Examine the diversity in tumour growth rates at relapse, particularly between intrathoracic and extrathoracic sites.
- Evaluate the predictive value of clinical tools (e.g., PET/CT) in identifying relapse patterns and the correlation between initial lymph node involvement and subsequent lymph node relapse.

2. Exploring the Heterogeneity of Progression:
    - Investigate site-specific relapse patterns and their impact on subsequent tumour progression and survival.
    - Investigate how tumour burden and location influence the rate and pattern of progression.
    - Explore the correlations between tumour growth rate and progression and their implications for clinical outcomes.
3. Exploring the Heterogeneity of Prognosis Based on Site-Specific Recurrence:
    - Assess the prognostic impact of early involvement of specific organs (e.g., bone, brain, lymph node) on prognosis.
    - Determine which relapse site (e.g., lung, brain) is associated with better or worse survival rates post-recurrence.

### 3.3 Aim Three:

To evaluate the role of surveillance frequency and identify key factors influencing progression-free survival (PFS) in non-small cell lung cancer (NSCLC). By analysing post-surgical and post-relapse tumour dynamics, this work proposes a framework to inform individualised surveillance and treatment strategies for improved patient outcomes.

**Objective Three:**

1. Examine the effect of surveillance frequency on prognosis.
2. Investigate predictive factors of tumour progression and overall survival.
3. Investigate how tumour growth dynamics and treatment response influence post-relapse outcomes.

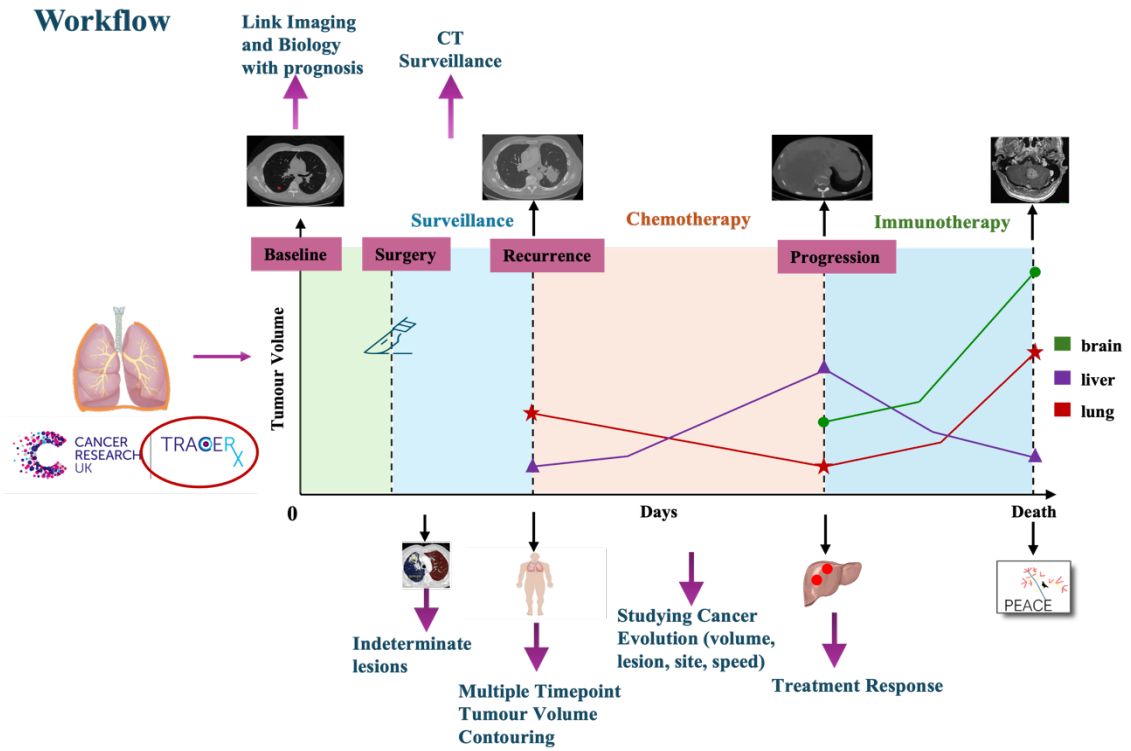


Fig. 1.1 Overview of study workflow across the disease trajectory in NSCLC patients.

# 4 Novel Contributions

## 4.1 Accurate Tumour Volume Measurement

Tumour volume is a significant predictor of outcomes in NSCLC. Previous studies have estimated tumour volume based on diameter, using the formula $\frac{4}{3}\pi r^3$, assuming the tumour is a perfect sphere. This method considers that proportional changes in volume correspond to changes in tumour diameter [49, 37, 126], which is often inaccurate. NSCLC tumours frequently exhibit irregular shapes, which challenges the accuracy of unidimensional measures, such as diameter, in capturing tumour complexity. Automatic segmentation algorithms can calculate volume, but their performance is limited by variability in tumour histology, location, and morphology [92–104,127,128]. Few studies have directly compared the tumour volume calculated by diameter with that obtained through manual contouring. In this research, diameter-based volumes and manually contoured volumes were compared, revealing a significant difference of 69%. The results show that using diameter alone does not accurately reflect tumour volume, emphasising the need for more precise approaches. Manual contouring, while more labour-intensive, can address these limitations by providing a more accurate representation of tumour volume.

### 4.2 Tumour Progression Evaluation Based on Tumour Volume

There is no universally accepted standard for evaluating tumour progression based on volume. This research introduced the application of volume-based RECIST (Response Evaluation Criteria in Solid Tumours) criteria. This cohort used Volume-RECIST criteria to define the complete response (CR) as total lesion disappearance, partial response (PR) as a minimum 30% volume reduction in the total volume, compared with the previous scan, and progressive disease (PD) as a 20% volume increase in the entire tumour volume or new lesions, including the non-target lesions. This approach identified progression earlier than traditional RECIST, which relies on changes in diameter.

### 4.3 The Biggest Scale of the Imaging Dataset from Diagnosis through to Death

Over the past few decades, research into tumour heterogeneity has revealed the presence of subclones within the primary tumour, contributing to different tumour growth rates and relapse patterns [4,107,108,129]. Given the variations in tumour growth rates and affected organs, a comprehensive understanding of progression diversity is crucial. The TRACERx study, the most extensive lung cancer study in the UK, launched in 2014 by Cancer Research UK and University College London Cancer Trials Centre, has been established to address this issue. It recruited 842 patients with early-stage lung cancer across 14 UK National Health Service hospitals, tracking them from diagnosis through to cure, relapse, and death, collecting multi-region tissue samples and imaging at baseline, recurrence, and periodic follow-up imaging post-surgery. I have developed a keyword-based extraction system from radiology reports to support natural language processing-based automation, established manual longitudinal contouring criteria, and created the largest TRACERx longitudinal imaging dataset globally, tracking the volume of each malignant lesion, lesion growth speed, and imaging characteristics from diagnosis to death. Over 2,400 scans and more than 3,200 individual lesions were longitudinally contoured, representing an unprecedented level of annotation in any prior study. This uniquely detailed dataset offers opportunities to analyse primary tumour evolution and metastasis over time.

### 4.4 Lesion-Specific Growth Rate Analysis: A Detailed Approach to Understanding Tumour Variations and Interdependencies in Individual NSCLC Patients

This study focuses on exploring the heterogeneity of longitudinal tumour evolution in non-small cell lung cancer (NSCLC) patients, emphasising anatomical locations and

volume changes. Unlike traditional bulk tumour volume analysis, this research takes a lesion-by-lesion approach, examining individual tumour growth rates and their variations within each patient. This more detailed analysis of individual lesions provides insight into the interdependencies of growth patterns, helping to identify specific factors that influence prognosis and response to treatment.

Routine surveillance imaging plays an essential role in monitoring patients with resected non-small cell lung cancer (NSCLC) to detect disease recurrence and new primary lung cancers. Despite existing guidelines [7], the intensity of surveillance varies widely in clinical practice. More than 50% of patients may experience early relapse before their scheduled examination, often due to the onset of symptoms [130]. Hence, many researchers have considered that high-intensity imaging checks can help detect early tumour relapse and potentially improve overall survival [131]. However, McMurry and his colleagues found that increased frequency of CT imaging does not improve survival [125]. Personalised surveillance strategies remain largely unexplored. This research investigated the frequency of surveillance across different subgroups to provide tailored surveillance schedules for individual patients.

### 4.5 Contributions to Other Research

I established a comprehensive lesion-based dataset, making the most extensive global imaging study in relapse and progression analysis. This dataset, which has become the foundation of the TRACERx study, includes detailed mappings of individual lesions' volumes, locations, and progression. The dataset is a valuable resource for ongoing research at the UCL Cancer Institute and the Francis Crick Institute. Future research will use these results to explore tumour evolution through genomics and circulating tumour DNA (ctDNA) data, aiming to construct phylogenetic trees of metastatic genes and uncover the mechanisms of metastasis seeding and treatment resistance. Specifically, one research study using my data, 'Characterizing evolutionary dynamics of cancer proliferation in single-cell clones with SPRINTER', has been published in *Nature Genetics*.

# Chapter Two

## Methodology

### 1. Overview of TRACERx Data Cohort

**Statement:** This study was a collaboration with the Cancer Institute, approved by the University College London (UCL), and used data from the TRACERx and PEACE studies. It aimed to create the most extensive global imaging dataset to track tumour evolution from diagnosis to death by contouring individual malignant lesions and recording imaging factors. Clinical characteristics and imaging scans were collected and transferred by the Cancer Institute. I was trained and worked as a radiation oncologist for six years, performing all the tumour contouring tasks in this project, using anatomic and volumetric information to understand tumour progression. Future TRACERx research will use anatomic imaging information, combining genomics and ctDNA data, to explore tumour evolution.

**Details of TRACERx and PEACE criteria:** The Tracking Cancer Evolution through Therapy (TRACERx) study (https://clinicaltrials.gov/ct2/show/NCT01888601), led by Charles Swanton, Principal Investigator at the Cancer Institute of UCL, is a landmark cancer study aimed at understanding the evolutionary trajectory of cancer tumours. Initiated in 2014 by Cancer Research UK and the University College London Cancer Trials Centre, the study recruited 842 patients with early-stage lung cancer across 14 National Health Service hospitals in the UK, tracking each patient from diagnosis to cure, relapse, and death. The TRACERx study collected tissue samples from multiple regions and performed imaging at baseline and recurrence, with periodic successive imaging surveillance post-surgery. All imaging scans, including CT, PET-CT, MRI, and bone scans, along with their corresponding reports, were collected. By analysing cancer's evolution and its response to treatment, TRACERx seeks to provide insights into mutation, heterogeneity, drug resistance and recurrence patterns.

The TRACERx project includes a UK national autopsy study called Posthumous Evaluation of Advanced Cancer Environment (PEACE)

(https://clinicaltrials.gov/study/NCT03004755), led by Mariam Jamal-Hanjani, which sampled patients frequently, aimed to analyse cells or ctDNA shed from tumours at surgery and from autopsy samples to understand how cancer spreads from the primary tumour site to distant locations genetically, thereby providing deeper insights into tumour evolution over space and time.

**1.1 TRACERx Study Inclusion Criteria:**
(https://clinicaltrials.gov/ct2/show/NCT01888601)
Collect multiple regions of tissue and perform longitudinal imaging.

1.1.1 Over 18 years old.

1.1.2 Written informed consent was obtained.

1.1.3 Early suspected or confirmed NSCLC and eligible for primary surgery.

1.1.4 The suspected lesion must be at least 15mm in diameter on pre-operative imaging, and once excised, at least two regions must likely be obtained.

1.1.5 Patients can not have any other current malignancy or malignancy diagnosed or relapsed at any time currently being treated (including hormonal therapy).

1.1.6 Patients cannot have any other current malignancy or malignancy diagnosed or relapsed within the past 3 years (other than non-melanomatous skin cancer, stage 0 melanoma in situ, and situ cervical cancer).

1.1.7 Primary surgery is planned in keeping with National Institute for Health and Care Excellence (NICE) UK guidelines.

1.1.8 Patients cannot have neoadjuvant therapy.

1.1.9 Performance status (ECOG) 0 or 1.

**1.2 TRACERx Study Exclusion Criteria:**
(https://clinicaltrials.gov/ct2/show/NCT01888601)

1.2.1 Any other malignancy diagnosed or relapsed at any time is currently being treated (including by hormonal therapy). Exceptions to other malignancies include non-melanomatous skin cancer, stage 0 melanoma in situ and situ cervical cancer.

1.2.2 Any other current malignancy or malignancy diagnosed or relapsed within the past 3 years. Exceptions to other malignancies include non-melanomatous skin cancer, stage 0 melanoma in situ and situ cervical cancer. An exception will be made for malignancies diagnosed or relapsed more than 2 years ago but less than 3 years ago, only if a preoperative lung lesion biopsy has confirmed an NSCLC diagnosis.

1.2.3 Insufficient tissue was collected.

1.2.4 Unable to comply with protocol requirements.

1.2.5 NSCLC is not confirmed.

1.2.6 A change in staging to IIIC or IV following surgery.

1.2.7 Treatment with neoadjuvant therapy for the current lung malignancy is deemed necessary.

1.2.8 Operative criteria are unmet (e.g., incomplete resection with macroscopic residual tumours).

1.2.9 Known HIV, hepatitis B virus, hepatitis C virus or syphilis infection.

**1.3 PEACE Study Inclusion Criteria:** (https://clinicaltrials.gov/study/NCT03004755)

Blood samples will be taken at baseline and follow-up time points before death. Tissue harvesting will be performed after death. The tissue will be collected from tumour and normal tissue sites, guided by either imaging performed before the patient's death or tissue harvest findings. Additionally, bone marrow and fluid will also be taken.

1.3.1 Over 18 years old.

1.3.2 Confirmed diagnosis of any form of solid malignancy with metastatic disease (where the site of origin is known or unknown), except primary brain tumour, where there may not be evidence of metastatic disease.

1.3.3 Oral and written informed consent from the patient to enter the study and to undergo tumour harvesting after death, or informed consent from a nominated representative or a person in a qualifying relationship after the patient has died.

**1.4 PEACE Study Exclusion Criteria:** (https://clinicaltrials.gov/study/NCT03004755)

1.4.1 Medical or psychiatric condition that would preclude informed consent.

1.4.2 History of intravenous drug abuse within the last 5 years.

1.4.3 Confirmed diagnosis of known high-risk infections (e.g. HIV/AIDS-positive, hepatitis B/C, tuberculosis, and Creutzfeldt–Jacob disease). Unless the patient's case is of scientific interest, and it must be agreed upon in advance with local mortuary staff and pathologists.

## 2. Details of Clinical Data Collection

Researchers in the TRACERx study recorded demographics, treatment modality, surgery sample data, recurrence date, and last follow-up or death date, details are listed below. This information can aid my analysis.

### 2.1 Clinical characteristics

Sex, age, race, smoking status, ECOG, mutations, FEV1, surgery types, tumour-nodes-metastasis [TNM] stage, pathology, pathology-positive lymph node and vascular invasion. The Cancer Institute transferred all data.

Smoking history, including the type, amount, and duration of smoking. All cigar and pipe consumption amounts were converted to equivalent cigarette counts. That is, one cigar corresponds to approximately 1.5 cigarettes, and for pipes, one bowl of tobacco is equal to 2.5 cigarettes [107]. Patients who had smoked fewer than 100 cigarettes in their lifetime were classified as never smokers. Ex-smokers were defined as patients who had smoked 100 or more cigarettes in their lifetime and had quit more than 1 year before registration. Patients who had smoked 100 or more cigarettes in their lifetime and were smokers at the time of registration were grouped as smokers. Patients who had smoked 100 or more cigarettes and had quit less than 1 year before enrollment were recent-ex smokers. The Smoking Index is then used in research to quantify the individual's exposure to tobacco over time.

Smoking Index = Cigarettes per day * smoking years.

Tumour-nodes-metastasis [TNM] stage classification used the 8$^{th}$ edition. Mutations were only detected at baseline.

### 2.2 Treatment modalities

Treatments include types, doses, given sites, and duration were transferred.

### 2.3 Diagnoses and recurrence date

Most patients had one prior diagnostic CT scan and a subsequent staging PET/CT scan at the time of diagnosis; therefore, I used the date of the last scan as the date of diagnosis. If the patients had only one scan at baseline, that date would be the date of diagnosis.

Furthermore, I used the date of recurrence from the clinical dataset confirmed by the Cancer Institute.

### 2.4 Last follow-up and death date

After completing the segmentation of one patient, I contacted the Cancer Institute to obtain the latest and most accurate follow-up or death dates.

## 3. Preparation Steps for Imaging Before Tumour Contouring

These were done in a collaboration between the Cancer Institute and my department.

### 3.1 Request scans

To create a large longitudinal imaging dataset with clinical treatment annotations and to subsequently contour 3D tumour volumes on a lesion-specific level for all patients with confirmed relapse of disease, the imaging manager in Mariam Jamal-Hanjani's team requested Computed Tomography (CT), Positron Emission Tomography (PET-CT), Magnetic Resonance Imaging (MRI) and reports from CTC group, covering14 hospitals. Staff from the 14 hospitals labelled all scans and reports with the hospital IDs, time points (Baseline, Follow-up, First recurrence, Progression, Last scan), and imaging types (CT, HRCT, CTPA, MRI, PET/CT). The following clinical time points where a scan has been performed (Fig. 2.1A):

3.1.1 Baseline (both the diagnostic CT and the staging PET/CT).

3.1.2 Follow-up after surgery/adjuvant therapy.

3.1.3 First recurrence (CT and PET-CT if both done, plus any other relevant scans).

3.1.4 Follow-up scans post-relapse.

3.1.5 All points of progression following the first recurrence.

3.1.6 Last scan prior to death.

Each scan was sent on a single disc from MACRO to RDS, not multiple scans on a single disc. The size of the DICOM files should remain the same (each DICOM file is usually 300MB–1.2GB). Each scan report should also be saved as a PDF corresponding to the scan date.

### 3.2 Scan Images

The imaging manager in Mariam Jamal-Hanjani's team asked sites to ensure that all scans and reports are labelled with the following details (Fig. 2.1B):

3.2.1 LTXID

3.2.2 Clinical Timepoint, including Baseline, First recurrence, First Progression, Second Progression

3.2.3 Scan type: CT (including HRCT, CTPA, contrast/non-contrast CT, CT head and CT bone), PET-CT, MRI, MRI spine and MRI head, etc.

3.2.4 Date of scan: This should match the date entered in the TRACERx MACRO database and should be the date the scan was performed, not the date it was reported or downloaded.

**A:**

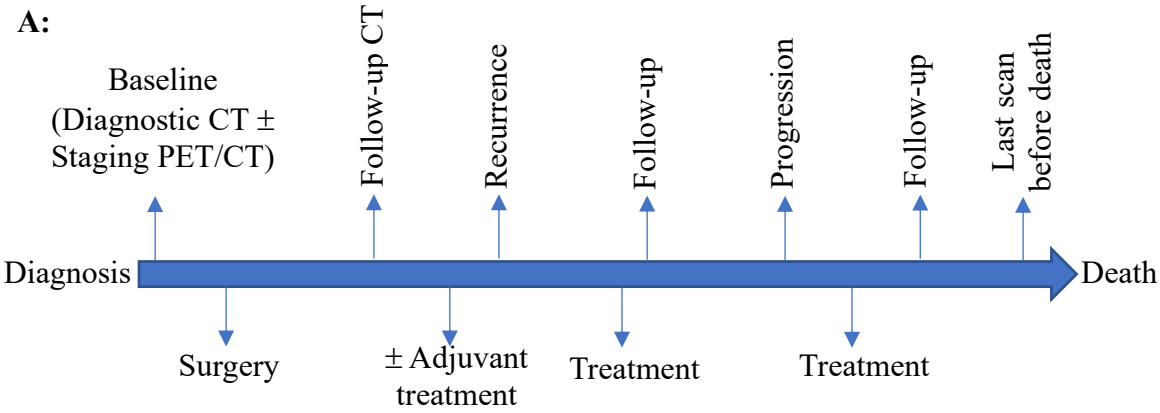


**B:**

Label format = HospitalID_LTX0000_TIMEPOINT_TYPE_01Jan2020
HospitalID: A, B, C, F, G, L, M, R, S, U, W, Y, V
TIMEPOINT: Baseline, FU, First Recurrence, First Progression, Second Progression, Third Progression, Fourth Progression and so on, New Lung Primary, Other Time Point, Last Scan Prior To Death
TYPE: CT, PET-CT, MRI, MRI head, CT head, Bone, MRI Spine, HRCT, CTPA, Other

Fig. 2.1 Timing and labelling of imaging scans used in this study. A: Overview of scan collection time points across the patient timeline, including diagnosis, follow-up, and post-relapse/progression imaging; B: Structure of scan labels, including patient ID, hospital ID, corresponding clinical timepoint and scan type.

None of the images of each patient can be transferred simultaneously. Scans were sent in different batches. Based on the quality monitoring results provided by the imaging manager at the Cancer Institute, any missing images were identified, and feedback was

given to the respective hospitals, requesting that they retrieve the missing images at various time points.

### 3.3 Scan Transfer

All the datasets, including DICOM format scans and reports, were then transferred in four batches over a three-year period to Royle's server by Catarina Isabel Correia Veloso Da Veiga, a member of Royle's team. Since images were transmitted by different sets, the new transfer might have contained the previous scans that had already been transferred, rather than just sending the newly retrieved images.

### 3.4 Convert Scan to NIfTI Format

Hyothaek Lee from Royle's team reviewed the scans' labelling, then created and ran a sorting code to check the metadata of the DICOM files against several criteria before being sorting them into scan-by-scan folders. He listed the sorting criteria priorities: the patient's unique ID, time point, and scan type. Each date folder from the original sites contains all DICOM files from the day of the scan, representing different scans in one folder, making it indistinguishable. Each scan's file name had a unique series number to indicate its source. The sorting process results in DICOM files representing each scan within a single folder. After sorting, the DICOM files within the individual scan folder are converted into a single NIfTI file format. The resolution of the images was not downgraded after converting. As DICOM files require several hundred individual files to represent a single image scan, converting to a single NIfTI is more convenient for image processing and keeping track of the files. After converting to the NIfTI format successfully, the corresponding DICOM files are compressed to reduce the file count and saved on the server for future reference. Our team chose the NIfTI format because its file size is tiny. Each file is usually 50MB–200MB. The images are easy to store and read faster, which can help researchers perform algorithmic computations and address other issues.

## 4. Hypotheses:

**4.1** Based on the previous study [126], tumour geometry is approximated as spherical. According to this hypothesis, when the diameter is 2r, the volume is $\frac{4}{3}\pi r^3$. However, in the real world, tumours are irregular in shape rather than perfectly round, making it

inaccurate to use diameter alone to represent the entire tumour. Therefore, I extracted the longest diameter initially and calculated the volume based on this diameter. Then, I manually contoured the tumour volume on three-dimensional images to compare the differences between the two methods.

**4.2** All patients had complete tumour resections, with no residual solid tumour remaining after surgery.

**4.3** The relapse tumour did not grow exponentially. I used follow-up scans taken post-surgery and before the confirmed relapse scan to longitudinally contour the growth pattern of the malignant lesion and verify its behaviour.

**4.4** The diagnostic CT scan and staging PET/CT scan were often taken 1–2 months apart. Linear growth is used to calculate the baseline growth rate.

**4.5** I calculated the treatment response, relapse, and progression growth speeds in a linear manner using scans taken before and after these events. This approach was chosen because the scans were conducted close to these events, and when one object is close to another, it can be linear. Since tumours may grow in various patterns, this is the most straightforward method, which is a priority of my study.

## 5 Procedures for Contouring Tumour Boundaries in Sequential Imaging Scans

I opted against auto-segmentation due to its limitations in handling tumours with blurred boundaries and its firm reliance on reference image similarity. Since my study encompasses imaging across baseline, recurrence, and progression, with heterogeneous relapse sites and tumour morphologies, automated models struggle to accurately segment all individual lesions. Additionally, developing a robust auto-segmentation model requires a large, well-annotated training dataset, which remains a challenge. As more tumours are manually contoured, the performance of auto-segmentation models can be progressively improved [92,93,96,95,98–101,102,103].

I am a clinical radiation oncologist with 6 years of clinical experience in tumour contouring. I completed all the tumour contouring, and 2440 scans were finally contoured. Each scan took me 1–3 hours to contour, and an additional 1 hour was required for each to be checked and reviewed. If I have any questions, I consult Dr. Crispin Hiley, a radiation oncologist and consultant at UCLH, as well as an associate professor at the Francis Crick Institute, for assistance. Once NIfTI files were uploaded, I manually verified the accuracy of each imaging file's patient ID and date on the Royle team's server.

## 5.1 Patient's Contour Criteria.

I chose the priorities for patients as follows:

5.1.1 Patients who experienced recurrence had baseline images, recurrence images, and at least two scans following recurrence. Corresponding radiology reports were also available.

5.1.2 Patients who did not recur had baseline images and more than three follow-up scans after surgery. The follow-up period post-surgery exceeded three years.

5.1.3 Patients from the PEACE study cohort with available autopsy samples.

## 5.2 Contouring Procedures

5.2.1 Firstly, based on the reports sent by the Cancer Institute, I created a dataset to record the entire tumour evolution process from diagnosis to death. I wrote down the scan type, contrast information, new lesion appearance event, individual lesion location in each organ, diameter size, SUV value, and diameter changes after treatment, and RECIST [132] criteria evaluation results at each imaging time point (baseline, follow-up, recurrence, the first progression, the second progression, the third progression, last scan before death etc.). This dataset can help contour the malignant lesions and determine the stage of the process.

5.2.2 I used ITK-SNAP (version 3.8.0, software copyright 1998–2019, Paul A. Yushkevich Guido Gerig), an open-source software, to open the imaging files. Adjust the imaging window level to obtain high-quality scans, which helps define the tumour boundary more precisely. The lung lesion was first delineated in the mediastinal window, followed by verification in the lung window, initially using the axial view, then the sagittal and coronal views. At the same time, I referred to imaging reports from hospital radiologists, which included annotations of biopsy-confirmed recurrences. Subsequently, I referenced positive autopsy findings from participants in the PEACE study. These reports helped clarify the locations of malignant lesions over time. Additionally, I used the brush in the toolbar to outline the tumour boundary and filled the target region in each axial slice section. After contouring slice by slice, 3D volume reconstructions were verified in sagittal and coronal planes. Each lesion was colour-coded and consistently tracked over time. Finished contours were saved in NIfTI format, with each segmentation named after its image file plus "SEG_Site (Lung, Abdominal, Brain, Bone, etc.)". Each segmentation NIfTI file represented one imaging file, ranging in size from 40 to 500 KB.

The figures in Fig. 2.2 illustrate how I contoured individuals and extracted volumes using ITK-SNAP. Furthermore, Figure 2.2D illustrates how autopsy biopsy findings from the PEACE study were used to identify positive malignant lesions that were not reported in the corresponding CT reports reviewed by senior radiologists.

**A:** Refer to CT reports identifying malignant tumours and adjust the CT contrast to enhance the visibility of the lesion's boundaries, making them more precise and distinguishable.

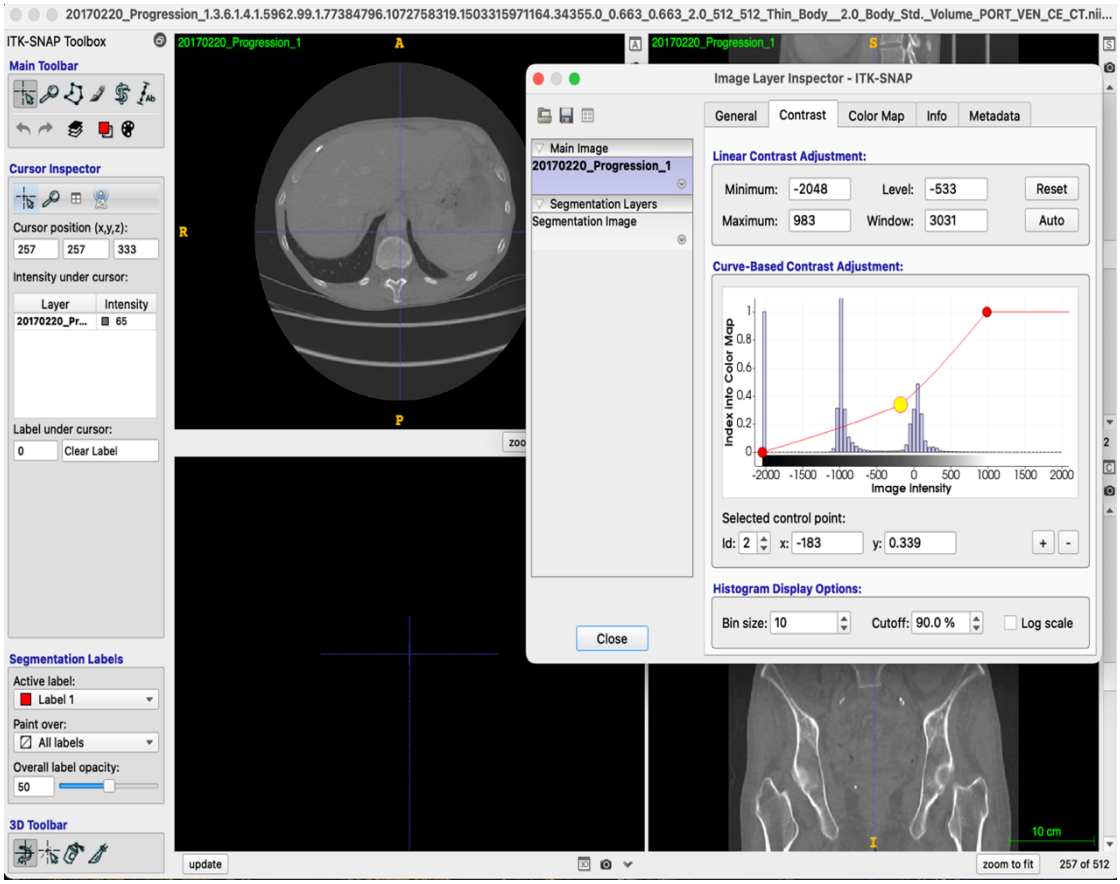

**B:** Contour the boundaries of each malignant lesion in the diaphragm, right kidney, and right adrenal gland. Fill each lesion on all slices using a distinct colour and appropriate label name.

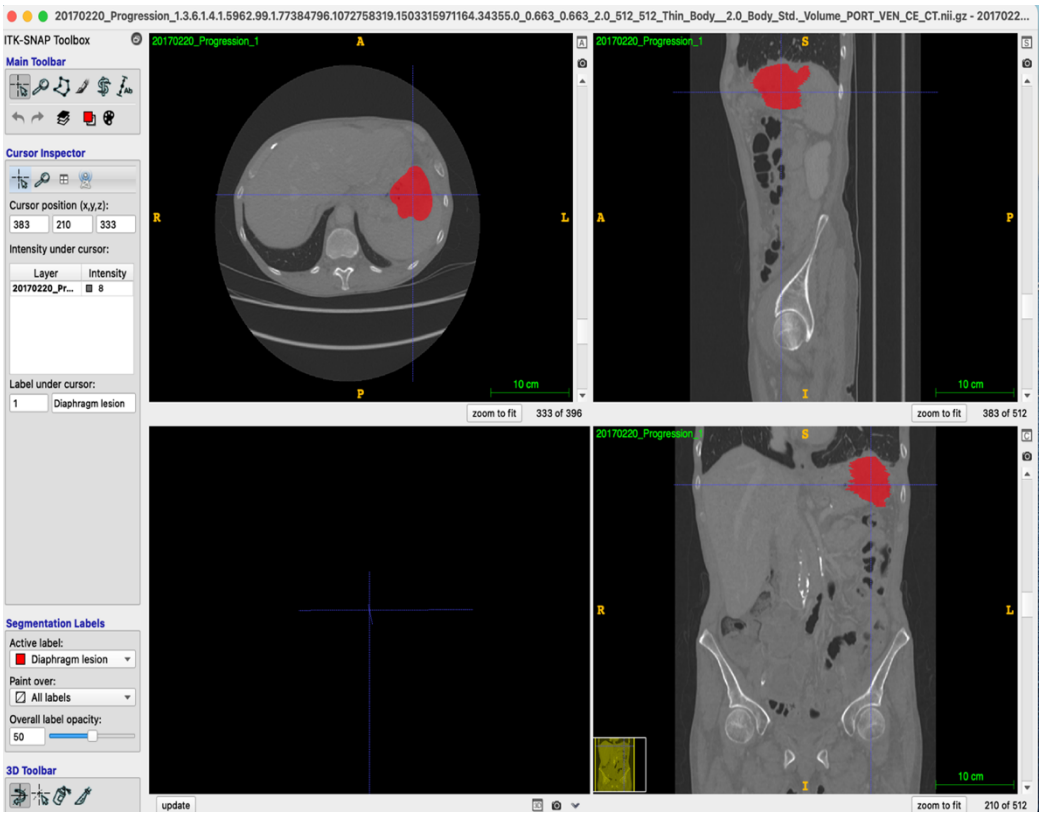


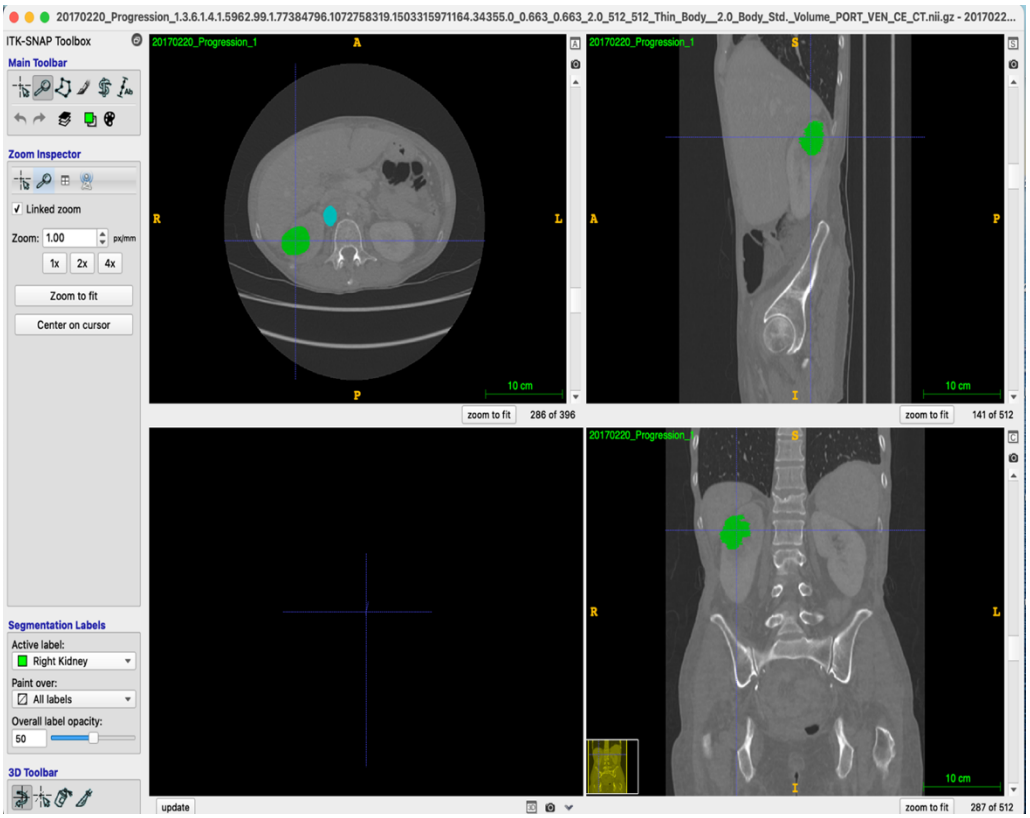

**C:** Extract tumour volumes using ITK-SNAP, based on pixel count within the contoured regions.


**D:** Identify autopsy-confirmed gastric lymph node that was not reported in the CT reports.

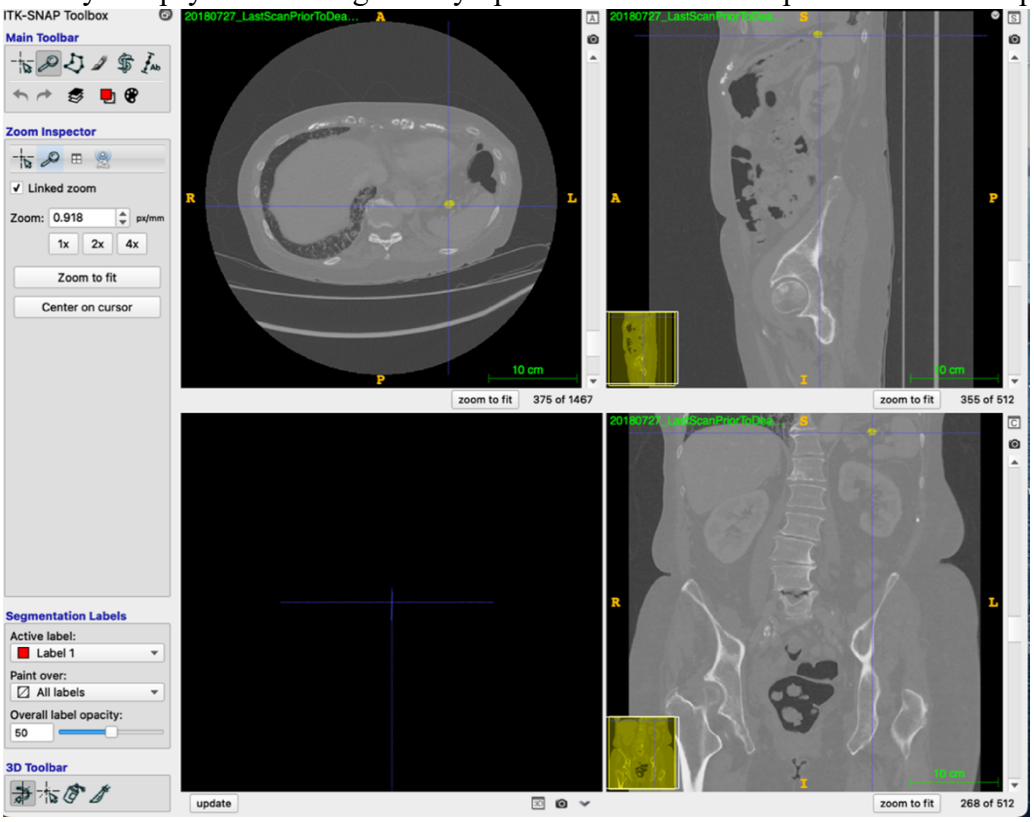


Fig. 2.2 Schematic diagrams illustrating the contouring procedures using ITK-SNAP.

5.2.3 Using imaging pixel calculations, the actual 3D tumour volume can be automatically extracted from the toolbar in ITK-SNAP software. ITK-SNAP also provides essential metadata, including scan type, scan thickness, and the X- and Y-axis dimensions of each scan. The slice thickness varies by imaging modality: CT (including HRCT and CTPA) ranges from 0.5 to 5 mm, MRI from 0.8 to 8 mm, and the CT component of PET/CT from 1 to 5 mm.

5.2.4 As scans were transferred in non-chronological batches, I manually matched new scans with previous segmentations, revising or replacing old segmentations to ensure accuracy.

5.2.5 To assess contouring variations, I randomly selected 10 patients. Each scan was contoured three times at different time points, with volumes recorded independently. The standard deviation was then used to calculate the 95% confidence interval. The results showed a 95% confidence interval difference ranging from 0.54% to 42.6%, with 90.9% of cases showing less than 20% variation. The coefficient of variation (CV) for each lesion ranged from 0.27% to 21.3%, with 90.9% of cases showing a CV below 10%, confirming the reliability of the contouring process. The mean contouring error per patient ranged from 2.69% to 7.60%, all of which were below 8%. Notably, larger tumours appeared to have higher contouring accuracy. (*Appendix 1, Table 1,* Fig. 2.3)

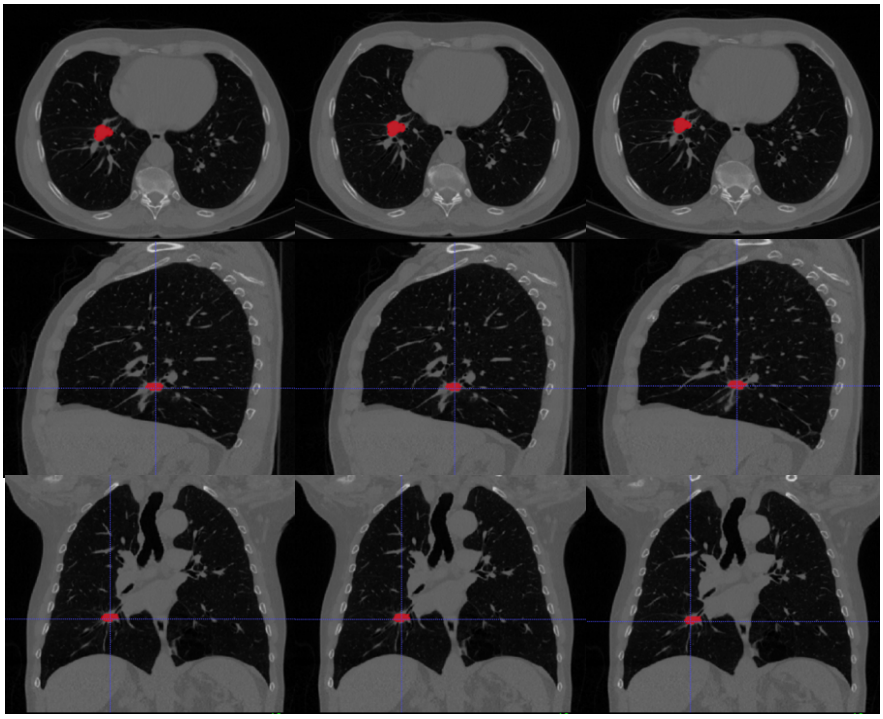

Fig. 2.3 Example of repeated tumour contouring on baseline CT scans for patient LTX0103.

5.2.6 In clinical practice, UK radiation oncologists typically use Eclipse for tumour contouring and radiotherapy planning. However, Eclipse supports only DICOM files and does not accept NIfTI formats. DICOM files are larger and slower to process, making the contouring of thousands of images in Eclipse impractical. To compare the contouring variability between ITK-SNAP and Eclipse, 10 patients were randomly selected for analysis on both platforms, with assistance from Catarina, who provided access to the Eclipse system. After checking the scans' ID, time point, and orientation, the same contouring procedures used in ITK-SNAP were replicated in Eclipse. Segmentations and corresponding files were saved separately on our server for traceability.

Compared to the mean tumour volumes contoured in ITK-SNAP, the tumour volumes measured in Eclipse varied from –47.76% to 22.14%. Overall, 93% of cases showed less than 10% variation. Smaller tumours showed greater discrepancies, likely due to the differences in contrast display and volume precision. Eclipse displays tumour volumes to one decimal place, whereas ITK-SNAP provides values to two decimal places, leading to more pronounced relative differences in smaller lesions. (*Appendix 1, Table 2,* Fig. 2.4)

**A:**

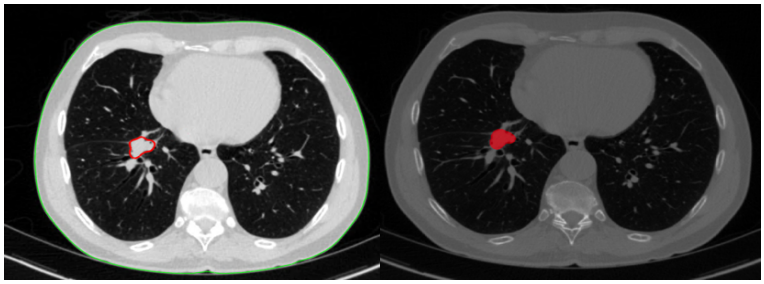

a b

**B:**

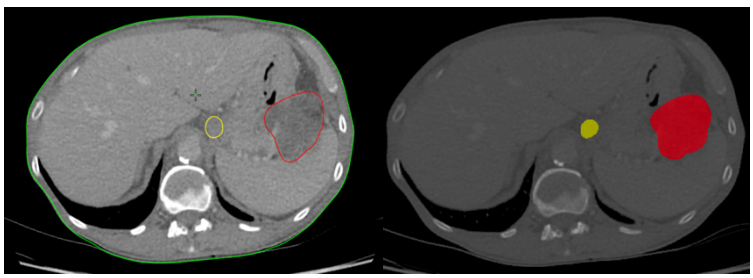

a b

**C:**

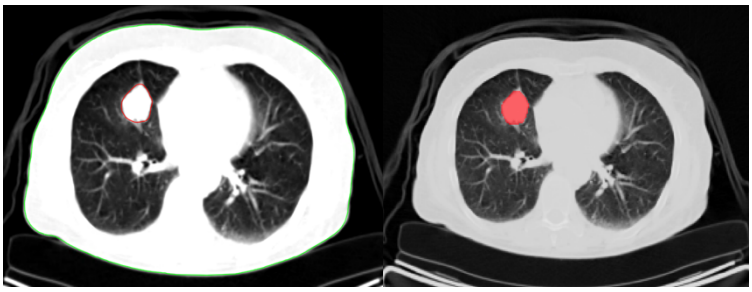

a b

**D:**

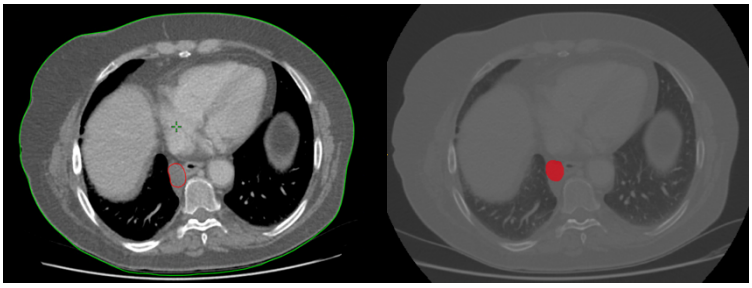

a b

Fig. 2.4 Example of tumour segmentation using Eclipse and ITK-SNAP for comparison. Tumour contours from four patients were manually segmented in both Eclipse (panels a) and ITK-SNAP (panels b) to evaluate consistency between clinical and research tools. A: patient LTX0103; B: LTX0474; C: LTX0582; D: LTX0817. Each pair shows the same tumour contoured in Eclipse (left) and ITK-SNAP (right).

5.2.7 Various algorithms have been developed for auto-segmenting and extracting 3D tumour volume, but none are currently capable of accurately contouring all lesion types across longitudinal scan series. Applying autopsy data to imaging using automated methods also remains challenging. In a previous TRACERx study [129], an algorithm was developed to automatically determine the primary tumour volumes for 163 patients. By accessing these data, I compared automated and manual contouring methods using the same patient set from both studies. Linear regression analysis of 64 patients revealed a strong correlation between the two methods ($r=0.97$, $P<0.0001$, Fig. 2.5), supporting the reliability of the manual volume measurements. However, due to variability in relapse patterns and the limited number of patients with comprehensive follow-up, automatic segmentation was less effective at mapping metastases, highlighting the importance of manual contouring in accurately capturing the

progression of metastatic disease across diverse sites and time points. Future research could enhance our understanding of tumour evolution by integrating lesion volumes with circulating tumour DNA (ctDNA), offering insights into primary tumour seeding dynamics.

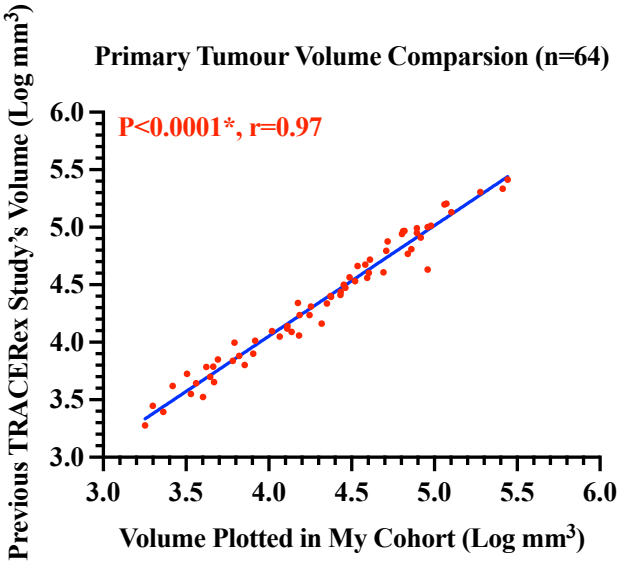


Fig. 2.5 Comparison of primary tumour volumes in 64 patients across two studies.

### 5.3 Contouring Procedures at Each Stage

The following contouring procedures were developed by me and applied consistently across all imaging stages. Detailed descriptions for each stage are provided below:

#### 5.3.1 Baseline Scans

At the baseline stage, I first reviewed the imaging reports provided by the hospital's senior radiologist to determine the location of the primary tumour. The tumour was then labelled according to its anatomical position within the lung. Following the initial contouring of the primary tumour, I identified and labelled any significant mediastinal lymph nodes.

- Lung labelling: 'Right Upper/Middle Lung', 'Right Lower Lung', 'Left Upper Lung', and 'Left Lower Lung'.
- Mediastinal Lymph Node labelling: 'Subcarinal Lymph Node', 'Right/Left Paratracheal Lymph Node', 'Right/Left Hilar Lymph Node', 'Pulmonary Artery Window Lymph Node', 'Suprascapular Lymph Node' and 'Oesophageal Lymph Node'.

Secondly, I extracted relevant imaging features from the radiology reports and verified each of them. These features included: lesion diameter, SUV value, clinical nodal (cN)

status, anatomical location, axial location, nodule attenuation, internal air bronchograms, necrosis, cavitation, nodule cysts, primary tumour margins, nodule shape, nodule calcification, primary tumour attachment to pleura, vessel, or bronchus, pleural retraction, nodule periphery, background ground-glass opacity, satellite nodules, background emphysema, bronchial wall thickening, bronchiectasis, tree-in-bud pattern, and atelectasis. All these imaging factors were systematically recorded.

Baseline CT scans typically include both the diagnostic CT scans and staging PET/CT scans. Tumours were initially contoured on the diagnostic CT scan and subsequently on the CT component of the staging PET/CT scan. The date of diagnosis was defined as the PET/CT scan date if available; otherwise, the diagnostic CT scan date was used.

- Baseline imaging interval = (Date of PET/CT) – (Date of CT).
- Surgery interval = (Surgery date) – (Date of PET/CT). If there was no PET/CT scan, then the surgery interval = (Surgery date) – (Date of CT).

In cases of pulmonary atelectasis, CT contrast window levels were adjusted in ITK-SNAP to improve the visual distinction between tumour and collapsed lung tissue. Any difficulties in defining lesion boundaries were documented.

Malignant lymph nodes were defined as those measuring greater than 15 mm in short-axis diameter and demonstrating high FDG uptake on PET imaging.

Satellite lesions were assessed relative to the primary tumour and labelled accordingly. Distinct labels were used to differentiate between potential synchronous primary tumours and true satellite lesions. Lesions were categorised based on their anatomical location as follows: within the same lobe as the primary tumour, within non-tumour lobes of the same lung, or within the contralateral lung. Satellite lesions adjacent to the primary tumour were initially contoured using the same label. However, if pathology confirmed a satellite lesion as a synchronous primary tumour, it was contoured separately with a distinct label.

Non-measurable lesions were also recorded and monitored using the categories ‘present’, ‘absent’, or ‘unequivocal progression’. Non-measurable lesions included tiny lesions (longest diameter less than 10mm) and other non-measurable lesions (leptomeningeal

disease, lymphangitic involvement of the lung, diffuse pleural or pericardial effusion, and hydrothorax).

### 5.3.2 Follow-up Scans Before Recurrence

For follow-up scans conducted before confirmed recurrence, I first reviewed lesions flagged in CT reports by expert radiologists, followed by the assessment of other equivocal lesions. Suspected malignant lesions were identified based on features consistent with RECIST and NCCN guidelines [132,133], including:

- Appearance of new lesions on imaging.
- Lesions present on previous scans but increasing in size on successive scans.
- Lesions that shrank following adjuvant therapy.
- Nodules with a diameter greater than 8 mm.
- Nodules with sharp, spiculated, lobulated, or irregular margins.
- Nodules with solid, semi-solid, necrotic, or cavitated density.
- Nodules located in the peripheral lung.
- Nodules reappearing near the resection margin rather than along a fissure.
- Nodules with irregular calcification.
- Enlargement of mediastinal lymph nodes.
- Evidence of vascular convergence around the nodules.
- Nodules adjacent to the broncho-vascular bundle.
- Tiny ground-glass opacities and interstitial changes are typically associated with inflammation rather than malignant progression.

I sequentially compared the size changes in equivocal lesions across successive follow-up scans, marking those that demonstrated persistent growth or morphological alteration after adjuvant therapy as notably suspicious. Simultaneously, I reviewed recurrence scans to identify relapsed malignant lesions and traced their presence and evolution retrospectively through post-surgical follow-up scans. Lesions that newly appeared or changed in size following therapy were also marked with high suspicion. The resolution of inflammatory findings, either spontaneously or following anti-inflammatory treatment, was taken into account to refine the classification of lesions. An expert radiation oncologist was consulted when necessary to validate suspicious lesions, ensuring the accuracy and reliability of lesion identification and analysis.

### 5.3.3 Recurrence

All patients underwent surgical resection with no apparent residual tumour remaining post-operatively. Recurrence was defined based on radiological or histological evidence of tumour reappearance, as recorded in follow-up scans or biopsy reports. For measurable lesions, the longest diameter was recorded, as confirmed by CT and supported by the maximum standardised uptake value (SUVmax) from PET/CT reports. Multiple non-target lesions within the same organ were documented as well.

Each lesion was contoured and labelled consistently across all imaging time points and categorised by organ of origin. Categories included: Lung, Intrathoracic Lymph Node, Extrathoracic Lymph Node, Intrathoracic Soft Tissue, Extrathoracic Soft Tissue, Intrathoracic Pleura, Extrathoracic Pleura, Liver, Spleen, Adrenal, Kidney, Pancreas, Bone, Brain, etc. Lesion names followed a predefined naming convention: 'Anatomy Location' ± 'Axial Location' + 'Organ', with additional description of the lesion's relationship to surrounding structures where applicable. For example: 'Right Upper Lobe Adjacent to Bronchus', 'Liver Segment VII', and 'Right third rib Pleura Invading Chest Wall'. The volume of each lesion, whole organ, and total tumour was recorded.

For metastatic lesions, when more than five were present within a single organ, they were grouped under a unified label and colour-coded accordingly. For example, six metastases in the right lung were contoured using the same colour and labelled as 'Right Lung Metastases', with their total tumour volume summed and recorded. Similarly, if more than five metastases were present in both the right and left lungs, they were colour-coded identically and labelled as 'Bilateral Lung Metastases', with the combined volume calculated. Mediastinal lymph nodes measuring greater than 15mm and abdominal lymph nodes larger than 10mm were considered positive. However, lymph node involvement confirmed by autopsy was considered positive regardless of size. Relapse sites were categorised as intrathoracic, extrathoracic, or both, depending on the anatomical distribution of recurrent disease.

Different techniques were used for various types of metastases:

- Brain metastases: MRI was the preferred modality for brain relapse, as it offered superior sensitivity. Contrast-enhanced T1-weighted MRI sequences were particularly effective in visualising tumour boundaries, as metastatic lesions typically exhibit contrast enhancement. T2-weighted MRI sequences, with or

without diffusion-weighted imaging (DWI), were used to distinguish surrounding oedema or swelling from the actual tumour mass, aiding in more accurate boundary delineation [134,135,136]. PET/CT was less effective in detecting brain metastases due to the high physiological glucose metabolism of normal brain tissue. FDG uptake was commonly observed in healthy brain tissue, making it challenging to distinguish metastatic lesions from background activity on 18F-FDG PET/CT scans. Therefore, contouring was performed primarily on contrast-enhanced T1-weighted MRI, while T2 and DWI sequences were used to refine lesion boundaries by identifying and excluding areas of oedema from the segmentation.

- Liver metastases: Identification can be prompted by a combination of portal venous phase CT images, typically acquired approximately 60–70 seconds after contrast injection, as well as T2-weighted, diffusion-weighted, and post-contrast sequences in MRI [137].

- Bone metastases: Sagittal images were used to identify vertebral levels, as they allowed easier top-to-bottom counting. Once identified, bone metastases were contoured on axial sections. Final 3D reconstructions were verified across all planes. Multiple vertebral lesions were labelled as 'Vertebral Bone Metastases'. Lesions too small to define were marked separately in the documentation.

### 5.3.4 Progression

Tumours may present a variety of responses to treatment. The World Health Organisation (WHO) first established criteria to evaluate tumour response in 1981 [86]. Various research groups have since adapted these criteria for specific clinical needs, leading to a diversity of assessment standards [87]. In response to the need for uniformity, the Response Evaluation Criteria in Solid Tumours (RECIST) criteria were published in 2000, offering a validated and practical guideline for predicting survival over a decade [88]**.** The emergence of new challenges, such as assessing total lesion numbers and evaluating lymph nodes, as well as integrating advanced imaging technologies like PET-CT [77], led to the release of an updated RECIST 1.1 in 2009 [89].

There are various response evaluation systems, including the RANO (Response Assessment Neuro-Oncology) criteria for glioblastomas, the International Working Group (Cheson) Criteria for lymphoma, the Revised Choi criteria for metastatic renal cell carcinoma treated with sunitinib, and the Immune-related Response Evaluation Criteria in Solid Tumours (irRECIST) for immunotherapy assessment [91]. Consequently, I used the RECIST 1.1 criteria [132] to evaluate NSCLC progression. (Details of the three criteria are provided in Table 2.1)

Table 2.1 Comparison of tumour response assessment criteria: WHO, RECIST 1.0, and RECIST 1.1.

| **Tumour response** | | **WHO criteria** [86] | **RECIST 1.0** [77,89] | **RECIST 1.1**[77,89] |
|---|---|---|---|---|
| 1. Complete Response (CR) | | Disappearance of all known disease | Disappearance of all target lesions (up to 5 per organ and up to 10 in total) | Disappearance of all target lesions (up to 2 per organ and up to 5 in total). Lymph nodes must shrink to <10mm in short-axis diameter |
| | *Illustration of lymph nodes assessment* | – | – | Short-axis measurements should be used: ≥15mm, target lesions; ≥10mm but <15 mm, non-target-lesions; <10mm, non-pathological |
| 2. Partial Response (PR) | *2.1 Bidimensional* | Single lesion shows ≥50% decrease in | | |

| | | | | |
|---|---|---|---|---|
| | | tumour area (longest diameter multiplied by the greatest perpendicular diameter) | | |
| | *2.2 Unidimensional* | ≥50% decrease in linear measurement | ≥30% decrease in the sum of the longest diameter of target lesions | ≥30% decrease in the sum of the longest diameter of target lesions |
| 3. No Change (NC) | | Total tumour size does not increase ≥25% or decrease ≥50% | | |
| 4. Stable Disease (SD) | | | Target lesions do not increase ≥20% or decrease ≥30% | Target lesions do not increase ≥20% or decrease ≥30% |
| 5. Progressive Disease (PD) | | ≥25% increase in one or more measurable lesions or appearance of new lesions | ≥20% increase in the sum of target lesions or appearance of new lesions | ≥20% increase in the sum of target lesions and an absolute increase of at least 5mm required, or the appearance of new lesions |

**Special notes for new lesions:**

- Missed lesions in previous scans: If a lesion is identified but was not scanned during previous follow-up imaging, its progression should be recorded based on the date of the confirmed imaging.
- Undetected lesions in earlier scans: If a lesion was not evident in earlier scans due to low FDG uptake or small size but is later confirmed as malignant with a positive FDG-PET scan after several treatments or scans, progression should be recorded on the confirmed imaging date. The lesion's corresponding volumes from previous scans should also be noted for analysis of growth rates.

**Special notes for evaluating the response of target lesions:**

- Diameter Comparison: To ensure accurate assessment of treatment response, tumour diameters should be measured and compared on the same CT scan slice before and after treatment. This consistency allows reliable tracking of size changes.
- Non-Nodular Lesions: For non-nodular lesions, sum the longest diameters of each lesion to determine the total size. If these lesions merge into a single mass post-treatment, measure the longest diameter of the combined lesion and compare it with the initial total. If a nodular lesion splits into multiple non-nodular lesions after treatment, sum the new longest diameters and compare them with the pre-treatment nodular lesion’s longest diameter for response assessment.

Furthermore, in the PEACE study, autopsies may reveal lesions that were not identified in the final scans. This discrepancy could be due to the rapid disease progression after the last scan, or lesions that were present but unreported or unconfirmed by radiologists at that time. In such cases, I would compare autopsy findings with the most recent available scans, dedicating over an hour per patient to thoroughly review and map each lesion’s presence and evolution, tracing it back to its initial appearance in earlier scans and documenting its volume.

Assessing disease progression in patients with both target and non-target lesions presents challenges, particularly when non-target lesions continue to grow while target lesions remain stable or show partial response to treatment. Therefore, it’s essential to record

target and non-target lesions distinctly to accurately measure disease dynamics and the impact of treatment. (Table 2.2).

Table 2.2 Response Evaluation Criteria 1.1

| Target lesions | Non-target lesions | New lesions | Overall response |
|---|---|---|---|
| CR | –/CR | No | CR |
| – | CR | No | CR |
| CR | Non-CR/non-PD | No | PR |
| CR | Not evaluated | No | PR |
| PR | Non-PD or not all evaluated | No | PR |
| SD | Non-PD or not all evaluated | No | SD |
| PD | Any | Yes/No | PD |
| Any | PD | Yes/No | PD |
| Any | Any | Yes | PD |
| – | Any | Yes | PD |

There is no universal standard for evaluating tumour progression based on volume. Research has shown that for spherical tumours, a 20% increase in diameter corresponds to a 72.8% increase in volume, while a 30% reduction in diameter results in a 65.7% decrease in volume [90]. Given the irregular shapes of most tumours, traditional diameter-based criteria may be inadequate. This cohort used Volume-RECIST criteria to define the complete response (CR) as total lesion disappearance; partial response (PR) as at least a 30% reduction in total tumour volume compared with the previous scan; and progressive disease (PD) as a more than 20% increase in total tumour volume or the appearance of new lesions, including non-target lesions. These assessments were supported by my manual contouring variability, which was predominantly less than 20%. This approach enabled earlier detection of progression compared to standard RECIST. For example, as shown in Figure 2.6, a treatment response classified as stable under RECIST was identified as progressive disease under Volume-RECIST. Among 130 relapsed patients, 21 were identified as experiencing progression earlier when using Volume-RECIST criteria. Such earlier detection may be instrumental in clinical decision-making, enabling

patients to benefit from timely interventions based on the identification of early disease progression.

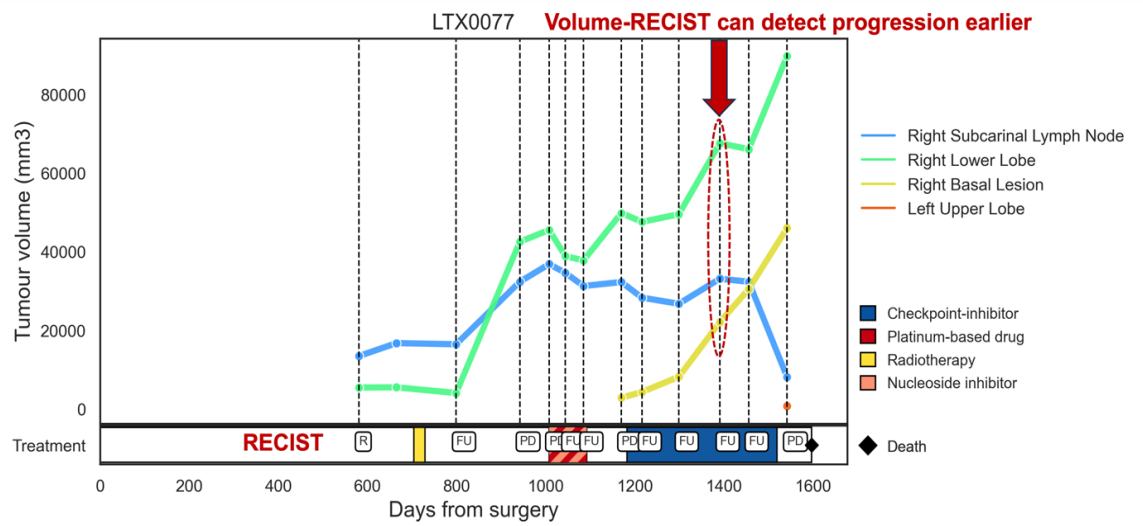


Fig. 2.6 Comparison between Volume-RECIST and standard RECIST Criteria for tumour progression detection.

### 5.4 Validation of Tumour Volume Estimates

To assess the reliability of tumour volume measurements in this study, diameter-based volume estimates were compared with volumes obtained through manual contouring. The diameter-based method applied the standard formula for the volume of a sphere, $\frac{4}{3}\pi r^3$, where r is the tumour radius. This approach, commonly used in previous studies [90], assumes a spherical shape and enables a straightforward comparison with manually segmented volumes. However, this spherical tumour assumption often does not reflect real-world clinical imaging, where tumour morphology is typically irregular. Therefore, this comparison aimed to validate the accuracy of volume estimates and to explore the differences between the two methods.

Given that volume can be estimated either geometrically (via diameter-based calculation) or anatomically (via manual contouring), it is essential to assess the consistency between these two methods. A scatter plot was generated to visualise the correlation between the two volume estimates (Fig. 2.7). A strong positive correlation was observed (Spearman's $r=0.9$, $P<0.0001$), indicating general consistency between the methods. However, correlation alone does not imply agreement. I did further analysis within tumour size

subgroups to better observe these differences. Among 199 eligible patients, diameter-based volume estimates were compared with manually contoured tumour volumes. A significant overall difference was observed (Fig. 2.8A). For subgroups with normally distributed data, a t-test was applied; otherwise, the Mann–Whitney U test was used (Fig. 2.8F). This analysis aimed to determine whether specific tumour size ranges show significant discrepancies, which may affect clinical interpretation. To ensure clinical relevance, subgroup cutoffs at 3 cm, 5 cm, and 7 cm were chosen based on the tumour size thresholds used in the TNM T-staging system. Volume discrepancy between the two methods was particularly significant in larger tumours (diameter>3 cm), likely because larger tumours more often exhibit complex and irregular shapes in clinical reality (Fig. 2.8C–E). To explore the clinical significance of these discrepancies on a case-by-case basis, a 20% threshold was chosen to define meaningful differences between the two volume estimation methods, reflecting the clinical relevance outlined in the RECIST criteria.

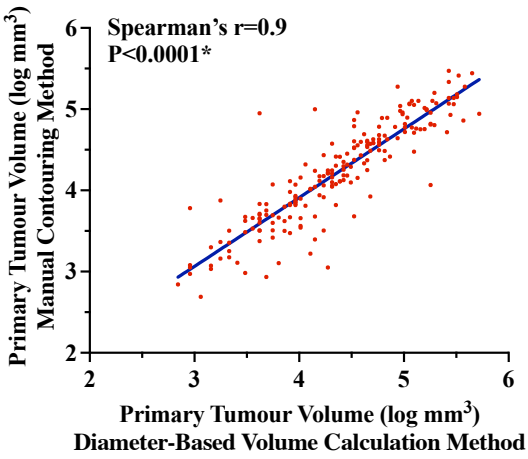


Fig. 2.7 Correlation between diameter-based and manually contoured tumour volumes.

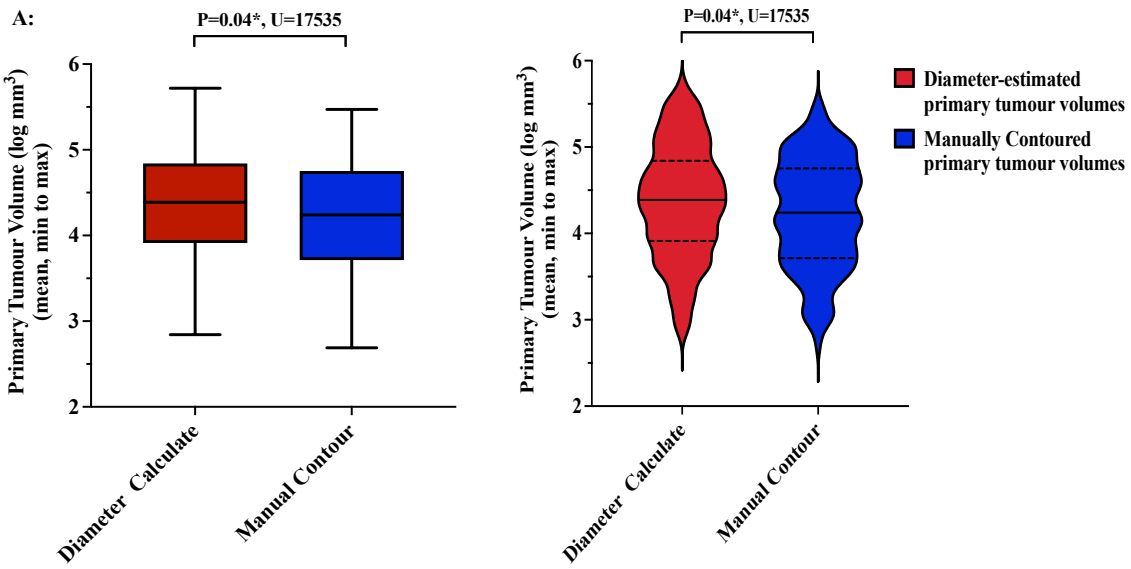
A:
P=0.04*, U=17535
Primary Tumour Volume (log mm3) (mean, min to max)
6
5
4
3
2
Diameter Calculate
Manual Contour
P=0.04*, U=17535
Primary Tumour Volume (log mm3) (mean, min to max)
Diameter Calculate
Manual Contour
Diameter-estimated primary tumour volumes
Manually Contoured primary tumour volumes

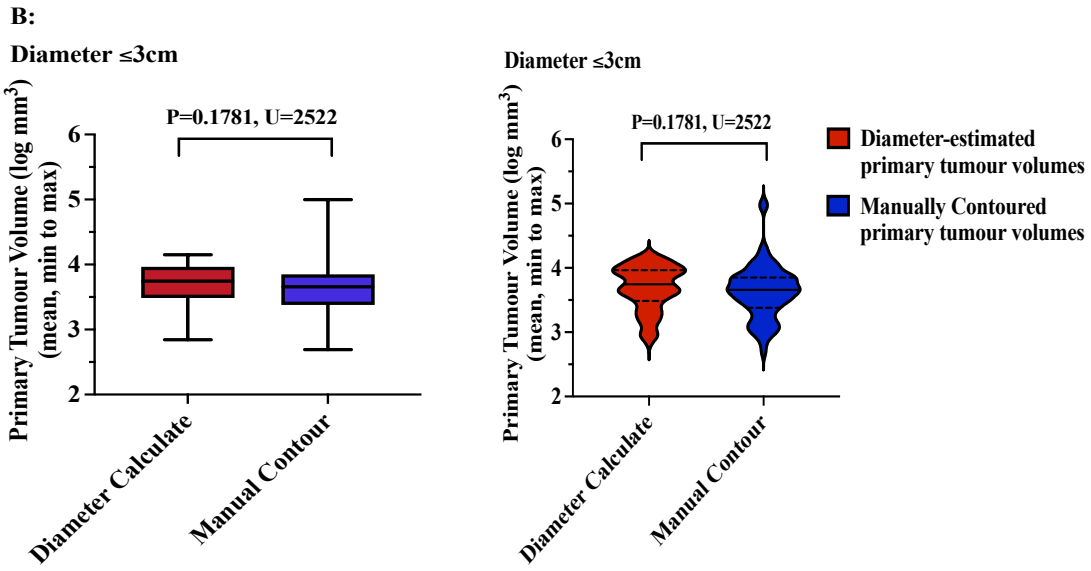
B:
Diameter ≤3cm
P=0.1781, U=2522
Primary Tumour Volume (log mm3) (mean, min to max)
6
5
4
3
2
Diameter Calculate
Manual Contour
Diameter ≤3cm
P=0.1781, U=2522
Primary Tumour Volume (log mm3) (mean, min to max)
Diameter Calculate
Manual Contour
Diameter-estimated primary tumour volumes
Manually Contoured primary tumour volumes

C:

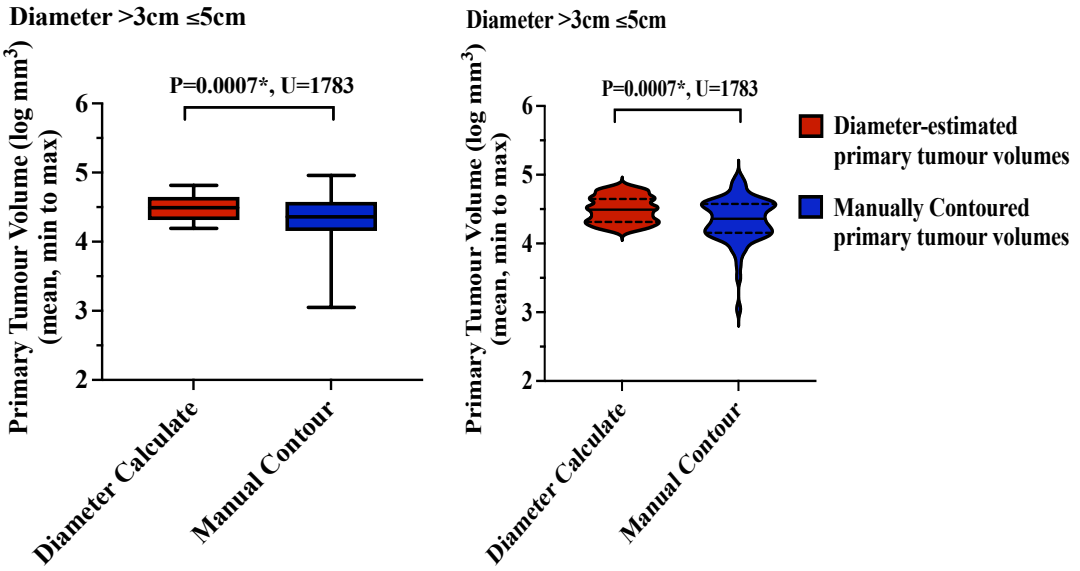
Diameter >3cm ≤5cm
P=0.0007*, U=1783
Primary Tumour Volume (log mm3) (mean, min to max)
6
5
4
3
2
Diameter Calculate
Manual Contour
Diameter >3cm ≤5cm
P=0.0007*, U=1783
Primary Tumour Volume (log mm3) (mean, min to max)
Diameter Calculate
Manual Contour
Diameter-estimated primary tumour volumes
Manually Contoured primary tumour volumes

D:

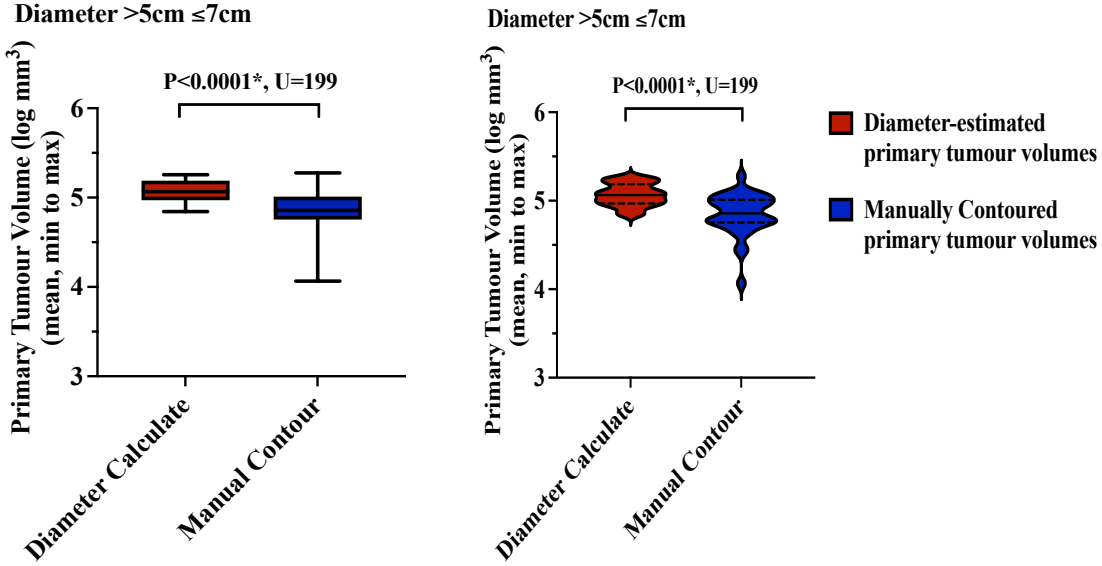
Diameter >5cm ≤7cm
P<0.0001*, U=199
Primary Tumour Volume (log mm3) (mean, min to max)
6
5
4
3
Diameter Calculate
Manual Contour
Diameter >5cm ≤7cm
P<0.0001*, U=199
Primary Tumour Volume (log mm3) (mean, min to max)
Diameter Calculate
Manual Contour
Diameter-estimated primary tumour volumes
Manually Contoured primary tumour volumes

E:

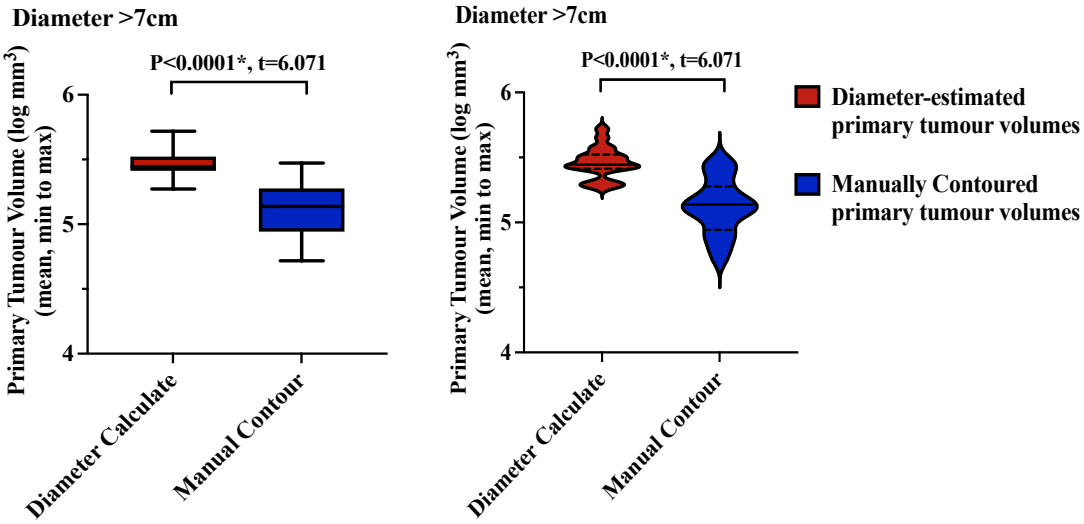
Diameter >7cm
P<0.0001*, t=6.071
Primary Tumour Volume (log mm3) (mean, min to max)
6
5
4
Diameter Calculate
Manual Contour
Diameter >7cm
P<0.0001*, t=6.071
Primary Tumour Volume (log mm3) (mean, min to max)
Diameter Calculate
Manual Contour
Diameter-estimated primary tumour volumes
Manually Contoured primary tumour volumes

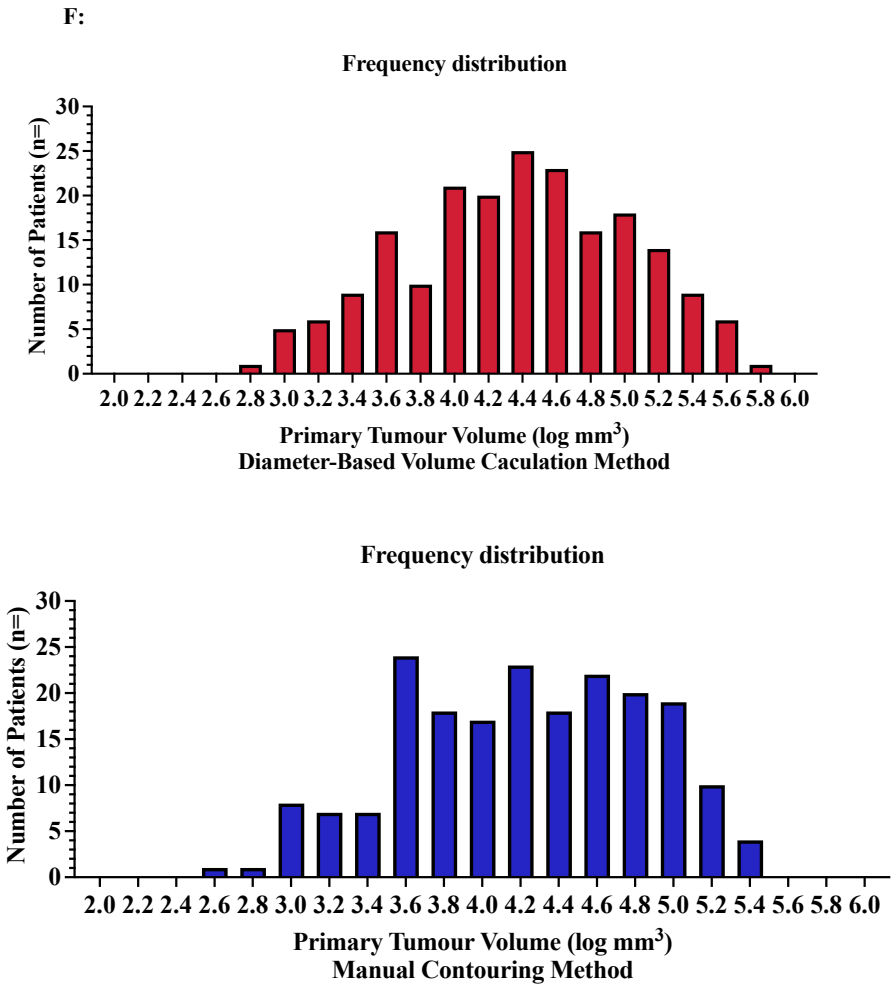


Fig. 2.8 Comparison of primary tumour volume (log-transformed) using diameter-based calculation and manual contour method. A: Overview of the whole cohort volumes between two calculation methods in box plots and violin plots; B: Comparison of lesion volumes between two calculation methods using box and violin plots (lesions ≤3 cm diameter); C: Comparison of lesion volumes between two calculation methods using box and violin plots (3<lesions diameter ≤5cm); D: Comparison of lesion volumes between two calculation methods using box and violin plots (5<lesions diameter ≤7cm); E: Comparison of lesion volumes between two calculation methods using box and violin plots (diameter>7cm); F: Frequency distribution of primary tumour volume based on two calculation methods. The diameter-based tumour volume calculation shows an approximately normal distribution, whereas manually contoured primary tumour volumes demonstrates a non-normal distribution.

In RECIST, a ≥20% increase in diameters is used to define progressive disease (PD), indicating a clinically significant change in tumour burden. Using this threshold for volume differences ensures alignment with widely accepted clinical decision-making criteria and highlights instances where measurement methods may impact clinical interpretation. The diameter-based calculation method overestimated tumour volume by more than 20% in 110 out of 199 patients, compared to manual contouring (Fig. 2.9A). In contrast, the manual contouring method overestimated tumour volume by more than 20% in 28 out of 199 patients (Fig. 2.9B). The remaining 61 patients had similar tumour volumes, as determined by both the diameter-based calculation and the manual contouring method (Fig. 2.9C). These results demonstrate that simple diameter-based calculations are insufficient for accurately measuring tumour volume due to the prevalence of irregular tumour shapes in clinical practice. Such oversimplified estimates may mislead clinical decision-making. In contrast, manual contouring provides a more precise and individualised assessment of tumour volume, especially for complex or non-spherical lesions.

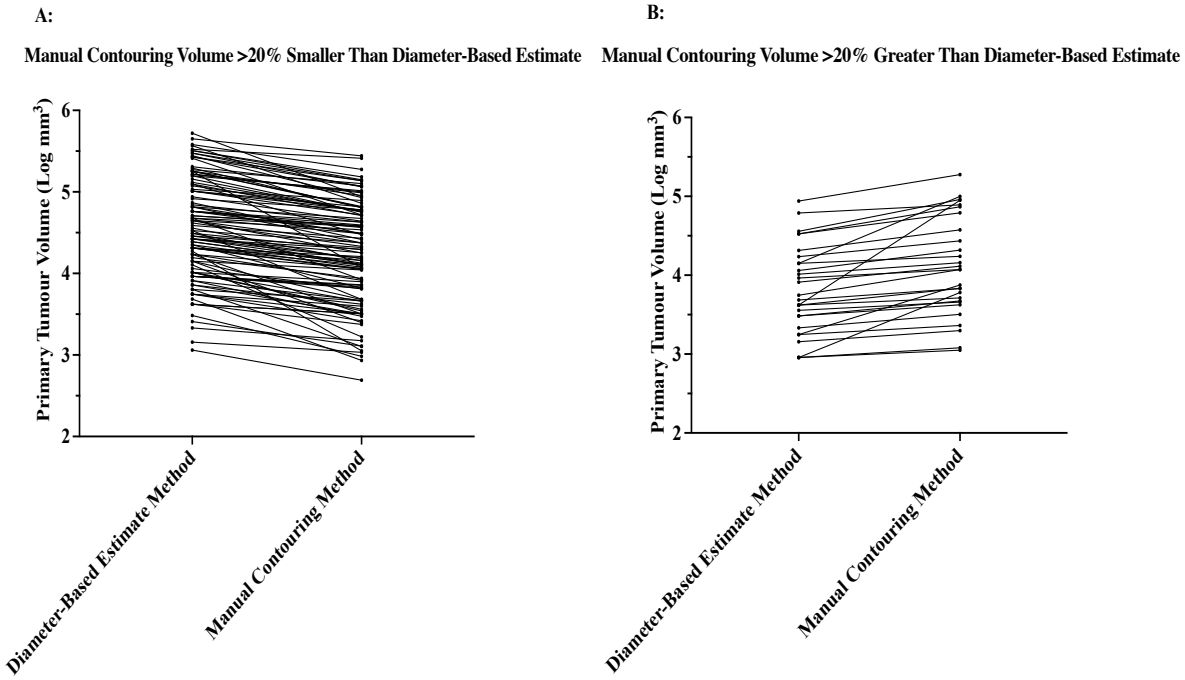

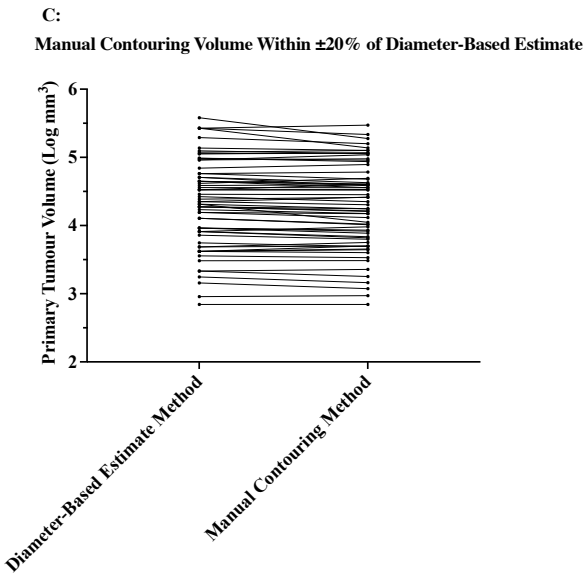


Fig. 2.9 Comparison of manual contouring and diameter-based tumour volume calculations across three agreement subgroups.

## 6 Completed Contouring of Imaging Scans: Information and Overview of Workload

The Cancer Institute followed 822 patients across 5075 scans until September 2023. Among the 306 patients who experienced recurrence, 170 had longitudinal imaging available. Additionally, 78 non-relapsed patients had more than 3 follow-up scans and at least three years of post-surgical surveillance (Fig. 2.10A–B).

Patients diagnosed with stage I–III NSCLC (eighth edition TNM staging) between October 21, 2013, and November 25, 2020, and who underwent complete surgical resection were included. This time frame was chosen because consistent clinical data collection began in 2013. All included patients had at least three scans during this period, comprising baseline imaging at diagnosis, recurrence scans, and follow-up scans.

**Scan Information:** A total of 2,440 scans from 208 patients (130 with relapse and 78 without relapse) were reviewed and segmented, including 408 PET/CT scans, 210 MRI scans, and 1,822 CT scans. This process required over 13,000 hours of work. A total of 425 baseline scans, 768 pre-relapse scans, 231 relapse scans, and 1,016 post-relapse scans were included (Fig. 2.10C). The median number of scans per patient was 10 (Interquartile Range [IQR], 7–14). For PET/CT, the median X-axis/Y-axis resolution and slice

thickness were 0.9766 mm and 3 mm, respectively. For CT, the median resolution and slice thickness were 0.7617 mm and 1 mm, respectively; for MRI, these values were 0.5134 mm and 5 mm, respectively. The distribution of segmented metastases is shown in Fig. 2.10D. After reviewing the clinical characteristics, 200 patients were ultimately recruited into the final cohort.

**A:**

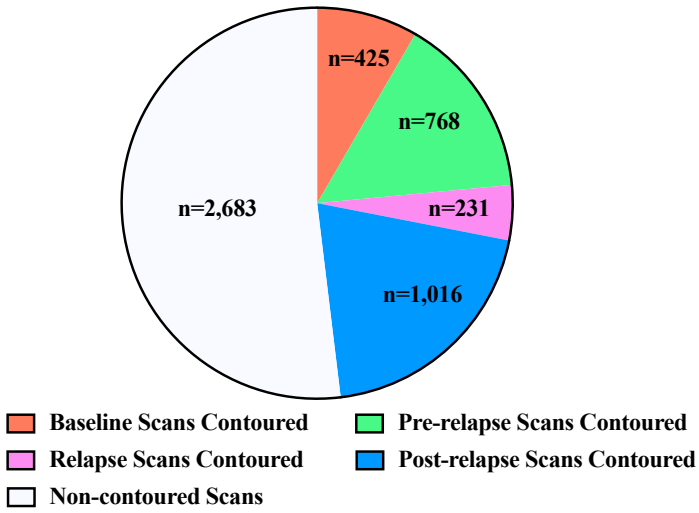


**Of 5,075 total scans, 2,440 scans were contoured (48% completion rate)**

**B:**

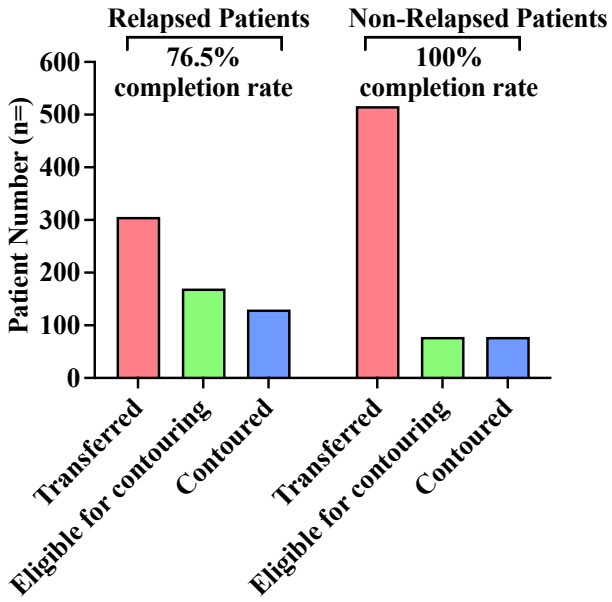


**Of 248 total eligible patients, 208 patients were contoured (84% completion rate)**

**C:**

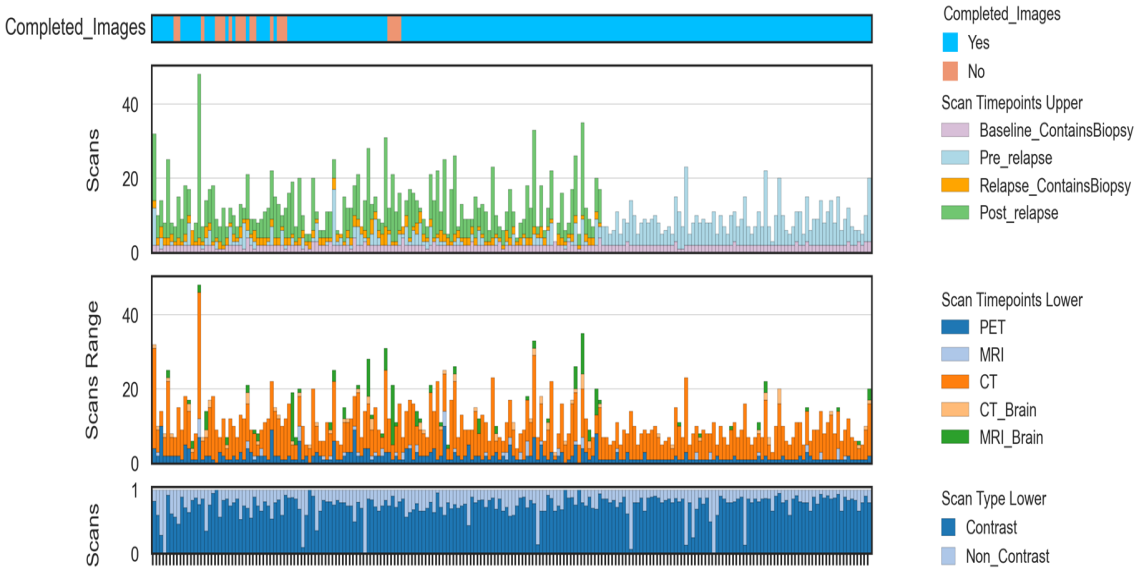


**D:**

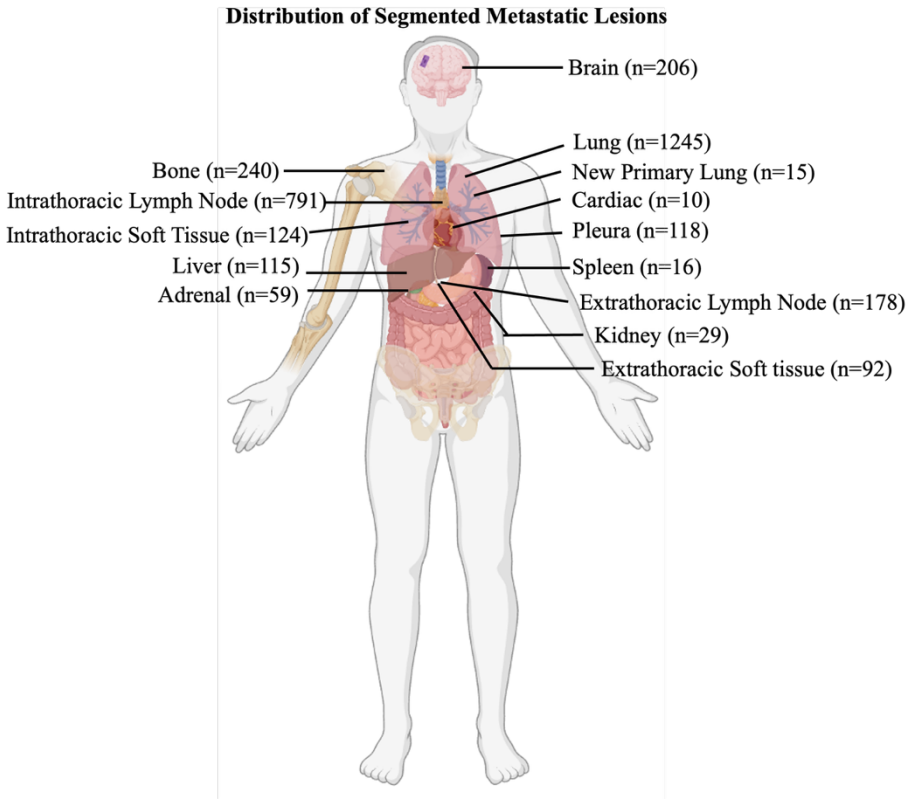


Fig. 2.10 Overview of scan inclusion and contouring in the study cohort. A: Total number of scans in the complete transferred TRACERx imaging dataset and the subset selected for contouring at each clinical time point (diagnosis, follow-up, relapse, etc.); B: Number of scans meeting contouring criteria and completion status; C: Summary of contoured

scans per patient among those selected for detailed segmentation; D: Distribution of segmented metastatic lesions in relapsed patients, showing lesion counts per organ.

**Labour-intensive workload:** The process of contouring tumours across 2,440 scans by myself was highly time-consuming, particularly due to the phased transmission of images. Each patient's images, covering stages like baseline, relapse, and progression, were sent in separate batches, often containing both previously transmitted and newly acquired scans from different time points. This discontinuity required manual verification of each new image set against the previous ones to ensure consistency. Any inconsistencies were reported to the Cancer Institute for tracing and confirmation. Additionally, I had to align autopsy and biopsy results with visible lesions on the scans, many of which were not documented in the imaging reports. As a result, each scan took me 1–3 hours to contour, followed by 2–3 hours for manual checking and review. Once all images were contoured, I spent an additional 1–2 hours per image reviewing the entire sequence from the first to the last scan before death. This final review involved organising the data, including imaging types, contrast details, scan axis information (X/Y/Z), lesion names, locations, label colours, times, and tumour volumes. In total, I spent more than **13000** hours establishing the whole imaging dataset.

## 7 Methods for Calculating the Tumour Growth Rate

### 7.1 Attempt to Fit of Gompertz Curves for Tumour Growth Modelling

Several methods for calculating tumour growth rates include Ordinary Differential Equations (ODEs), ranging from simple exponential models to more advanced approaches such as the Gompertz model; however, these assumptions may not apply universally. Partial Differential Equations (PDEs) provide more detailed spatial analysis but are computationally demanding. Stochastic models account for tumour variability through randomness but require large datasets. Deep learning models provide detailed insights, but their complexity, data volume demands, and high computational requirements limit their interpretability and practicality in real-world applications [105,113,138,139].

To explore a convenient and biologically informed method for estimating tumour growth rates in this cohort, the Gompertz model was initially selected. This model is widely used in tumour dynamics as it captures key features of tumour growth, including an initially

exponential phase that slows over time as the tumour approaches a carrying capacity. It particularly works well under stable conditions. However, fitting failed in a large proportion of patients, and notable heterogeneity was observed in the growth patterns of individual lesions within the example patient (Fig. 2.11). The model often produced biologically unrealistic growth curves. For example, several curves predicted early plateauing or even regression despite radiological evidence of progression. Others overestimated tumour burden at later time points or generated unrealistic exponential growth well beyond the observed data range. These fitting failures appeared more significant in lesions with fewer than three time points, long intervals or inconsistent timing between scans, post-treatment tumour shrinkage or pseudo-responses, slow-growing behaviour with limited volumetric change, and irregular, immune-influenced growth patterns. Even when curve fitting was mathematically successful, parameter estimates (e.g., time to plateau or maximum volume) varied widely and lacked robustness, often influenced by outliers or sparse time points. Additionally, the model's starting point did not accurately reflect the actual biological onset of the tumour growth, introducing inter-patient heterogeneity. These limitations illustrate that while the Gompertz model captures general tumour growth principles, it was ultimately unsuitable for this dataset due to real-world variability in imaging frequency, lesion characteristics, treatment response, and follow-up duration.

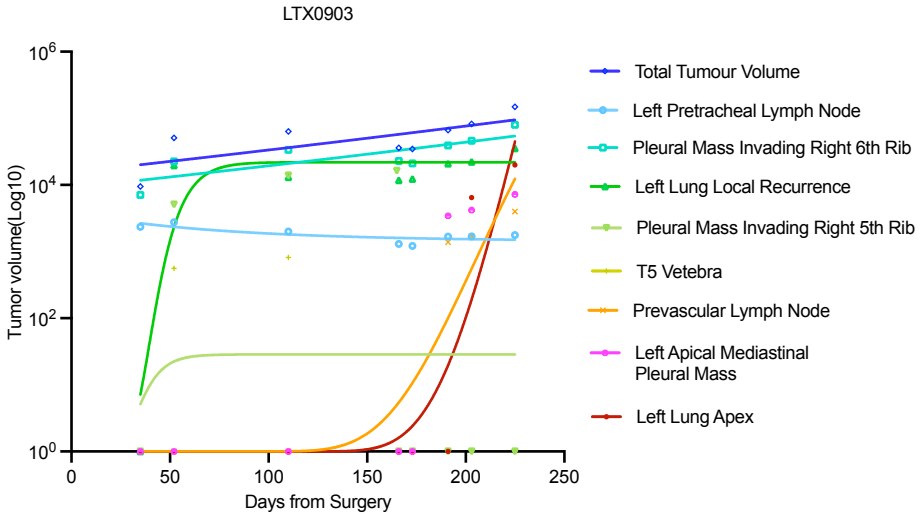


Fig. 2.11 Tumour volume changes over time fitted with the Gompertz model.

## 7.2 Verify Tumour Growth Patterns

Similar to findings from a 5-year lung cancer screening study [140], many tumours did not exhibit exponential growth patterns. These heterogeneities make the model unsuitable for universal application across all patients and even across different lesions within a single individual.

To verify tumour growth patterns, I contoured the malignant lesion on the confirmed relapse scan and traced it back on previous post-surgical follow-up scans. Tumour volumes at each time point were plotted, with days post-surgery on the x-axis and tumour volume ($mm^3$) on the y-axis. Growth patterns varied significantly among patients: some showed exponential growth, others linear, and some had slow initial growth followed by a sharp increase or vice versa (Some examples are listed in *Appendix 1, Fig. 1)*. This variability, combined with imbalanced scan frequencies, heterogeneous growth patterns both within and across patients, and a small cohort size, highlights the limitations of the Gompertz model and underscores the need for more advanced methods, such as deep learning algorithms and larger cohorts, to improve prediction accuracy.

The most straightforward approach was to use a line plot to connect tumour volumes at each scan point, particularly when scans occurred close to treatment, relapse, or progression events, as simplicity and reasonable accuracy were my priorities. The x-axis showed the time of successive scans, and the y-axis showed the logarithmic transformation of tumour volume. Lesions were plotted using distinct colours, while treatments during progression were noted at the bottom of the graph (using Jupyter Notebook 6.4.3). (Fig. 2.12)

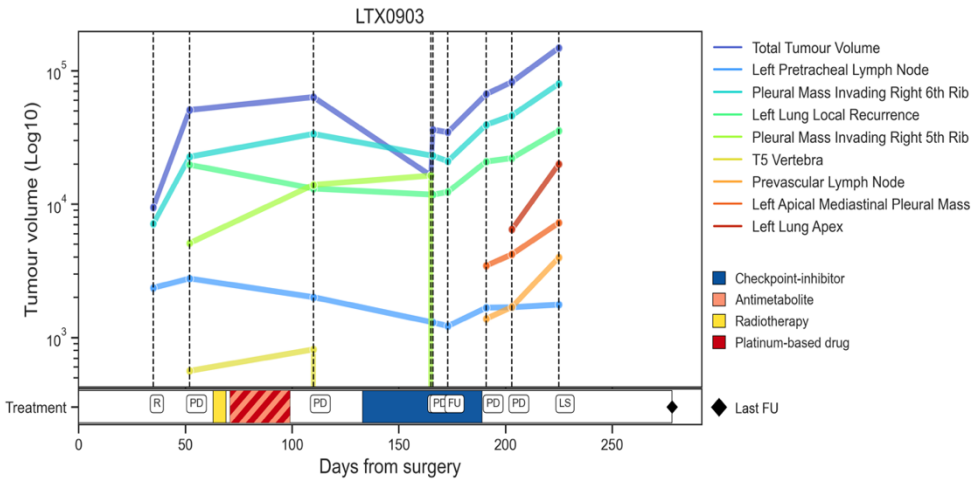


Fig. 2.12 Line plot showing tumour volume progression using linear interpolation between scans.

Scenarios for determining relapse speed:

- Confirmed relapse date: The confirmed relapse date recorded in the clinical dataset was used as the reference point (Date 2). The corresponding scan provided the relapse tumour volume (Volume 2). If another relapse-related scan had been performed shortly before this scan (typically, two scans are done within a short period, such as a CT followed by a PET/CT), the earlier scan was used to determine the initial relapse volume (Volume 1) for calculating relapse speed, as shown in the formula below.
- Post-surgery surveillance scans available: If only surveillance scans were available between surgery and the confirmed relapse scan (Volume 2), the most recent surveillance scan prior to relapse was used to obtain Volume 1, as shown in the formula below.
- No prior scans before confirmation: If no surveillance or earlier relapse-related scans were available prior to confirmation, the volume at surgery was assumed to be zero (Volume 1=0), as no residual tumour was present. The relapse speed was then calculated between the surgery date (Date 1) and the date of the relapse scan (Date 2) (Fig. 2.13).

**Formula:**

Tumour Growth Rate ($mm^3$/day) = (Volume 2 – Volume 1) / (Date 2 – Date 1)

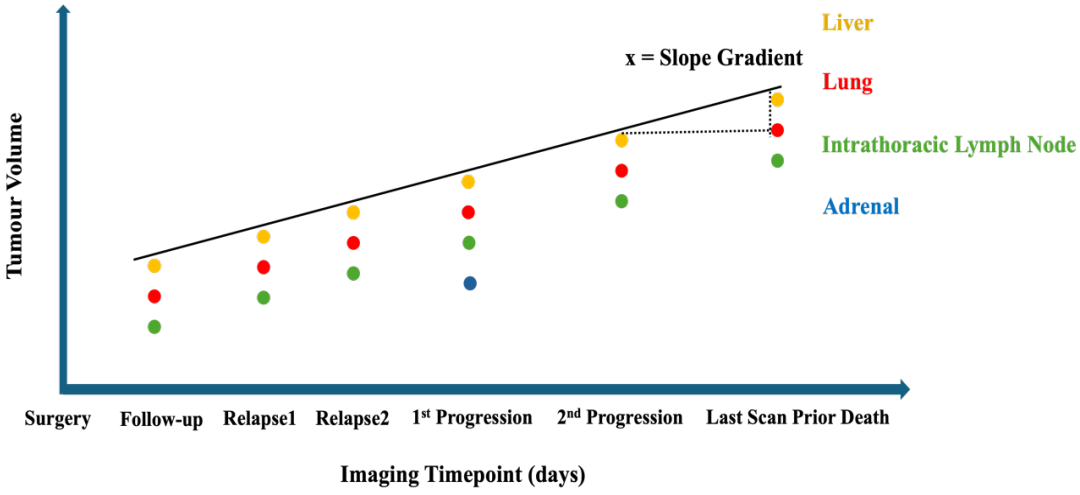


Fig. 2.13 Illustration of the method used to calculate tumour growth rate in this study based on segmented tumour volumes and the time interval between two relevant scans.

## 8 Disease-free survival, Progression-free survival (PFS), Post-surgery survival and Post-relapse survival (PRS)

Progression was assessed using the RECIST 1.1 criteria, which align with current clinical protocols for making treatment decisions. For analyses involving tumour volume, Volume-RECIST criteria were applied to monitor progression.

- Disease-free survival (DFS) was defined as the time from surgery to the confirmed relapse event. If no relapse occurred, the last follow-up date was used as the reference.
- Progression-free survival (PFS) was defined as the time from the start of post-relapse treatment to disease progression, death or last follow-up. For patients who did not receive therapy, PFS was calculated from the date of the corresponding scan to the date of progression, death, or last follow-up.
- Post-surgery survival was defined as the time from surgery to death or last follow-up.
- Post-relapse survival (PRS) was defined as the time from the first recurrence to death or last follow-up.

## 9 Definition of Oligometastatic and Polymetastatic Disease

Based on the literature review, oligometastatic disease is often defined as having up to five metastases and involving up to three organs.

## 10 Statistical Analysis

Descriptive and summary statistics were generated for patient demographics, tumour characteristics, and initial treatments, including the median, mean, quartiles, and percentages. The Kaplan–Meier method was used for the initial visualisation and comparison of survival curves, while Cox regression was applied to assess the impact of covariates on survival outcomes [141–144].

**10.1 Kaplan–Meier** was used to analyse and plot annual recurrence rates and survival probabilities [141–144]. Survival curves were generated by calculating the probability of remaining event-free (e.g., recurrence or death) at each observed event time. Initially, all patients were assumed to have a 100% survival probability. At each event time, the

survival probability was updated based on the proportion of patients who remained event-free. The method appropriately accounts for censored data, including patients lost to follow-up or those who did not experience an event during the study period. This method provides a clear visual comparison of survival trends. When combined with the log-rank test, it enables statistical comparison of survival distributions between groups. Despite its widespread use, Kaplan–Meier analysis has notable limitations. It only handles one categorical variable at a time and does not adjust for confounding variables, such as age, disease severity, or clinical management decisions. Clinical practices, such as more frequent surveillance for high-risk patients, can also introduce bias into survival estimates. Therefore, Kaplan–Meier curves are useful for initial exploratory analysis and must be interpreted carefully. To address these limitations, multivariate methods such as Cox regression should also be used to adjust for confounding factors and provide more robust insights.

**10.2 Cox regression** analysis was used for multivariable survival analysis to quantify the effects of multiple predictors on survival time [141–144]. In this study, univariable Cox regression models were first used to assess the associations between recurrence or death days and patient characteristics across groups. A stepwise method [144,145] was then applied in multivariable Cox regression, where variables with a univariable P-value of ≤0.2 were entered into a stepwise backwards selection algorithm to create a more efficient and interpretable final model [146]. Stepwise selection helps reduce the number of variables, improve model efficiency, and minimise overfitting. Despite its widespread use, the stepwise selection has notable limitations. It assumes a linear relationship between covariates and the log hazard, but the method can still result in overfitting, particularly in small datasets with many variables and few events. Moreover, stepwise selection relies solely on statistical significance for variable inclusion, which may exclude clinically or biologically meaningful predictors that are not statistically significant.

**10.3 Statistical Tests**: A range of statistical tests was used to ensure the appropriate analysis for different data types in this study. For normally distributed groups, the t-test (for two groups) and the ANOVA (for more than two groups) were used. For non-normally distributed data, non-parametric alternatives were used, such as the Wilcoxon Rank-Sum test (for two groups) and the Kruskal–Wallis test (for more than two groups). Categorical data were analysed using the Chi-squared or Fisher's exact tests (for small sample sizes). Pearson correlation and Spearman rank correlation were

used to assess linear and non-linear relationships, respectively, ensuring robust analysis across various scenarios [144].

**10.4 Pearson Correlation and Spearman Rank Correlation:** Correlation tests were used to measure the strength and direction of relationships between variables [144].

- **Pearson Correlation:** was used to measure the strength and direction of a linear relationship between two normally distributed continuous variables. Values range from –1 (perfect negative correlation) to +1 (perfect positive correlation), with 0 indicating no linear relationship. Point-biserial correlation is a special case of Pearson correlation, measuring the relationship between a binary variable and a continuous variable. The Phi coefficient measures the association between two binary variables.
- **Spearman Rank Correlation:** was used to measures the strength and direction of a monotonic relationship (not necessarily linear) between two non-normally distributed variables. It is based on ranked values rather than actual data points. Kendall's Tau is another non-parametric measure of monotonic association based on the number of concordant and discordant pairs in small sample sizes or tied ranks.
- Correlation strength was categorised as weak (r: 0–0.3), moderate (r: 0.3–0.6), or strong ($r > 0.6$).

**10.5 ROC (Receiver Operating Characteristic) Curve** was used to evaluate the performance of a binary classification model. It plots the true positive rate (sensitivity) against the false positive rate (1 – specificity) at various threshold settings. The ROC curve helps to assess how well a model distinguishes between two classes (e.g., recurrence vs. no recurrence). The ROC curve is often summarised by calculating the AUC (Area Under the Curve). The AUC quantifies the overall ability of the model to discriminate between positive and negative classes. The DeLong was used to statistically compare the AUC values of two or more correlated ROC curves [147,148].

**10.6 X-tiles Analysis** is a statistical tool developed at Yale University [149], commonly used in biomedical research to identify optimal cutoff points in continuous variables for survival analysis. It helps to stratify patients into groups (e.g., low, medium, and high risk) by finding thresholds that maximise the statistical differences between these groups.

**10.7 P-values** [150] represents the probability of observing the current result, assuming the null hypothesis (no difference or no association) is true. It does not measure the size or importance of an effect but indicates the level of statistical evidence against the null hypothesis. Statistical significance refers to the likelihood of a result occurring

due to chance. A P-value <0.05 indicates that the observed result is unlikely due to chance alone, supporting the rejection of the null hypothesis (statistical significance). A P-value ≥0.05 indicates insufficient evidence to reject the null hypothesis. Statistical significance does not necessarily equate to clinical relevance. Conversely, clinically meaningful effects might lack statistical significance due to limited sample sizes or variability. Therefore, interpretation of results should consider clinical context, study design, potential confounders, and existing evidence. A two-tailed P-value <0.05 was considered statistically significant in this thesis. Prism (Version 9.0.0), RStudio (Version 4.4.1, 2024-06-14), and Jupyter Notebook 6.4.3 were used to analyse and plot the figures.

### 10.8 Multiple test correction [151]:

Analysing multiple statistical tests simultaneously may increase the likelihood of false positive results (Type I errors), as each additional test introduces more opportunities for random findings to appear significant. To address this, multiple testing correction methods are applied to adjust P-values and reduce the risk of reporting false positive results. The Benjamini–Hochberg False Discovery Rate (FDR) correction method was primarily used in this study due to its balance between sensitivity and specificity. It works by ranking all P-values from smallest to largest and comparing each to a calculated threshold based on its rank. The largest P-value that passes this threshold, and all smaller ones, are considered significant. Adjusted P-values (Q-values) reflect statistical significance after correcting for multiple comparisons, balancing the need to detect actual effects while limiting the risk of false positives.

# Chapter Three

# Analysing Recurrence Rates and Using Clinical and Imaging Factors to Predict Disease-free Survival in Non-Small Cell Lung Cancer

## Highlights

**Aims:** Create the largest global imaging dataset to track tumour evolution from diagnosis to death by contouring individual malignant lesions and recording imaging factors. The goal is to better understand how recurrence rates vary across different subgroups of non-small cell lung cancer (NSCLC) patients, with particular emphasis on evaluating primary tumour volumes and growth rates as predictors of relapse.

**Methods:** See the Methodology chapter about how to contour the tumour volume and how to calculate the primary tumour growth speed. Kaplan–Meier analysis was used to analyse and plot annual recurrence rates, stratified by gender, age, histology, TNM stage, tumour volume, and adjuvant therapy conditions. Univariable and multivariate Cox regression models were applied to identify factors associated with tumour relapse, offering deeper insights into the variables most strongly linked to recurrence. Pearson correlation or Spearman rank correlation was used to detect the relationship between primary volume and growth rate. T-tests and ANOVA were used to compare the means of two, three, or more normally distributed groups separately. The Wilcoxon Rank-Sum Test (also known as the Mann–Whitney U Test) and the Kruskal–Wallis Test were used to compare the medians of two, three, or more independent groups when the data were not normally distributed. The Benjamini–Hochberg FDR method was used for multiple test correction. The ROC curve was used to find the best cutoff value.

**Results:**

- **Recurrence Timing and Tumour Characteristics:** Over a median follow-up of 1732 days, half of the NSCLC patients experienced relapse within the first two years post-surgery, with a slight increase in relapse rates observed thereafter.
- **Tumour Volume as a Prognostic Indicator:** Manually contoured primary tumour volume showed stronger association with relapse risk (HR=2.68, 95%CI 1.54–4.65), recurrence volumes, recurrence rates and extrathoracic relapses, compared to diameter-based volume calculation, pT staging, and pTNM staging.
- **Recurrence Patterns by Histology, Gender, and Smoking Status:** In this cohort, histology (LUAD vs. LUSC), gender and smoking status were not statistically associated with DFS. Smoking and TNM stages did not show a stepwise relationship with relapse tumour burden as well. However, current smokers showed an increased risk of relapse after 2.5 years post-surgery. Males accounted for 62.5% of relapses during the 9–12-month peak. LUSC relapse peaked at 9–12 and 15–18 months post-surgery; LUAD peaked at 12–15 months. LUSC, central, and advanced tumours were prone to having larger tumours, consistent with previous findings. These trends should be interpreted cautiously due to limited subgroup sizes.
- **Volume Thresholds in pT2N0M0:** In a subgroup analysis of patients with pT2N0M0 tumours, preliminary thresholds for tumour volume (>17,010 $mm^3$) and growth rate (>58 $mm^3$/day) were associated with an increased risk of relapse. These values should be viewed as preliminary thresholds, given the small sample size, which limits statistical power.

**Conclusions:** Manually contoured primary tumour volume is a stronger predictor of relapse than diameter-based calculation, pT stage and pTNM stage. Larger tumours are associated with earlier relapse, extrathoracic relapse and higher recurrence burden. In pT2N0M0 tumours, preliminary thresholds for tumour volume (>17,010 $mm^3$) and growth rate (>58 $mm^3$/day) are identified. While these metrics may help stratify adjuvant therapy, they are not clinically applicable without further prospective validation.

# Introduction

Prostate, breast, colorectal and lung cancers rank as the most common malignancies worldwide. Despite a gradual decrease in mortality rates over the last twenty years, lung cancer remains the leading cause of cancer-related deaths, accounting for approximately 125,070 deaths annually and representing 20% of all cancer-related mortality [1]. Non-small cell lung cancer (NSCLC), accounting for approximately 85% of lung cancer cases, is the predominant form of lung cancer [2]. While early-stage NSCLCs (stage IA) can expect a five-year survival rate of up to 70% post-complete resection [152], this figure drastically falls to less than 20% for stage IIIA and below 5% for stage IV [153], indicating worse outcomes for advanced stages. When considering NSCLC holistically, the overall 5-year survival rate has increased from 12% to 25% [1]. Over recent decades, the number of averted deaths has been approximately twice as high in men as in women, mainly due to higher smoking cessation rates among men [1]. These trends underscore the urgency of investigating recurrence patterns to inform clinical decision-making.

Surgery is the gold standard treatment method for NSCLC. The debate continues over the application of adjuvant therapy in patients with pT2N0M0 lung cancer. Post-surgical cancer recurrence is common, with about 30% of patients experiencing relapse within five years and the average recurrence-free survival is 15.7 months [154]. Although advances in chemoradiotherapy, targeted therapy, and immunotherapy have significantly improved locoregional control and overall survival in advanced NSCLC, disease progression remains common following initial response. The two-year relative survival rate remains limited at only 42% [132].

Several risk factors have been identified for NSCLC relapse, including smoking status, tumour size over 4cm, vascular invasion, poor differentiation, marginal resection, positive regional lymph nodes and visceral pleural involvement [155]. It has been observed that NSCLC tumours typically present irregular shapes rather than uniform roundness, challenging the conventional reliance on unidimensional measures of tumour diameter for capturing tumour complexity. A promising and unexplored area is the use of primary tumour volume and pre-treatment inner tumour growth rate as novel predictive parameters for relapse. Tumour volume and growth dynamics could significantly

influence disease management and monitoring strategies. This research has the largest known dataset on relapse, encompassing tumour volume, location, lesion characteristics, and progression procedures. This pioneering work is also being used at the UCL Cancer Institute, where the dataset is combined with genomic and circulating tumour DNA (ctDNA) data to elucidate tumour evolution, establish a metastatic gene phylogenetic tree, and investigate mechanisms of treatment resistance.

# Results

## 1. Patients' Clinical Characteristics and Tumour Volume in the Study Cohort

### 1.1 Patients' Clinical Characteristics

By June 26, 2024, a total of 200 stage I–III non-small cell lung cancer (NSCLC) cases were included in the analysis, including 130 patients who experienced post-surgery recurrence and 70 who did not relapse (Fig. 3.1). The median follow-up period was 1,732 days (range: 88–3,018 days).

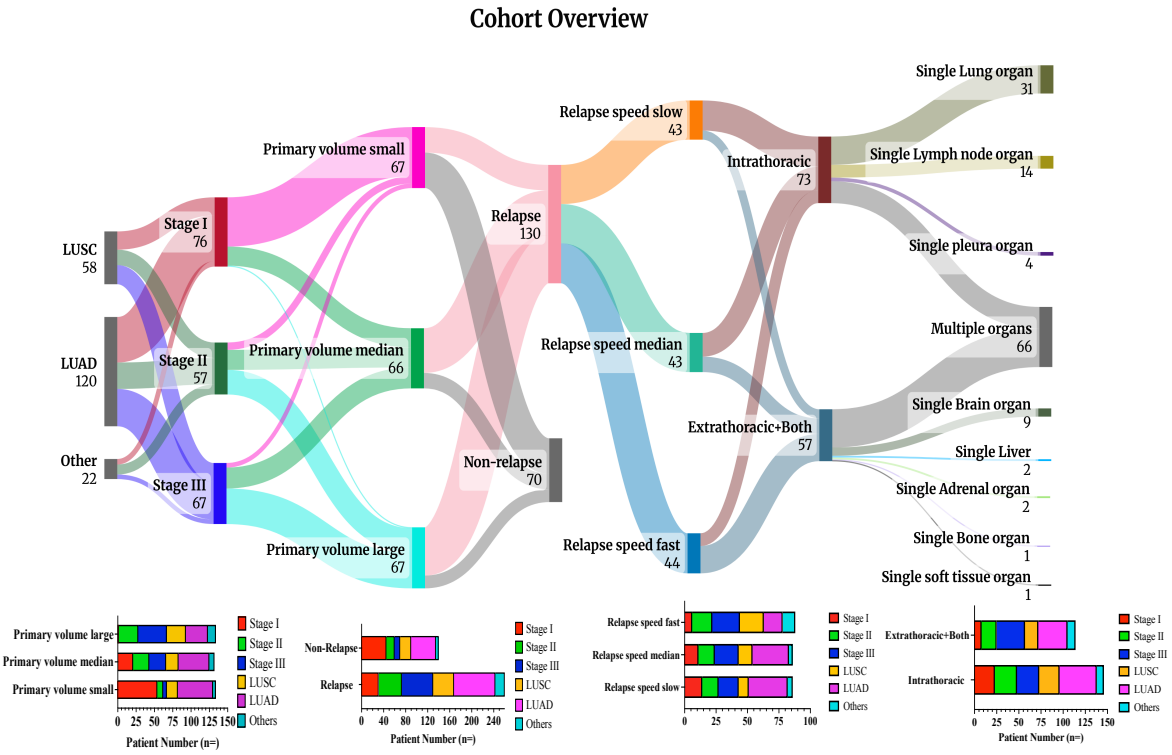


Fig. 3.1 Overview of contoured patients in the TRACERx longitudinal Imaging cohort.

Dominant clinical characteristics are listed in Table 3.1. The cohort predominantly consisted of males, with the majority being under 75 years old. A significant portion, 91%, had a history of smoking, with 9.5% identified as current smokers at diagnosis. Most patients were White, while 8% were from other ethnic backgrounds, including Caribbean, Indian, and African. Less than 5% of primary tumours harboured EGFR or ALK mutations. T2-stage tumours were the most common, followed by T1, T3 and T4. Stages II and III had comparable patient numbers, both slightly fewer than those in Stage I.

Invasive adenocarcinoma (LUAD) and squamous cell carcinoma (LUSC) were the most prevalent histological subtypes. In contrast, other types, such as large cell carcinoma (LCC) and pleomorphic carcinoma, accounted for only 11% of the cases. 83% of patients underwent Lobectomy surgery. Primary tumours were frequently located in the right upper or middle lung and less commonly in the left lower lung. Peripheral primary tumours represented 68% of cases. Most surgeries achieved R0 resection. The median interval from diagnosis to surgery was 38 days (Interquartile range [IQR], 29–49). A total of 157 patients underwent both diagnostic CT and staging PET/CT, with a median interval of 19 days (Interquartile range [IQR], 12–34) between scans. 63% of patients did not receive adjuvant therapy post-surgery, 30.5% underwent adjuvant chemotherapy, 4.5% received adjuvant radiotherapy, and 2% had chemoradiotherapy.

Table 3.1 Clinical and demographic characteristics of 200 patients included in this study

| **Factors** | | **Patient Number (n=200)** | **2-Year Relapse (n=105)** | **2-Year Non-Relapse (n=95)** | **Adjusted P-value** |
|---|---|---|---|---|---|
| *Sex* | Male | 111(55.5%) | 58(55%) | 53(56%) | 0.938 |
| | Female | 89(44.5%) | 47(45%) | 42(44%) | |
| *Age* | <66 | 74(37%) | 41(39%) | 33(35%) | 0.553 |
| | 66–75 | 85(42.5%) | 40(38%) | 45(47%) | |
| | >75 | 41(20.5%) | 24(23%) | 17(18%) | |
| *Smoking Status* | Ex-smoker | 100(50%) | 50(48%) | 50(53%) | 0.938 |
| | Recent Ex-smoker | 63(31.5%) | 34(32%) | 29(31%) | |
| | Current smoker | 19(9.5%) | 11(10%) | 8(8%) | |
| | Never smoker | 18(9%) | 10(10%) | 8(8%) | |
| *Smoking Pack Years* | ≤36.83 | 105(52.5%) | 56(53%) | 49(52%) | 0.938 |
| | >36.83 | 95(47.5%) | 49(47%) | 46(48%) | |
| *Ethnicity* | White British | 163(81.5%) | 83(79%) | 80(84%) | 0.391 |
| | White Irish | 13(6.5%) | 5(5%) | 8(9%) | |
| | White Other | 8(4%) | 6(6%) | 2(2%) | |
| | Other | 16(8%) | 11(10%) | 5(5%) | |

| | | | | | |
|---|---|---|---|---|---|
| *pT* | T1 | 49(24.5%) | 10(9.5%) | 39(41%) | 0.651 |
| | T2 | 76(38%) | 45(43%) | 31(33%) | |
| | T3 | 46(23%) | 29(27.5%) | 17(18%) | |
| | T4 | 29(14.5%) | 21(20%) | 8(8%) | |
| *pN* | 0 | 132(66%) | 52(49.5%) | 80(84%) | 0.0005* |
| | 1 | 32(16%) | 25(24%) | 7(7%) | |
| | 2 | 36(18%) | 28(26.5%) | 8(9%) | |
| *pTNM* | I | 76(38%) | 18(17%) | 58(61%) | 0.0005* |
| | II | 57(28.5%) | 36(34%) | 21(22%) | |
| | III | 67(33.5%) | 51(49%) | 16(17%) | |
| *Histology* | LUSC | 58(29%) | 29(28%) | 29(31%) | 0.263 |
| | LUAD | 120(60%) | 60(57%) | 60(63%) | |
| | Other | 22(11%) | 16(15%) | 6(6%) | |
| *Surgery* | Lobectomy | 166(83%) | 82(78%) | 84(88%) | 0.051 |
| | Segmentectomy or Wedge | 15(7.5%) | 7(7%) | 8(9%) | |
| | Pneumonectomy | 12(6%) | 11(10%) | 1(1%) | |
| | Others | 7(3.5%) | 5(5%) | 2(2%) | |
| *Resection Margin* | R0 | 184(92%) | 91(87%) | 93(98%) | 0.012* |
| | R1–2 | 16(8%) | 14(13%) | 2(2%) | |
| *Primary Tumour Location* | Left Lower | 27(13.5%) | 14(13%) | 13(14%) | 0.398 |
| | Right Lower | 50(25%) | 29(28%) | 21(22%) | |
| | Left Upper | 46(23%) | 28(27%) | 18(19%) | |
| | Right Upper/Middle | 77(38.5%) | 34(32%) | 43(45%) | |
| *Axial Location* | Central | 64(32%) | 41(39%) | 23(24%) | 0.058 |
| | Peripheral | 136(68%) | 64(61%) | 72(76%) | |
| *Adjuvant Therapy* | Chemotherapy | 61(30.5%) | 45(43%) | 16(17%) | 0.0005* |
| | Radiotherapy | 9(4.5%) | 8(8%) | 1(1%) | |
| | Chemoradiotherapy | 4(2%) | 2(2%) | 2(2%) | |
| | None | 126(63%) | 50(47%) | 76(80%) | |

P values were adjusted using the Benjamini–Hochberg False Discovery Rate (FDR) method to account for multiple comparisons (n=14 tests).

More than half of the patients experienced relapse within two years post-surgery, with a gradual increase observed thereafter. Specifically, 28% relapsed within the first year, 23% in the second year, 6% in the third year, 6.1% in the fourth year, 1.1% in the fifth year, and 2.1% in the sixth year, with no relapses in the seventh and eighth years. (Fig. 3.2)

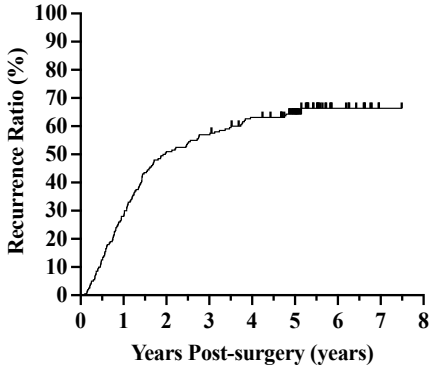


Fig. 3.2 Each year recurrence proportion post-surgery.

### 1.2 Tumour's Primary Tumour Volume and Inner Growth Rate

Half of the patients relapsed within 2 years after completing resection in this cohort. Comparisons in Table 3.2 were made between patients who experienced recurrence within 2 years post-surgery and those who remained disease-free beyond that period.

Table 3.2 200 patients' primary tumour volume and tumour growth rate

| **Primary Tumour** | **Group** | **Median** | **Interquartile Range** | **Adjusted P-value** |
|---|---|---|---|---|
| *Diameter (cm)* | All | 3.6 | 2.5–5.1 | 0.0003* |
| | 2-Year relapse | 4.4 | 3.4–5.8 | |
| | 2-Year non-relapse | 2.7 | 2.1–3.9 | |
| *Volume-Diameter Based Calculation ($mm^3$)* | All | 24429 | 8181–69456 | 0.0003* |
| | 2-Year relapse | 43116 | 20579.5–102160.4 | |
| | 2-Year non-relapse | 10306 | 4849–33510 | |
| *Volume-Manual Contouring ($mm^3$)* | All | 17390 | 5405–54410 | 0.0003* |
| | 2-Year relapse | 37520 | 14757.5–86817.5 | |
| | 2-Year non-relapse | 6611 | 3196.5–19310 | |
| *Primary Growth Rate Pre-surgery ($mm^3/d$)* | All | 37.84 | 6.52–149.2 | 0.014* |
| | 2-Year relapse | 103.8 | 21.02–350 | |
| | 2-Year non-relapse | 12.21 | 2.4–46.69 | |
| *Volume Increase Ratio (%)* | All | 8.3 | 1.11–22.86 | 0.046* |
| | 2-Year relapse | 10.22 | 2.51–26.45 | |
| | 2-Year non-relapse | 6.6 | 0.41–16.86 | |
| *SUV* | All | 10 | 6–15.65 | 0.0004* |
| | 2-Year relapse | 12.35 | 8.13–18 | |
| | 2-Year non-relapse | 7.85 | 3.95–13.25 | |
| *Blood SUV* | All | 5.1 | 2.38–5.8 | 0.1 |
| | 2-Year relapse | 5.1 | 2.6–5.8 | |
| | 2-Year non-relapse | 4.6 | 2.3–5.7 | |

P values were adjusted using the Benjamini–Hochberg False Discovery Rate (FDR) method to account for multiple comparisons (n=7 tests).

To visualise tumour volume distributions in the relapse and non-relapse groups, violin plots were generated to compare diameter-based volume estimates with volumes derived from manual contouring (Fig. 3.3). The distributions exhibit a bell-shaped structure and are approximately symmetric around the median, indicating that they are approximately normally distributed. P-values were adjusted using the Benjamini–Hochberg False Discovery Rate (FDR) method to account for multiple comparisons (n=2 tests).

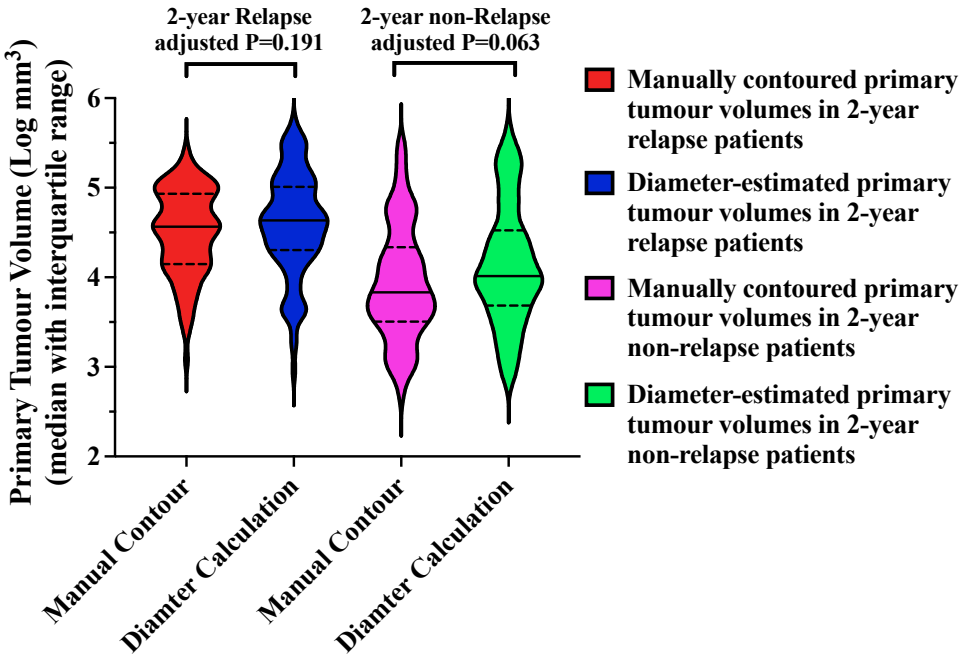


Fig. 3.3 Distribution of manually contoured and diameter-based primary tumour volumes in patients stratified by 2-year relapse status.

Patients who relapsed within 2 years post-surgery had a larger primary tumour volume, a faster primary tumour growth rate, a more significant volume increase ratio, and a higher SUV than non-relapsed patients. The difference was more significant in manually contoured volumes; the median contour volume in the relapse group was over five times higher than in the non-relapse group (Table 3.2), underscoring the important role of manual contouring in assessing clinically relevant tumour burden.

To reduce errors, the Blood SUV (background) values were compared between the two groups. The analysis showed no significant differences, indicating that despite variations in clinical techniques, the baseline Blood SUVs were standardised (Table 3.2).

### 1.3 Predictors of Recurrence.

Cox regression analysis was used to investigate the parameters that could predict recurrence-free survival (Table 3.3). In the univariate analysis, several factors exhibited significant differences, including primary tumour volume, baseline tumour growth rate, SUV value, pT, pN, pTNM, adjuvant therapy, primary tumour location, primary tumour texture, nodule shape, primary tumour attachment to vessel, bronchus or pleura, presence of equivocal lesions, and atelectasis. Interestingly, smoking status (P=0.511), age (P=0.919), and histology (LUSC vs. LUAD vs. Other, P=0.118) were not significantly associated with recurrence. Notably, univariate Cox regression analysis revealed that diameter-based tumour volume was not predictive of relapse (HR =1.00), whereas manually contoured volume was significantly associated with an increased relapse risk (HR=2.504), highlighting the advantage of contoured volume over diameter-based estimates in relapse prediction.

Subsequently, a backward stepwise multivariate analysis was conducted to further investigate these parameters. The analysis identified manually contoured primary tumour volume (HR = 2.68, 95% CI 1.54–4.65), pTNM stage, pN stage, irregular primary tumour shape, pleural or bronchial attachment, satellite nodules, fibrosis, and nodule calcification as factors associated with DFS, suggesting their potential prognostic value.

Table 3.3 Univariate and multivariate Cox regression analyses of clinical and tumour-related factors associated with recurrence

| **Characteristic Factors** | **Univariate Analysis** | | |
|---|---|---|---|
| | **P value** | **HR** | **95%CI** |
| Primary Tumour Growth Rate (Slow vs Fast) | <0.001 | 1.6 | 1.05–2.43 |
| Primary Tumour Size (Manual Contouring, log $mm^3$) | <0.001 | 2.5 | 1.89–3.32 |
| Primary Tumour Size (Diameter-Based Estimate, log $mm^3$) | <0.001 | 1 | 1–1 |
| Scan Number Before Relapse | <0.001 | 0.62 | 0.56–0.68 |
| pT stage (T1–2 vs T3–4) | <0.001 | 1.8 | 1.27–2.55 |
| pN stage (N0 vs N1–2) | <0.001 | 3.07 | 2.16–4.38 |
| TNM Stage (I vs II vs III) | <0.001 | | |
| I vs II | <0.001 | 2.93 | 1.84–4.67 |
| I vs III | <0.001 | 4.41 | 2.83–6.87 |
| Adjuvant Therapy | <0.001 | 0.64 | 0.54–0.77 |
| Primary Tumour Location (Central/ Peripheral) | 0.033 | 1.22 | 1.02–1.45 |
| Equivocal Lesions | <0.001 | 2.9 | 1.87–4.49 |
| Primary Tumour Texture (Non-solid) | 0.002 | 0.63 | 0.47–0.85 |
| Nodule Shape (Irregular) | 0.011 | 1.25 | 1.05–1.48 |
| Vascular Attachment | 0.021 | 1.64 | 1.08–2.49 |
| Bronchial Attachment | 0.011 | 1.61 | 1.11–2.32 |
| Pleural Attachment | <0.001 | 2.26 | 1.56–3.29 |
| Atelectasis | 0.023 | 1.49 | 1.06–2.11 |
| SUV | <0.001 | 1.05 | 1.02–1.07 |

| Characteristic Factors | Multivariate Analysis | | |
|---|---|---|---|
| | P value | HR | 95%CI |
| Primary Tumour Volume (Manual Contouring) | <0.001 | 2.68 | 1.54–4.65 |
| pTNM | 0.84 | | |
| I vs II | 0.043 | 2.07 | 1.02–4.21 |
| I vs III | 0.501 | 1.41 | 0.52–3.80 |
| pN | 0.022 | | |
| N0 vs N1 | 0.26 | 1.49 | 0.75–2.96 |
| N0 vs N2 | 0.006 | 3.06 | 1.38–6.78 |
| Irregular Shape | <0.001 | 2.62 | 1.61–4.27 |
| Pleural Attachment | 0.129 | 1.45 | 0.9–2.35 |
| Bronchial Attachment | 0.094 | 0.64 | 0.38–1.08 |
| Satellite Nodules | 0.02 | 1.72 | 1.09–2.71 |
| Fibrosis | 0.036 | 1.81 | 1.04–3.13 |
| Nodule Calcification | 0.069 | 2.08 | 0.94–4.6 |

I explored whether primary tumour volume at diagnosis was associated with patterns of recurrence, with a specific focus on anatomical location and relapse burden. This analysis was motivated by previous studies suggesting that larger tumours may have a greater potential for distant metastasis; however, few studies have investigated the association between primary tumour burden and relapse burden [69,71]. Findings from this study showed that larger primary tumour volumes were associated with a higher probability of extrathoracic relapse (Fig. 3.4A), but not with polymetastatic relapse (Fig. 3.4B), suggesting that the relapse burden is not solely determined by primary tumour size. They may be affected by additional factors such as immune surveillance or molecular subtypes.

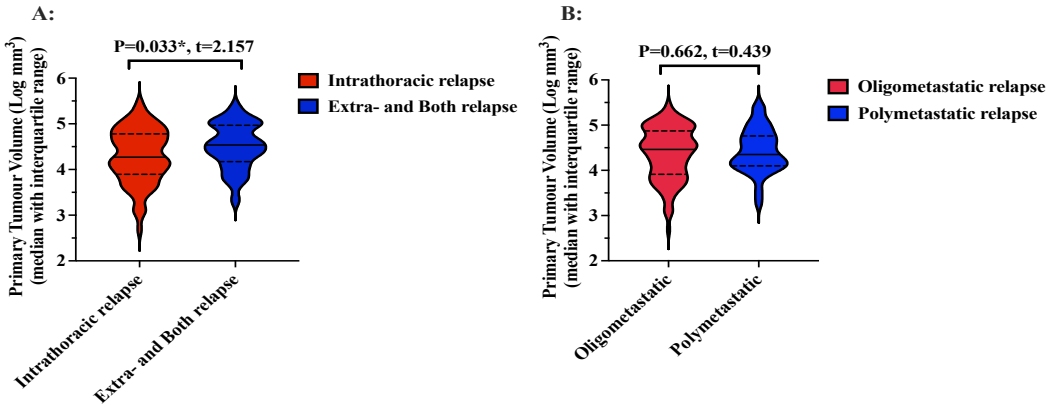

Fig. 3.4 Relationship between primary tumour volumes and relapse characteristics. A: Distribution of primary tumour volumes stratified by relapse site: intrathoracic, extrathoracic and both. B: Comparison of primary tumour volumes across relapse burden groups. In both panels, the distributions are approximately normal and exhibit a bell-shaped pattern.

In summary, these findings suggest that parameters such as primary tumour volume may be important in guiding post-surgical surveillance and management strategies aimed at reducing the risk of recurrence.

**1.4 Primary Tumour Volume as a Predictor of Overall Survival.**

To evaluate whether primary tumour volume provides prognostic value for overall survival, X-tile analysis—previously used in relation to DFS—was applied to determine the optimal cutoff values for manually contoured primary tumour volumes (11,120$mm^3$, 3,172$mm^3$), for diameter-based volume calculations (15,599$mm^3$, 3,054$mm^3$), these thresholds were used to stratify patients into high-, moderate-, and low-risk groups, predicting overall survival post-surgery accordingly.

This analysis was based on the rationale that volumetric tumour burden reflects underlying tumour biology more accurately than linear measurements and T stage. Survival curves demonstrated that stratification by manually contoured primary tumour volume provided greater distinction in overall survival compared to diameter-based estimates, pT and pTNM staging (Fig. 3.5), although the patient numbers were imbalanced across the volume-based risk subgroups. The respective AUC values were 0.69, 0.64, 0.62, and 0.66, and the corresponding C-index values were 0.67, 0.63, 0.65, and 0.68. Notably, the low-risk classification based on manually contoured tumour volume provided clearer separation of survival curves than those based on pT and pTNM staging, suggesting improved predictive performance. In future analyses, expanding the cohort and integrating primary tumour volume with pTNM staging may further improve the predictive accuracy for overall survival.

**A:**

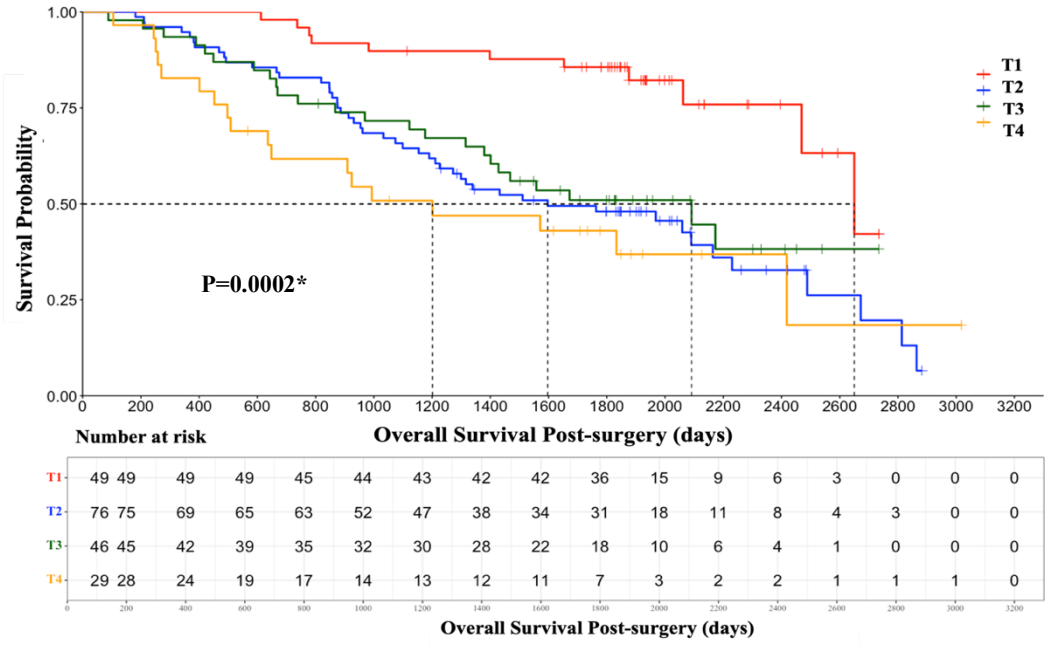
Survival Probability
1.00
0.75
0.50
0.25
0.00
T1
T2
T3
T4
P=0.0002*
0 200 400 600 800 1000 1200 1400 1600 1800 2000 2200 2400 2600 2800 3000 3200
Overall Survival Post-surgery (days)
Number at risk
T1 49 49 49 49 45 44 43 42 42 36 15 9 6 3 0 0 0
T2 76 75 69 65 63 52 47 38 34 31 18 11 8 4 3 0 0
T3 46 45 42 39 35 32 30 28 22 18 10 6 4 1 0 0 0
T4 29 28 24 19 17 14 13 12 11 7 3 2 2 1 1 1 0
Overall Survival Post-surgery (days)

**B:**

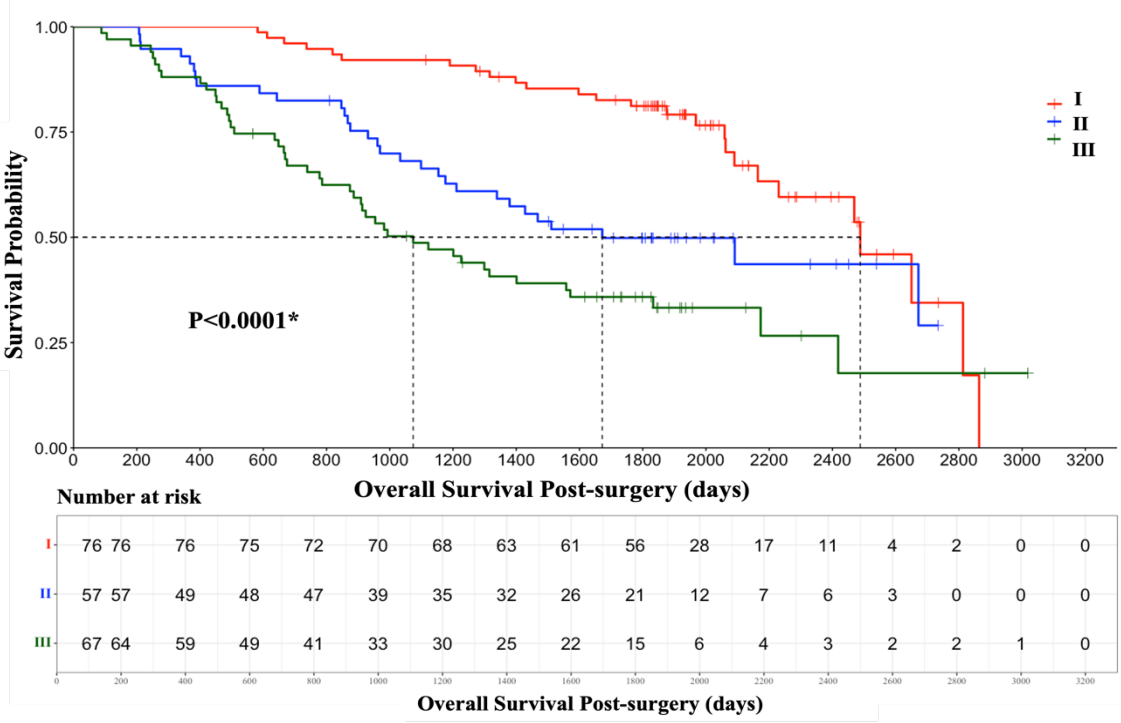
Survival Probability
1.00
0.75
0.50
0.25
0.00
I
II
III
P<0.0001*
0 200 400 600 800 1000 1200 1400 1600 1800 2000 2200 2400 2600 2800 3000 3200
Overall Survival Post-surgery (days)
Number at risk
I 76 76 76 75 72 70 68 63 61 56 28 17 11 4 2 0 0
II 57 57 49 48 47 39 35 32 26 21 12 7 6 3 0 0 0
III 67 64 59 49 41 33 30 25 22 15 6 4 3 2 2 1 0
Overall Survival Post-surgery (days)

**C:**

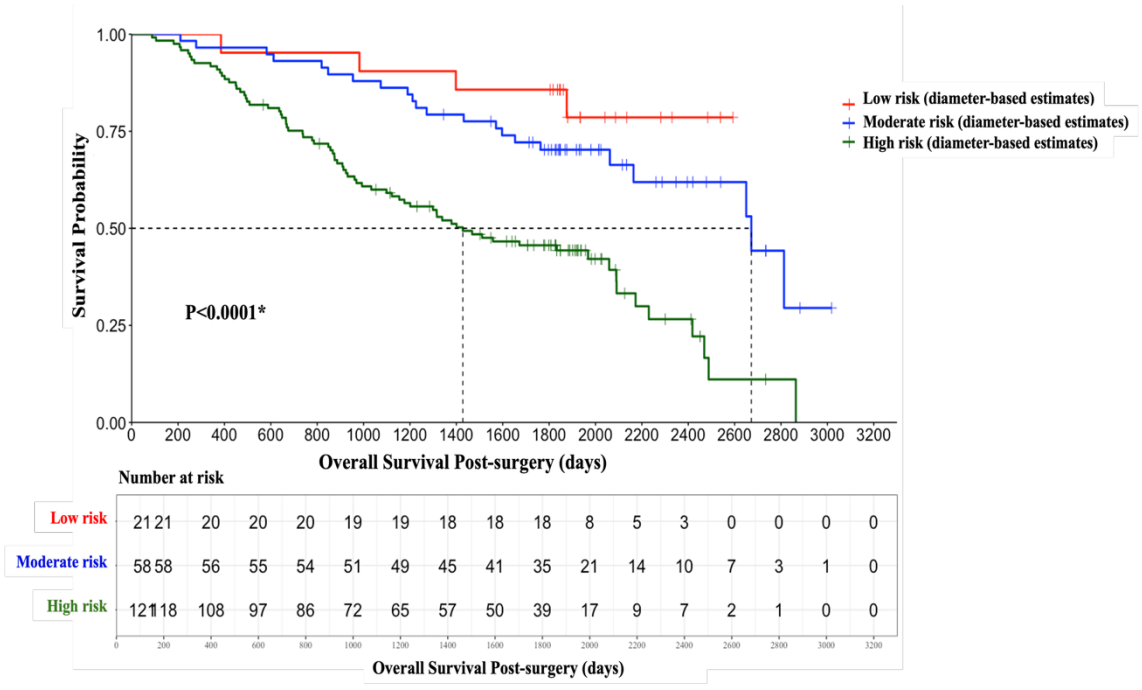


**D:**

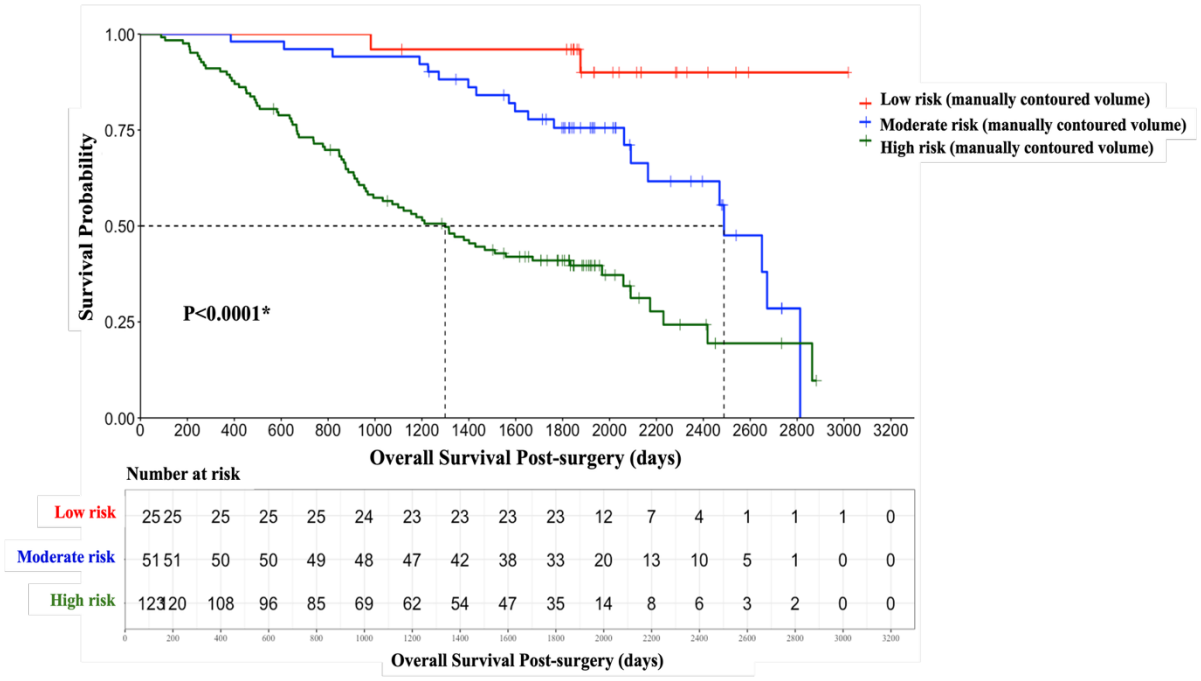


Fig. 3.5 Overall survival post-surgery across pT, pTNM and primary volume risk groups. A: Overall survival post-surgery by pT stage; B: Overall survival post-surgery by pTNM stage; C: Overall survival post-surgery by diameter-based primary tumour volume risk groups; D: Overall survival post-surgery by manually contoured primary tumour volume risk groups.

## 2. Yearly Recurrence Ratios in Different Subgroups

To further explore how the recurrence ratio varied across different groups, yearly recurrence ratios across multiple subgroups were analysed. The aim was to determine whether recurrence risk profiles differ across demographic, pathological and treatment-related variables, thereby identifying factors that may inform clinical decision-making.

### 2.1 Yearly Recurrence Ratios by Gender, Age, Histology, Smoking status, TNM Stage, and Adjuvant Therapy.

Firstly, yearly recurrence ratios across clinical characteristics subgroups, including gender, age, histology, smoking status, TNM stage, T stage, and adjuvant therapy, were assessed to evaluate the distribution of recurrence rates. The aim was to identify factors associated with early or late recurrence. Key results are presented in Fig. 3.6.

There was no significant difference in recurrence rates across gender and age groups within the first two years. (Fig. 3.6A–B). However, early relapse (within 9–12 months) appeared more common in males, consistent with the previous findings that males (62.5%) are prone to early relapse [156], raising the possibility of sex-related biological influences on relapse dynamics.

Histology-specific trends provided meaningful insights. LUAD and LUSC showed similar overall recurrence rates (Fig. 3.6C), but the timing of relapse differed, with LUSC showing a higher peak at 9–12 months post-surgery and LUAD at 12–15 months (Fig. 3.7B). Pleomorphic carcinomas, a rare subtype, exhibited aggressive behaviour, with all cases relapsing within 9 months (Fig. 3.7A). These preliminary findings suggest that post-surgery surveillance schedules may benefit from histology-informed adjustments, with intensified monitoring during the most relapse-prone intervals for each subtype.

Smoking status and tobacco exposure did not significantly affect the recurrence ratio (Fig. 3.6D, H), including within the LUAD subgroup (P=0.34); these findings differ from previous clinical commonalities and may be partially due to the limited sample size. However, a notable acceleration in relapse beyond 2.5 years was observed among current smokers. While this may be influenced by cohort size, it also potentially reflects biological processes such as late-emerging subclonal mutations, delayed immune escape, or treatment-driven selection of resistant subclones. Previous TRACERx studies support

this hypothesis, which found that smoking-related mutational SBS4 is enriched in the upper or right lung, particularly in LUAD, and is associated with subclonal evolution [107,115]. Moreover, immune escape mechanisms have been identified in later subclones or under specific conditions, including HLA loss, neoantigen editing, T cell infiltration, and PD-L1 upregulation [108,112,157,158]. All these results highlight the possibility that smoking-related tumour evolution may emerge over time and be influenced by tumour location and microenvironment factors. These preliminary findings require further genomic and immunological analyses to elucidate the underlying biological mechanisms of late relapse patterns in smokers.

TNM staging and T-stage alone showed the clearest associations with recurrence (Fig. 3.6E–F). Stage III patients had a higher likelihood of relapse rates within the first 0–3 months, while stage II initially peaked at 3–6 months (Fig. 3.8), indicating that stage-specific intensified surveillance during these high-risk intervals may be beneficial.

Interestingly, patients who received adjuvant therapy had higher recurrence rates (Fig. 3.6G). However, this may be due to selection bias, as nearly all adjuvant-treated patients were in advanced stage (99%), compared to only 40% of those who did not receive adjuvant therapy. Among advanced-stage matched subgroups, adjuvant therapy did not significantly reduce recurrence rates (P=0.45), suggesting that it may provide limited benefit for certain patients. It's essential to find the predictors for these patients.

In summary, despite variations in subgroup sizes and some statistical fluctuations in the curves, the main trends—particularly those related to stage and histology—were consistent with clinical expectations. An exception was observed for smoking status, which did not follow the expected pattern. These results support the need for tailored surveillance intervals and underscore the urgent need to uncover the biological mechanisms in specific subgroups.

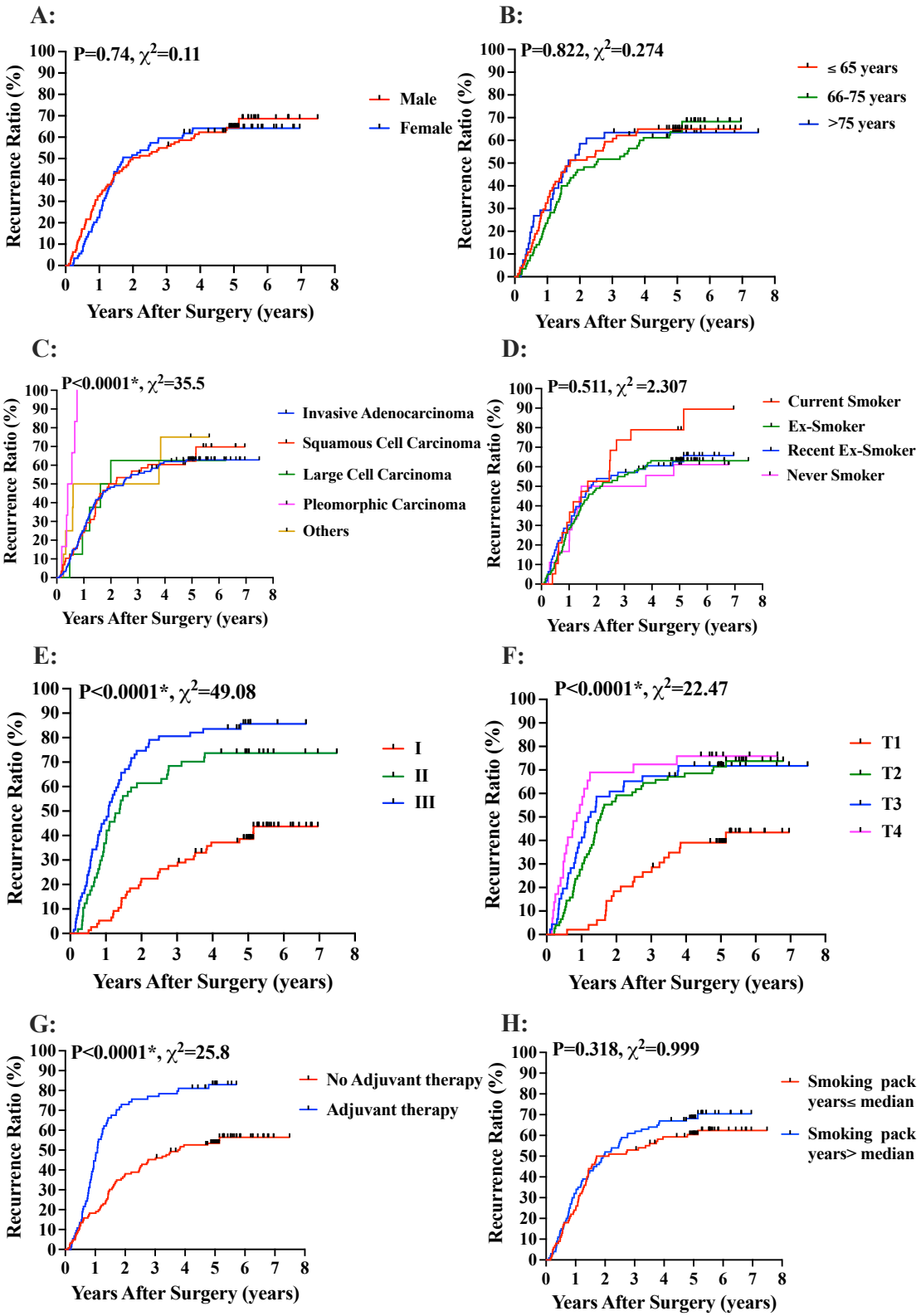


Fig. 3.6 Annual recurrence ratios after surgery across clinical and demographic subgroups. A: Recurrence ratios by gender; B: Recurrence ratios by age group; C: Recurrence ratios by histological subtype; D: Recurrence ratios by smoking status; E: Recurrence ratios by pathological TNM stage; F: Recurrence ratios by pathological T stage; G: Recurrence

ratios by receipt of adjuvant therapy; H: Recurrence ratios by smoking pack-year categories.

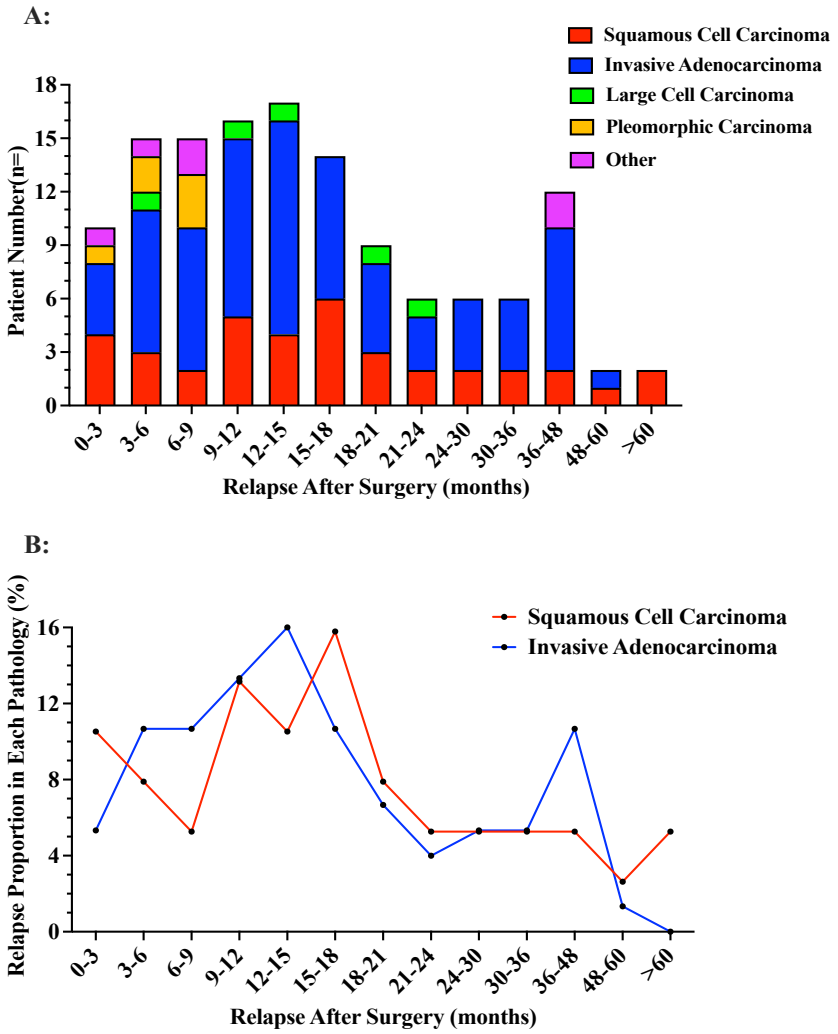


Fig. 3.7 Distribution of relapse timing (in months) stratified by histological subtypes.

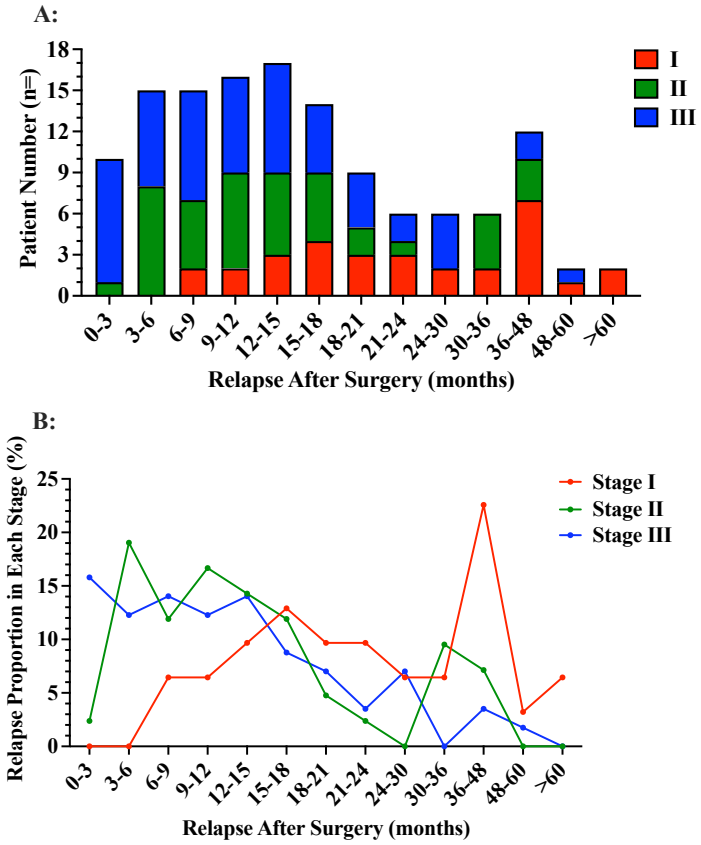


Fig. 3.8 Distribution of relapse timing (in months) stratified by pathological TNM stage.

### 2.2 Recurrence Patterns of Primary Tumour Volume Subgroups

Previous results identified primary tumour volume as a key predictor of recurrence. However, few studies have explored how volume-based recurrence dynamics vary in different clinical subgroups. To address this gap, I analysed yearly recurrence ratios across subgroups to explore whether the predictive value of primary tumour volume remains consistent or varies across specific patient groups.

The patients were grouped into three subgroups according to tertiles of primary tumour volume: ≤33% (small), 34–66% (median), and 67–100% (large), to explore how primary tumour volume affects the disease-free survival (DFS). This tertile-based cutoff method was selected to ensure an even distribution of patients across subgroups, helping to minimise bias from imbalanced subgroup sizes. Unlike the fixed linear thresholds used in TNM staging, tertile-based stratification ensures sufficient patient numbers within each subgroup, allowing trends to emerge without enforcing arbitrary clinical rules. This approach also avoids binary classification, which can overlook meaningful variations in

this data. As demonstrated in this study, manually contoured tumour volume may better reflect actual tumour burden and heterogeneity compared to linear dimensions or diameter-based volume estimates.

The summarised results presented below provide valuable insights for clinical practice, illustrating the relationships between tumour sizes and various factors such as gender, sex, histology, smoking habits, and the use of adjuvant therapy. These findings may help inform more individualised approaches to patient care and treatment planning based on tumour volume and related clinical characteristics. In the future, a tick-box-style guideline could be developed to support clinical decision-making in routine practice.

**Manually Contoured Primary Tumour Volume: A Predictor of Recurrence.**

The analysis was conducted to determine whether manually contoured primary tumour volume provides better relapse prediction than traditional staging methods and diameter-based volume estimates. The study found that small, medium, and large primary tumour volumes (stratified by tertiles of manually contoured volume) had distinct relapse probabilities (Fig. 3.9A). The large-sized group (upper tertile) had the highest relapse rate within the first year (46%), while the medium-sized group peaked around the second year. In contrast, small tumours recurred more gradually, with a peak around the fourth year. Manually contoured primary tumour volume was a better predictor of 1-, 2- and 3-year relapse than diameter-based volume calculation, pT stage, and pTNM stage (AUC values are shown in Fig. 3.9B). The ROC curves exhibited non-smooth patterns, likely reflecting sampling variability due to the small cohort size and uneven subgroup distributions. Nonetheless, the area under the curve (AUC) remains a valid comparative metric, and the overall trends are still interpretable. Future studies with larger and more balanced datasets are needed to validate these findings. The Concordance index (C-index) for DFS was also higher in the manually contoured primary tumour volume (0.67) than in the diameter-based estimates (0.66) and pT stage (0.65) and was comparable to the pTNM stage (0.68). In summary, these results suggest that manually contoured primary tumour volume may provide improved relapse risk stratification compared to traditional metrics.

**A:**

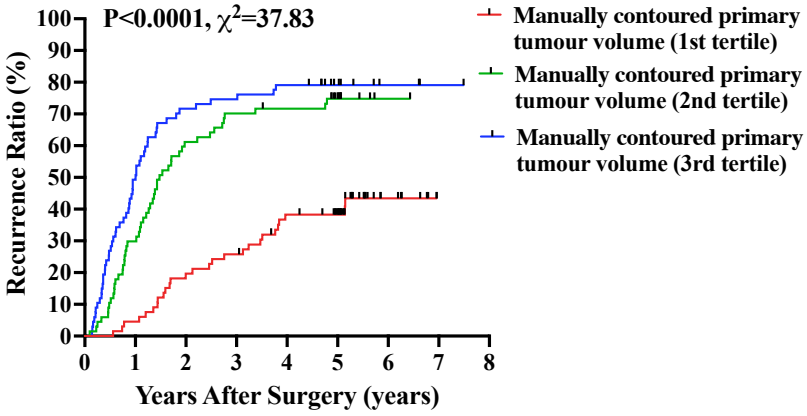
P<0.0001, $\chi^2$=37.83
Recurrence Ratio (%)
Years After Surgery (years)
Manually contoured primary tumour volume (1st tertile)
Manually contoured primary tumour volume (2nd tertile)
Manually contoured primary tumour volume (3rd tertile)

**B:**

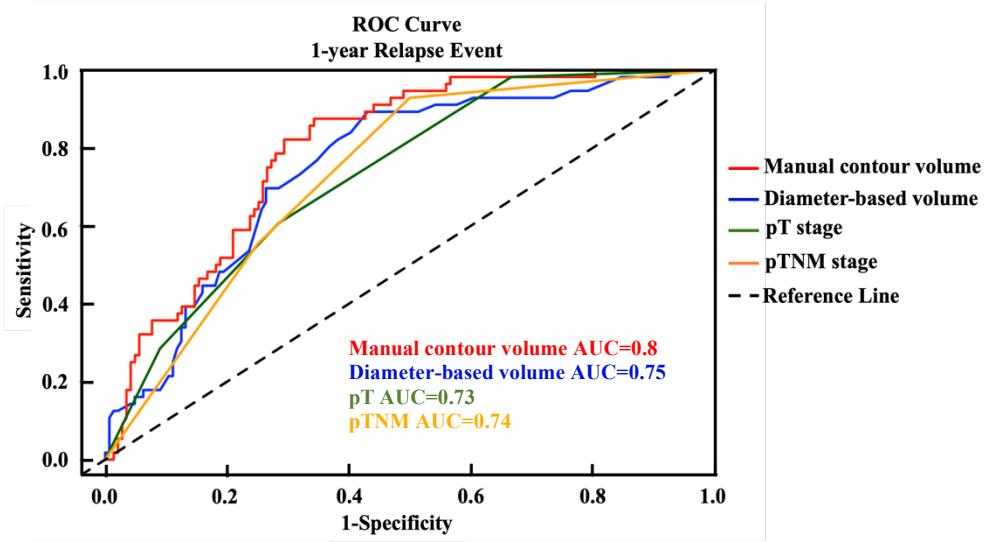
ROC Curve
1-year Relapse Event
Sensitivity
1-Specificity
Manual contour volume
Diameter-based volume
pT stage
pTNM stage
Reference Line
Manual contour volume AUC=0.8
Diameter-based volume AUC=0.75
pT AUC=0.73
pTNM AUC=0.74

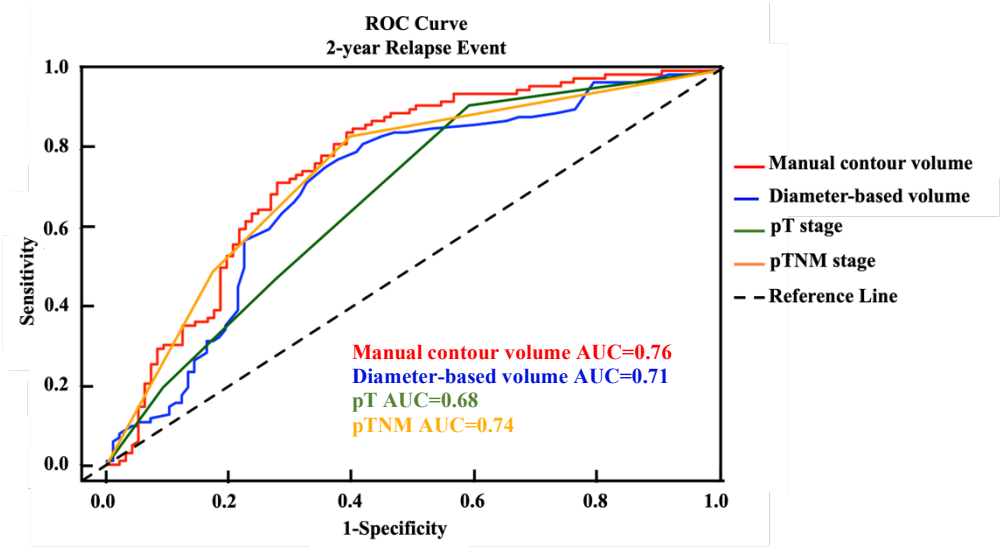
ROC Curve
2-year Relapse Event
Sensitivity
1-Specificity
Manual contour volume
Diameter-based volume
pT stage
pTNM stage
Reference Line
Manual contour volume AUC=0.76
Diameter-based volume AUC=0.71
pT AUC=0.68
pTNM AUC=0.74

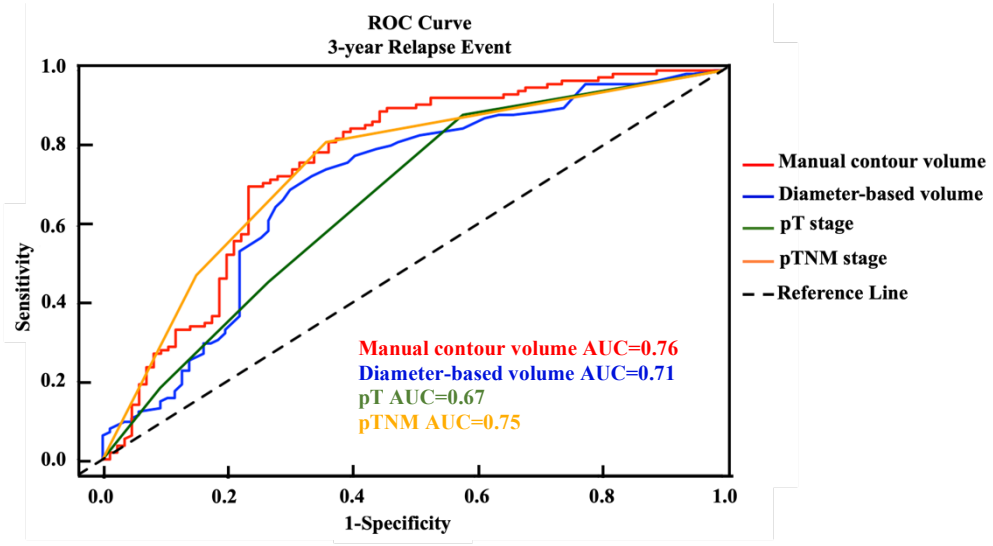


Fig. 3.9 Yearly recurrence ratios by primary tumour volume subgroups and ROC curves for manually contoured primary tumour volume, diameter-based volume, pT stage, and pTNM stage.

**Subgroup Insights**

**Age and Gender:** No significant interaction between age or gender and tumour volume was observed. Recurrence rates increased with tumour size across all age groups and in both genders. Females had slightly higher 2-year relapse rates in the moderate- and large-sized groups, with recurrence rates of 66% and 75% for females, respectively, compared to 50% and 65% for males. However, these differences were not statistically significant.

**Histology:** Across volume subgroups, recurrence patterns varied modestly by histological type, although no significant interaction with volume was observed (P=0.508). LUAD showed slightly higher recurrence rates than LUSC in the moderate-sized group after 3 years post-surgery (74% vs 53%) and in the large-sized group after 1.5 years (70% vs 62%). Large cell lung cancer and pleomorphic subtypes, although limited by small sample sizes, showed the poorest recurrence outcomes, particularly within the first year post-surgery.

In an exploration of tumour growth characteristics across different lung cancer subtypes within a specific cohort, the study aimed to validate whether lung adenocarcinoma (LUAD) – typically characterised by smaller tumour size and slower growth, but with a higher metastatic potential compared to lung squamous cell carcinoma (LUSC) [159] –

showed similar patterns. The analysis included 40 out of 58 LUSCs and 90 out of 119 LUADs, focusing on calculating the baseline inner tumour growth rates for each histological subtype.

The proportions of LUSC and LUAD among stages I, II, and III were insignificant (P= 0.619), indicating the distribution of LUSC and LUAD did not vary significantly with the stage of cancer. I hypothesised that larger tumours would be associated with rapid growth rates, reflecting a more aggressive biological behaviour. A strong positive correlation was observed between tumour volume and inner growth rate in both LUSC and LUAD (Fig. 3.10A), indicating that faster-growing tumours are generally associated with larger tumour burdens across histologies, which helps identify patients at higher risk of aggressive tumour behaviours. Previous studies have demonstrated that LUAD has smaller tumours and slower growth rates, but has a higher metastatic potential compared to LUSC [107,159]. Hence, I explored whether LUSC and LUAD differed in baseline and relapse tumour burden. LUSC displayed larger initial volumes than LUAD, although significant differences were not found in some stages. Stage III LUSC had the largest primary tumour volume (Fig. 3.10B). Similarly, relapse volume showed a positive correlation with relapse speed in both LUSC and LUAD (Fig. 3.11A), indicating that faster-growing tumours at relapse tend to be associated with larger relapse tumour burdens. LUSC had a faster relapse speed and larger relapse volume than LUAD. (Fig. 3.11B–C). There were variations in the relapse growth rate group, but the distributions are approximately normal. In summary, LUSC is associated with larger initial volumes, faster relapse, and a higher relapse burden than LUAD, supporting tumour volume and histology as clinically relevant indicators of tumour behaviour.

**A:**

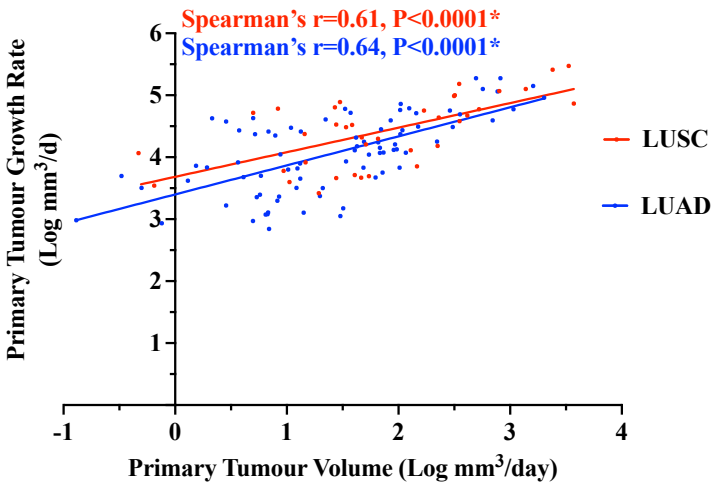

B:

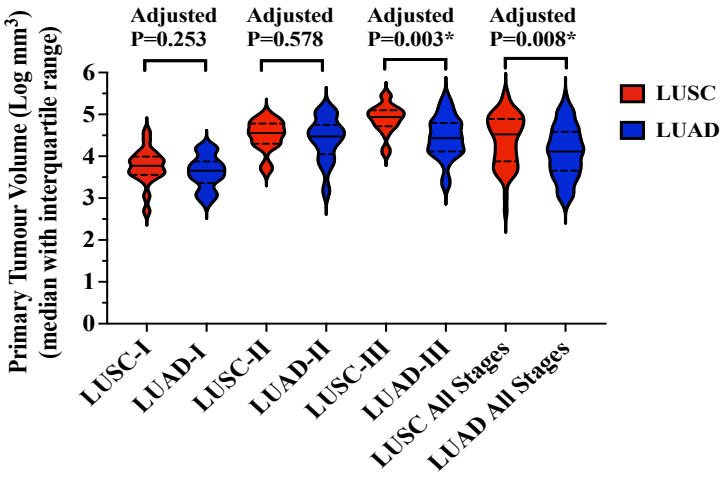


Fig. 3.10 Relationship between primary tumour growth rates and primary tumour volumes across histological subtypes. A: Correlation between primary tumour growth rates and primary tumour volumes across histological subtypes; B: Comparison of primary tumour volumes across histological subtypes by TNM stages. P values were adjusted using the Benjamini–Hochberg False Discovery Rate (FDR) method to account for multiple comparisons (n=4 tests).

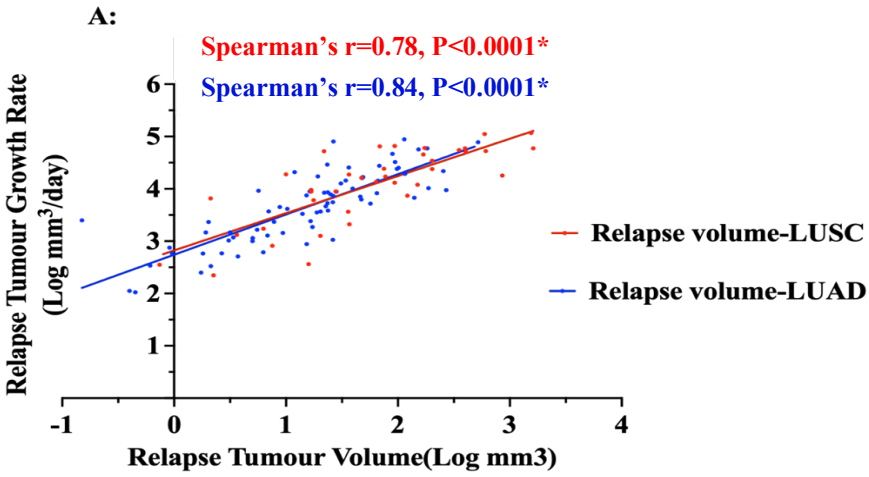

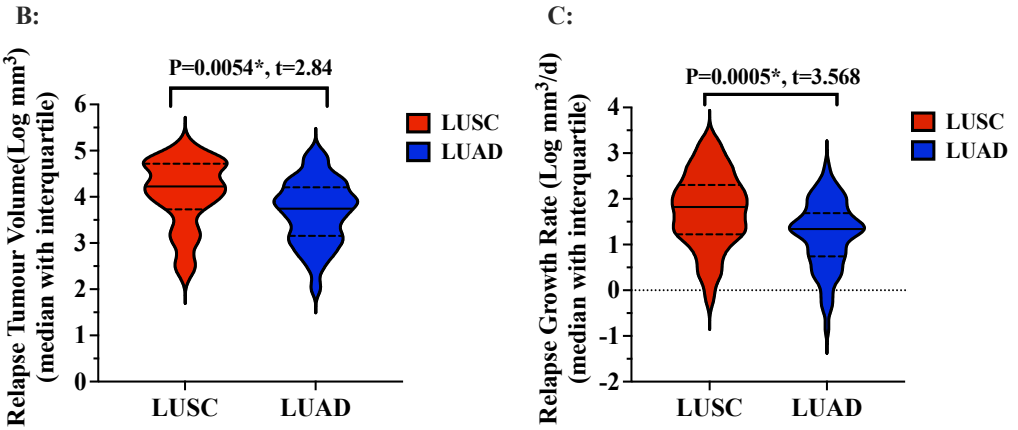


Fig. 3.11 Relationship of relapse tumour growth rate and volume in different histologies.

**Smoking:** Smoking pack years and smoking status can't help to distinguish the recurrence risks (Fig. 3.12). However, current smokers had a higher relapse risk after 2 years in the small-volume group and after 1 year in the large-volume group. There was a strong positive correlation between relapse volume and relapse speed across smoking status subgroups: current smoker (r=0.86), ex-smoker (r=0.86), recent ex-smoker (r=0.85), never smoker (r=0.72). However, no significant differences were found in relapse volume (P=0.878, 0.617) or relapse speed (P=0.663, P=0.193) among the smoking status and pack-years subgroups, indicating that smoking status may influence the timing of relapse but not its size or growth rate; further mutational analysis is essential.

**Adjuvant Therapy:** Adjuvant therapy was not associated with a significantly reduced risk of recurrence (Fig. 3.12). 5 out of 10 patients with a small tumour burden who received adjuvant therapy experienced relapse within two years post-surgery, contrary to the expectations based on current treatment paradigms. This unexpected result may reflect confounding factors, such as lymph node involvement not accounted for in this analysis, and highlights the need to identify compound predictors of adjuvant therapy benefit.

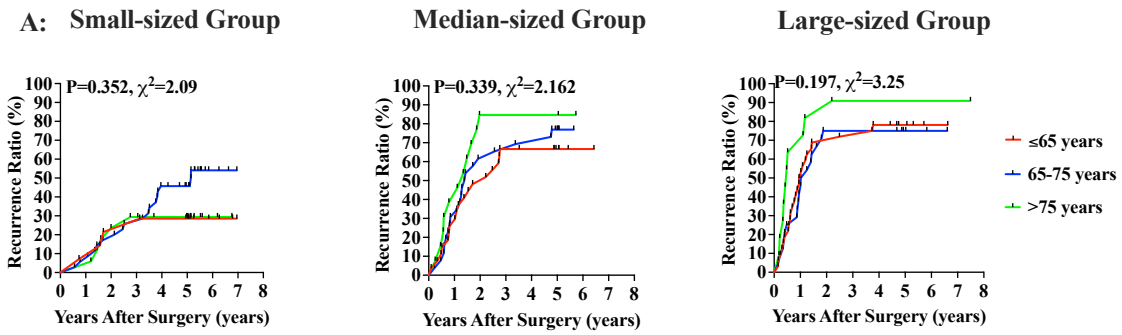

B: Small-sized Group

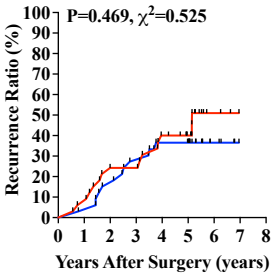


Median-sized Group

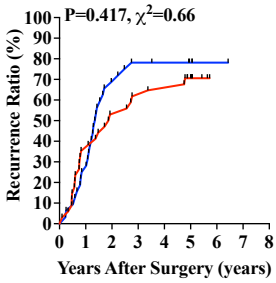


Large-sized Group

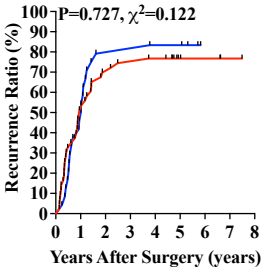


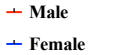


C:

Small-sized Group

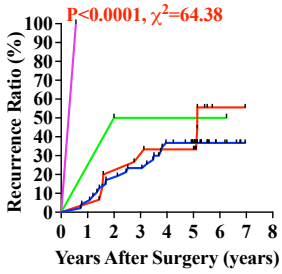


Median-sized Group

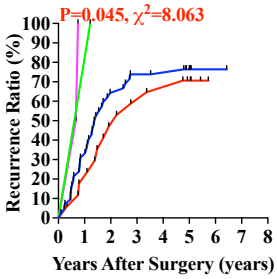


Large-sized Group

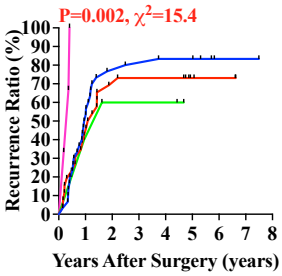


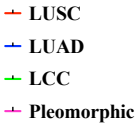


D:

Small-sized Group

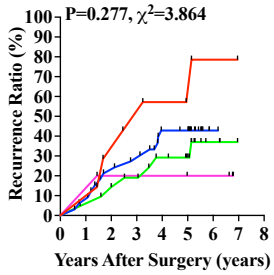


Median-sized Group

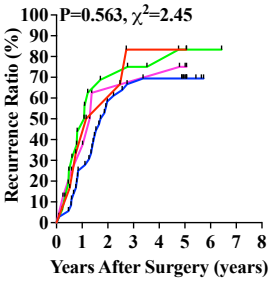


Large-sized Group

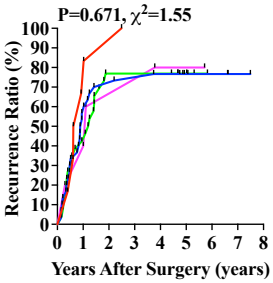


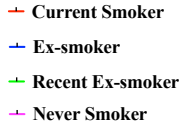


E:

Small-sized Group

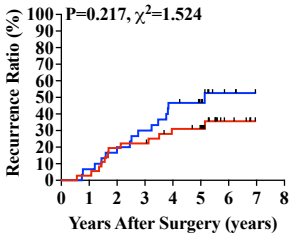


Median-sized Group

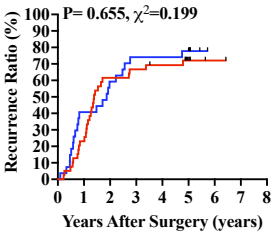


Large-sized Group

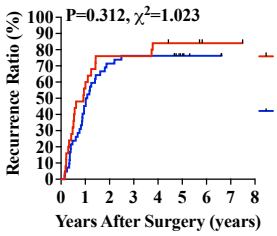


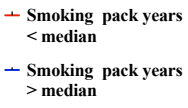


F:

Small-sized Group

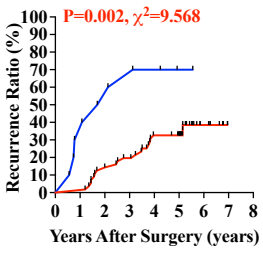


Median-sized Group

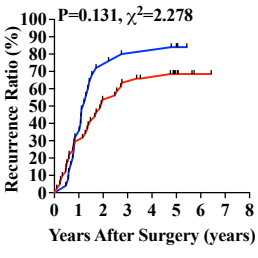


Large-sized Group

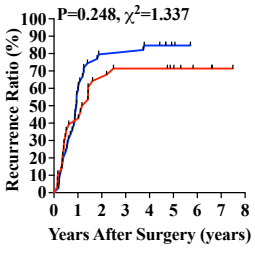


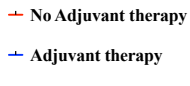

Fig. 3.12 Annual recurrence hazard ratios across primary tumour volume groups (small, median, and large), stratified by clinical and demographic subgroups. A: Age; B: Gender; C: Histology; D: Smoking status; E: Smoking pack years; F: Adjuvant therapy status. These plots illustrate how recurrence risk trends vary across tumour size categories within each subgroup.

## 3. Relationship between Primary Tumour Volume and Tumour Growth Rate

### 3.1 Primary Tumour Volume and Primary Growth Rate.

Tumour volume is known as a prognostic factor. However, few studies have explored whether there is a positive relationship between volume and growth rate. To explore this relationship, linear regression was used to assess the association between primary tumour volume and growth rate. Primary tumour volume showed a moderate positive correlation with primary tumour growth rate (Spearman's $r=0.58$, $P<0.0001$), suggesting that larger tumours are more likely to exhibit aggressive growth behaviour. The interval between diagnostic CT and staging PET/CT did not show a significant correlation with tumour growth rate ($P=0.64$). This weak correlation may be due to the fact that tumours don't always grow steadily over short periods, especially in slow-growing tumours. Apparent changes in size may also result from inflammation or necrosis rather than true tumour progression. Additionally, the limited cohort size may cause bias. Despite these limitations, ROC analysis identified a 17-day threshold to distinguish rapidly growing tumours (AUC 0.57), potentially helping to minimise delays between scans. Further validation in larger datasets using robust tumour growth modelling techniques is needed.

**TNM Stage Influence:** The hypothesis is that the baseline tumour growth rate would increase with advancing TNM stage, reflecting a more aggressive disease type in later stages. To test this, baseline burden across TNM stages was compared. In some cases, the initial scan may capture tumour necrosis or inflammation, leading to an overestimation of volume. Subsequent volume reduction may reflect resolution of inflammation rather than true tumour regression. While variations in baseline growth rate were observed, the distributions are approximately normal and consistent with overall trends in this study (Fig. 3.13). Patients in stages II–III had significantly faster baseline tumour growth rates than those in stage I, supporting the hypothesis that tumour growth accelerates with disease progression.

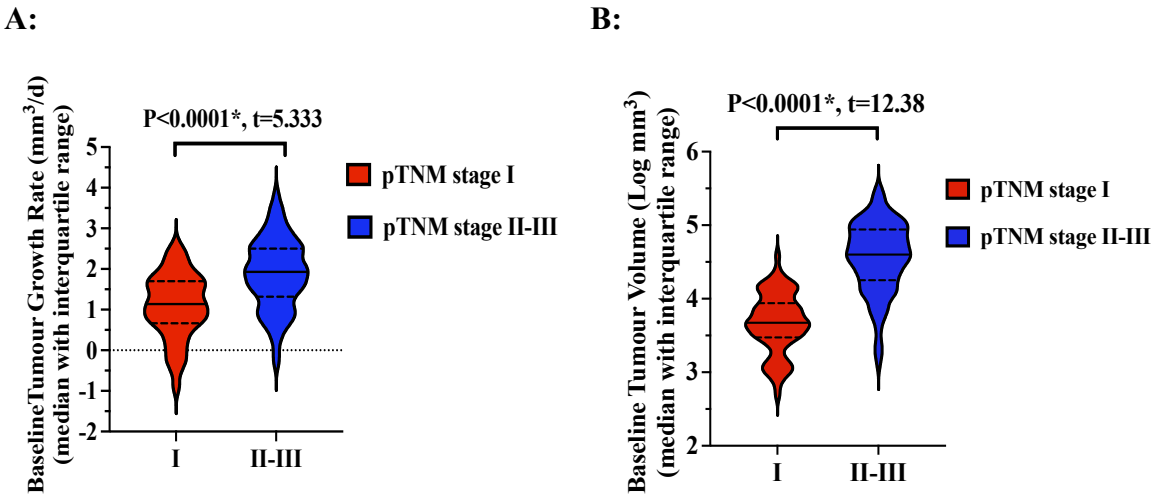


Fig. 3.13 Comparison of baseline tumour volume and growth rate across TNM stages.

Next, the relationship between relapse speed and relapse tumour burden was evaluated, based on the hypothesis that aggressive recurrence is associated with larger tumour volumes. A strong positive correlation was observed between relapse speed and relapse volume, indicating that faster-growing tumours at relapse are typically associated with greater relapse tumour burden (Fig. 3.14A). Interestingly, tumour stage at diagnosis was not positively correlated with either the size or the pace of recurrence (Fig. 3.14B–C), indicating that the TNM stage at diagnosis does not necessarily predict the relapse burden. These findings underscore the complexity of relapse biology and the limitations of staging in predicting post-treatment progression.

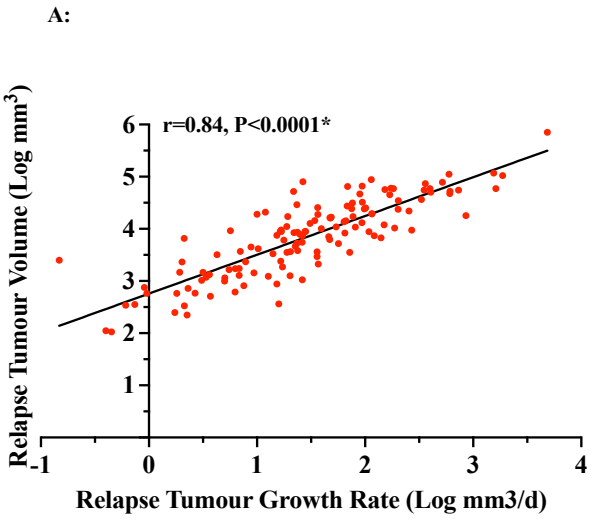

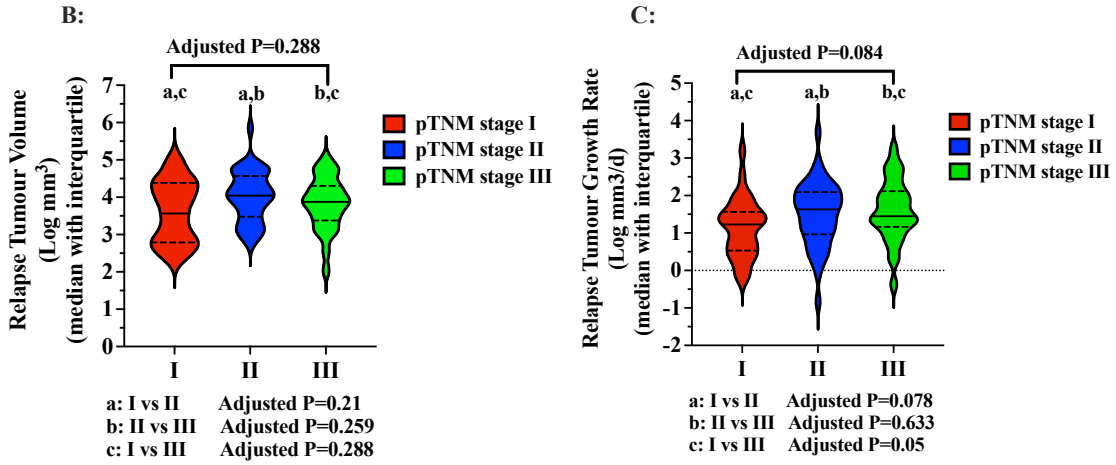


Fig. 3.14 Relationship of relapse tumour volume and growth rate in different TNM stages. P values were adjusted using the Benjamini–Hochberg False Discovery Rate (FDR) method to account for multiple comparisons (n=4 tests), both in figure B and C. The distributions are approximately normal in growth subgroups but not in volume subgroups.

**Location Influence:** Previous studies have shown that central tumours are prone to having larger tumours [160,161]. In this study, tumour volume showed a strong positive correlation with growth rate. Primary tumours located in the central lung were prone to be larger and having a faster growth rate, suggesting a potentially more aggressive behaviour (Fig. 3.15). These observations suggest that tumour location may influence growth patterns and could serve as an additional parameter for risk stratification. However, the anatomical definitions of "central" may vary across studies. Further validation in a larger cohort with uniform location criteria is needed.

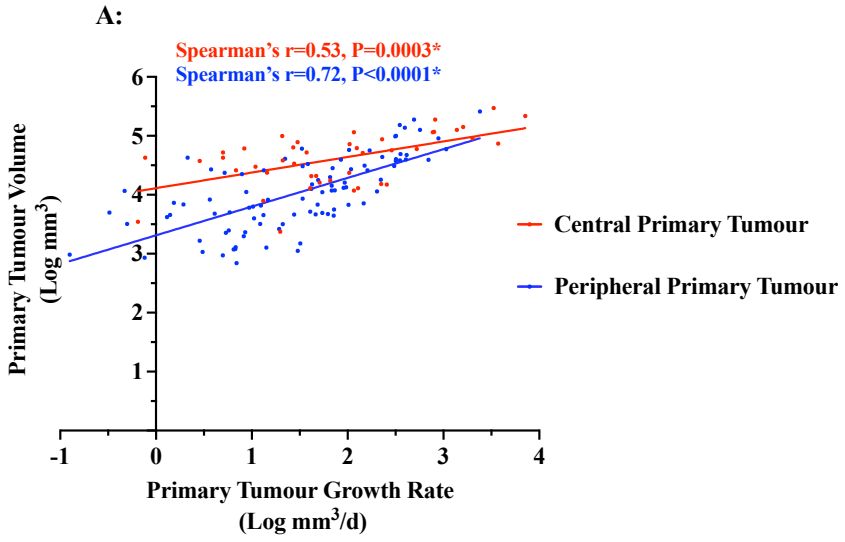

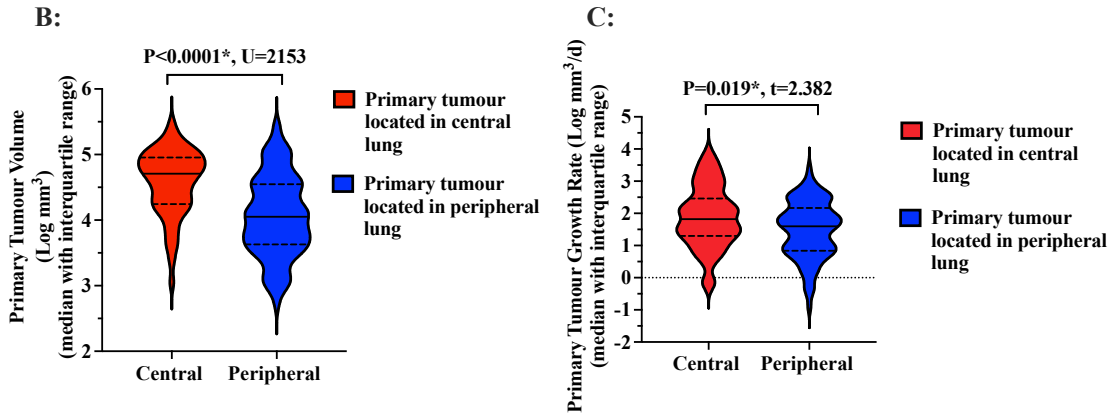


Fig. 3.15 Relationship between primary tumour volume and growth rate across distinct primary tumour locations. The distributions in figure B and C are both approximately normal.

**Metabolism Influence:** PET/CT scans, a noninvasive diagnostic tool for malignancies, offer insights into tumour metabolism through standardised uptake value (SUV). Analysis of this cohort revealed that both baseline tumour size (P<0.0001, Spearman's r=0.53) and tumour growth rate (P<0.0001, Spearman's r=0.48) moderately correlated with SUV values. However, variations in SUV measurement across hospitals might contribute to inconsistency in these associations.

### 3.2 Primary Tumour Volume and Relapse Growth Rate

Whether baseline volume is associated with relapse volume was tested, based on the assumption that larger tumours may seed more micrometastatic disease in clinical practice. Relapse volume exhibited a strong positive correlation with relapse speed across different primary tumour volume categories, with r values of 0.79, 0.73, and 0.62 for the first, second, and third tertiles, respectively (P<0.0001), suggesting that large tumours may contribute to more aggressive relapse. Additionally, primary tumour volume categories were significantly associated with relapse volume (P=0.028, F=3.674, Fig. 3.16A). Moreover, baseline volume showed a moderate negative correlation with DFS (Spearman's r= –0.52, P<0.0001), with smaller baseline volumes linked to longer DFS durations (Fig. 3.16B). In contrast, baseline tumour growth rate (initial growth rate) showed a weak correlation with relapse growth rate (Fig. 3.16C). These findings underscore the significance of initial tumour size in predicting both the likelihood and timing of post-surgery relapse. They suggest that larger initial tumours may be associated with more rapid and aggressive relapse, but treatment and the immune microenvironment

can also shape tumour dynamics. Further analysis, combining genomic and microenvironmental data, is needed.

**A:**

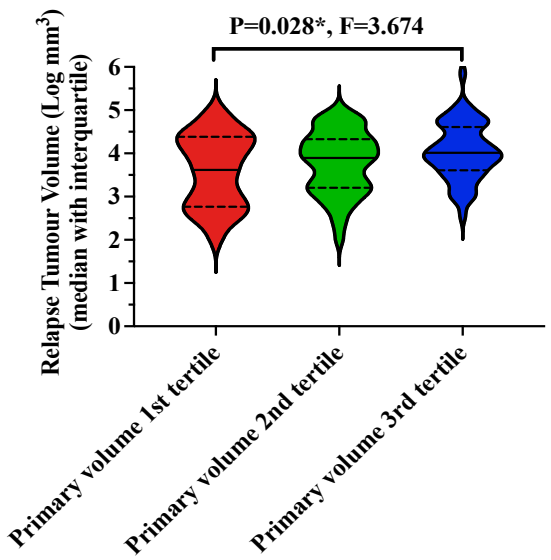


**B:**

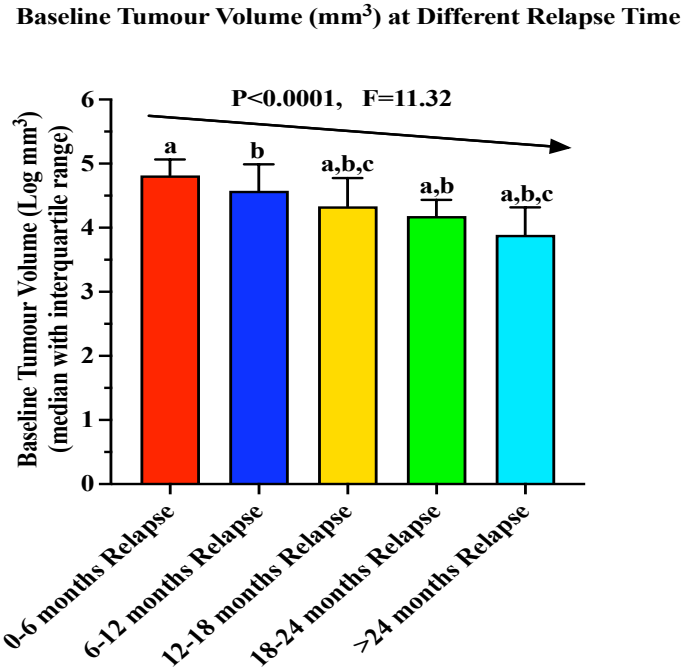

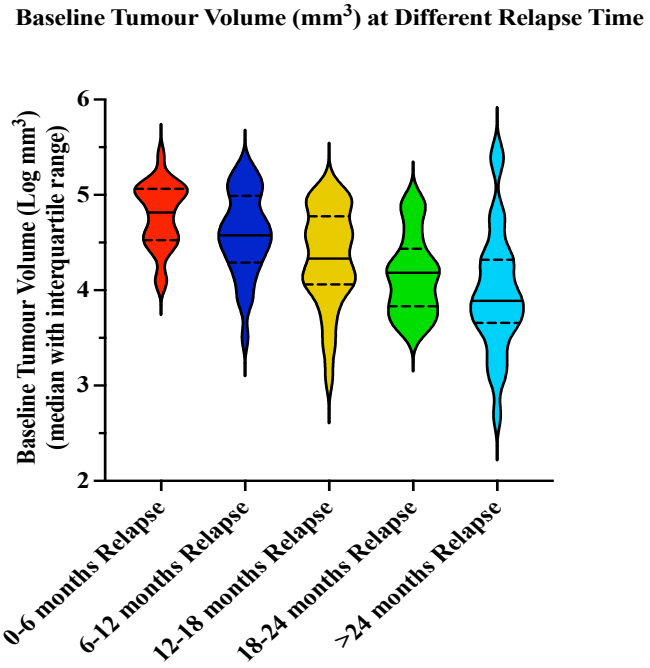


**C:**

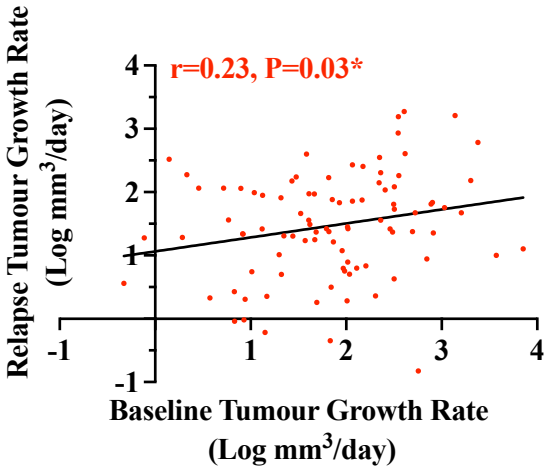


Fig. 3.16 Relationship between primary tumour volume, relapse volume, relapse speed and DFS. A: Distribution of relapse tumour volume across primary tumour volume subgroups. The distributions within each subgroup are approximately normal. B: Distribution of primary tumour volume among different relapse periods. The violin plot shows higher heterogeneity in primary tumour volumes among patients who relapsed beyond 24 months, primarily due to the presence of new primary tumours within this group, which could exhibit distinct biological behaviours. C: Relationship between primary tumour speed and relapse speed.

## 4. Primary Tumour Volume as a Predictor of Adjuvant Therapy Benefit in Stage IB

The optimal post-surgical management of Stage IB lung cancer remains under debate. According to the 7th edition of the AJCC TNM staging system, the NCCN recommended adjuvant therapy for patients with Stage II–III NSCLC after radical resection and advised considering it for high-risk Stage IB patients (pT2N0M0) [162,163]. With the updated 8th TNM staging system, former Stage IB patients are now categorised as either Stage IB (pT2aN0M0, with a tumour diameter under 4cm) or Stage IIA (pT2bN0M0, with a tumour diameter over 4cm) [162–164]. Research suggests that adjuvant chemotherapy is most beneficial for pN0 NSCLC tumours larger than 4cm [163]. To explore this further, a subgroup of 42 patients with pT2N0M0 tumours was analysed. Only three individuals received adjuvant therapy post-surgery, and they all experienced recurrence within 79, 399, and 443 days post-surgery. While limited by cohort size, these outcomes highlight the need for improved risk stratification markers in this population, particularly using manually contoured primary tumour volume. Univariate Cox regression analysis identified several factors associated with disease-free survival (DFS) in pT2N0M0 patients, including primary tumour size, growth rate, tumour stage, location and tumour morphology. Further multivariate Cox regression analysis demonstrated that primary tumour size, nodule necrosis, vessel attachment, emphysema, and margin status were significantly associated with DFS (Table 3.4).

Table 3.4 Univariate and multivariate Cox regression analyses identifying factors associated with recurrence in patients with stage pT2N0M0 NSCLC

| **Characteristic Factors** | **Univariate Analysis** | | |
|---|---|---|---|
| | **P value** | **HR** | **95%CI** |
| Primary Tumour Growth Rate | 0.002 | 1.01 | 1.00–1.01 |
| Primary Tumour Size | 0.001 | 8.61 | 2.3–32.24 |
| TNM Stage (IB vs IIA) | 0.012 | 2.85 | 1.21–6.69 |
| Location (Central vs Peripheral) | 0.023 | 0.35 | 0.14–0.9 |
| Vessel Attachment | 0.001 | 8.38 | 1.77–39.67 |
| Emphysema | 0.013 | 2.92 | 1.21–7.05 |
| Bronchial wall thickening | 0.034 | 2.73 | 1.08–6.88 |
| Nodule Shape | 0.037 | 1.52 | 1.02–2.26 |

| Characteristic Factors | Multivariate Analysis | | |
|---|---|---|---|
| | P value | HR | 95%CI |
| Primary Tumour Size | 0.013 | 5.92 | 1.46–24.06 |
| Nodule Necrosis | 0.018 | 6.15 | 1.37–27.55 |
| Vessel Attachment | 0.05 | 10.16 | 1–103.03 |
| Emphysema | 0.002 | 6.19 | 2–19.16 |
| Margin Status | 0.004 | 29.34 | 2.94–292.77 |

The receiver operating characteristic (ROC) curve analysis supported these findings, revealing that primary tumour size (AUC 0.72) and growth rate (AUC 0.74) are predictors of recurrence events (Fig. 3.17). Notably, the ROC curves exhibit non-smooth patterns, likely due to sampling variability—an expected limitation given the small cohort size and uneven subgroup distributions. Despite this limitation, the area under the curve (AUC) remains a valid factor, and the observed trends are still interpretable.

Similarly, C-index values from Cox models indicated that tumour volume (C-index = 0.7) and growth rate (C-index = 0.68) had reasonable discriminatory power in predicting DFS. Based on these findings, thresholds of 17,010 $mm^3$ in primary tumour volume or 58 $mm^3$/day in growth rate may help identify higher-risk patients (Fig. 3.17). While these results are not sufficient to guide treatment decisions, they suggest that volume and growth rate could be predictors in future risk-stratification strategies. Further validation of these values in a larger cohort is needed.

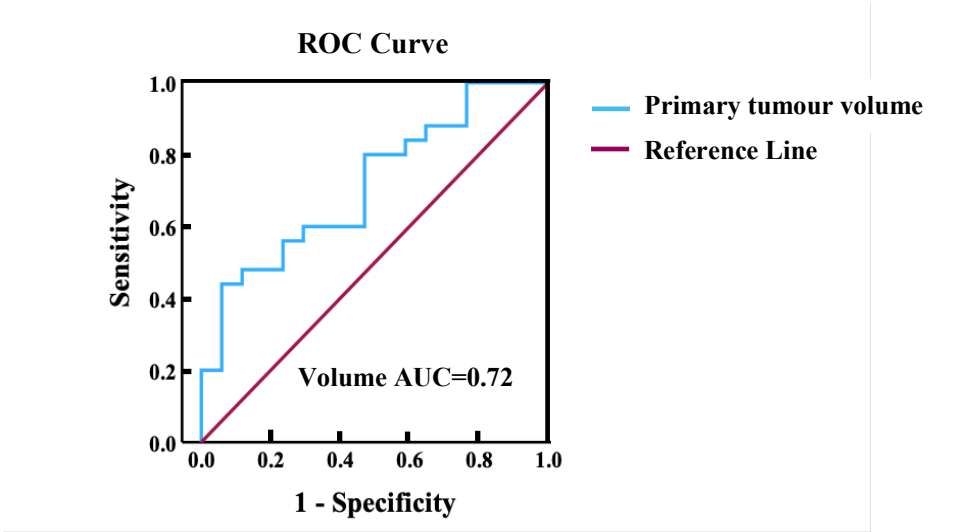


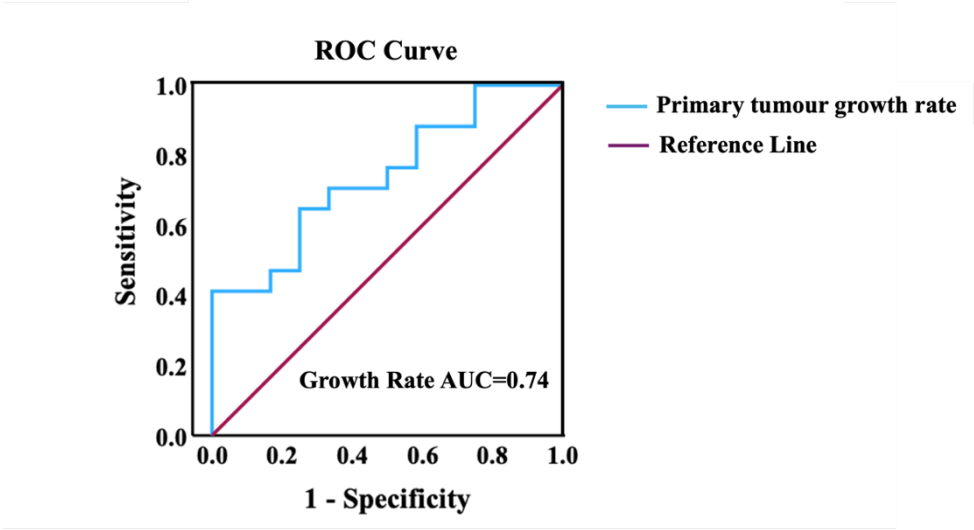


Fig. 3.17 Receiver Operating Characteristic (ROC) curve illustrating the predictive performance of tumour volume and growth rate for relapse in pT2N0M0 NSCLCs.

## Results Summary

1. **Tumour Volume as a Prognostic Indicator:** Manually contoured primary tumour volume showed a stronger association with relapse risk (HR=2.68, 95%CI 1.54–4.65), recurrence volumes, recurrence rates and extrathoracic relapses, compared to diameter-based volume calculation, pT staging, and pTNM staging.
2. **Recurrence Patterns by Histology, Gender and Smoking Status:** In this cohort, histology (LUAD vs. LUSC), gender and smoking status were not statistically associated with DFS. Smoking and TNM stages did not show a stepwise relationship with relapse tumour burden as well. However, current smokers showed an increased risk of relapse after 2.5 years post-surgery. Males accounted for 62.5% of relapses during the 9–12-month peak. LUSC relapse peaked at 9–12 and 15–18 months post-surgery; LUAD peaked at 12–15 months. LUSC, central, and advanced tumours were prone to having larger tumours, consistent with previous findings. These trends should be interpreted cautiously due to limited subgroup sizes.
3. **Volume Thresholds in pT2N0M0:** In a subgroup analysis of patients with pT2N0M0 tumours, preliminary thresholds for tumour volume (>17,010 $mm^3$) and growth rate (>58 $mm^3$/day) were associated with an increased risk of relapse. These values should be viewed as preliminary thresholds, given the small sample size, which limits statistical power.

# Discussion

Lung cancer remains one of the most fatal diseases in the world, with non-small cell lung cancer (NSCLC) taking up approximately 85% of all cases [2]. Surgery is the leading treatment for early-stage NSCLC [165]; however, the 5-year survival rate after surgery varies widely, ranging from 20% to 70% [152,153]. A major challenge in post-surgical management is the high probability of recurrence, ranging from 30% to 55% [166], largely attributed to the presence of undetected micrometastases at the time of surgery and the possibility that surgical or biopsy procedures may disseminate tumour cells [167]. In this cohort, 28% of patients relapsed within the first year post-surgery, with a decrease in relapse rates in subsequent years, leading to 64.2% experiencing a recurrence event by the fifth year. This result contrasts with findings from larger cohorts (>800 patients), which reported a 5-year recurrence rate of approximately 90% [146,168]. Such variation may be due to the differences in cohort size and composition, including the inclusion of small-cell lung cancers, which are associated with higher recurrence rates. The 1, 2, and 5-year recurrence rates in this cohort were 3.9%, 21.05% and 48.68% for stage I; 35.09%, 59.65% and 80.7% for stage II; 44.78%, 73.13% and 91.04% for stage III, respectively. These findings highlight that advanced stages are strongly associated with a faster recurrence trajectory, consistent with previous research [169–173]. Notably, the recurrence rate significantly declines after five years, aligning with broader research findings [174]. These findings underscore the urgent need to identify the factors that can predict recurrence.

Hence, this study focuses on understanding recurrence mechanisms and identifying predictive markers for clinical outcomes. Imaging is a novel, noninvasive method for detecting lung recurrence and is widely used today. In this study, I longitudinally contoured diagnostic, follow-up, relapse/progression, and final pre-mortem scans for 200 patients. In total, over 2,400 scans and more than 3,200 individual lesions were manually contoured. This comprehensive dataset enables continuous calculation of lesion-specific volume and growth rate across the disease course. To date, no prior study has achieved this level of detailed, lesion-level longitudinal annotation. Among imaging factors, primary tumour size emerges as a key predictive marker. Traditionally, the largest axial diameter is used to represent tumour size. Unfortunately, reliance on two-dimensional measurements performed by radiologists leads to inter- and intra-observer variability and

fails to capture the complexity of irregular tumour morphology [175–177]. Notably, in this cohort, the manual contouring method resulted in a ≥20% reduction in volume for 55% of patients compared to the CT diameter-based volumetric calculations. In contrast, 14% of patients showed a ≥20% increase in volume. Additionally, the diameter measurements may be biased due to tissue shrinkage after removal from the patients. Advanced auto-segmentation algorithms have been explored to address these limitations by extracting three-dimensional tumour volumes. However, challenges remain, particularly for ground-glass nodules with low contrast [178,179]. This study contributes to this ongoing exploration but is limited by its small cohort size and the absence of a comparative analysis between auto-segmented and manually contoured outcomes [180]. Wormanns [177] utilised the Siemens LungCare software to determine the volume of 151 pulmonary nodules in 10 patients, addressing the variability of tumour volume measurements. Subsequent manual verification by radiation oncologists showed 95% limits of agreement ranging from –20.4% to 21.9%, with greater variation observed in smaller lung tumours [178]. Controversy remains between auto-segmentation and manual contouring [181], particularly in my cohort, which involves target regions from diverse anatomical sites and variable imaging conditions. This research utilised the largest imaging dataset on tumour progression, laying the groundwork for using precisely plotted tumour volumes to predict and explore the factors influencing recurrence patterns. With more than 90% of volume measurements agreeing within a 20% margin after manual contouring and individual lesion variation remaining below 8%, this work also establishes a benchmark for future improvements in auto-segmentation techniques.

Tumour volume, unlike conventional linear diameter used in pT staging or RECIST criteria, provides more comprehensive information on the actual tumour burden, especially for irregular tumours. The findings from this study show that manually contoured primary tumour volume is a stronger predictor of relapse risk, recurrence patterns, and overall survival than diameter-based volume estimates, pT staging, and pTNM staging. These findings suggest that volumetric assessment may enhance risk classifications, particularly in borderline-stage groups. There is ongoing controversy regarding adjuvant treatment for small tumours, especially in early-stage patients. According to the 7$^{th}$ edition of the AJCC TNM staging system, the NCCN recommended adjuvant therapy for Stage II–III NSCLC patients after radical resection, and advised consideration for high-risk Stage IB patients (pT2N0M0) [162,163]. The Lung Adjuvant

Cisplatin Evaluation (LACE) meta-analysis demonstrated a trend toward benefit in IB and a significant benefit in II N1 and IIIA (especially N2), with an average improvement of 5% in 5-year survival [182]. With the updated 8th TNM staging system, former Stage IB patients are now categorised as either Stage IB (pT2aN0M0, with a tumour diameter under 4cm) or Stage IIA (pT2bN0M0, with a tumour diameter over 4cm) [162–164]. Previous research suggests that adjuvant chemotherapy is most beneficial for pN0 NSCLC tumours larger than 4cm [163]. However, linear dimensions alone can't reflect true tumour burdens. In this small cohort, volumetric assessment provided additional discriminatory value and could help refine treatment recommendations, showing its potential as a routine clinical predictor in future guidelines.

Baseline tumour growth rates showed a strong correlation with baseline volumes but a weak correlation with relapse growth rates; this may be because of the impact of treatments and immune microenvironmental factors. This weak correlation in post-treatment growth rates aligns with findings from the TRACERx studies, which showed that treated micro-metastases post-surgery frequently harbour private monoclonal driver mutations absent in the primary tumour, indicating treatment-driven evolution of resistant clones. In contrast, untreated metastases remain polyclonal, like primary tumours [23,26]. Apoptotic cells or cancer stem cells can also stimulate repopulation post-irradiation, further complicating growth dynamics. Immune escape mechanisms, including neoantigen editing or loss of HLA expression, play a vital role in shaping tumour evolution. LUAD tends to experience truncal immune selection, while LUSC shows more subclonal selection, suggesting different evolutionary pressures [107]. While the intervals between CT and PET/CT did not correlate significantly with tumour growth rate, this may reflect the variability in growth dynamics, particularly in slow-growing tumours. Although genetic mutations such as EGFR and ALK mutations, subclonal copy number alterations, and the subclonal mutations index [39,42,107,183,184] have been linked to aggressive tumour behaviour, no study to date has directly linked specific genomic features to baseline growth rate. Identifying genetic predictors could reduce the need for follow-up imaging and help tailor surveillance intensity in future clinical practice.

Apart from the tumour volume, other researchers have demonstrated that age, smoking status, TNM stage, pT, pN, SUV value, the status of lymphovascular, and visceral pleural invasion can predict prognosis in NSCLC [173,185,186]. In this dataset, univariate Cox

regression analysis identified several factors associated with disease-free survival (DFS) in NSCLC patients. Further multivariate analysis highlighted that baseline tumour volume, combined with other clinical and imaging factors, was a key predictor of recurrence risk. Unlike pTNM staging, tumour volume showed a stepwise relationship with both relapse volume and speed, suggesting that TNM staging alone may not be a sufficient predictor of recurrence. Large-sized tumours had the highest recurrence rate (nearly 50%) within the first year, median-sized tumours peaked in the second year, and small tumours showed a steady increase, peaking in the fourth year. Previous studies have confirmed that gross tumour volume predicts prognosis more effectively than pT and pTNM staging; however, these studies were limited to advanced, inoperable lung cancers [187–189] and didn't explore the relationship between primary tumours, relapse sites, and relapse burdens [190]. In contrast, this study specifically showed that primary tumour volume performs better in predicting prognosis, relapse site and relapse tumour burden compared to pT and pTNM staging. These findings suggest that using primary tumour volume to guide clinical practice may be more effective than traditional staging systems.

To further explore the potential differences in recurrence trajectories, it would be valuable to analyse patients based on distinct clinical characteristics and imaging parameters. These variables may influence the timing of recurrence and could provide important insights into how different subgroups experience disease progression.

The role of age in lung cancer recurrence remains complex, with studies offering diverse results. Some research [191,192] has reported that age is a significant prognostic factor for lung cancers, suggesting that older age may be associated with poorer outcomes. Other observations challenge this assertion. Goodgame's [193] study showed no significant disparity in recurrence rates between younger and older cohorts, though older patients showed poorer overall survival. Similarly, Zhu [194] demonstrated that patients aged 65 and above faced an increased risk over time, indicating the impact of age on post-surgery outcomes. However, the argument persists that age alone might not serve as a reliable prognostic marker due to the increased risk of comorbidities and complications in the elderly, which could bias outcomes independently of cancer progression. This perspective is supported by the findings from this study, which reveal a complex relationship between age and annual recurrence rates. Tumour recurrence rates did increase with tumour size across all age subgroups, but no clear overall correlation between age and recurrence rates

was observed. Younger patients with smaller tumours had lower hazard ratios, whereas those aged 65–75 with smaller primary tumours showed an increase in recurrence rates after three years post-surgery. Similarly, Yamamoto also found that primary tumour size was related to survival across different age groups [195]. These findings challenge the use of chronological age alone as a prognostic indicator.

Interestingly, smoking status did not show a significant correlation with DFS, which contrasts with the conventional understanding of its impact on lung cancer outcomes. This discrepancy may be due to the limited cohort size. Expanding the cohort size in future studies would be necessary to further investigate these findings. Zhu [194] demonstrated distinct hazard rate curves for smokers and non-smokers, with smokers experiencing a lower initial hazard peak, suggesting an earlier risk of recurrence. This observation aligns with my data, which indicates current smokers face a substantially increased risk of recurrence over time, surpassing that of ex-smokers, never smokers, and recent ex-smokers after 2.5 years, although the difference was not statistically significant. The relationship between smoking status and lung cancer outcomes is complicated, revealing significant differences in recurrence rates and genetic mutations based on smoking history. A previous study has shown that LUAD has a higher clonal and subclonal mutational burden in smokers, indicating worse outcomes [109]. In this cohort, no significant difference was observed in DFS between current smokers and non-smokers with LUAD. A 2023 study published in *Nature* [107] may help explain this phenomenon, revealing that 8% of lung adenocarcinoma (LUAD) cancers did not display tobacco-induced mutagenesis markers despite a smoking history and presented similar oncogenic mutation rates to those of never smokers. Moreover, smoking status may show a propensity in primary tumour anatomical location, with research noting an increased prevalence of truncal SBS4-associated mutations located on the right side of the lung compared with the left side and in the upper or middle lobe compared with the lower lobe areas more susceptible to tobacco carcinogen exposures [107]. In my cohort, the tobacco exposure ratio in the right lung for NSCLC was 76/4 (13 current smokers, 36 ex-smokers, 27 recent ex-smokers and 4 never smokers), which is higher than in the left lung, highlighting the potential that smokers are more likely to have tumours in the right lung. Personalised prognosis and treatment strategies that account for the complex influences of smoking history and anatomical tumour characteristics on lung cancer outcomes are highly needed.

Histology plays a crucial role in determining the prognosis of lung cancer, with distinct patterns of recurrence observed across different histological types. Research has indicated that LUSC and LUAD follow different trajectories in terms of hazard peaks, with LUSC peaking at 9 months and LUAD at 15 months post-surgery window [156]. This trend was confirmed by this cohort data, showing that the 12–15 months post-surgery window is the most prevalent period for recurrence in LUAD, with LUSC exhibiting an initial peak in recurrences between 9–12 months, followed by a second peak at 15–18 months, particularly among male patients. Furthermore, LUAD tends to present with smaller tumours and slower growth rates, but it metastasises more easily compared to LUSC [159]. Similar results were shown within my cohort: LUAD had smaller sizes than LUSC in both primary and relapse tumours. Within this cohort, LUSC patients displayed a mild increase in recurrence hazard at later stages (after 5 years post-surgery) compared to LUAD in smaller tumours. LUAD patients with larger tumours showed higher recurrence rates than LUSCs, although the difference is not significant. Central tumours were prone to having larger sizes and faster growth rates, suggesting a more aggressive behaviour, as confirmed by previous studies as well [160,161]. However, due to the limited sample size in this cohort, these conclusions should be considered preliminary and require validation in larger datasets before they can be applied to clinical practice.

The analysis of recurrence patterns by gender reveals slight differences. A study has identified distinct temporal peaks in recurrence risk post-surgery, with males experiencing a peak increase in recurrence risk at 9 months, while females show a more prolonged risk, period peaking at 15 months [156]. This pattern aligns with Watanabe's findings of an acute recurrence peak within the first year for men and a broader peak occurring between 2 and 3 years for women [196]. Findings from this cohort further support these observations, although the difference in recurrence timing between genders was not significant. It was noted that a higher proportion of males (62.5%) experienced recurrence within 9–12 months post-surgery compared to females. Exploring the relationship between primary tumour size and gender in greater detail, the results showed that females had a slightly higher recurrence rate than males after 1 year post-surgery, particularly in larger tumour sizes. These findings may potentially aid in predicting relapse time across genders, although no significant difference was observed.

SUV values derived from PET/CT scans reflect tumour metabolic activity. In this cohort, a moderate positive correlation was observed between primary tumour volume measured from CT components and SUV values. This moderate correlation suggests that tumour volume, as delineated by CT, might not adequately reflect tumour metabolic activity, likely due to the inclusion of necrotic, cavitary, or metabolically inactive regions that dilute the PET signal. Additionally, the variability in SUV measurements across different institutions may introduce further bias. Further studies should normalise the SUV standards and exclude non-metabolically active regions to ensure more accurate and consistent assessments.

In summary, tumour volume and growth rate can be promising imaging biomarkers that could improve relapse stratification, complement current staging systems, and aid in clinical decision-making. However, this study has several limitations that should be considered in future research: First, the small cohort size and missing follow-up scans for some patients may have introduced bias and limited the generalisability of the results. Second, this study did not include genetic data; future research could explore the relationships between gene mutations, circulating tumour DNA (ctDNA), and tumour volume to better understand recurrence mechanisms. Third, the precision of tumour contouring was affected by variability in imaging quality, techniques and modalities across different hospitals. As this is a ten-year study, advancements in imaging techniques during this period introduced variability that affected consistency. These discrepancies introduce errors, particularly impacting the accuracy of smaller tumour measurements. Future research could quantify error margins by anatomical location to improve reliability. Despite these challenges, most contouring variations remained within a 10% threshold, supporting the credibility of the findings. Additionally, as a retrospective study, potential confounders (e.g., treatment heterogeneity, comorbidities) further limit the ability to draw definitive criteria for clinical decision-making. In conclusion, despite the presence of limitations, this work provides valuable preliminary evidence supporting the prognostic value of primary tumour volume and growth rate in NSCLC, laying the groundwork for future comprehensive studies.

# Conclusions

Manually contoured primary tumour volume is a stronger predictor of relapse than diameter-based calculation, pT stage and pTNM stage. Larger tumours are associated with earlier relapse, extrathoracic relapse and higher recurrence burden. In pT2N0M0 tumours, preliminary thresholds for tumour volume (>17,010 $mm^3$) and growth rate (>58 $mm^3$/day) are identified. While these metrics may help stratify adjuvant therapy, they are not clinically applicable without further prospective validation.

# Chapter Four

# Patterns and Outcomes of Recurrence and Progression: Tumour Dynamics, Timing, and Location in Non-Small Cell Lung Cancer

## Highlights

**Aims:** This study aims to explore and characterise the heterogeneity of relapse, progression, and prognosis across different tumour sites and growth patterns in non-small cell lung cancer. Specifically, it seeks to:

1. Investigate the temporal and spatial diversity of tumour relapse.
2. Examine the patterns of progression with an emphasis on tumour burden, anatomical location, and growth rate.
3. Assess the prognostic impact of site-specific recurrences on patient outcomes.

**Methods:** Relapse speed was calculated as described in the Methodology chapter. Cox regression models were applied to assess differences in survival across groups. Pearson correlation analysis was used to detect the relationship between volume and growth rate. For group comparisons, either the t-test or the Mann–Whitney U test was applied for two groups, and ANOVA or the Wilcoxon rank-sum test was used for three or more groups, depending on the data distribution. A Sankey plot was generated to visualise the progression pathways of tumour recurrence.

**Results:**

**1. Heterogeneity of relapse:**

- **Temporal and anatomical diversity:** 9–15 months post-surgery was the most common period for relapse events, with the lung being the most common initial site for intrathoracic relapse, irrespective of the tumour's extent, consistent with previous studies. Local lung relapsed earliest (median 346 days), while intrathoracic lymph node (especially N2) ranked as the second most common relapse site. No consistent link was found between lymph node status at diagnosis and later relapse,

differing from prior literature. Bone emerged as the most frequent extrathoracic relapse site in this cohort, and this contrasts with previous literature, which reported the brain as the most common extrathoracic site.

Limited intrathoracic tumour burden corresponded with the longest DFS, whereas extensive extrathoracic tumour burden resulted in the shortest DFS, as evidenced by other researchers as well. This study specifically revealed that a subset of initial oligometastatic relapses progressed to widespread tumour burden and had earlier relapses. Site-specific burden also differed: poly-extrathoracic relapse frequently involved the bone, whereas the brain was more common in oligo-extrathoracic relapse.

- **Relapse growth rate diversity:** This study notably revealed that relapse tumour growth rates increased alongside lesion growth speed, particularly in extrathoracic sites, leading to a massive total tumour burden and a worse prognosis, but was not associated with the number of progression events. Interestingly, the relapse tumour growth rate before treatment correlated weakly with the post-treatment tumour growth rate. These insights suggest that dynamic growth features may offer prognostic value.

**2. Heterogeneity of progression:**

- **Site-specific relapse and subsequent progression:** Ipsilateral lung relapse was the most common relapse type in single-lung relapse, and the median PFS was 244 days for new lesion progression. Key indicators of ipsilateral relapse included a primary tumour in the right upper lung, slow relapse speed, female gender, diagnosis of LUAD, and pleural attachment. Predictors of exclusive brain relapse were related to advanced stages (at least stage IIB), large primary tumours in the peripheral lung, LUAD, and pleural involvement (as confirmed by other studies as well), rapid relapse speed, and the absence of air bronchogram. These findings remain exploratory due to the limited sample size.
- **Impact of tumour volumes and lesion counts on progression:** New findings in this research showed that relapse growth rate correlated with both larger tumour volume and faster progression speeds. In contrast, lesion count alone did not predict growth or survival. These results suggest that tumour volume and speed may better reflect biological aggressiveness than lesion number.

- **Site and progression patterns:** New findings in this research showed that patients with intrathoracic relapses tended to develop new lesions. In contrast, extrathoracic relapses often experienced a mix of new lesions and local expansions, indicating more complex and aggressive progression modes. Progression into or within extrathoracic locations was associated with shorter survival and greater aggressiveness.

**3. Site-specific prognosis:**

Early involvement of the bone, intrathoracic pleura, extrathoracic lymph node, brain and extrathoracic soft tissue can impact prognosis. Patients with lung-only relapses had better outcomes than those who never relapsed in the lung or who had multiorgan relapses. Conversely, brain metastases were linked to the worst survival outcomes, consistent with previous findings. While these site-specific findings are clinically relevant, small subgroup sizes limit statistical power and generalisability.

**Conclusions:** This study identifies several novel findings: larger tumour volumes, faster progression, and extrathoracic involvement are associated with higher initial relapse rates and poorer outcomes, highlighting that volume and speed may serve as stronger prognostic indicators than lesion count alone. Relapse and progression patterns vary by timing, anatomical location, and growth characteristics, with intrathoracic recurrence—especially in the lung—being most common and generally associated with better outcomes. Poor prognosis is observed in patients with relapses involving multiple organs or the brain, consistent with previous research. Notably, intrathoracic relapses often present as new lesions or localised expansions, while extrathoracic relapses frequently involve both new and expanding lesions, indicating more complex progression and worse survival.

# Introduction

Non-small cell lung cancer (NSCLC) remains a leading cause of cancer-related death, with about a 25% 5-year overall survival rate and more than 60% of patients experiencing relapse [1]. Survival rates vary significantly depending on the type of relapse—regional, localised, or distant—at 30.8%, 57.4%, and 5.2%, respectively [197]. The timing and location of relapse remain contentious, with some studies highlighting early and frequent distant recurrences, notably in the central nervous system. In contrast, others identify the lung as the primary site for relapse [90,146,169]. Moreover, a meta-analysis showed that 60% of NSCLCs develop brain recurrence, followed by metastases to the contralateral lung, lymph nodes, liver, and adrenal glands [8]. These results underscore the need to identify predictive markers for recurrence sites and their progression pathways.

*Oligometastatic* disease represents a condition with limited tumour spread, typically defined by no more than five metastases and involvement of up to three organs [9,10]. *Polymetastatic* disease represents an advanced stage of cancer characterised by widespread tumour dissemination, often requiring systemic treatment. Mortality rates vary significantly with sites and the number of metastases, as illustrated by a study analysing the outcomes of 45423 NSCLCs with distant metastases. The results demonstrated that the highest mortality was associated with liver and multiorgan involvement [28]. Furthermore, the number and location of extracranial metastases in NSCLC patients with brain involvement may have a different impact on survival [198]. Interestingly, the late phase of liver regeneration has been shown to promote lung metastases in colorectal cancers [30]. All these findings above suggest that the organ-specific and temporal characteristics of metastases are associated with distinct clinical outcomes, potentially explaining why many lung cancers fail to respond to current treatment strategies despite ongoing advances.

Research into tumour heterogeneity over the past decades has shed light on the presence of distinct subclonal populations within the primary tumour, contributing to variability in tumour growth rates and relapse patterns [4,107,108,129]. Notably, early metastatic divergence tends to occur more in smaller tumours and among smokers. Less than 20% of metastatic relapses are attributed to primary lymph node involvement, indicating that metastatic

potential varies among patients and is unrelated to the route of subsequent recurrences [115]. Given the observed differences in tumour growth dynamics and affected organs, a comprehensive understanding of progression diversity is essential to be further discussed.

In this study, progression-free survival (PFS) is defined as the interval from the initiation of post-relapse treatment to disease progression, death, or last follow-up. For patients who did not receive therapy, PFS is measured from the date of the corresponding scan to progression, death, or last follow-up. This study aims to investigate the heterogeneity of relapse in non-small cell lung cancer (NSCLC), with a specific focus on the sequence of anatomical involvement and changes in tumour volume. The ultimate goal is to uncover patterns or factors that may influence prognosis and treatment strategies for NSCLC. Understanding the variability in relapse characteristics could facilitate more personalised and practical approaches for managing and potentially preventing relapse in lung cancer patients.

# Results

## 1. Relapsed Patients' Clinical Characteristics and Imaging Factors in the Study Cohort

130 stage I–III non-small cell lung cancer (NSCLC) patients relapsed between 6 January 2015 and 10 March 2022. The last follow-up was 22 January 2024. The median follow-up duration was 1183 days (range: 88–3018 days). The median interval between diagnostic CT and staging PET/CT was 18 days (Interquartile Range [IQR], 12–34 days). The median time from PET/CT to surgery was 36 days (Interquartile Range [IQR], 29–49 days). Most patients had right upper lobe tumours (35%), peripheral primary tumours (64%), and invasive adenocarcinomas (LUAD, 58%). At initial relapse, 56% of patients presented with intrathoracic disease, 20% with extrathoracic relapse, and 24% with both. Relapse burden was classified as limited at initial relapse in 56% of patients, oligometastatic with later progression to polymetastatic in 20%, and presenting as multiple metastases at the first recurrence in 24% of cases. Half of the patients experienced relapse in a single organ, primarily in the lung, with the bone being the most distant organ of relapse. More than half the patients presented with 2–5 lesions at relapse (Details are listed in Table 4.1).

Table 4.1 Clinical characteristics of 130 patients included in the relapse analysis cohort

| **Factors** | | **Patient Number (n=)** | **Early Relapse (n=65)** | **Late Relapse (n=65)** | **Adjusted P-Value** |
|---|---|---|---|---|---|
| *Sex* | Male | 73 | 39 | 34 | 0.551 |
| | Female | 57 | 26 | 31 | |
| *Age* | <66 | 48 | 28 | 20 | 0.459 |
| | 66–75 | 56 | 24 | 32 | |
| | >75 | 26 | 13 | 13 | |
| *Smoking Status* | Ex-Smoker | 63 | 30 | 33 | 0.875 |
| | Recent Ex- | 40 | 22 | 18 | |
| | Current Smoker | 16 | 7 | 9 | |
| | Never Smoker | 11 | 6 | 5 | |

| | | | | | |
|---|---|---|---|---|---|
| *Smoking* | ≤36.75 (median) | 66 | 34 | 32 | 0.862 |
| *Index* | >36.75 (median) | 64 | 31 | 33 | |
| *Ethnicity* | White British | 117 | 50 | 57 | 0.187 |
| | White Irish | 6 | 4 | 2 | |
| | White European | 6 | 6 | 0 | |
| | Other | 11 | 5 | 6 | |
| *Mutation* | None | 122 | 61 | 61 | 1 |
| | EGFR | 6 | 3 | 3 | |
| | ALK±EGFR | 2 | 1 | 1 | |
| *pT* | T1 | 20 | 1 | 19 | 0.001* |
| | T2 | 55 | 25 | 30 | |
| | T3 | 33 | 21 | 12 | |
| | T4 | 22 | 18 | 4 | |
| *pN* | 0 | 69 | 29 | 40 | 0.042* |
| | 1 | 28 | 21 | 7 | |
| | 2 | 33 | 15 | 18 | |
| *pTNM* | I | 31 | 4 | 27 | 0.001* |
| | II | 42 | 26 | 16 | |
| | III | 57 | 35 | 22 | |
| *Histology* | LUSC | 38 | 17 | 21 | 0.382 |
| | LUAD | 75 | 36 | 39 | |
| | Other | 17 | 12 | 5 | |
| *Surgery* | Lobectomy | 106 | 52 | 54 | 0.447 |
| | Segmentectomy or Wedge | 9 | 3 | 6 | |
| | Others | 15 | 10 | 5 | |
| *Resection Margin* | R0 | 117 | 57 | 60 | 0.709 |
| | R1 or R2 | 13 | 8 | 5 | |
| *Primary Tumour Location* | LLL | 17 | 7 | 10 | 0.875 |
| | RLL | 36 | 17 | 19 | |
| | LUL | 32 | 17 | 15 | |
| | RU/ML | 45 | 24 | 21 | |
| | Central | 47 | 27 | 20 | 0.382 |

| | | | | | |
|---|---|---|---|---|---|
| *Axial Location* | Peripheral | 83 | 38 | 45 | |
| *Adjuvant Therapy* | Chemotherapy | 50 | 33 | 17 | 0.025* |
| | Radiotherapy or Chemoradiation | 11 | 7 | 4 | |
| | None | 69 | 25 | 44 | |
| *Relapse Location* | Intrathoracic | 73 | 28 | 45 | 0.042* |
| | Extrathoracic | 26 | 17 | 9 | |
| | Both | 31 | 20 | 11 | |
| *Relapse Organ Number* | 1 | 66 | 28 | 38 | 0.321 |
| | 2 | 33 | 16 | 17 | |
| | 3 | 20 | 14 | 6 | |
| | >3 | 11 | 7 | 4 | |
| *Relapse Lesion* | 1 | 44 | 20 | 24 | 0.277 |
| | 2–5 | 65 | 38 | 27 | |
| | >5 | 21 | 7 | 14 | |
| *Metastasis Pattern* | Oligometastatic | 72 | 35 | 37 | 0.709 |
| | Oligo to Poly | 27 | 16 | 11 | |
| | Polymetastatic | 31 | 14 | 17 | |

P values were adjusted using the Benjamini–Hochberg False Discovery Rate (FDR) method to account for multiple comparisons (n=19 tests).

The first 15 months post-surgery was the most common period for relapse events, especially between 12–15 months, followed by 9–12 months (Fig. 4.1). However, due to the small number of patients in each timeframe, the differences may not be statistically significant but still indicate a potential trend. Specifically, a fluctuation was observed in the 36–48 months period, during which some new primary lung tumours recurred. The median time from post-surgery to relapse was 404 days (Interquartile Range [IQR], 216–676 days). Hence, early relapse was defined as recurrence within 404 days (13 months) post-surgery. The median disease-free survival (DFS) for patients with early versus late relapse was 214 and 681 days, respectively. Patients in the early relapse group showed more advanced stages (T, N, and overall TNM stages) and were more likely to have received adjuvant therapy than those in the late relapse group (Table 4.1).

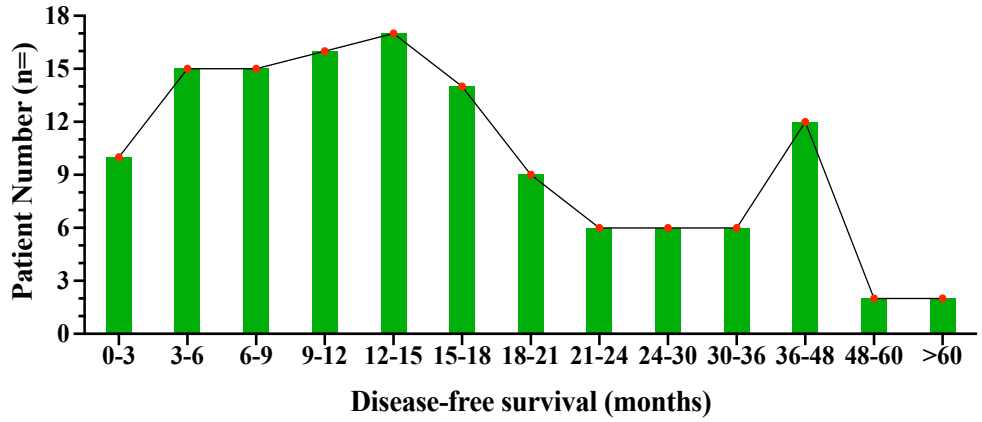


Fig. 4.1 Distribution of disease-free survival (DFS) times among relapsed patients following surgery.

## 2. Heterogeneity of Relapses in Resected NSCLC

### 2.1 Diversity in the Timing of Initial Organ Relapse

To explore the frequency and timing of organ initial relapse in NSCLC patients, the time of each organ's appearance was calculated among 130 relapsed patients. The results showed that different organs had distinct patterns of recurrence, with the lung emerging as the most common organ for intrathoracic recurrence, independent of tumour burden. Furthermore, the median time from surgery to lung recurrence varied by stage: 712 days for Stage I (n=18), 357 days for Stage II (n=26), and 333 days for Stage III (n=30), with an overall median of 428 days across 74 patients. Additionally, eight patients developed new primary lung tumours, with a median time to emergence of 686 days, indicating a separate trajectory of progression. (Fig. 4.2A–B)

Among all types of lung recurrence, local relapse occurred the earliest, followed by bilateral lung relapse and then only contralateral lung relapse. The analysis further detailed that the time to local recurrence decreased with advancing tumour stage, suggesting that more advanced tumours tend to relapse more quickly. Specifically, among lung relapse cases, stage III patients with local recurrence had the earliest median relapse at 191 days (n=4), while stage II patients with contralateral lung recurrence had the latest relapse with 1374 days (n=1). (Fig. 4.2B)

The second most frequent organ of recurrence was the intrathoracic lymph node, with a median recurrence time of 345 days across 56 patients. Among these, 52 patients had positive lymph nodes identified on diagnostic scans, while 11 were subsequently found to be overstaged, resulting in a positive predictive value of 78.8% in this cohort. Out of 78 patients who showed no lymph node involvement on diagnostic scans, 20 were found to have pathology-confirmed nodal metastases upon surgical resection, resulting in a false-negative rate of 25.6% and a sensitivity value of 67.2%. Among the 56 patients with intrathoracic lymph node recurrence, 24 had baseline PET/CT evidence of nodal involvement, 29 had positive lymph nodes found in surgical samples, and 17 were positive on both. These findings showed that the presence of a positive lymph node at baseline did not consistently predict lymph node relapse. Although previous studies have suggested a potential association between ground-glass opacity (GGO) and lymph node recurrence, this was not supported in this cohort. Neither the presence of GGO within the primary tumour nor its peritumoural distribution was associated with an increased risk of nodal relapse. Within the various lymph node relapse groups, N2 station involvement was the most common site, with its median time to recurrence being slightly slower than that of N1 (321 vs 302 days) but faster than N3 (321 vs 471 days), especially in cases of the N2 station recurrence with advanced stage, which showed the earliest relapse with a median of 182 days. (Fig. 4.2C)

The third most common relapse organ was bone, occurring at a median of 323 days in 22 patients. Other relapse locations included intrathoracic soft tissue (median 358 days, n=18), brain (median 258 days, n=16), extrathoracic lymph node (median 293 days, n=16), extrathoracic soft tissue (median 239 days, n=12), liver (median 361 days, n=10), adrenal (median 392 days, n=8), kidney (median 374 days, n=2), pancreas (median 607 days, n=2), Lymphangitis (1866 days, n=1), mesentery (169 days, n=1). (Fig. 4.2A)

A:

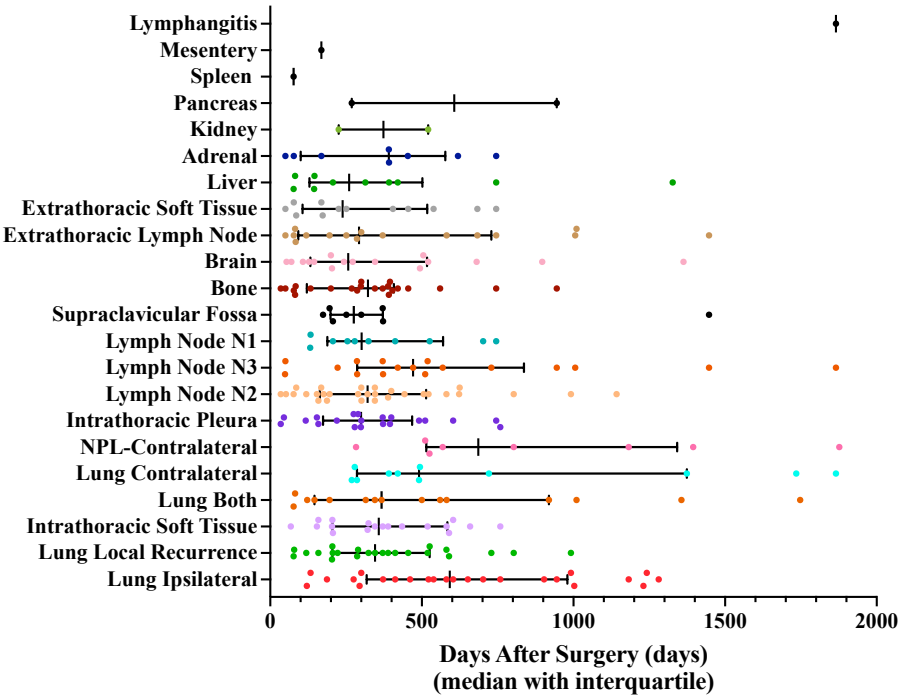
Timing of Relapse Across All Organs
Lymphangitis
Mesentery
Spleen
Pancreas
Kidney
Adrenal
Liver
Extrathoracic Soft Tissue
Extrathoracic Lymph Node
Brain
Bone
Supraclavicular Fossa
Lymph Node N1
Lymph Node N3
Lymph Node N2
Intrathoracic Pleura
NPL-Contralateral
Lung Contralateral
Lung Both
Intrathoracic Soft Tissue
Lung Local Recurrence
Lung Ipsilateral
0
500
1000
1500
2000
Days After Surgery (days)
(median with interquartile)

B:

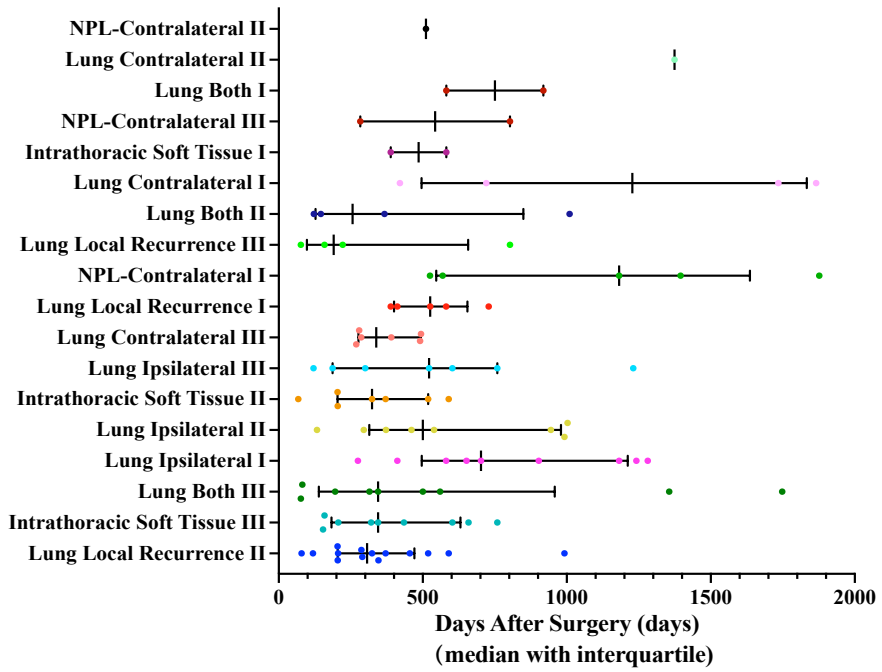
Timing of Lung Recurrence
NPL-Contralateral II
Lung Contralateral II
Lung Both I
NPL-Contralateral III
Intrathoracic Soft Tissue I
Lung Contralateral I
Lung Both II
Lung Local Recurrence III
NPL-Contralateral I
Lung Local Recurrence I
Lung Contralateral III
Lung Ipsilateral III
Intrathoracic Soft Tissue II
Lung Ipsilateral II
Lung Ipsilateral I
Lung Both III
Intrathoracic Soft Tissue III
Lung Local Recurrence II
0
500
1000
1500
2000
Days After Surgery (days)
(median with interquartile)

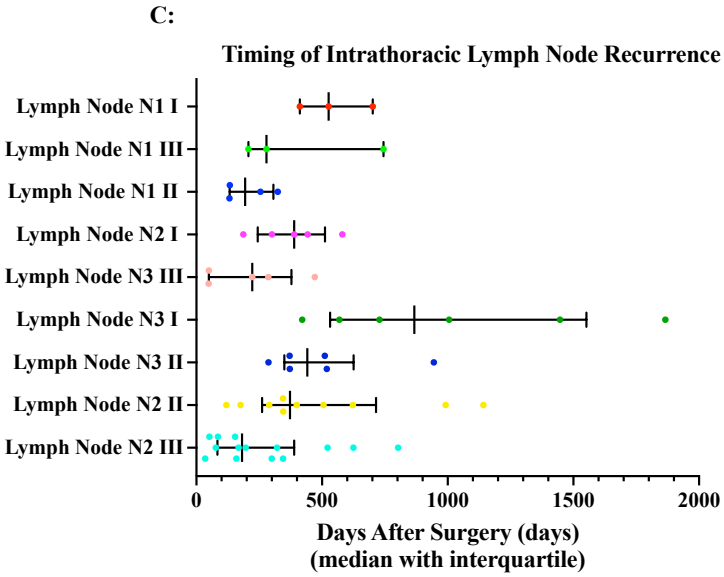


Fig. 4.2 Scatter plot of relapse timing by anatomical organ and subsite. Organs are displayed on the y-axis and are ordered from bottom to top according to overall initial relapse frequency across the cohort. Within each organ group, subsites are ordered from bottom to top according to the frequency of occurrence within this organ.

### 2.2 Diversity of Relapse Sites: Intrathoracic or Extrathoracic

This study explored whether the anatomical site of initial relapse influences disease-free survival (DFS), based on the hypothesis that the distribution and burden of relapse reflect distinct biological behaviours and may affect post-surgical prognosis [199]. The 130 relapsed patients were stratified into three groups according to their initial relapse sites: intrathoracic, extrathoracic, and both intrathoracic and extrathoracic.

**DFS varied by relapse site:** The distribution of DFS among relapse sites indicates a non-normal distribution (Fig. 4.3). The intrathoracic site was the most common recurrence site (n=73) and had the longest DFS (median, 509 days; [IQR], 288–908 days). In contrast, patients whose initial relapse involved both intrathoracic and extrathoracic sites (n=31) had a shorter DFS (median, 299 days; [IQR], 174–539 days), and those with only extrathoracic metastatic disease (n=26) had a median DFS of 346 days ([IQR] 169–521 days) (Fig. 4.3). These results suggest that anatomical site of relapse is associated with differences in DFS and may provide insight into tumour evolution and prognosis.

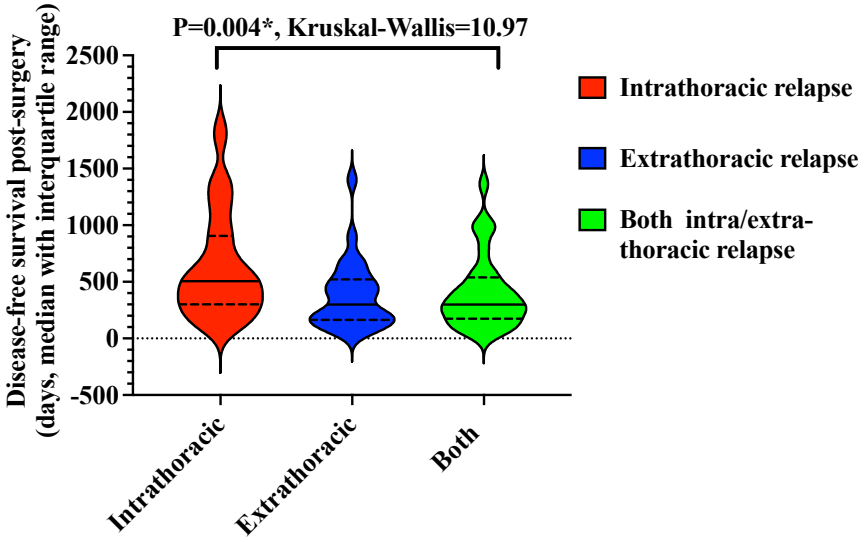


Fig. 4.3 Difference of DFS among Intrathoracic, Extrathoracic and Both relapse sites.

**DFS varied by tumour burden and anatomical location:** Notable variation emerged when tumour burden was stratified by anatomical location. However, relapse tumour burden alone was not significantly associated with DFS (Fig. 4.4). Intrathoracic relapses had longer DFS. In contrast, patients with widespread extrathoracic tumour burden had the shortest DFS, with these relapses typically being detected within 3 months post-surgery, followed by oligo extrathoracic in 3–6 months (Fig. 4.4). Notably, bone was the most frequent site of recurrence in the poly-extrathoracic group, while brain metastases were most common in the oligo-extrathoracic group.

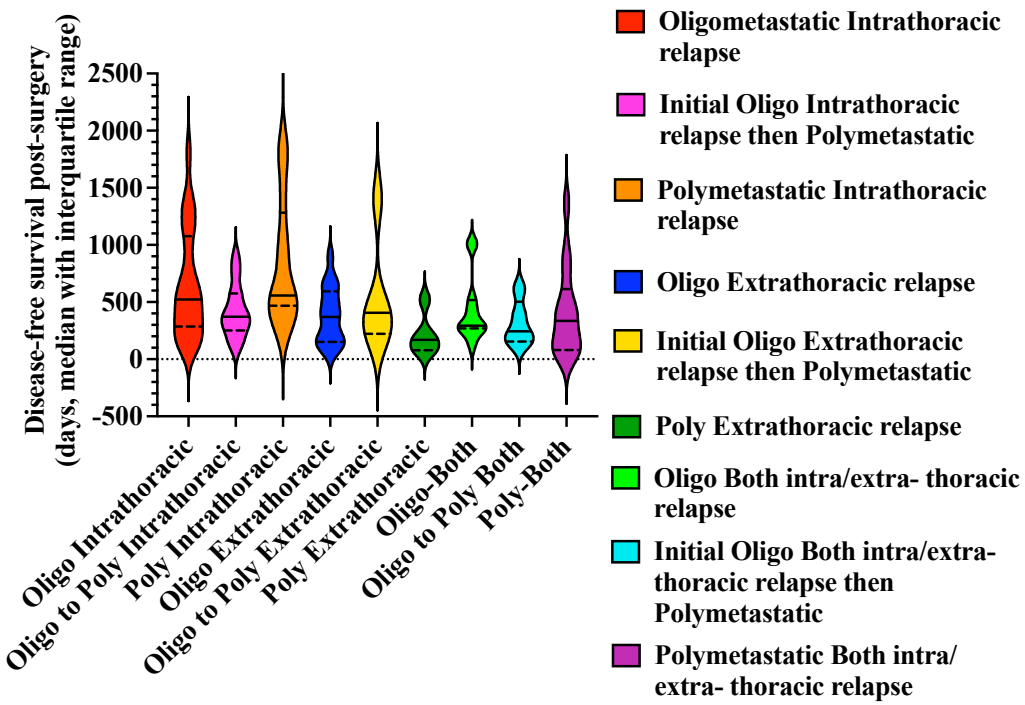


Fig. 4.4 DFS distributions among relapse sites and tumour burden categories

Intrathoracic relapse was commonly associated with a longer DFS. A subset of patients who initially presented with oligometastatic intrathoracic relapse had a shorter DFS and eventually progressed to polymetastatic disease (Fig. 4.5A). This observation is clinically meaningful, as it suggests that oligometastatic patients with earlier relapses, particularly within 9–12 months post-surgery, are more likely to experience widespread disease progression later. Future research should explore the genomic characteristics of these patients to better understand the mechanisms behind their widespread disease progression, potentially leading to more efficient treatments or uncovering tumour evolution. There was no significant difference in DFS across tumour burdens within extrathoracic involvement (Fig. 4.5B). Additionally, the number of relapse lesions was not correlated with DFS (Spearman's r= –0.05, P=0.544), suggesting that lesion count alone may not be a reliable predictor in this subgroup. These findings underscore the importance of considering both relapse site and overall tumour burden when evaluating prognosis. Site-specific patterns of relapse may hold the potential to help future clinical stratification frameworks.

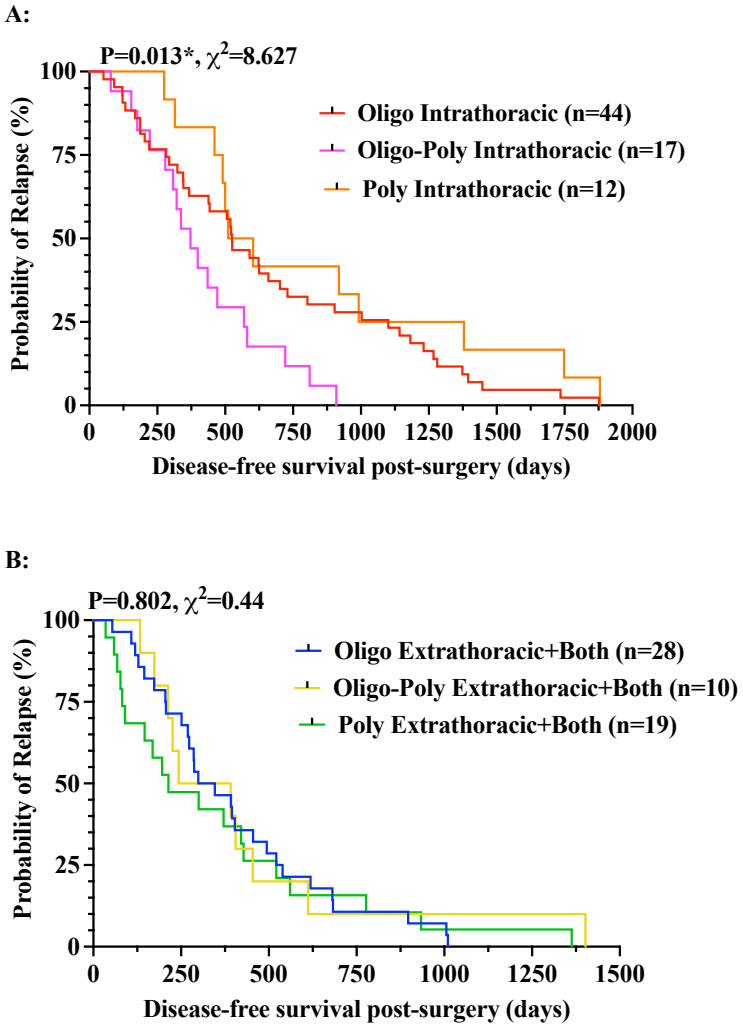


Fig. 4.5 Relapse probability among tumour burdens and relapse site.

### 2.3 Diversity of Relapse Growth Rates among Sites

Previous studies have found that genetic mutations are more common in extrathoracic metastases and are associated with a worse prognosis [34,39,44–47]. TRACERx studies have found that extrathoracic metastases often arise from aggressive subclones and are associated with poor prognosis [107,109,157,200]. Larger tumours have been shown to be associated with greater intratumour heterogeneity behaviour [201]. However, limited papers have explored how relapse rates impact recurrence sites and prognosis.

**Relapse growth rates vary by anatomical site:** In this cohort of 130 relapsed cases, relapse growth rates were stratified into three distinct categories based on tertiles: relapse speed first tertile (slow), relapse speed second tertile (median), and relapse speed third tertile (rapid). Tertile-based cutoffs ensure sufficient patient numbers within each subgroup,

allowing for the identification of trends and avoiding binary grouping, which can overlook meaningful variations. A clear tendency was observed: higher relapse growth rates were associated with a greater likelihood of extrathoracic involvement (Fig. 4.6A, P=0.0001). Additionally, higher relapse tumour growth rates were associated with increased lesion growth speed, particularly in extrathoracic sites, leading to a massive tumour burden and a worse prognosis (Fig. 4.6B–D). These findings highlight relapse growth rate as a novel and clinically relevant biomarker with the potential to inform prognosis. There was a positive relationship between relapse speed and total tumour volume (Spearman's r=0.68, P<0.0001). This positive relationship may be because larger tumours contain more heterogeneous subclone populations, which is related to aggressive tumour biology [107,200]. These findings highlight that relapse growth rate could guide risk stratification post-relapse and prioritise patients for urgent therapeutic intervention. Interestingly, the relapse tumour growth rate before treatment weakly correlated with the tumour growth rate post-treatment (Spearman's r=0.38, P<0.0001), indicating that growth rates may be affected by treatment selection pressure, favouring the expansion of therapy-resistant clones that dominate post-treatment tumour populations [26,202]. Such changes may also be driven by the tumour microenvironment, as previously described [157].

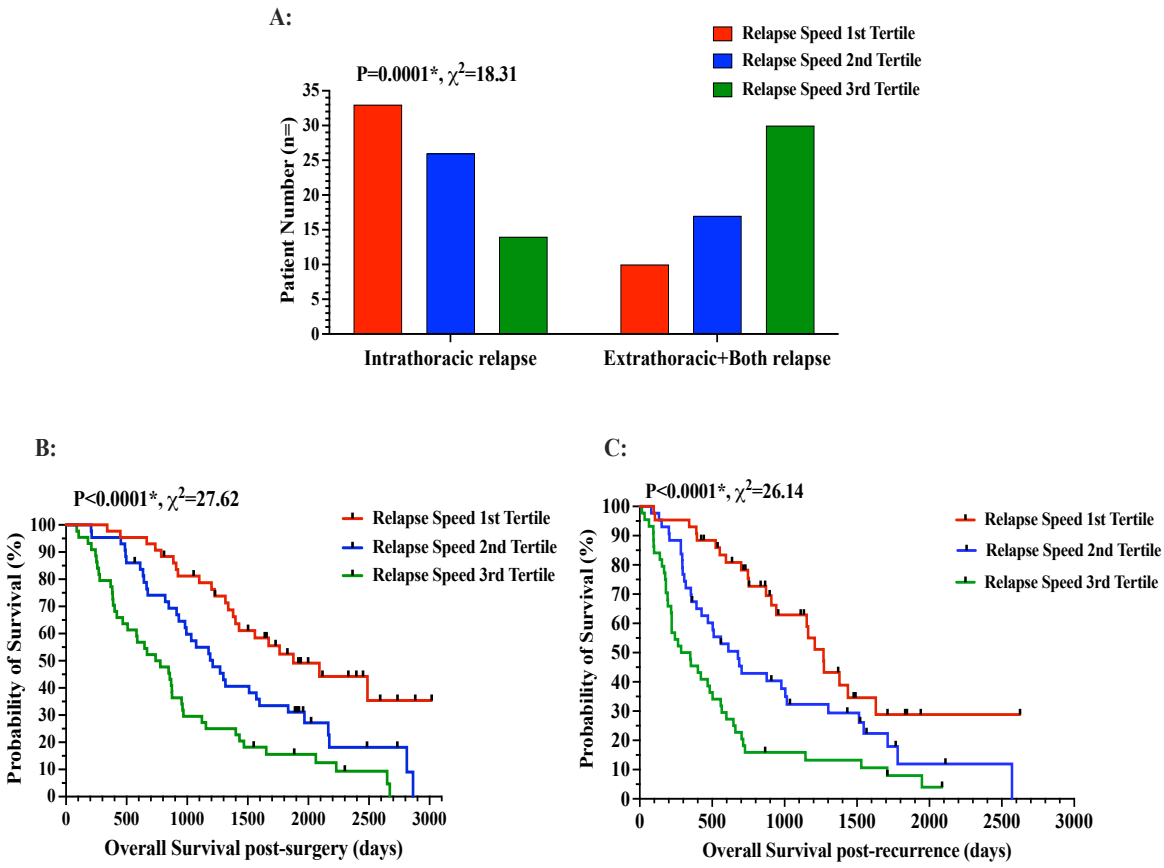

**D:**

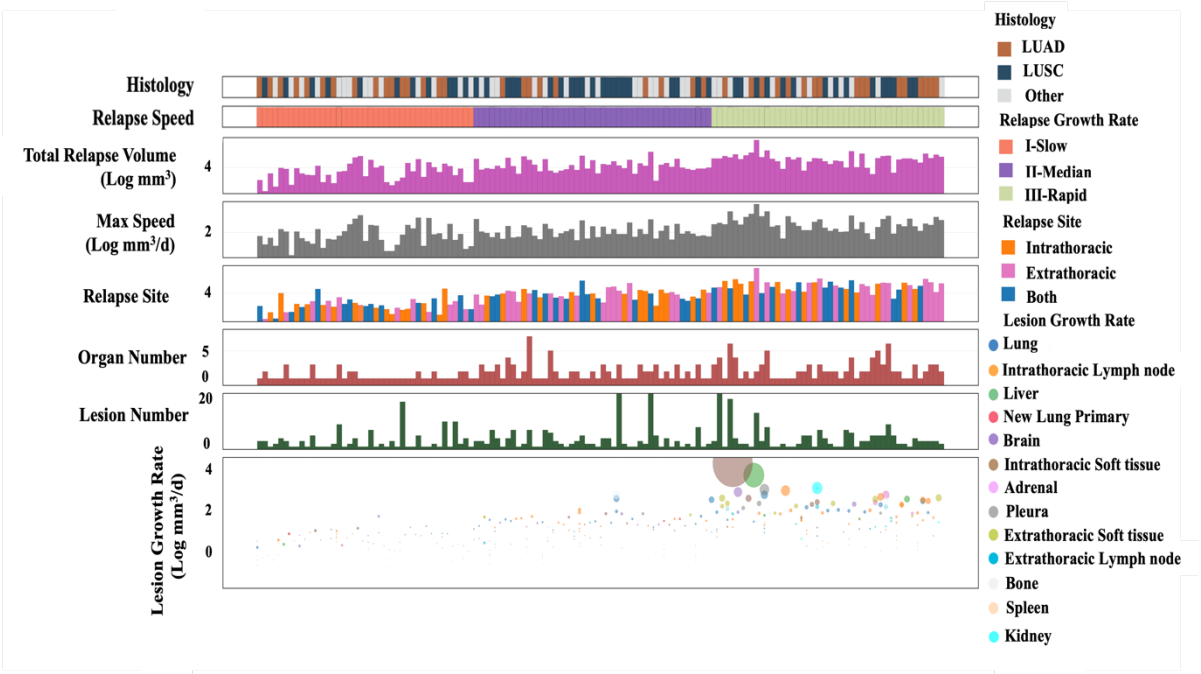


Fig. 4.6 Patterns of relapse growth and its association with tumour burden, site, and survival. A: Distribution of relapse sites stratified by relapse growth rates; B: Overall survival post-surgery stratified by relapse growth rate; C: Overall survival post-recurrence stratified by relapse growth rate; D: Subplots illustrating relapse characteristics across different relapse speed categories, including histology, total relapse volume, maximum growth rate, relapse site, number of involved organs and lesions, and lesion-level growth rates. Higher relapse growth rates were associated with faster lesion-level growth, particularly in extrathoracic sites, a greater probability of extrathoracic involvement, increased total tumour burden, and poorer survival outcomes.

## 3. Heterogeneity of Progression Patterns in Relapsed NSCLC

### 3.1 Diversity in the Timing of Organ-Specific Progression

The timing of each organ's involvement, as determined by imaging, was quantified to capture both the initial recurrence and subsequent tumour progression phases. The results revealed a diverse pattern of organ-specific progression across the dataset (Fig. 4.7A). During tumour evolution, the lung was identified as the most common site of involvement (n=108), including intrathoracic soft tissue (n=25). Notably, local recurrence within the lung was the earliest detected event, occurring at a median of 323 days after surgery. Intrathoracic lymph node (n=66), especially N2, was the second most common site of recurrence. The median progression time of intrathoracic lymph nodes followed a

sequential pattern through the mediastinal stations, with N1 being the earliest, followed by N2 and then N3.

Other notable sites included bone (n=35), pleura (n=31), brain (n=30), extrathoracic lymph node (n=25), extrathoracic soft tissue (n=21), liver (n=19), and adrenal gland (n=15). The liver was not the most frequent site of extrathoracic disease, but it showed an earlier relapse with a median of 332 days, compared to the bone, the organ where disease progressed most frequently in extrathoracic disease, with a median of 389 days (Fig. 4.7A).

Intrathoracic progression was more easily seen in oligometastatic disease. Extrathoracic progression was more easily seen in polymetastatic diseases. Interestingly, exceptional organs can be found. Brain metastases, as the extrathoracic progression, were observed in 50% of cases within the oligometastatic disease. In contrast, intrathoracic involvements, including bilateral lung nodules (77%), intrathoracic pleura (73%) and intrathoracic soft tissue (60%), were more commonly detected in polymetastatic disease. These findings underscore the complexity of disease progression in cancer patients and suggest that the metastatic burden of the disease influences the site of metastasis.

Lung, intrathoracic lymph nodes, and bone were the most common sites identified in the last scan prior to death (Fig. 4.7B). Interestingly, not all the patients showed an increased tumour burden at the last scan before death, with 23 out of 97 dead patients displaying stable or reduced tumour volumes. This variability may be attributed to accelerated disease progression following the last scan in some patients, as well as to cancer-related complications such as leptomeningeal disease (n = 1), brain progression (n = 1), and atelectasis (n = 2), or non-malignant events such as pulmonary embolism.

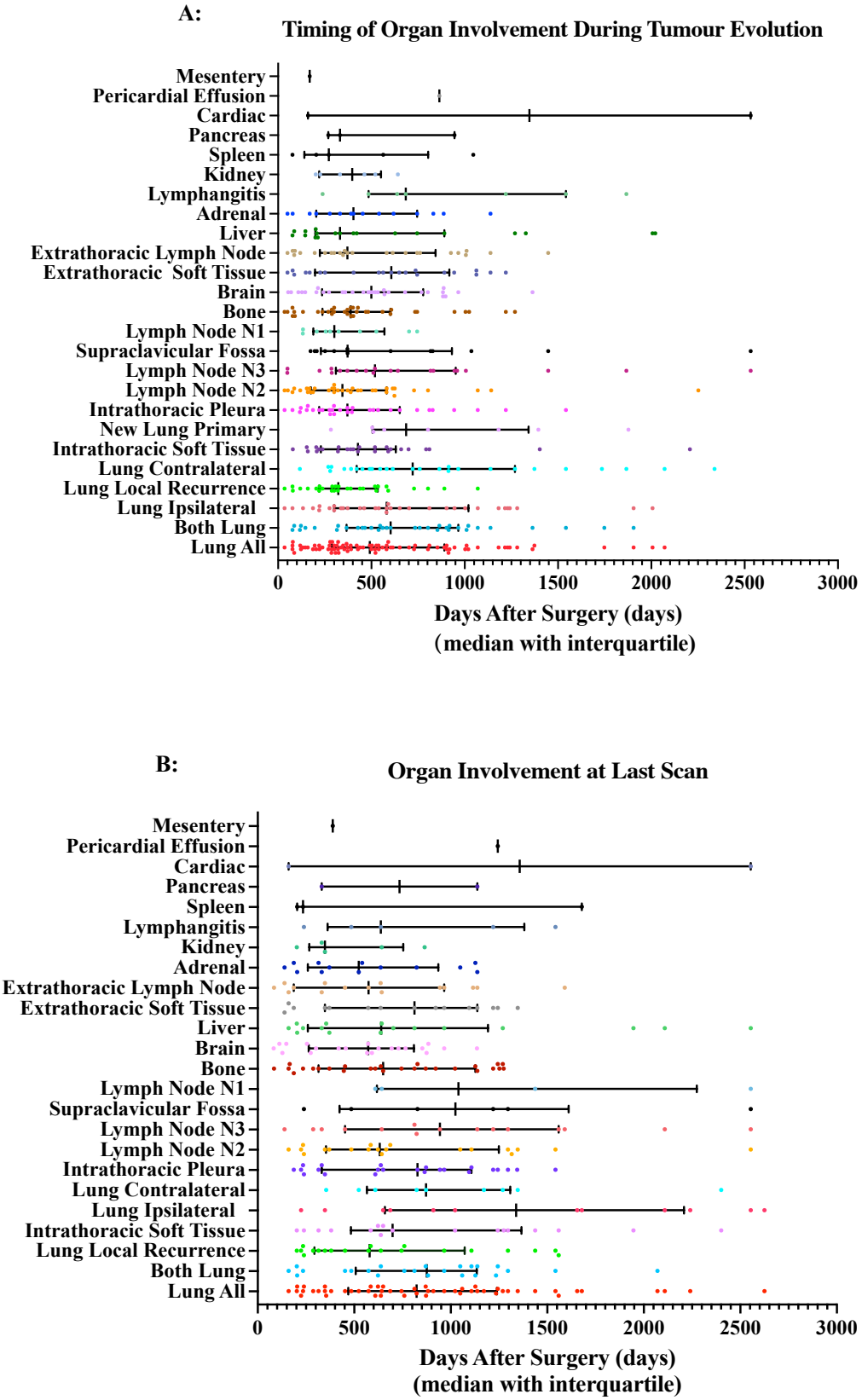


Fig. 4.7 Scatter plot of overall relapse timing and last scan before death by anatomical organ and subsite. Organs are displayed on the y-axis and are ordered from bottom to top according to their overall relapse or last scan frequency across the cohort. Within each

organ group, subsites are ordered from bottom to top according to the frequency of occurrence within this organ. There is a diverse pattern of organ progression across the dataset.

### 3.2 Heterogeneity of Prognosis Based on Organ-Specific Recurrences

Previous research has highlighted significant differences in mortality rates based on the site of relapse, particularly those involving the brain [199,203]. However, no study to date has specifically explored the prognostic impact of early versus late relapse within individual organs. To determine whether specific relapsed organs influence clinical outcomes, I identified four organs frequently associated with high relapse rates in this cohort: the lung (including lung soft tissue but excluding new primary lung tumours), intrathoracic lymph nodes, bone, and brain. The results indicated that an initial lung and intrathoracic lymph node relapse did not affect post-recurrence survival (Fig. 4.8L, P). However, patients who experienced their first relapse in the brain and bone had significantly poorer post-recurrence survival rates (Fig. 4.8J, O). Additionally, patients with evidence of relapse in the bone and brain on their final scan prior to death exhibited worse post-recurrence survival compared to those without such involvement (Fig. 4.8B–C). These findings underscore the critical role of the bone and brain in tumour evolution.

Other organs, which were less frequently involved than the previously mentioned ones in initial relapse scans, including the extrathoracic lymph nodes, extrathoracic soft tissue, and adrenal gland, were found to have worse overall survival and post-recurrence survival when affected at the last scan before death compared to those not affected (Fig. 4.8F, H, I). Especially early intrathoracic pleura, extrathoracic lymph node, and extrathoracic soft tissue involvement shortened the survival time (Fig. 4.8K–O). However, initial liver and adrenal gland relapses didn't impact the clinical outcomes (Fig. 4.8P–R).

A:

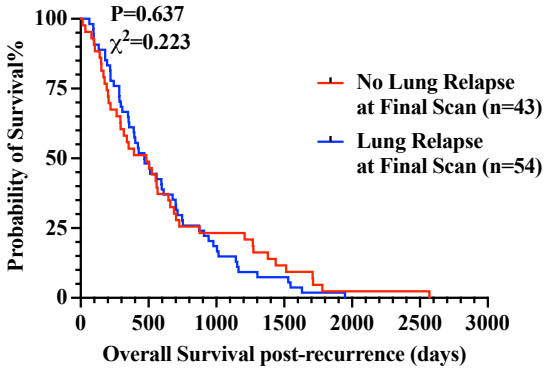
P=0.637
$\chi^2$=0.223
No Lung Relapse at Final Scan (n=43)
Lung Relapse at Final Scan (n=54)
Probability of Survival%
Overall Survival post-recurrence (days)

B:

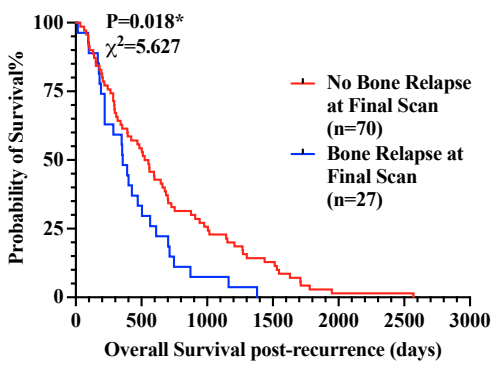
P=0.018*
$\chi^2$=5.627
No Bone Relapse at Final Scan (n=70)
Bone Relapse at Final Scan (n=27)
Probability of Survival%
Overall Survival post-recurrence (days)

C:

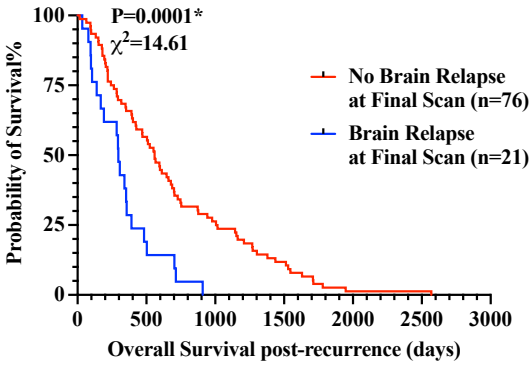
P=0.0001*
$\chi^2$=14.61
No Brain Relapse at Final Scan (n=76)
Brain Relapse at Final Scan (n=21)
Probability of Survival%
Overall Survival post-recurrence (days)

D:

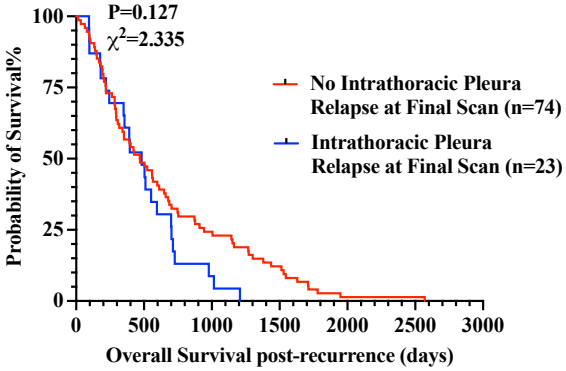
P=0.127
$\chi^2$=2.335
No Intrathoracic Pleura Relapse at Final Scan (n=74)
Intrathoracic Pleura Relapse at Final Scan (n=23)
Probability of Survival%
Overall Survival post-recurrence (days)

E:

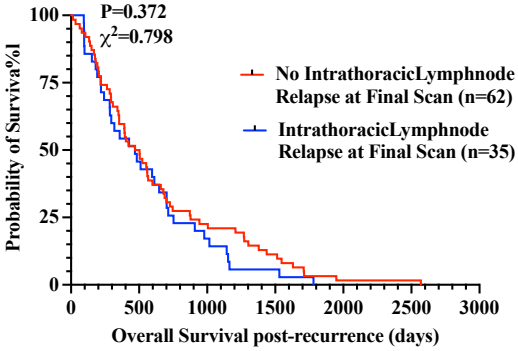
P=0.372
$\chi^2$=0.798
No IntrathoracicLymphnode Relapse at Final Scan (n=62)
IntrathoracicLymphnode Relapse at Final Scan (n=35)
Probability of Survival%l
Overall Survival post-recurrence (days)

F:

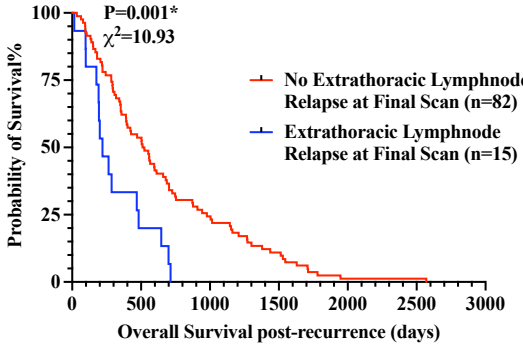
P=0.001*
$\chi^2$=10.93
No Extrathoracic Lymphnode Relapse at Final Scan (n=82)
Extrathoracic Lymphnode Relapse at Final Scan (n=15)
Probability of Survival%
Overall Survival post-recurrence (days)

G:

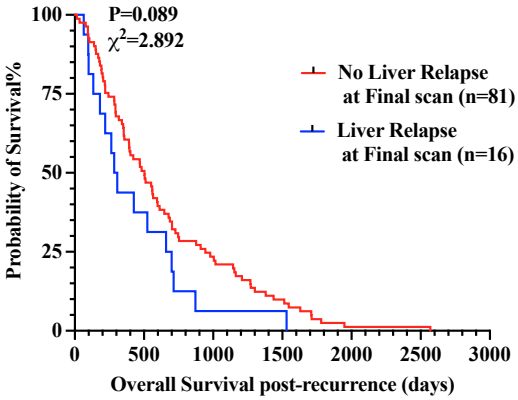
P=0.089
$\chi^2$=2.892
No Liver Relapse at Final scan (n=81)
Liver Relapse at Final scan (n=16)
Probability of Survival%
Overall Survival post-recurrence (days)

H:

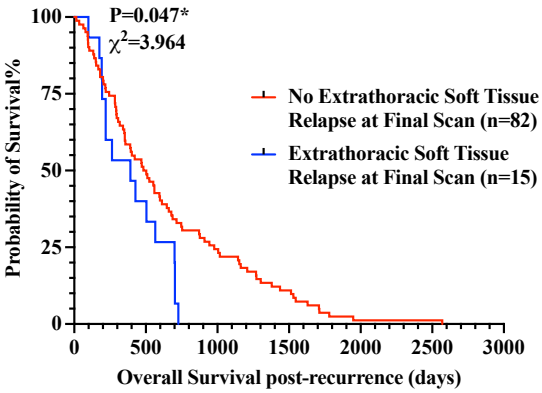
P=0.047*
$\chi^2$=3.964
No Extrathoracic Soft Tissue Relapse at Final Scan (n=82)
Extrathoracic Soft Tissue Relapse at Final Scan (n=15)
Probability of Survival%
Overall Survival post-recurrence (days)

I:

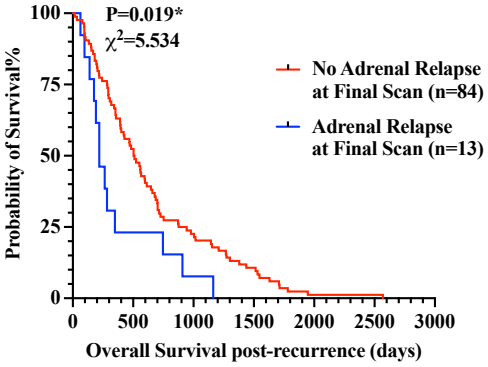
P=0.019*
$\chi^2$=5.534
No Adrenal Relapse at Final Scan (n=84)
Adrenal Relapse at Final Scan (n=13)
Probability of Survival%
Overall Survival post-recurrence (days)

J:

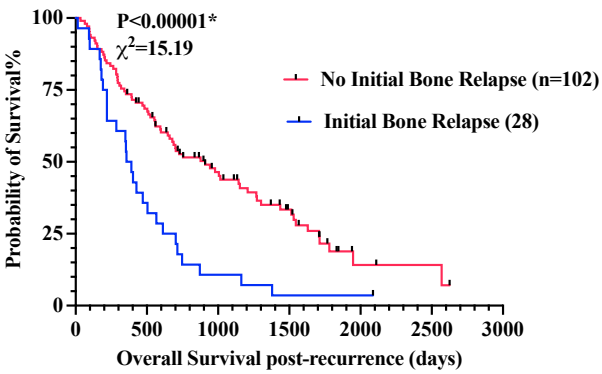
P<0.00001*
$\chi^2$=15.19
No Initial Bone Relapse (n=102)
Initial Bone Relapse (28)
Probability of Survival%
Overall Survival post-recurrence (days)

K:

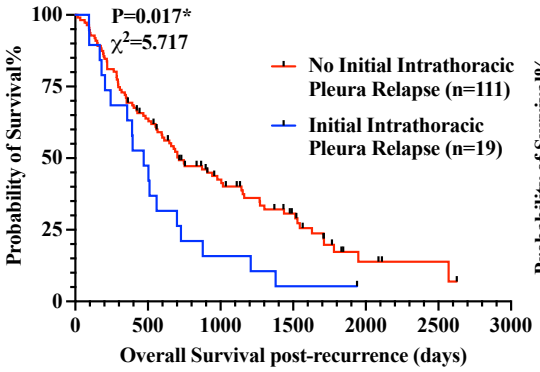
P=0.017*
$\chi^2$=5.717
No Initial Intrathoracic Pleura Relapse (n=111)
Initial Intrathoracic Pleura Relapse (n=19)
Probability of Survival%
Overall Survival post-recurrence (days)

L:

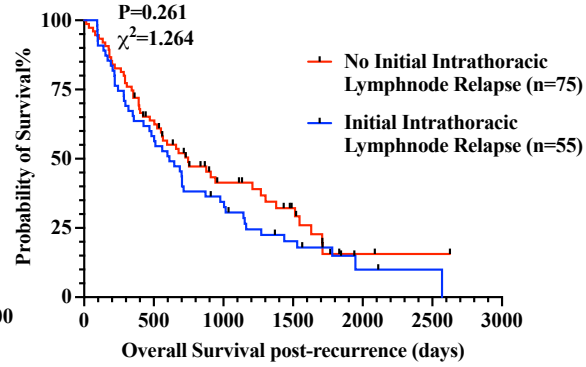
P=0.261
$\chi^2$=1.264
No Initial Intrathoracic Lymphnode Relapse (n=75)
Initial Intrathoracic Lymphnode Relapse (n=55)
Probability of Survival%
Overall Survival post-recurrence (days)

M:

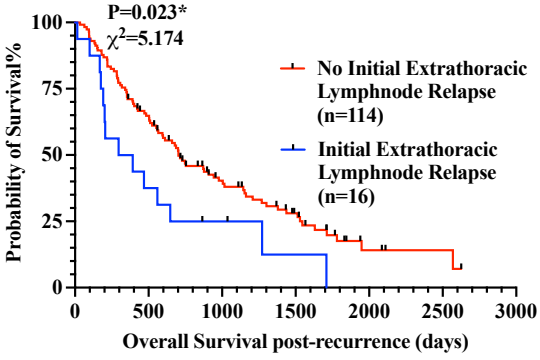
P=0.023*
$\chi^2$=5.174
No Initial Extrathoracic Lymphnode Relapse (n=114)
Initial Extrathoracic Lymphnode Relapse (n=16)
Probability of Survival%
Overall Survival post-recurrence (days)

N:

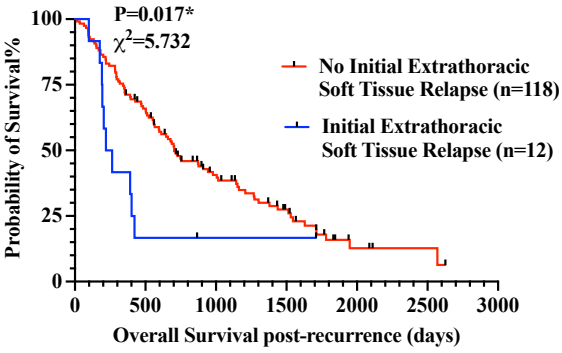
P=0.017*
$\chi^2$=5.732
No Initial Extrathoracic Soft Tissue Relapse (n=118)
Initial Extrathoracic Soft Tissue Relapse (n=12)
Probability of Survival%
Overall Survival post-recurrence (days)

O:

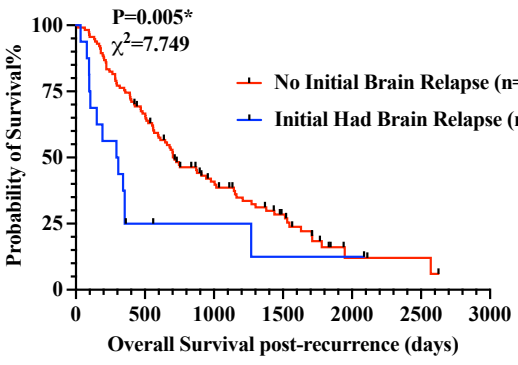
P=0.005*
$\chi^2$=7.749
No Initial Brain Relapse (n=114)
Initial Had Brain Relapse (n=16)
Probability of Survival%
Overall Survival post-recurrence (days)

P:

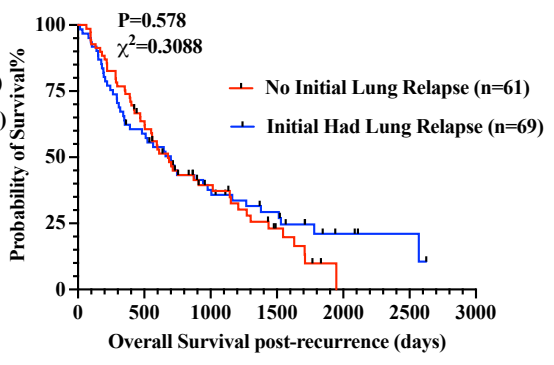
P=0.578
$\chi^2$=0.3088
No Initial Lung Relapse (n=61)
Initial Had Lung Relapse (n=69)
Probability of Survival%
Overall Survival post-recurrence (days)

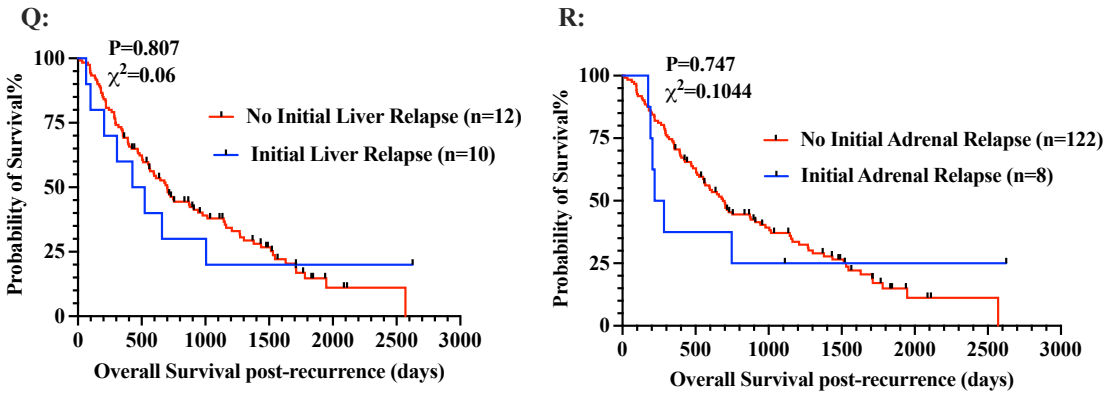


Fig. 4.8 Kaplan–Meier survival curves comparing overall survival post-recurrence according to the presence or absence of initial relapse and final scan in the lung, bone, brain, liver, pleura, intrathoracic and extrathoracic lymph node, extrathoracic soft tissue, liver and adrenal glands. A–R: In each plot, the survival of patients with relapse in that organ is compared to that of patients without relapse. The patient numbers are imbalanced among some groups, but this can still reveal preliminary trends.

To find how relapse affects prognosis, I regrouped patients to do more profound research. Patients who had only lung or intrathoracic soft tissue metastases during the entire progression period showed a better post-relapse survival rate than those who never had lung or intrathoracic soft tissue relapse and those who had both lung and other organ relapses. Still, there was no difference between patients who never had a lung or intrathoracic soft tissue relapse and those with relapses both in the lung and other organs (Fig. 4.9A, Relapse only in lung vs Relapse in lungs and other sites, Adjusted P=0.0003; Relapse only in lung vs No lung relapse, Adjusted P=0.0003; Relapse in lungs and other sites vs No lung relapse, Adjusted P=0.896. P values were adjusted using the FDR method, n=3 tests). In contrast, brain relapse was associated with markedly worse outcomes. Patients who experienced brain metastases—either as the only site of relapse or in combination with other organs—had significantly shorter post-relapse survival than those who never developed brain metastases (Fig. 4.9B, Relapse only in brain vs Relapse in brains and other sites, Adjusted P=0.264; Relapse only in brain vs No brain relapse, Adjusted P<0.001; Relapse in brains and other sites vs No brain relapse, Adjusted P=0.003. P values were adjusted using the FDR method, n=3 tests).

**A:**

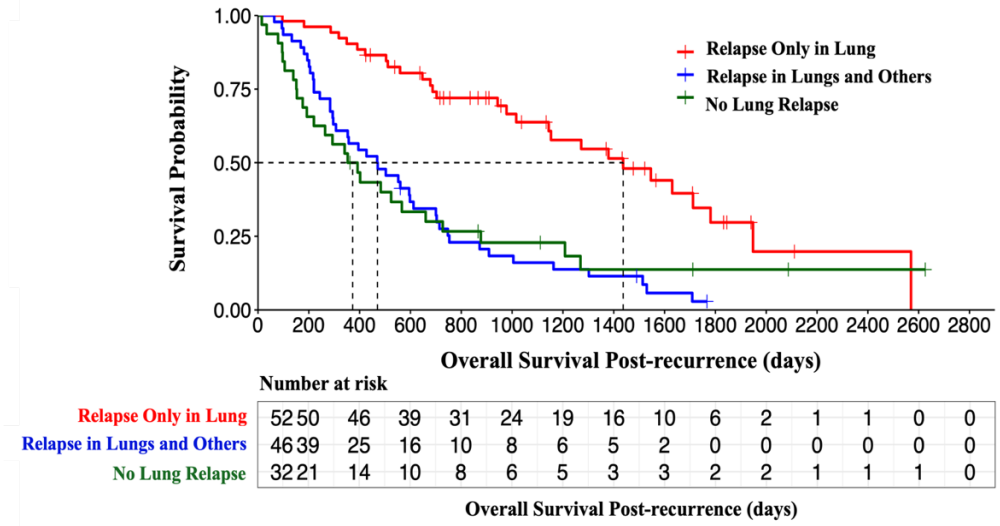


**B:**

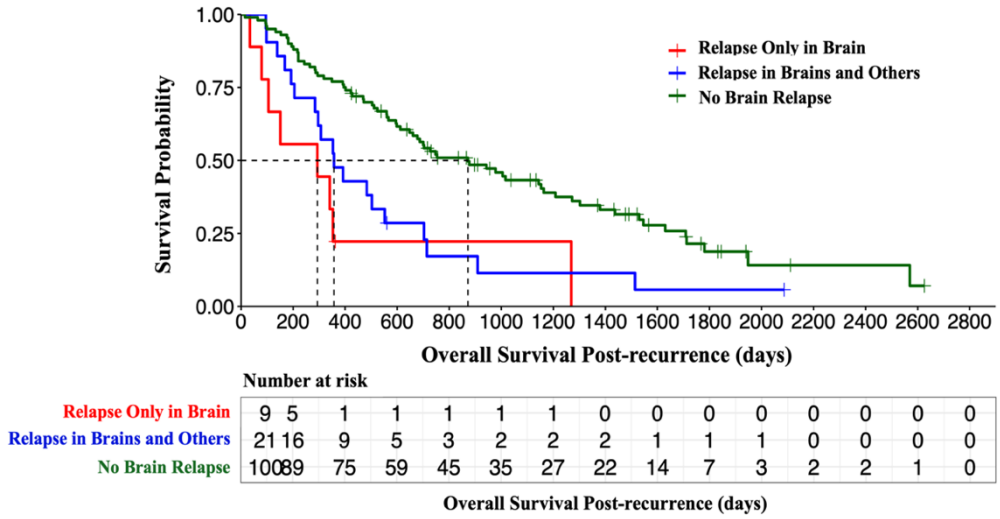


Fig. 4.9 Survival curves illustrating the impact of lung and brain relapse on post-recurrence overall survival. A: Survival outcomes in patients grouped by lung involvement; B: Survival outcomes in patients grouped by brain involvement.

In summary, early involvement of the bone, intrathoracic pleura, extrathoracic lymph nodes, brain, and extrathoracic soft tissue can impact prognosis, in contrast to the involvement of the lung, intrathoracic lymph nodes, liver, and adrenal glands. Patients with only lung metastases performed better than those who never had lung relapse or those who had both lung and other sites relapse. Patients with brain metastases had worse post-recurrence survival rates than those who never had brain relapse. Due to the small and imbalanced cohort size, these observations are preliminary and need further validation in larger cohorts.

## 3.3 Patterns and Outcomes of Cancer Progression

The 130 relapsed patients' progression patterns were diverse. An initial progression event was observed in 115 patients (with a median of progression-free survival of 153 days). Subsequently, 88 patients experienced a second progression event, and 66 patients progressed to a third event. 17 patients died at the first progression, 16 died at the second progression, and another 16 died at the third progression. The median number of progression events per patient was 2.5, and 97 patients eventually died during the follow-up period. No statistically significant difference in the distribution of progression events was observed between patients with initial intrathoracic versus extrathoracic relapse ($P=0.911$, $x^2=0.013$).

### 3.3.1 Single Site-Specific Relapse and Subsequent Progression Routes:

Previous results have shown that the lung and intrathoracic lymph nodes are the most common sites of recurrence. In this study, I focused exclusively on three common single-organ relapse patterns to explore clearer pathways and characteristics of progression, thereby effectively minimising the confounding effects of simultaneous multiple-organ relapses, which complicate the identification of metastasis patterns.

***Lung*** emerged as the predominant site for single-organ relapse events, with the right upper lobe displaying the highest likelihood of relapse. Among these, ipsilateral lung relapse, including local lung recurrence, was the most common recurrence pattern, with 12 out of 16 cases originating from the right lung, where the upper lobe was slightly more affected than the lower. Notably, the majority of these patients were female (9 of 16), and the relapse speed was predominantly slow (8 of 16), compared to median (6 of 16) and rapid (2 of 16). Additionally, nearly all patients (11 of 16) were diagnosed with LUAD. Internal air bronchogram signs were found in 8 patients, and 10 of 16 patients' primary tumours showed pleural attachment on baseline CT scans. (Fig. 4.10, Table 4.2)

Within the ipsilateral lung relapse cohort, the most prevalent progression pattern was the emergence of new pulmonary lesions (7/16). Post-relapse treatment modalities varied, with 5 patients receiving radical radiotherapy, 3 patients receiving palliative radiotherapy, 1 patient receiving chemotherapy, and 2 patients receiving immunotherapy. The median progression-free survival (PFS) after treatment was 244 days. Among progression

patterns, the emergence of new lesions was the most common, followed by localised lesion expansion. Of the 8 patients who experienced the first progression as localised lesion expansion, 3 didn't receive any treatment (median PFS was 140 days), 2 received palliative treatment (PFS was 1423 and 289 days), 1 underwent chemotherapy (PFS was 244 days) and 1 received immunotherapy (PFS was 340 days). A particularly aggressive pattern involved the simultaneous emergence of new lung lesions and localised progression. Most cases exhibiting this pattern at first progression originated from contralateral or bilateral lung relapse. (Fig. 4.10, Table 4.2)

These results suggest that specific characteristics, such as a primary tumour in the right upper lung (particularly the right upper lung), slow relapse speed, female gender, LUAD histology, and the presence of pleural attachment, are signs of ipsilateral lung relapse.

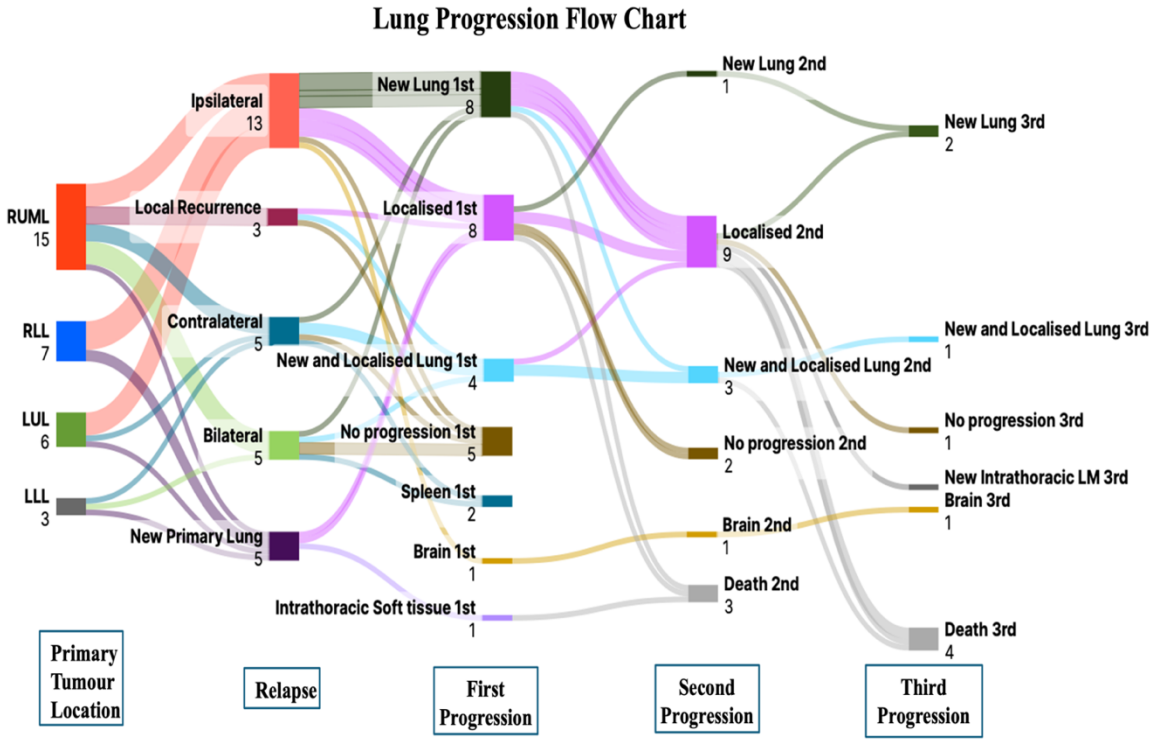


Fig. 4.10 Progression trajectories of patients with initial relapse within the lung.

Table 4.2 Clinical and tumour characteristics associated with single-lung relapse

| Characteristics | Dominant characteristics (n) |
|---|---|
| 1. Primary tumour location of common relapse sites | RUL (12/16) |
| 2. Common relapse site | Ipsilateral (16/31) |
| 3. First progression post common relapse type | New lung lesions (7/16) |
| 4. Gender | Female (9/16) |
| 5. Primary tumour histology | LUAD (11/16) |
| 6. Relapse Speed | Slow (8/16) |
| 7. Pleural Involvement | + (10/16) |
| 8. Bronchial aerogram | +/– (8/16) |
| 9. PFS days post-relapse (radical treatment to common first progression) | 244 |
| 10. PFS days post-relapse (no treatment) | 140 |

***Intrathoracic lymph node*** was the second most common site of single-organ relapse (n=14). Among these cases, the left lung, particularly the left lower lobe, was more susceptible to relapse. N2 nodal involvement was the most prevalent pattern of those recurrences, with 7/11 primary tumours in the upper lung lobes. Additionally, 10/11 showed a faster relapse speed.

Similar to ipsilateral lung relapse, patients with N2 recurrence demonstrated a higher likelihood of pleural involvement (8/11), while air bronchogram signs were notably absent. Five patients with intrathoracic lymph node relapse did not progress during follow-up. All received radical treatment: three underwent radical radiotherapy, one received chemotherapy followed by sequential radiotherapy, and one was treated with EGFR-targeted therapy. (Fig. 4.11, Table 4.3)

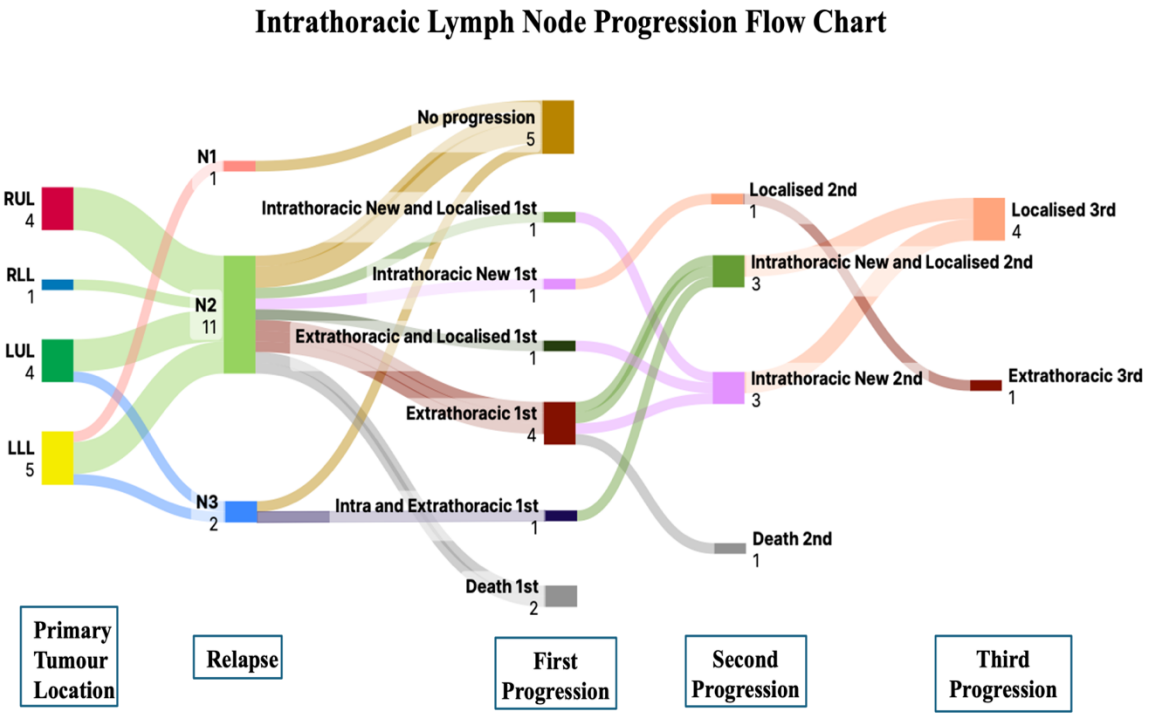


Fig. 4.11 Progression trajectories of patients with initial relapse within the intrathoracic lymph node.

Table 4.3 Clinical and tumour characteristics associated with single-intrathoracic lymph node relapse

| Characteristics | Dominant characteristics (n) |
|---|---|
| 1. Primary tumour location of common relapse sites | Upper lobe (7/11) |
| 2. Common relapse site | N2 (11/14) |
| 3. First progression post common relapse type | No progression (5/14) |
| 4. Relapse Speed | >Slow (10/11) |
| 5. Pleural Involvement | + (8/11) |
| 6. Bronchial aerogram | – (11/11) |
| 7. PFS days post-relapse (radical treatment to common first progression) | No progression |

***Brain*** was the most common site of extrathoracic single-organ relapse (n=9), with a higher probability of the primary tumour originating from the upper lung, particularly the right upper lung. Among these patients, 7 patients had advanced TNM stage (above IIB), 6 patients had large primary tumours, 6 patients were male, 6 patients were diagnosed with peripheral lung cancer, and 8 patients were histologically confirmed as LUAD. Pleural involvement was observed in 7 patients, and 6 patients showed no signs of air bronchogram on baseline scans. Additionally, 6 patients showed a faster relapse speed.

6 patients who received palliative radiotherapy post-relapse or no treatment died within a median period of 129 days. In contrast, 3 patients who received radical radiotherapy had longer PFS with a median of 1176 days, including one patient who did not progress during the follow-up period. (Fig. 4.12, Table 4.4)

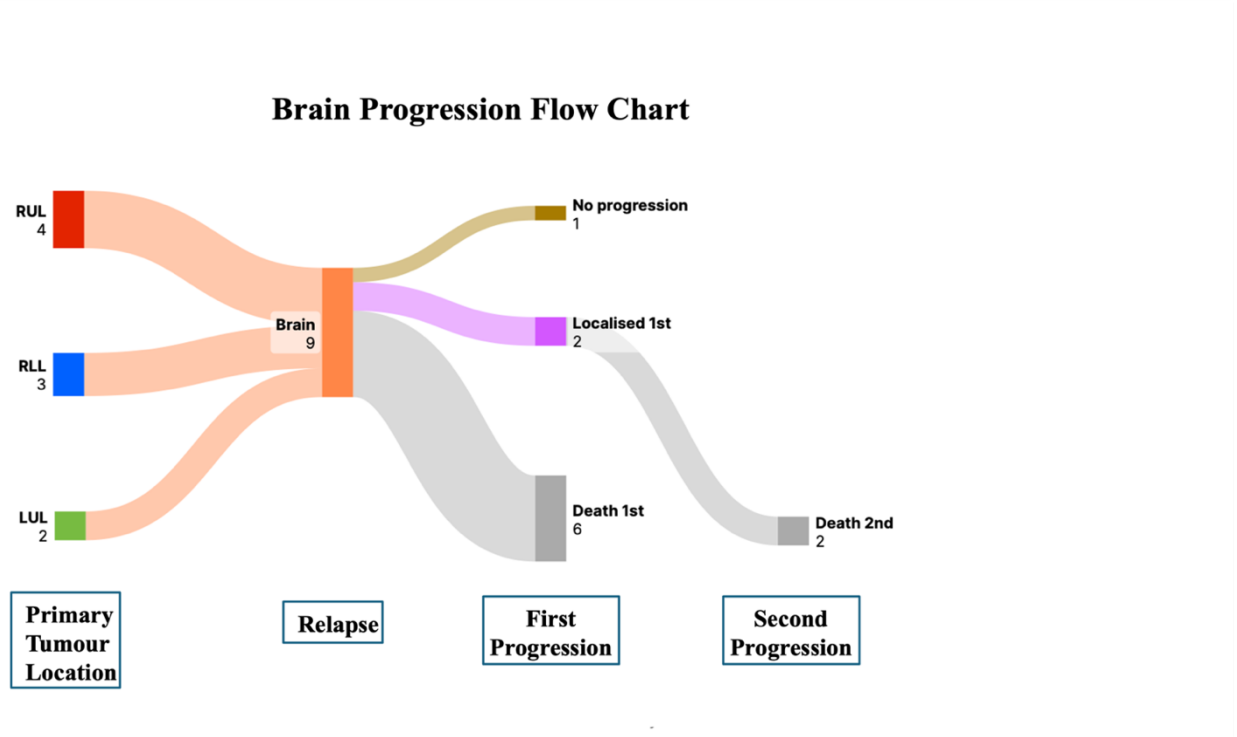


Fig. 4.12 Progression trajectories of patients with initial relapse within the brain.

Table 4.4 Clinical and tumour characteristics associated with single-brain relapse

| Characteristics | Dominant characteristics (n) |
|---|---|
| 1. Primary tumour location of common relapse sites | Upper lobe peripheral (6/9) |
| 2. First progression post common relapse type | Death (6/9) |
| 3. Gender | Male (6/9) |
| 4. Primary tumour size | Big (6/9), above IIB (7/9) |
| 5. Primary tumour histology | LUAD (8/9) |
| 6. Relapse Speed | >Slow (6/9) |
| 7. Pleural Involvement | + (7/9) |
| 8. Bronchial aerogram | – (6/9) |
| 9. PFS days post-relapse (radical treatment to common first progression) | 1176 |
| 10. PFS days post-relapse (no treatment) | 129 |

Single-organ relapse, including those in the lung and intrathoracic lymph nodes, were associated with significantly better post-recurrence survival compared to multiple-organ relapses ($P<0.0001$, $x^2=26.22$). No significant difference in post-recurrence survival was observed between patients with lung-only and intrathoracic lymph node-only relapses. Additionally, patients with brain-only relapse had similar survival outcomes to those with multi-organ relapses, highlighting the particularly poor prognosis associated with brain metastases and the need for heightened clinical attention. These findings are illustrated in Fig. 4.13. However, given the small and imbalanced subcohort sizes, validation in larger, independent cohorts is needed.

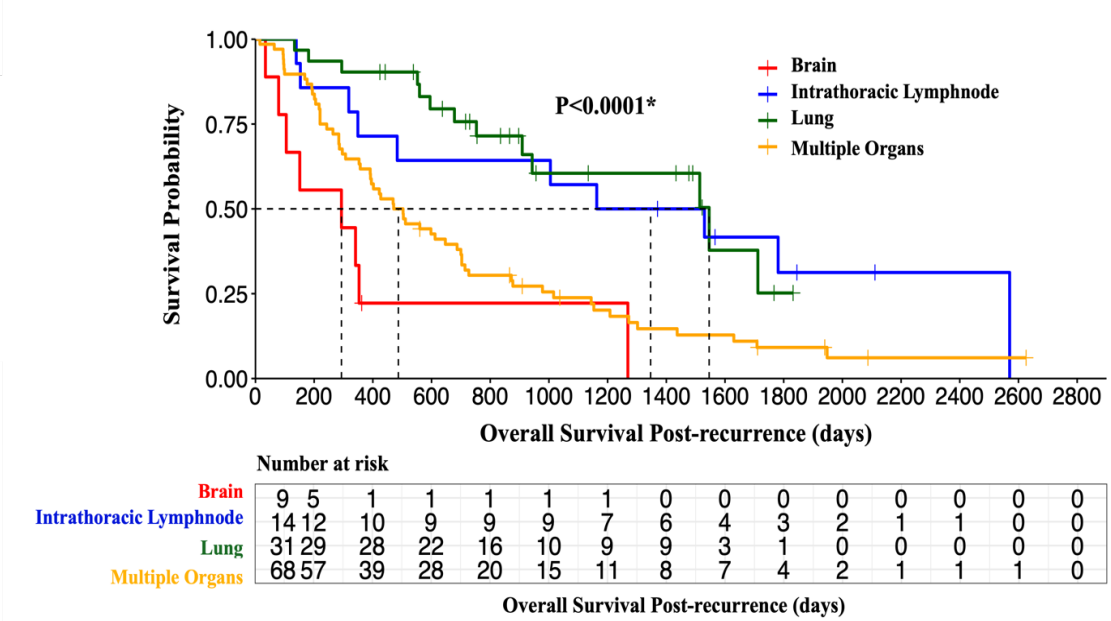


Fig. 4.13 Overall survival post-recurrence stratified by relapse site: lung, intrathoracic lymph node, brain, and multiple-organ relapse.

### 3.3.2 Impact of Tumour Burden Dynamics During Tumour Evolution

This section investigates whether the number and volume of metastatic lesions over time are associated with clinical outcomes. The primary aim is to determine whether lesion count alone is a reliable prognostic marker or whether incorporating additional metrics—such as tumour volume and growth rate—provides a more accurate reflection of metastatic aggressiveness.

**Tumour Number Burden and Relapse Dynamics:**

The relationship between the number of lesions and survival was analysed first. Patients were stratified into three groups based on relapse speed: slow (1$^{st}$ tertile), median (2$^{nd}$ tertile), and fast (3$^{rd}$ tertile). This approach was chosen to ensure balanced group sizes and to explore potential trends. As no established clinical thresholds for relapse speed currently exist, this stratification is considered an exploratory analysis. In previous analyses of this cohort, lesion count at initial relapse did not significantly correlate with disease-free survival (DFS). According to previous literature [9], oligometastatic disease is defined as metastatic disease with no more than five lesions and involvement of up to three organs. In this study, no significant difference in overall survival was found between patients with initial oligometastatic disease and those with initial polymetastatic disease (Fig. 4.14A). To further explore the prognostic relevance of lesion count, address group

size imbalances, and better capture non-linear trends, patients were grouped into three categories based on the number of lesions at initial relapse: single lesion, 2–5 lesions, and more than 5 lesions. This categorisation was based on existing literature, where five lesions are commonly used as the threshold to distinguish between widespread and oligometastatic disease. Interestingly, Kaplan–Meier analysis demonstrated unexpected trends: patients with 2–5 lesions appeared to have worse outcomes than those with more than 5 lesions, with crossing survival curves (Fig. 4.14B), suggesting that lesion number alone may not consistently reflect tumour evolution.

**A:**

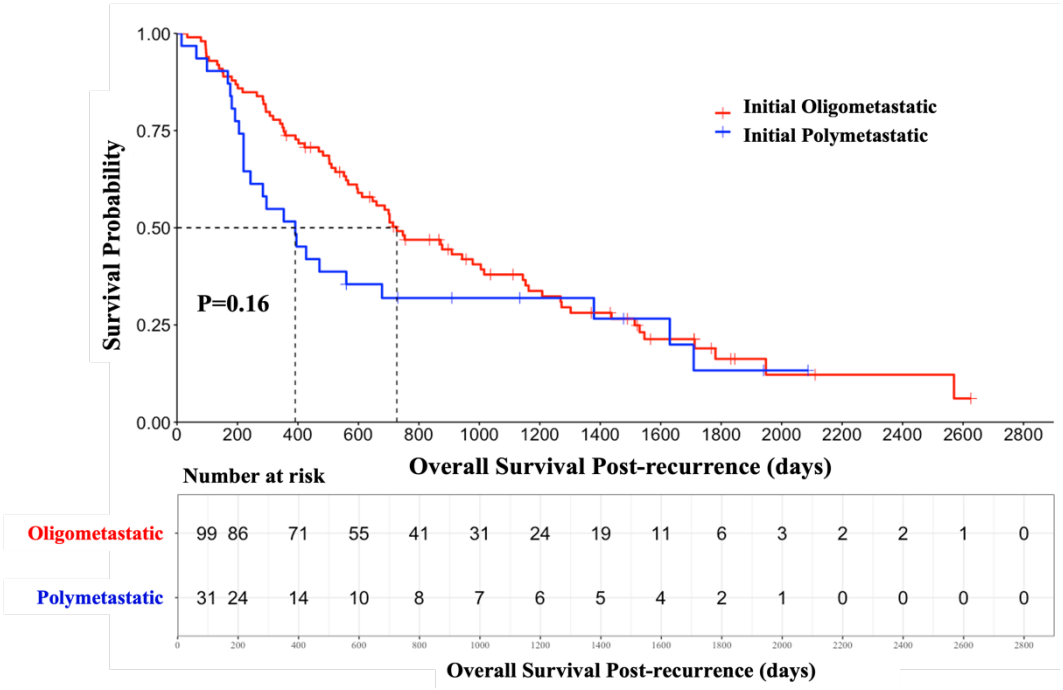

**B:**

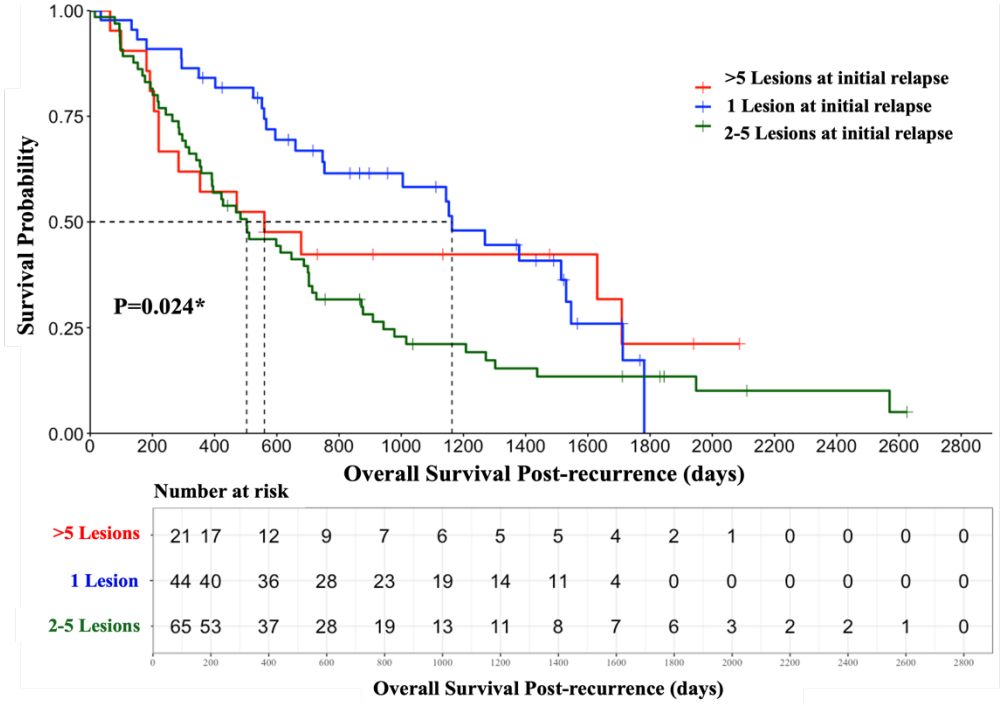


Fig. 4.14 Overall survival post-recurrence stratified by initial metastatic status and lesion count. A: The overall survival post-recurrence between initial oligometastatic relapse and initial polymetastatic relapse; B: The overall survival post-recurrence among different lesion count groups.

The relationship between lesion number and relapse rates is barely explored. Hence, patients were divided into tertiles based on relapse growth rate, and lesion counts were compared across successive progression events. This analysis aimed to test the assumption that tumour aggressiveness would increase through both faster relapse and an increasing number of lesions over time. During tumour progression, neither the number of lesions nor the increase in lesion numbers showed a positive trend with the relapse tumour growth rate (Fig. 4.15). Furthermore, lesion counts across successive progression events (first, second, and third) did not show a significant difference among the relapse speed groups (P=0.269, 0.04, 0.065), nor did the increases in lesion number (P=0.466, 0.522, 0.07). These results suggest that tumour number dynamics alone do not reflect tumour biological aggressiveness, highlighting the importance of considering additional metrics, such as tumour volume and growth rate, to improve risk stratification strategies.

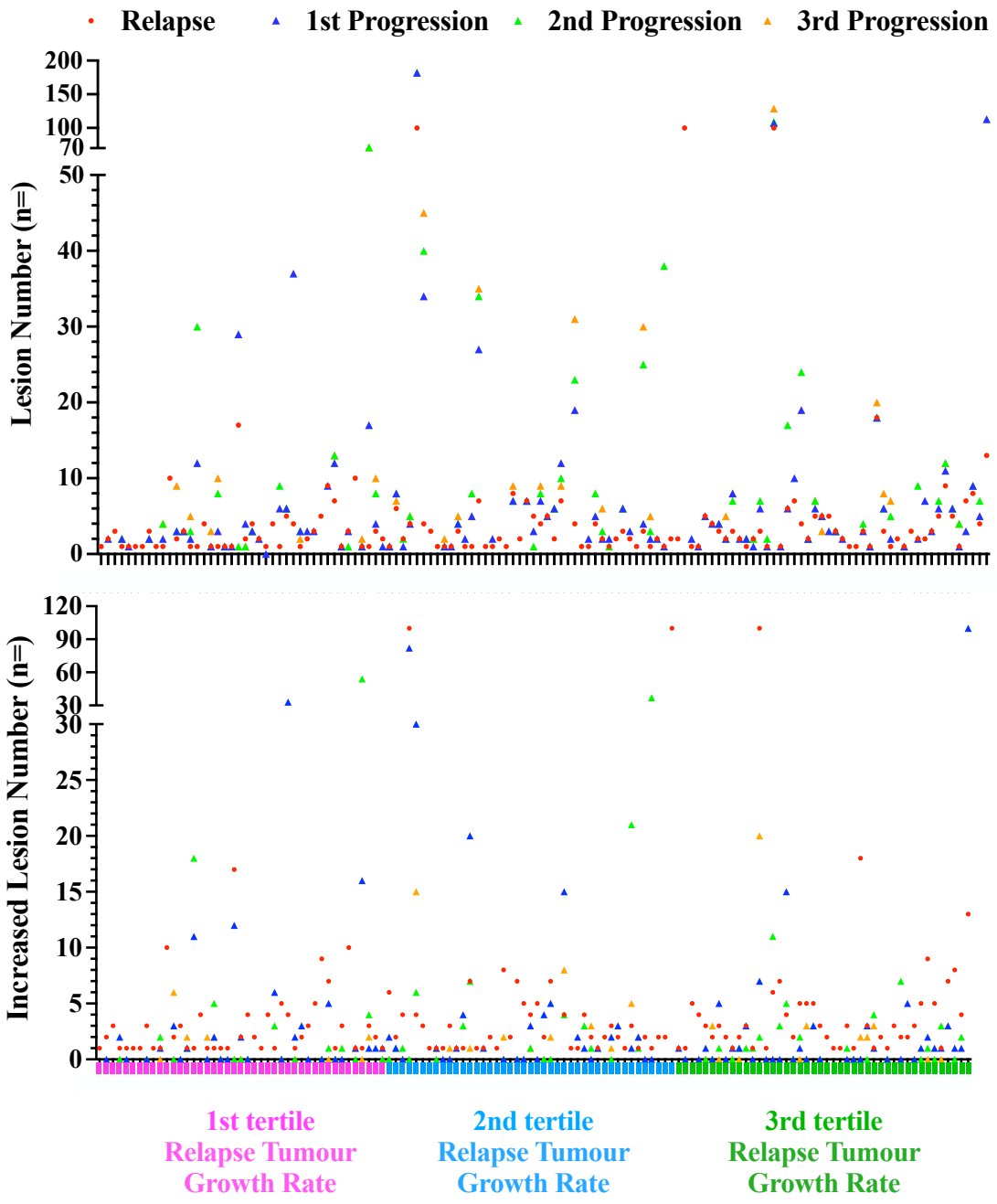


Fig. 4.15 Tumour number and increased number at relapse and progressions across different relapse growth rate categories

**Tumour Volume Burden and Relapse Dynamics:** Next, the relationship between relapse volume burden and progression dynamics was explored. This analysis was hypothesis-driven and informed by previous findings, which demonstrated that larger tumours tend to harbour greater intratumour heterogeneity, potentially contributing to more aggressive relapse behaviour [201]. However, to date, the association between relapse

speed and tumour burden across successive progression events remains largely unexplored. In this cohort, relapse speed was positively associated with relapse volume (Fig. 4.16A), and both relapse speed and volume were associated with greater tumour volumes at subsequent progression events (Fig. 4.16B–C). Patients with faster relapse speed had more progression events (median=3) than those with slower relapse (median=2). However, no positive correlation was identified between the relapse growth rate and the number of progression times (Spearman's r=0.11, P=0.2). Patients were divided into tertiles based on relapse growth rate. Due to the limited number of patients experiencing three progression events, the corresponding error bars were wide. Nevertheless, the observed results remained consistent throughout the analysis, indicating that faster relapse rates are associated with significantly larger tumours and faster progression speeds compared to those with slower recurrence rates (Fig. 4.17A–G).

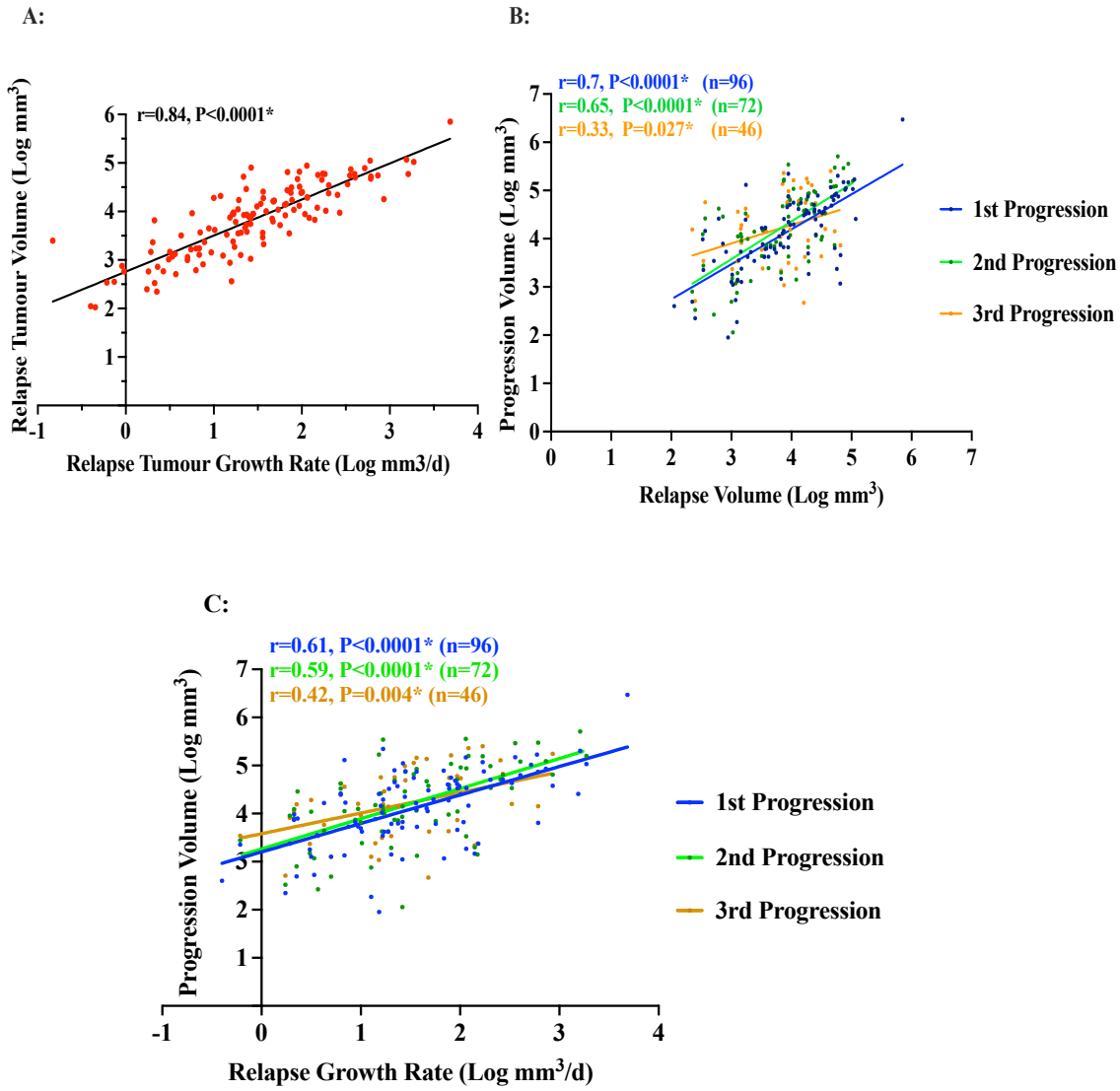

Fig. 4.16 Relationship between volume and speed across progression events. A: Relationship between relapse speed and volume; B: Relationship among relapse volume, first progression volume, second progression volume and third progression volume; C: Relationship among relapse speed, first progression volume, second progression volume and third progression volume.

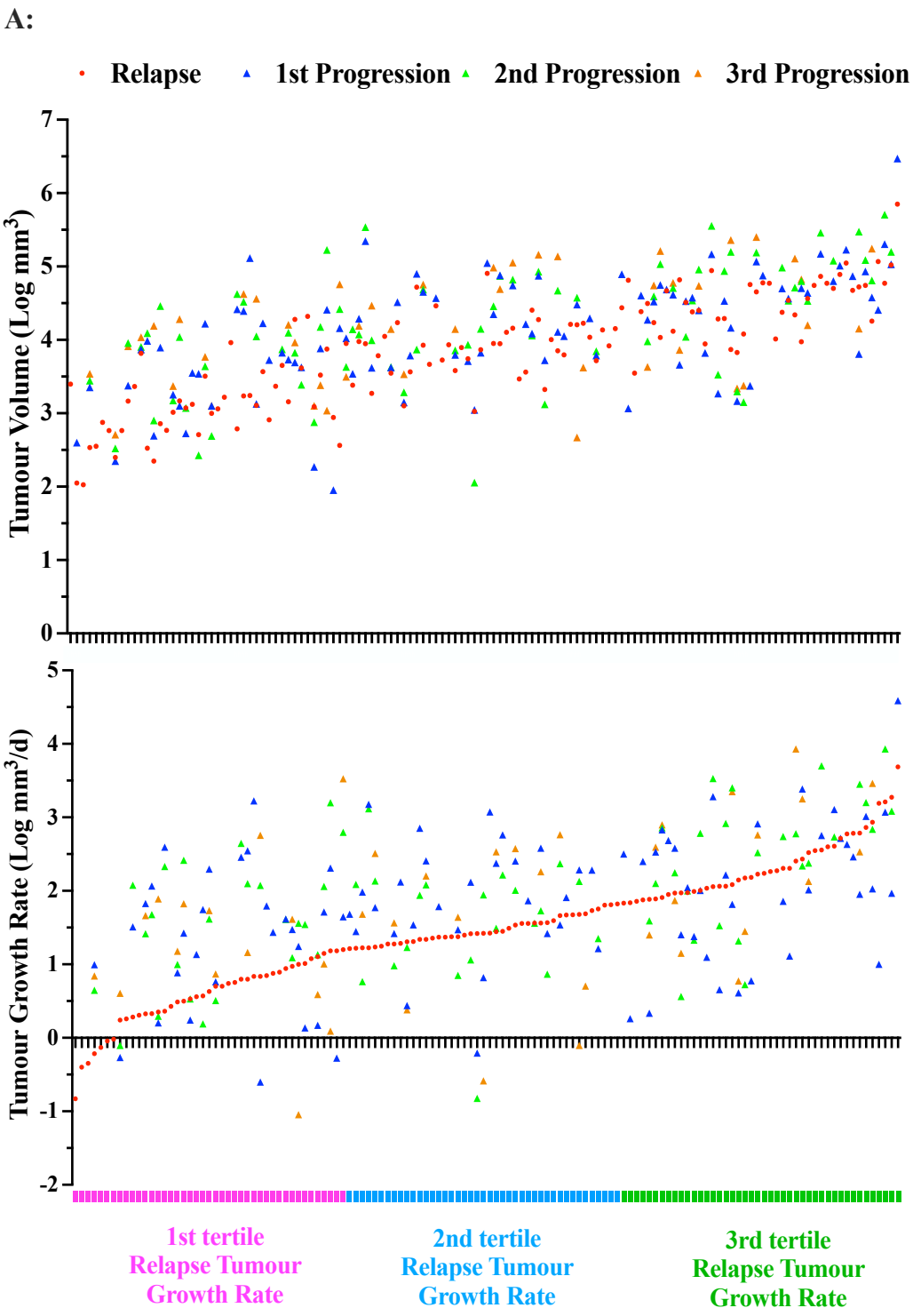

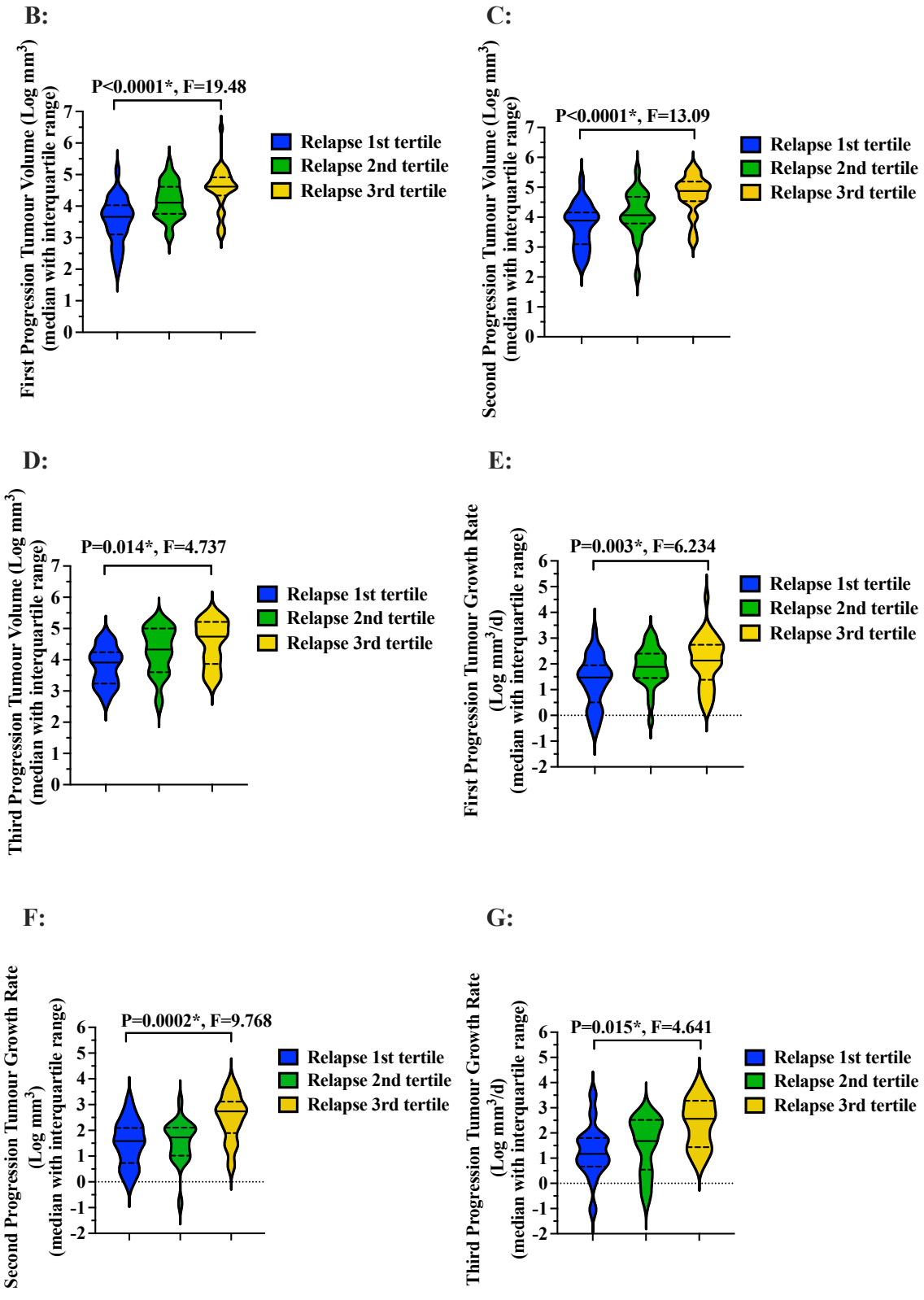


Fig. 4.17 Relationship between relapse growth rates and progression volumes at the first relapse, first progression, second progression and third progression. A: Comparison of tumour volume and growth rate at initial relapse and subsequent progression events across

different relapse speed categories (slow, medium, fast); B: First progression volume stratified by relapse speed; C: Second progression volume stratified by relapse speed; D: Third progression volume stratified by relapse speed; E: First progression speed stratified by relapse speed; F: Second progression speed stratified by relapse speed; G: Third progression speed stratified by relapse speed.

In summary, these findings suggest that tumour volume may better reflect metastatic behaviours than lesion number. This result may be because larger tumours may harbour more subclonal diversity, increasing the chance of aggressive and treatment-resistant subclone growth. Volumetric burden combines lesion counts, which may provide more precise prognostic information.

### 3.3.3 Impact of Tumour Location Dynamics During Tumour Evolution

**Progression Trajectories of Intra/Extrathoracic Relapses:** Limited research has systematically explored the longitudinal patterns of anatomical relapse sites, their progression modes, and associated prognoses. In this cohort, a predominant recurrence pattern was identified within the intrathoracic region, with subsequent progression often following an intrathoracic trajectory. A similar pattern was found in extrathoracic relapses and multiple relapse sites (concurrent intrathoracic and extrathoracic areas). (Fig. 4.18)

Although intrathoracic relapse generally followed a thoracic progression pattern, exceptions were observed. A subgroup of 23 patients initially relapsed within the thorax but later progressed to extrathoracic sites, with a median time to extrathoracic progression of 171 days (Fig. 4.18). The most common extrathoracic progression site post intrathoracic relapse was bone. Notably, a subset of 8 patients progressed from intrathoracic relapse to combined intrathoracic and extrathoracic disease, representing a particularly widespread progression phenotype (Fig. 4.18). This subgroup demonstrated a predominance of left-sided primary tumours (6/8) and exhibited relapse involving multiple intrathoracic organs. In addition, they showed faster relapse growth rates, indicating that higher relapse burdens are prone to widespread progress.

9 patients initially experienced intrathoracic relapse followed by extrathoracic progression. These cases were characterised by a primary tumour located in the upper, especially the left upper lobe, typically involving a single intrathoracic organ relapse, with relapse speed at or above the medium level and all patients only receiving localised treatments. Among the 130 relapse cases, 15 patients achieved a stable disease status post-relapse, with approximately 90% being intrathoracic relapses. This subgroup shared commonalities, such as a single intrathoracic organ relapse, a slow relapse speed, and receipt of radical local treatments.

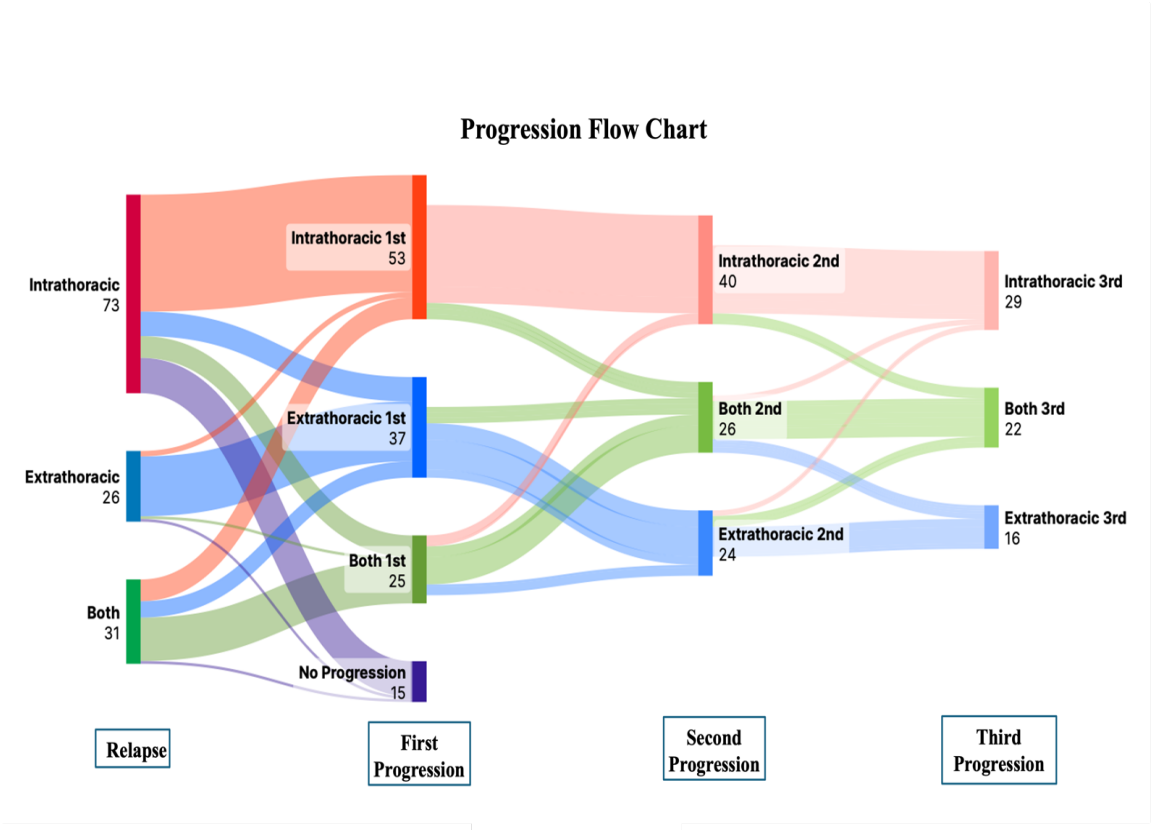


Fig. 4.18 Progression trajectories.

**Outcomes of Extrathoracic Progressions**: Interestingly, regardless of the initial site of relapse, involvement of extrathoracic regions during tumour evolution was associated with significantly poorer outcomes compared to cases where the disease remained confined to the intrathoracic region ($P<0.0001$, $\chi^2=25.81$, Fig. 4.19). This finding underscores the prognostic importance of anatomical spread, highlighting the adverse impact of extrathoracic dissemination on patient survival.

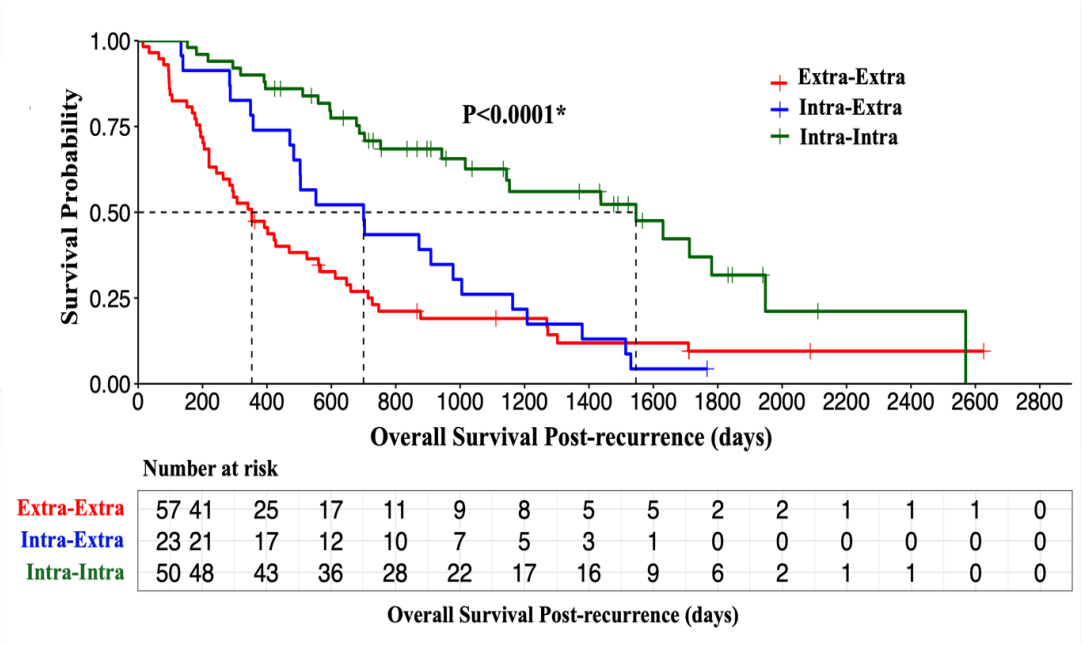


Fig. 4.19 Overall survival post-recurrence stratified by progression trajectories.

### 3.3.4 Impact of Tumour Location and Growth Rate on Dynamics During Tumour Evolution

To elucidate the relationships among relapse location, relapse speed, progression times, and progression mode at first, second, and third progression, I have categorised progression events into death, emergence of new lesions and expansion of localised lesions at the same time, expansion of localised lesions only, emergence of new lesions only, and absence of progression. Regardless of the treatment types, the likelihood of experiencing localised progression versus the emergence of new lesions was comparable. However, as the number of progression events increased, there was a shift towards more localised progression and a decrease in the exclusive emergence of new lesions. Concurrently, there was an increase in mortality rates, while non-progression decreased (Fig. 4.20A).

Patients with intrathoracic relapse tended to develop new lesions, followed by localised progression. In contrast, patients with extrathoracic relapse were more prone to experiencing a new lesion emergence and localised lesion expansion simultaneously. Individuals with extrathoracic relapse had more complicated and more aggressive progression modes than those with intrathoracic relapse, which may explain why extrathoracic progressions had poorer outcomes (Fig. 4.20B).

Unfortunately, there was no significant correlation between the speed of relapse and the mode of progression (Fig. 4.20C). This weak association may reflect earlier findings in this study, which showed that tumour growth was not necessarily linked to an increased number of lesions.

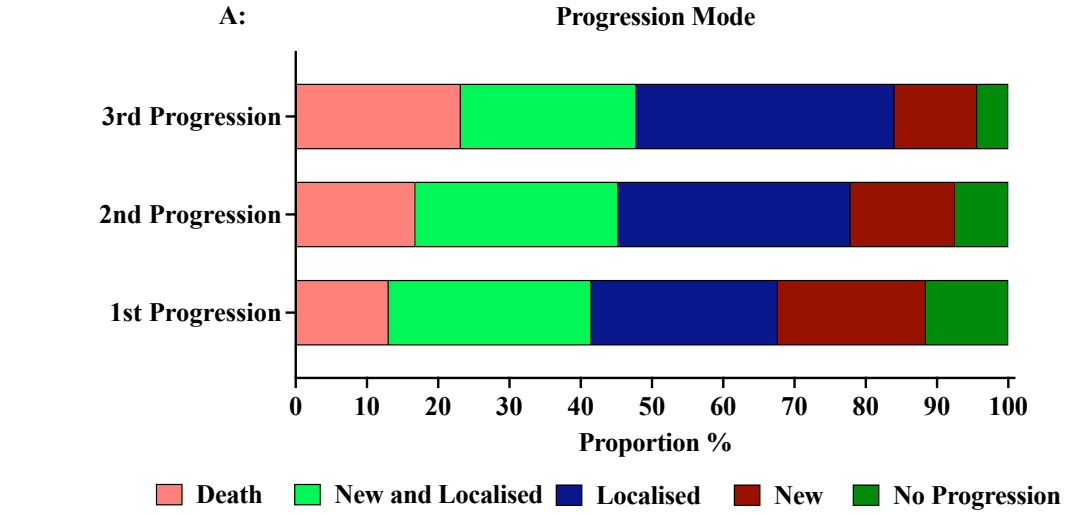


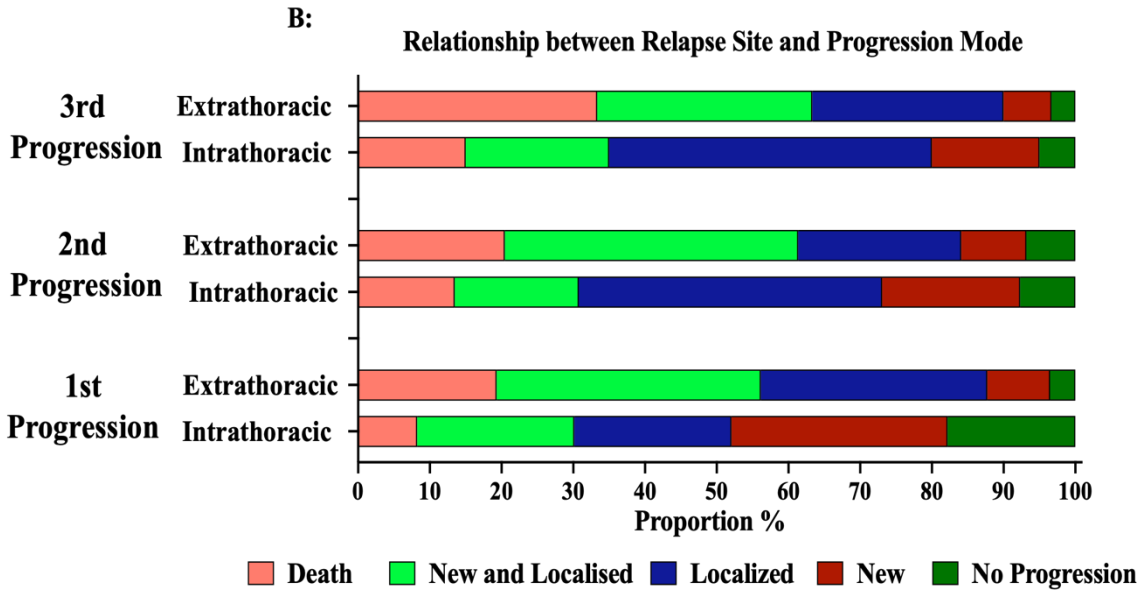

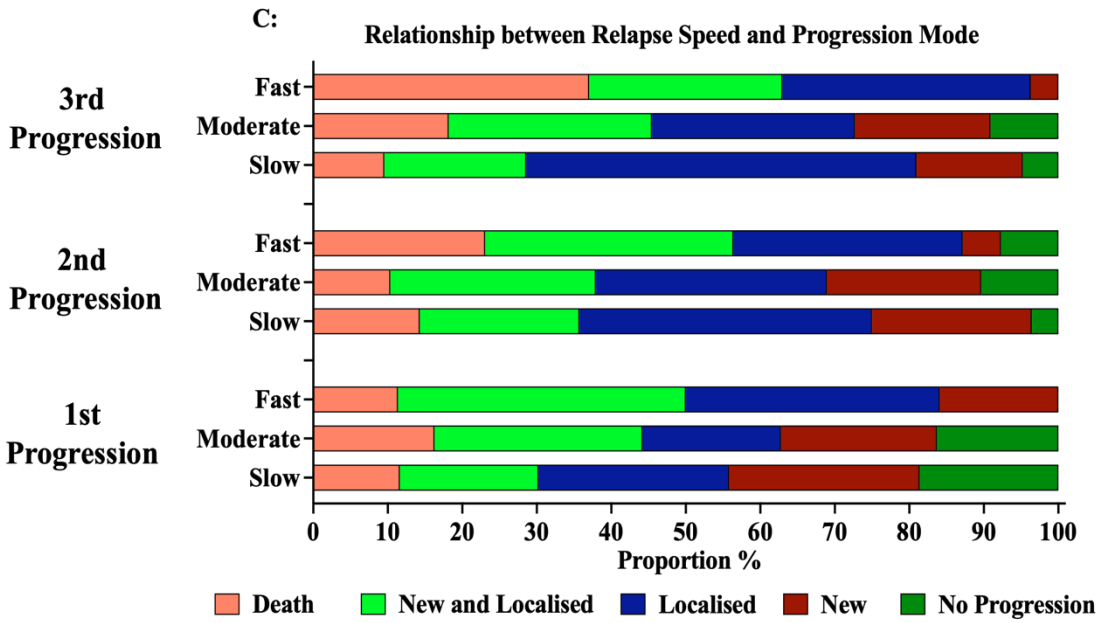


Fig. 4.20 Relationship between the relapse site, relapse speed, and progression mode at the first, second, and third progressions. A: Stacked bar plots illustrating the distribution of progression modes (new lesions only, localised expansion only, or both) across successive progression events. There was a shift towards more localised progression and a decrease in the exclusive emergence of new lesions as a result of progression. B: Stacked bar plots showing progression mode distribution according to the anatomical site of initial relapse. Intrathoracic relapses were more often associated with new lesion emergence, while extrathoracic relapses frequently involved both new lesions and localised expansions, indicating more complex progression dynamics. C: Stacked bar plots depicting progression mode distribution across relapse speed categories (slow, moderate, rapid) for each progression event. No consistent pattern was observed between relapse speed and progression mode.

# Results Summary

1. **Heterogeneity of relapse:**

- **Temporal and anatomical diversity:** 9–15 months post-surgery was the most common period for relapse events, with the lung being the most common initial site for intrathoracic relapse, irrespective of the tumour's extent, consistent with previous studies. Local lung relapsed earliest (median 346 days), while intrathoracic lymph node (especially N2) ranked as the second most common relapse site. No consistent link was found between lymph node status at diagnosis and later relapse, differing from prior literature. Bone emerged as the most frequent extrathoracic relapse site in this cohort, and this contrasts with previous literature, which reported the brain as the most common extrathoracic site.

  Limited intrathoracic tumour burden corresponded with the longest DFS, whereas extensive extrathoracic tumour burden resulted in the shortest DFS, as evidenced by other researchers as well. This study specifically revealed that a subset of initial oligometastatic relapses progressed to widespread tumour burden and had earlier relapses. Site-specific burden also differed: poly-extrathoracic relapse frequently involved the bone, whereas the brain was more common in oligo-extrathoracic relapse.
- **Relapse growth rate diversity:** This study notably revealed that relapse tumour growth rates increased alongside lesion growth speed, particularly in extrathoracic sites, leading to a massive total tumour burden and a worse prognosis, but was not associated with the number of progression events. Interestingly, the relapse tumour growth rate before treatment correlated weakly with the post-treatment tumour growth rate. These insights suggest that dynamic growth features may offer prognostic value.

2. **Heterogeneity of progression:**

- **Site-specific relapse and subsequent progression:** Ipsilateral lung relapse was the most common relapse type in single-lung relapse, and the median PFS was 244 days for new lesion progression. Key indicators of ipsilateral relapse included a primary tumour in the right upper lung, slow relapse speed, female gender, diagnosis of LUAD, and pleural attachment. Predictors of exclusive brain relapse were related to advanced stages (at least stage IIB), large primary tumours in the peripheral lung,

LUAD, and pleural involvement (as confirmed by other studies as well), rapid relapse speed, and the absence of air bronchogram. These findings remain exploratory due to the limited sample size.

- **Impact of tumour volumes and lesion counts on progression:** New findings in this research showed that relapse growth rate correlated with both larger tumour volume and faster progression speeds. In contrast, lesion count alone did not predict growth or survival. These results suggest that tumour volume and speed may better reflect biological aggressiveness than lesion number.
- **Site and progression patterns:** New findings in this research showed that patients with intrathoracic relapses tended to develop new lesions. In contrast, extrathoracic relapses often experienced a mix of new lesions and local expansions, indicating more complex and aggressive progression modes. Progression into or within extrathoracic locations was associated with shorter survival and greater aggressiveness.

**3. Site-specific prognosis:**

Early involvement of the bone, intrathoracic pleura, extrathoracic lymph node, brain and extrathoracic soft tissue can impact prognosis. Patients with lung-only relapses had better outcomes than those who never relapsed in the lung or who had multiorgan relapses. Conversely, brain metastases were linked to the worst survival outcomes, consistent with previous findings. While these site-specific findings are clinically relevant, small subgroup sizes limit statistical power and generalisability.

.

# Discussions

As disease-free survival (DFS) is identified as a critical factor in predicting patient outcomes [204], this study explores the recurrence patterns of non-small cell lung cancers (NSCLC), with a focus on how these patterns vary by relapse speed and anatomical site. Reported recurrence rates range widely from 17.8% to 71%, with lower rates observed in early-stage NSCLC (stages I–II, 11.1%–22%) and significantly higher rates in advanced-stage IIIA disease (52%–72%) [205]. Conforti [206] found that the highest risk of recurrence occurs within the initial 18 months after surgery, with a peak between 6–12 months and gradually increasing until the fourth year post-operation [207]. Consistent with prior studies, this study found a notable frequency of relapse within 9–15 months. Several studies have shown that neoadjuvant or adjuvant therapies can prolong DFS [208,209], with a median DFS of more than 46 months. Such treatments were less commonly used in this cohort.

Organ-specific relapse timing and probabilities in NSCLC vary widely, as one investigation into relapse patterns indicated that advanced NSCLC often primarily relapses with brain metastases [210]. At the same time, most studies have shown that locoregional recurrence, especially within the lung, is the most common relapse site in stage IB–IIIA NSCLC, including EGFR-positive tumours [207,211,212,213]. Another study from the USA [214] found that nearly 33% of lung relapse cases were local lung recurrences, having a median of 11 months earlier relapse, and recurrence days became shorter as the primary tumour stage increased, which aligns closely with my findings, despite the diversity of temporal relapse, lung remained the most frequent site for initial relapse, primarily through local recurrence about 11 months after surgery. Relapse time varied according to the primary tumour's stage and location; stage III tumours with local lung recurrence had the earliest relapse, and stage II tumours with contralateral lung recurrence had the latest relapse. The second most frequent site of relapse was the intrathoracic lymph nodes, particularly at the N2 station. Notably, the diagnostic accuracy of baseline PET/CT in predicting lymph node involvement at surgery was limited in this cohort, with a positive predictive value (PPV) of 78.8%, which is similar to another study, reporting a 64% positive predictive value [215]. Furthermore, lymph node status at baseline or in surgical specimens did not consistently correspond with subsequent lymph node relapse in this study. Similarly, the presence of ground-glass opacity (GGO) within or around the

primary tumour showed no correlation with lymph node recurrence, aligning with the findings from Wang et al [216]. Lymph node skip metastasis to mediastinum occurred in a small proportion of cases (4.85%–7%), and N2 involvement emerged as a prognostic factor for overall survival (OS) [216–218]. Differing from the previous results, in this cohort, lymph node metastases progressed in a sequential time frame, with N1 occurring the earliest, followed by N2 and N3. Bone was the most common extrathoracic metastasis in this cohort, similar to Wang's study [219]. The liver was not the most frequent extrathoracic relapse site, but it relapsed earlier than the bone. Furthermore, liver metastases can influence the growth of the primary lesion and the extent of metastases in other organs [29,30], suggesting that liver metastases are associated with a more aggressive biological behaviour.

The anatomical distribution and growth dynamics of NSCLC recurrences are heterogeneous, with some studies noting that extrathoracic metastatic recurrence rates were comparable to intrathoracic recurrence rates. In contrast, both intrathoracic and extrathoracic metastatic rates were lower, ranging from 4% to 19% [207,205,213]. An analysis of a subset of my dataset revealed a predominance of intrathoracic relapse (56%) [220], which was further supported as my cohort expanded, showing a majority (56.2%) with longer DFS. When stratifying by relapse tumour burden, intrathoracic oligometastatic disease tended to relapse later, whereas multiple extrathoracic metastases were associated with the earliest relapses, often within three months post-surgery. However, the number of progression events did not significantly differ between intrathoracic and extrathoracic relapses, likely due to the limited sample size. Further validation in larger cohorts is needed. Distinct patterns of tumour evolution in NSCLC were associated with differing clinical outcomes. An extensive population-based study involving 45,423 NSCLCs with distant metastases demonstrated substantial variability in mortality depending on the metastatic site [28]. Consistently, in this cohort, early involvement of the bone, intrathoracic pleura, extrathoracic lymph nodes, brain, and extrathoracic soft tissue was significantly associated with poorer prognosis.

This study offers novel insights by exploring a uniquely detailed imaging dataset comprising serial volumetric measurements across baseline, relapse, and post-treatment time points—an approach that has been rarely explored in previous NSCLC research. Distinct biological and clinical patterns between intrathoracic and extrathoracic relapses

were initially observed. Intrathoracic relapses, particularly those that progressed within the lung, were associated with better DFS and post-recurrence survival compared to extrathoracic or combined intrathoracic and extrathoracic involvements, consistent with previous findings [203]. Their progression patterns varied as well. Patients with intrathoracic relapse tended to maintain disease progression within the thorax, typically developing new lesions followed by localised expansion. While outcomes worsened once extrathoracic involvement occurred. Among patients who initially relapsed intrathoracically, the median time to subsequent extrathoracic progression was 171 days. Treatment after relapse, especially when involving multiple therapies, was found to extend extrathoracic progression-free days. Extrathoracic relapses were related to fast relapse speed. They were more inclined to experience the emergence of new lesions and localised lesion expansion simultaneously, indicating that extrathoracic relapse had more complicated progression modes than intrathoracic relapse. This more invasive progression mode may reflect underlying biological differences. Previous studies have found that genetic mutations are more common in extrathoracic metastases and related to worse prognosis [34,39,44–47], indicating that extrathoracic relapse has more aggressive behaviours. Previous TRACERx studies [107,109,157, 200] have demonstrated that spatial and temporal heterogeneity in NSCLC is shaped by branched evolution, with extrathoracic metastases often arising from subclones or polyclones under selective pressure. These subclones may harbour more aggressive subclones that carry immune escape characteristics, such as HLA loss or the presentation of new antigens, which contribute to a poorer prognosis. Furthermore, subclonal copy number alterations (SCNA ITH) have been proven to be associated with extrathoracic metastasis. Additionally, larger tumours have been shown to be associated with greater intratumour heterogeneity [201]. However, the relationships between relapse volume, growth rate, lesion count, and relapse sites have not been systematically characterised until now.

Hence, I did further exploration of the relationship between relapse burdens and anatomical relapse sites. The increased rate of relapse was associated with greater total tumour volume, accelerated progression dynamics, and extrathoracic involvement, all of which contributed to poorer prognosis. However, relapse speed was not associated with the total number of progression events. In contrast, the lesion count did not consistently correlate with the tumour growth rate or overall survival, which may explain why relapse speed showed no clear association with progression modes—such as the emergence of

new lesions—in this analysis. All these findings highlight the greater prognostic value of volumetric and kinetic measures over conventional lesion-based metrics. Interestingly, not all the patients died with a massive tumour burden at the last scan before death. Some may have died from cancer-related complications, while others likely experienced rapid disease progression between the last imaging and death. This result further underscores the importance of understanding the complexity of NSCLC relapse patterns and timing, and customised therapeutic strategies are crucial for improving patient outcomes.

To date, few studies have systematically investigated the relationship between tumour growth rates at baseline, during relapse, and following treatment. This novel study is the first to investigate tumour volume and growth rates longitudinally, encompassing baseline, relapse, pre-treatment, post-treatment and follow-up periods. Baseline tumour growth rates strongly correlated with initial volumes but showed only a weak correlation with relapse growth rates. Similarly, relapse growth rates correlated with relapse volumes, but there was a weak correlation between the speed before first-line treatment and post-first-line treatment. These results in this cohort demonstrated that tumour growth rates are dynamic and may be significantly influenced by treatment. This observation aligns with previous findings that metastatic lesions often harbour private monoclonal driver mutations absent from the primary tumour, suggesting treatment-driven clonal selection and the evolution of resistant subclones [23,202]. Additionally, apoptotic tumour cells or cancer stem cells can stimulate repopulation post-irradiation, leading to renewed tumour growth [221]. Moreover, TRACERx and other studies [107,112,114] have further shown that the immune microenvironment plays an important role in shaping distinct tumour evolution: LUADs tend to undergo truncal selection and are characterised by lower CD8+ T-cell infiltration, dispersed immune cells and localised clusters, while LUSCs are more at subclonal selection level, with higher CD8+ T-cell infiltration, and more structured immune-rich regions. Other factors, such as extracellular matrix (ECM) remodelling or tumour hypoxia, can also influence heterogeneity [222]. All these factors together further explain the heterogeneity in cancer evolution patterns, supporting the results that growth dynamics are not only dependent on intrinsic proliferative potential but also shaped by treatment pressure, immune selection, and microenvironmental factors.

Studying patients with single-organ relapse provides a clearer framework for analysing progression pathways than studying patients with multiple-site relapse, which can reduce

confounding factors. Consistent with findings from a Japanese study [117], the lung emerged as the most common site of single-organ relapse in this study, with the right upper lobe being particularly susceptible. Recurrences within the ipsilateral lung were predominant, typically presenting in females with right primary tumours, slow relapse speed, LUAD histology, and the presence of pleura involvement on baseline CT scans, which is similar to Guerra's findings, where visceral pleural invasion was a predictive value, but they only analysed locoregional recurrence [63]. The most prevalent post-relapse progression pattern was the emergence of new pulmonary lesions, with a median PFS of 244 days. A particularly aggressive progression involved simultaneous new lung lesions and localised lesion growth, often originating from contralateral or bilateral lung relapse. Patients who didn't receive treatment post-relapse were more likely to have localised tumour progression, with a median PFS of 140 days. Therefore, clinical strategies within this period are crucial for extending PFS. Some researchers demonstrated that patients with initial lung recurrence had better recurrence-free survival than those without [223]. A similar result was found in this cohort, patients who had only lung metastases showed a more prolonged post-recurrence survival than those who didn't undergo lung recurrence.

Single-organ relapse also frequently involves intrathoracic lymph nodes. The left lung, particularly the lower lobe, was more susceptible to this type of relapse. N2 nodal involvement is the most prevalent pattern among lymph node relapses. Patients with primary tumours in the left lung, rapid relapse, and baseline CT evidence of pleural involvement but lacking air bronchogram signs, were more likely to experience N2 lymph node relapse. The brain was the most common site of extrathoracic single-organ relapse. Wang's research demonstrated that in NSCLCs with brain metastases, the number and anatomical location of extracranial metastases may affect survival, although the association did not reach statistical significance [198]. Similarly, Isaka reported that multiple-site recurrences are associated with poor post-recurrence survival [117]. In this study, the cohort of patients with brain metastases was too small to permit an analysis of how the number and anatomical location of brain tumours might influence prognosis. Nevertheless, both groups with brain-only and multiple-site relapses showed worse outcomes compared to those with relapses confined to the lung or intrathoracic lymph nodes, highlighting the aggressive behaviour of brain metastasis. A study in 2007 found a 36% prevalence of brain metastases, correlating with larger primary tumours, LUAD histology, and advanced intrathoracic lymph node stage [224]. Similar results were

observed in this cohort: a higher probability of large primary tumour in the upper lung–particularly the right upper and peripheral regions–higher TNM stages (at least IIB), a predominance of LUAD, presence of pleural involvement on baseline CT scans, and absence of bronchial aerogram signs, although the subgroup size was limited.

In clinical practice, the anatomical site of relapse is already considered when guiding post-relapse treatment decisions, e.g., isolated brain metastasis may be treated with radical radiotherapy. However, relapse speed and tumour volume are not routinely incorporated into clinical decision-making. The exploratory findings from this study suggest that combining anatomical relapse patterns with new prognostic dimensions (tumour volume and speed) may provide a more comprehensive framework for post-relapse risk stratification than lesion count alone. This multidimensional approach could inform more personalised treatment strategies and surveillance protocols. However, several limitations should be acknowledged, including the relatively small cohort of relapsed patients and variability in imaging intervals. Further validation in larger, independent cohorts is required. In particular, molecular profiling of rapidly growing extrathoracic relapses may help uncover key genomic drivers or immune-related mechanisms underlying their aggressive behaviour.

## Conclusions

This study identifies several novel findings: larger tumour volumes, faster progression, and extrathoracic involvement are associated with higher initial relapse rates and poorer outcomes, highlighting that volume and speed may serve as stronger prognostic indicators than lesion count alone. Relapse and progression patterns vary by timing, anatomical location, and growth characteristics, with intrathoracic recurrence—especially in the lung—being most common and generally associated with better outcomes. Poor prognosis is observed in patients with relapses involving multiple organs or the brain, consistent with previous research. Notably, intrathoracic relapses often present as new lesions or localised expansions, while extrathoracic relapses frequently involve both new and expanding lesions, indicating more complex progression and worse survival.

# Chapter Five

# Recommendations for NSCLC Surveillance and Optimal Tumour Reduction Post-Treatment for Improved Prognosis

## Highlights

**Aims:** This chapter aims to evaluate the role of surveillance frequency and identify key factors influencing progression-free survival (PFS) in non-small cell lung cancer (NSCLC). By analysing post-surgical and post-relapse tumour dynamics, this work proposes a framework to inform individualised surveillance and treatment strategies for improved patient outcomes.

1. Examine how frequent imaging follow-ups affect prognosis and surveillance considerations.
2. Investigate predictive factors of tumour progression and overall survival.
3. Investigate how tumour growth dynamics and treatment response influence post-relapse outcomes.

**Methods:** A Cox regression model was used to assess the effect of different surveillance frequencies on overall survival (OS), taking into account various clinical characteristics. The model also explored how progression-free survival (PFS) and treatment outcomes could inform personalised clinical management. Additionally, ROC curve analysis was utilised to identify the optimal threshold for tumour volume reduction during initial therapy as a predictor of prognosis, providing insights into early treatment effectiveness and long-term outcomes.

**Results:**

- **Frequency of Scans and Prognosis:** 30% of patients presented with equivocal lesions post-surgery, with 68.9% later confirmed malignant. Frequent imaging follow-ups were more common in large-sized primary tumours. High frequency did not improve overall survival, especially in early-stage and smaller tumours, consistent with previous findings. Additionally, high-frequency imaging did not correlate with the earlier detection

of smaller relapse volumes. These observations suggest a limited benefit from intensified surveillance; however, the findings should be interpreted cautiously due to the cohort size and potential confounders.

- **Post-Relapse Treatment Timing Considerations:** The findings from this study primarily demonstrated that the speed of relapse did not significantly impact progression-free survival (PFS) across relapse sites. However, differences in post-relapse progression patterns were observed. Lung and intrathoracic-dominant relapses were generally associated with more stable disease courses, while brain and other extrathoracic relapses appeared to progress more rapidly. While no definitive surveillance interval can be proposed based on these data, the observed site-specific differences may have important implications for future research.
- **Progression-free survival (PFS) and Tumour Burden as Predictive Factors:** The findings from this study primarily demonstrated that PFS, best response to initial therapy (as assessed by Volume-RECIST), tumour volume, and growth rate at first progression, were indicative factors of progression speed and volume, all of which influenced overall survival. Notably, a tumour volume reduction greater than 65% following initial treatment was associated with improved prognosis (AUC = 0.81).
- **Maximum tumour burden related to Heterogeneity:** The findings from this study primarily demonstrated that patients reaching maximum tumour burden earlier in the disease course tended to have smaller tumour burden and better prognosis compared to those with later peak volumes. Later-peak tumours more frequently showed lesion increase and higher heterogeneity, potentially contributing to immunotherapy resistance.

**Conclusions:** Current follow-up protocols, based solely on the TNM stage, may be insufficient for optimising surveillance. Site-specific relapse patterns may help to tailor follow-up intensity in the future. Key prognostic indicators include PFS, the best initial therapy response (particularly volume reduction of>65%), and tumour burden. Additionally, rapid tumour growth and high heterogeneity are associated with larger, more resistant relapses. These results support the potential value of personalised surveillance strategies in NSCLC.

# Introduction

Approximately 1.5 million pulmonary nodules are identified annually in the United States through the use of CT imaging. Around 5% of detected nodules are malignant. In current practice, 22% of patients with indeterminate lesions on imaging undergo unnecessary invasive biopsies [225], leading to a unique dilemma in the surveillance of NSCLC patients. Surgical resection remains the gold standard treatment for early-stage non-small cell lung cancers (NSCLC), providing long-term disease control. Despite achievements in surgery, the post-resection landscape is interrupted by recurrence. Routine surveillance imaging plays an essential role in monitoring patients with resected non-small cell lung cancer (NSCLC) to detect disease recurrence and new primary lung cancers. A recent inquiry from a cohort of 140 patients receiving annual chest CT scans revealed that 30 of 168 scans showing equivocal lesions, only 14, less than half, actually represented recurrent disease [121]. According to NCCN guidelines, early-stage NSCLCs should undergo imaging checks every six months for the first two years post-radical resection and then annually up to the fifth year [7]. Despite these guidelines, surveillance intensity varies widely in clinical practice. More than 50% of patients may experience early relapse before their scheduled examination due to the onset of symptoms [130]. In contrast, some patients relapse after five years, and others might never relapse at all. There is still a controversy about the optimal frequency of imaging scans.

Previous studies have not been able to establish a precise follow-up guideline for resected NSCLC due to the wide range of reported recurrence rates. 5-year local recurrence rates vary from 15 to 38.5% [226], while recurrence rates drop to 10% in early-stage lung cancers [227]. Additionally, circulating tumour cells shed from the primary tumour may lead to an early relapse post-resection. However, such relapses remain undetectable until the formation of a solid tumour, which is identifiable through imaging. Generally, it is believed that tumours contain approximately $1x10^7$ cells when they reach a diameter of 1 millimetre, which is roughly the smallest size detectable by certain highly sensitive imaging technologies [7]. Many researchers have considered that high-intensity imaging checks can help detect early tumour relapse and potentially improve overall survival [131]. However, McMurry and his colleagues reviewed more than 4000 NSCLC patients and found that the increased frequency of CT imaging did not improve survival [125]. Diverse

recommendations exist for surveillance intervals post-relapse as well. Initially, imaging should be conducted every 2–3 months to assess the disease and plan further treatment. For patients in stable status after treatment, the frequency of imaging can be reduced to every 3–6 months. For patients on maintenance therapy, less frequent monitoring, typically every 6 months, may be sufficient.

Based on these findings, it is essential to select factors that guide personalised monitoring for post-operation and post-relapse patients. Tailored methods can improve tumour detection, enhance treatment effectiveness, and reduce clinical costs.

# Patients and Methods

## Tumour Progression Estimation

1. RECIST standard criteria

It is the same as the Methodology Chapter.

2. Volume-RECIST

There is currently no universally accepted criterion for assessing progression using tumour volume. In my cohort, I defined a complete response (CR) as lesions disappearing. A partial response (PR) was deemed to be at least a 30% reduction in the sum of the whole targeted tumour volume compared with the previous scan. Progressive disease (PD) was defined as a 20% or greater increase in the entire tumour volume or the appearance of one or more new lesions.

3. Definition of Dominant Lesion

The lesion occupying at least 50% of the total tumour volume at relapse was defined as the dominant lesion, and the organ containing this lesion was defined as the dominant organ at relapse.

4. Progression-free survival (PFS) was defined as the interval from the start date of post-relapse treatment (radiation/chemotherapy) to disease progression, death or last follow-up. If the patient did not receive therapy, PFS was calculated from the date of the corresponding scan to the date of progression, death, or last follow-up.

## Tumour Growth Rate and Volume Calculation

1. Relapse tumour growth rate calculation formula: defined in Methodology Chapter

2. Tumour progression growth rate and progression volume calculation formula:

Date2 is the date of the scan showing progression and Date1 is the date of the preceding scan.

Progression Tumour Growth Rate ($mm^3$/day) = (Volume2 – Volume1) / (Date2 – Date1)

Progression Tumour Volume ($mm^3$) = Volume2 – Volume1

3. Tumour growth rate and volume before treatment:

To assess tumour growth prior to therapy, two pre-treatment scans were selected. Scan A refers to the imaging scan immediately before the initiation of treatment, and Scan B is the scan preceding Scan A. The following formulas were used.

Before Treatment Tumour Growth Rate ($mm^3$/day) = (Volume A – Volume B) / (Date A – Date B)

Before Treatment Tumour Volume ($mm^3$) = Volume A – Volume B

Days before treatment (days) = Treatment start date – Scan A date

If the imaging taken before the start of treatment is significantly dated from the initiation of therapy, a new image is available around the time of treatment. The tumour volume and time indicated on this image at the start of therapy can be used to represent the pre-treatment tumour volume and start time. This approach was taken to calculate the tumour growth rate precisely. The median interval between the final pre-treatment scan and the start of therapy was 29 days (Interquartile Range [IQR], 13–50 days).

4. Tumour growth rate and volume after treatment:

To estimate post-treatment tumour growth, I used the first scan following the completion of therapy (Scan A) and the most recent scan prior to the end of treatment (Scan B). This choice was necessary because no dedicated scan was routinely taken at the exact end of treatment in many cases. As a result, Scan B may reflect ongoing treatment effects, potentially underestimating early post-treatment regrowth. The median interval between the end of treatment and Scan A was 16 days (Interquartile Range [IQR], 1–72 days), indicating that growth rate estimates largely reflect the early post-treatment period. The growth rate was calculated as:

After Treatment Tumour Growth Rate ($mm^3$/day) = (Volume A – Volume B) / (Date A – Date B)

After Treatment Tumour Volume ($mm^3$) = Volume A – Volume B

Days after treatment (days) = Scan A date – Treatment end date

5. Total tumour volume calculation:

For each patient, the total tumour volume was calculated by first summing the volumes of all lesions at each progression event, then averaging these values across all progression events. This method is illustrated in Fig. 5.1.

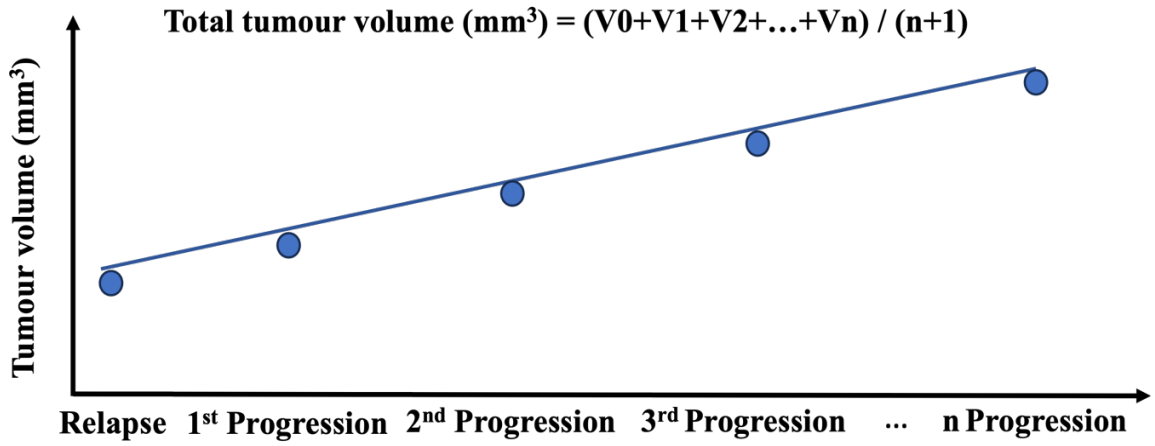


Fig. 5.1 Illustration of the method of total tumour volume calculation.

**Treatment regimens post-recurrence**

Details of the treatment regimens administered after recurrence are summarised in the table below.

Table 5.1 Treatment characteristics of patients following relapse

| Regimens | First line | Second line | Third line | Fourth line | Fifth line | Sixth line |
|---|---|---|---|---|---|---|
| Chemotherapy | 12 | 11 | 5 | 1 | | 1 |
| Radical Radiotherapy | 26 | 1 | 2 | 1 | 1 | 1 |
| Immunotherapy | 20 | 10 | 17 | 1 | | |
| Targeted therapy | 11 | 6 | 2 | 1 | | |
| Metastectomy | 7 | 3 | 1 | | | |
| RFA | 2 | 5 | | | | |
| Palliative Radiotherapy | 18 | 6 | 1 | 2 | 2 | 1 |
| Chemotherapy and Immunotherapy | 4 | 1 | | | 1 | |
| Chemoradiotherapy and Immunotherapy | 2 | 1 | 1 | | | |
| Chemoradiotherapy | 9 | 3 | 1 | | | |
| Radiotherapy and Immunotherapy | 2 | 2 | 1 | | | |
| Metastectomy and Radical Radiotherapy | 2 | | | | | |

**Follow-up CT surveillance post-operation**

31 patients with equivocal lesions on surveillance CT were eventually diagnosed with malignancy.

1. Surveillance days of each year

Due to scheduling limitations in routine clinical practice and individual patient circumstances, follow-up imaging in the first year after surgery was not always performed precisely at the 12-month mark. In this cohort, the first post-operative year was defined as the period from 0 to 14 months after surgery. Subsequent years were similarly defined

in 12-month intervals with a 2-month buffer to reflect real-world clinical variation in scan timing: the second year as 14 to 26 months, the third year as 26 to 38 months, the fourth year as 38 to 50 months, and the fifth year as 50 to 62 months. Follow-up beyond five years was defined as more than 62 months post-operation (Fig. 5.2). The endpoint of surveillance was the detection of recurrence.

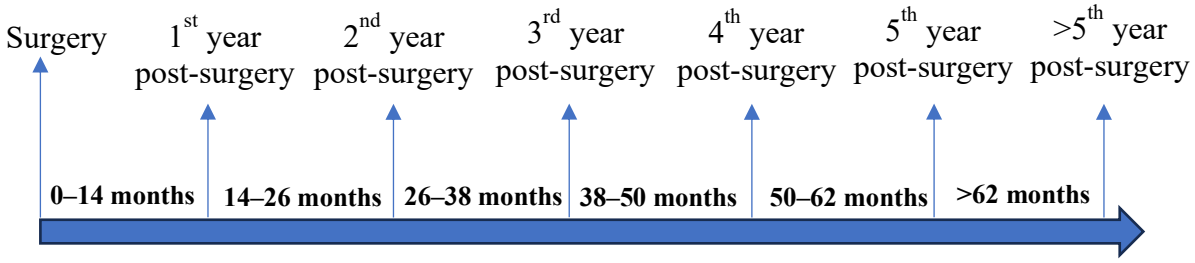


Fig. 5.2 Definition of the post-operation year in this study.

2. Different surveillance intensity groups

McMurry and his colleagues reviewed more than 4000 NSCLC patients. They separated them into three groups based on the timing of their first post-operative scan: high-intensity (>2.5 months to <5 months), moderate-intensity (≥5 months to <9 months), and low-intensity (≥9 months to <14 months) surveillance groups [125]. In alignment with this approach, I also created time-based visit windows to categorise patients based on the interval between surgery and their first surveillance CT scan. The visit windows were defined as follows: 0 to 120 days (0–4 months), 121 to 243 days (4–8 months), and 244 to 425 days (8–14 months), corresponding to high-intensity (3 months), moderate-intensity (6 months), and low-intensity (1 year) surveillance groups, respectively. Alternative stratification methods were explored but led to significant group imbalances or lacked relevance to real-world clinical practice (*Appendix 2*).

The number of surveillance CT scans performed within the first two years after surgery, as well as the average number of scans per year during this period, was calculated. As clinical follow-up appointments often vary in timing and do not always strictly adhere to scheduled intervals in real-world practice, follow-ups intended for two years may extend up to 26 months post-surgery. Therefore, the two-year surveillance window was defined as the period from the date of surgery to 26 months thereafter.

3. Criteria for defining surveillance scans post-operation and prior to relapse.

3.1 Post-operative chest X-rays were not considered as follow-up surveillance imaging.

3.2 Head CT or MRI was not classified as standard routine surveillance. However, if the first site of recurrence was the brain, then the initial head CT or MRI identifying the recurrence was considered the first surveillance scan.

3.3 In this cohort, chest CT scan, including thoracic and upper abdominal sections, with or without contrast, and regardless of whether a full abdominal CT was performed, was classified as a standard surveillance scan. Bone or spine CT was not considered standard follow-up surveillance.

3.4 Based on worldwide guidelines, PET/CT is not routinely used for post-operative surveillance. Suppose a CT scan and a PET/CT scan were performed within a short timeframe (within 1–2 months) for the same purpose of checking symptoms or equivocal lesions. In that case, they should be considered as part of a single standard follow-up surveillance imaging. In this case, the date of the initial CT scan was used to calculate the duration of surveillance. For brain metastases, when a head CT was followed shortly by a brain MRI for clarification, these scans were considered part of a single diagnostic event. In such cases, the date of the head CT was used to determine surveillance timing, as the MRI served primarily to refine lesion characterisation.

**Flow chart of optimal surveillance strategy analysis across different phases of tumour evolution**

Surveillance strategies may be optimised by aligning with distinct phases of tumour evolution, specifically the post-surgical, post-relapse, and post-first progression periods. (Fig. 5.3)

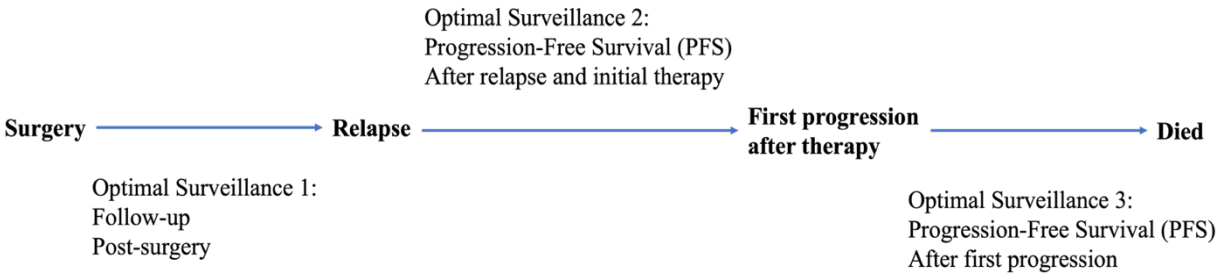


Fig. 5.3 Flow chart of surveillance strategy analysis across different phases.

# Results

## 1. Optimal surveillance periods between post-surgery and relapse

### 1.1 Patients with high-, moderate-, and low-intensity surveillance schedules before relapse

**Study Population:** Among 200 patients, the median number of days to the first standard surveillance scan post-operation was 194 (Interquartile Range [IQR], 107–332).

**Relapse and Surveillance Intervals:**

- Relapsed patients: Among the 130 patients who experienced relapse, the median surveillance days before relapse were 180 (Interquartile Range [IQR], 104–278), supporting a potential benefit of imaging at approximately 6-month intervals.
- Non-relapsed patients: The 70 non-relapsed patients had a median surveillance period of 339 days (Interquartile Range [IQR], 217–373) from surgery to last follow-up. (Fig. 5.4A)

**Annual Surveillance Analysis:** Across the entire cohort, the median surveillance intervals post-resection and prior to relapse were as follows:

- First Year: 175 days (approximately 6 months, [IQR] 105–246)
- Second Year: 265 days (approximately 9 months, [IQR] 167–376)
- Third Year: 340 days (nearly 1 year, [IQR] 191–391)
- Fourth Year: 362 days (nearly 1 year, [IQR] 240–423)
- Fifth Year: 371 days (about 1 year, [IQR] 324–438)
- Over Fifth Year: 368 days (1 year, [IQR] 248–493)

The median number of surveillance scans per year was 1. Within the first year (defined as 0–14 months) after surgery, 73 patients experienced relapse, with a median surveillance interval of 142 days. In contrast, non-relapsed patients had a longer median surveillance interval of 183 days (Fig. 5.4B).

**A:**

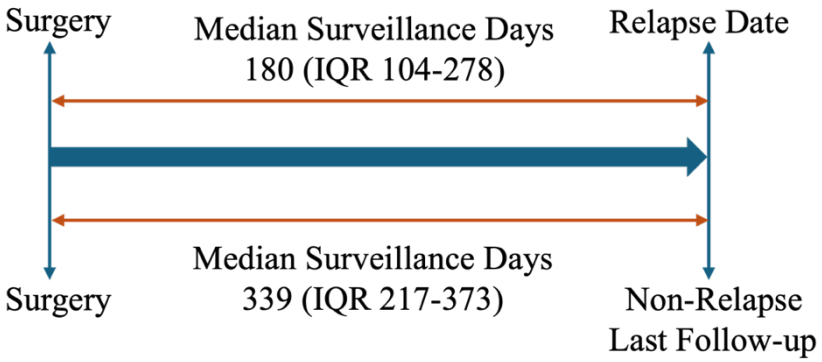


**B:**

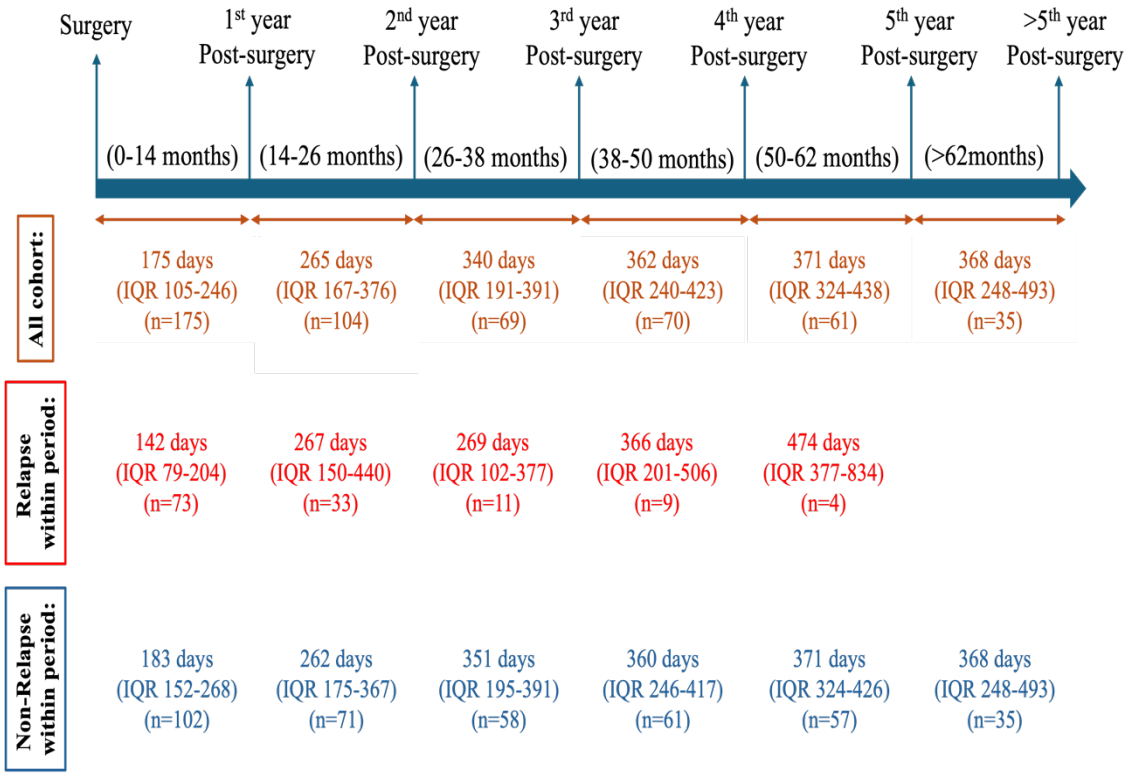


Fig. 5.4 Surveillance timing following surgery. A: Median surveillance intervals among patients who experienced relapse versus those who did not, measured from the date of surgery to the last follow-up or recurrence event; B. Duration of surveillance during each follow-up year across the entire cohort, including both relapsed and non-relapsed patients within the corresponding surveillance periods.

These data suggest that more frequent imaging (every 3–6 months) may be associated with the detection of early relapse. However, as surveillance intensity is often influenced

by clinical judgement, this may introduce potential bias. These findings underscore the need for individualised surveillance strategies.

**Surveillance Intensity Groups:** To explore the effect of the surveillance intensity on clinical performance, patients were categorised into high-, moderate- and low-intensity groups based on the timing of their first standard follow-up scan (55, 67, and 53 patients, respectively, with 25 excluded due to delayed first CT scans). Patients who had delayed their first standard CT scans may have received chest X-ray checks instead of CT scans or missed follow-up scans. After excluding those 25 patients, the remaining 175 patients had a median of 175 days from the surgery to the first follow-up scan. The distribution of times from surgery to first surveillance imaging, categorised by surveillance intensity group, is shown in Fig. 5.5, and patients' characteristics are listed in Table 5.2.

There were no significant differences in overall relapse rates among the three surveillance groups. The low-intensity surveillance group contained a higher proportion of early-staged NSCLCs, which partially explains the observed lower 2-year recurrence rates in this group despite similar long-term recurrence rates. This result reflects underlying clinical decision-making, where clinicians increase surveillance frequency in response to the perceived risk of relapse.

There were no significant differences in age, gender, smoking status, histology, adjuvant therapy, types of surgery, inner tumour growth rate, and the anatomical location of the primary tumour across the groups. There were also no significant differences in oligo relapse status, single lesion relapse and relapse sites across the three intensity groups. Despite receiving more scans during the initial two years, patients in the high-intensity surveillance group had shorter surveillance periods and disease-free survival (DFS).

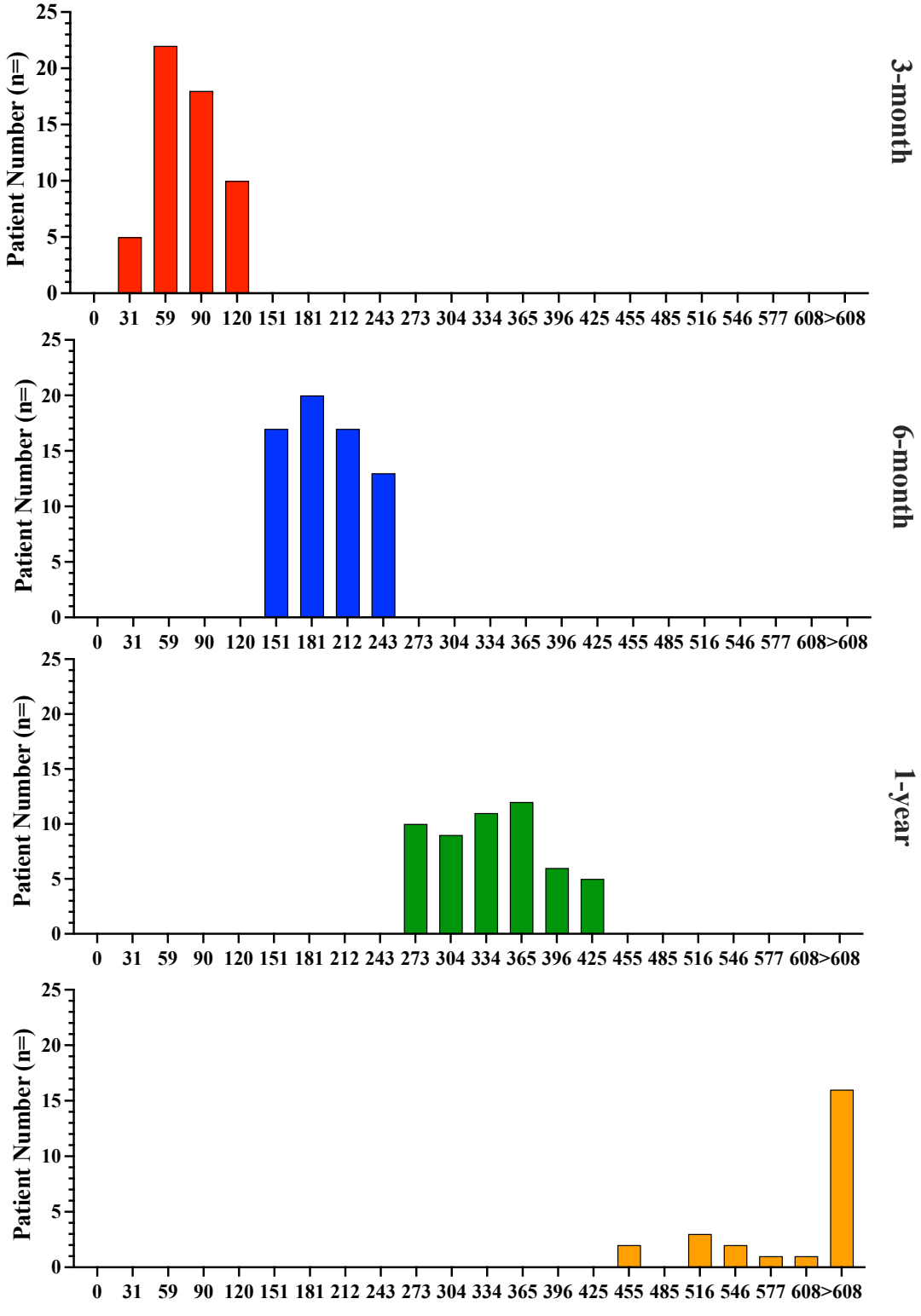


Fig. 5.5 Time from surgery to first surveillance imaging by surveillance intensity group.

Table 5.2 Patient demographics for the 3 surveillance groupings, presented as n (%) for categorical variables and median for continuous variables.

| **Characteristics (n=)** | **3-month** | **6-month** | **1-year** | **Adjusted P-Value** |
|---|---|---|---|---|
| n | 55 | 67 | 53 | |
| Relapse within period | 12 (22%) | 17 (25%) | 16 (30%) | 0.728 |
| 24 months relapse | 42 (76%) | 34 (50%) | 23 (43%) | 0.009* |
| Overall Relapse | 44 (80%) | 45 (67%) | 29 (55%) | 0.068 |
| Age (Median±SD) | 70 (9.5) | 68 (8.9) | 67 (9.5) | 0.557 |
| Gender (male) | 29 (53%) | 38 (57%) | 31 (58%) | 0.856 |
| Smoking Status | | | | |
| *Current smoker* | 3 (5%) | 9 (13%) | 5 (9%) | 0.678 |
| *Ex-smoker* | 26 (47%) | 34 (51%) | 29 (55%) | |
| *Recent Ex-smoker* | 19 (35%) | 18 (27%) | 17 (32%) | |
| *Never smoker* | 7 (13%) | 6 (9%) | 2 (4%) | |
| Histology | | | | |
| *LUSC* | 18 (33%) | 17 (25%) | 16 (30%) | 0.694 |
| *LUAD* | 28 (51%) | 44 (66%) | 31 (59%) | |
| *Other* | 9 16%) | 6 (9%) | 6 (11%) | |
| Pathologic TNM stage | | | | 0.039* |
| *I* | 8 (15%) | 29 (43.3%) | 23 (43%) | |
| *II* | 21 (38%) | 17 (25.4%) | 12 (23%) | |
| *III* | 26 (47%) | 21 (31.3%) | 18 (34%) | |
| Adjuvant therapy | 24 (44%) | 24 (36%) | 21 (40%) | 0.733 |
| Surgery Type | | | | 0.733 |
| *Lobectomy* | 44 (80%) | 58 (87%) | 47 (89%) | |
| *Segmentectomy or wedge* | 5 (9%) | 5 (7%) | 2 (4%) | |
| *Bilobectomy or Pneumonectomy* | 6 (11%) | 4 (6%) | 4 (7%) | |
| Primary Tumour Volume ($mm^3$, median, IQR) | 35970 (13390–87590) | 13955 (5073–39480) | 14480 (4749–62765) | 0.027* |

| | | | | |
|---|---|---|---|---|
| Primary Tumour Growth Rate ($mm^3$/d, median, IQR) | 94.87 (8.59–318.7) | 20.89 (6.803–56) | 54.33 (6.45–128.6) | 0.243 |
| Anatomical Location | | | | 0.674 |
| *RU/ML* | 22 (40%) | 26 (39%) | 18 (34%) | |
| *RLL* | 13 (24%) | 15 (22%) | 17 (32%) | |
| *LUL* | 14 (25%) | 19 (28%) | 8 (15%) | |
| *LLL* | 6 (11%) | 7 (11%) | 10 (19%) | |
| Central Location | 19 (35%) | 22 (33%) | 17 (32%) | 0.991 |
| Pleural Attachment | 40 (73%) | 42 (63%) | 28 (53%) | 0.243 |
| Bronchial Attachment | 21 (38%) | 13 (19%) | 16 (30%) | 0.21 |
| Air Bronchogram | 20 (36%) | 26 (39%) | 24 (45%) | 0.728 |
| Atelectasis | 29 (53%) | 26 (39%) | 22 (42%) | 0.467 |
| Pleural Retraction | 24 (44%) | 29 (43%) | 18 (34%) | 0.678 |
| Relapse Site | | | | 0.245 |
| *Intrathoracic* | 22 (40%) | 28 (42%) | 14 (27%) | |
| *Extrathoracic* | 9 (16%) | 9 (13%) | 6 (11%) | |
| *Both* | 13 (24%) | 8 (12%) | 9 (17%) | |
| *None* | 11 (20%) | 22 (33%) | 24 (45%) | |
| New primary tumour | 2 (4%) | 7 (10%) | 2 (4%) | 0.365 |
| Oligo relapse status | 33 (60%) | 36 (54%) | 22 (42%) | 0.307 |
| Single lesion relapse | 13 (24%) | 18 (27%) | 7 (13%) | 0.349 |
| Scans in the first 2-year, (n, median, IQR) | 3 (2–4) | 2 (1–3) | 2 (1–2) | 0.027* |
| Scans in the first 2-year, n/per year (n, median, IQR) | 1 (1–2) | 1 (1–2) | 1 (1–1) | 0.027* |
| Surveillance days in the first 2-year (median, IQR) | 102 (68–151) | 187 (147–232) | 301 (244–342) | 0.001* |
| Surveillance days at relapse or last follow-up (media, IQR) | 102 (68–150) | 191 (148–247) | 315 (258–369) | 0.001* |

P values were adjusted using the Benjamini–Hochberg False Discovery Rate (FDR) method to account for multiple comparisons (n=27 tests).

### 1.2 Survival in high-, moderate-, and low-intensity surveillance group

The clinical benefit of frequent surveillance remains controversial, especially in early-stage tumours [118,122–124,228,229]. The findings from this study indicated that the low-intensity surveillance group had the lowest 2-year recurrence rates. However, this introduces potential bias, as surveillance intensity was not randomly assigned. Patients deemed at higher risk by clinicians were more likely to receive frequent imaging. Additionally, some patients in the low-intensity group underwent delayed imaging due to external factors such as the COVID-19 pandemic, which may have contributed to later detection of relapse. These factors complicate the interpretation of surveillance intensity as an independent predictor of disease-free survival (DFS). While there were no significant differences in overall relapse rates among surveillance groups, the role of surveillance intensity in predicting long-term survival remains uncertain. Further analysis showed that the survival rates were similar in low- and moderate-intensity surveillance groups. The high-intensity surveillance group demonstrated the worst overall survival rates (P=0.009, Fig. 5.6). A previous TRACERx study [109] recommended adjusting for factors such as age, smoking pack-years, histological subtype, adjuvant therapy, and TNM staging in multivariate analysis. In this cohort, after applying these adjustments, surveillance intensity was not a significant predictor of survival (Table 5.3). This insignificant result may be partially because the treatment strategy post-relapse also plays a significant role in outcomes.

Nevertheless, it is essential to strategically utilise high-frequency scanning within specific subgroups to maximise its benefits across various parameters. This deeper analysis is critical given the ongoing controversy over whether early-stage tumours require high-intensity surveillance.

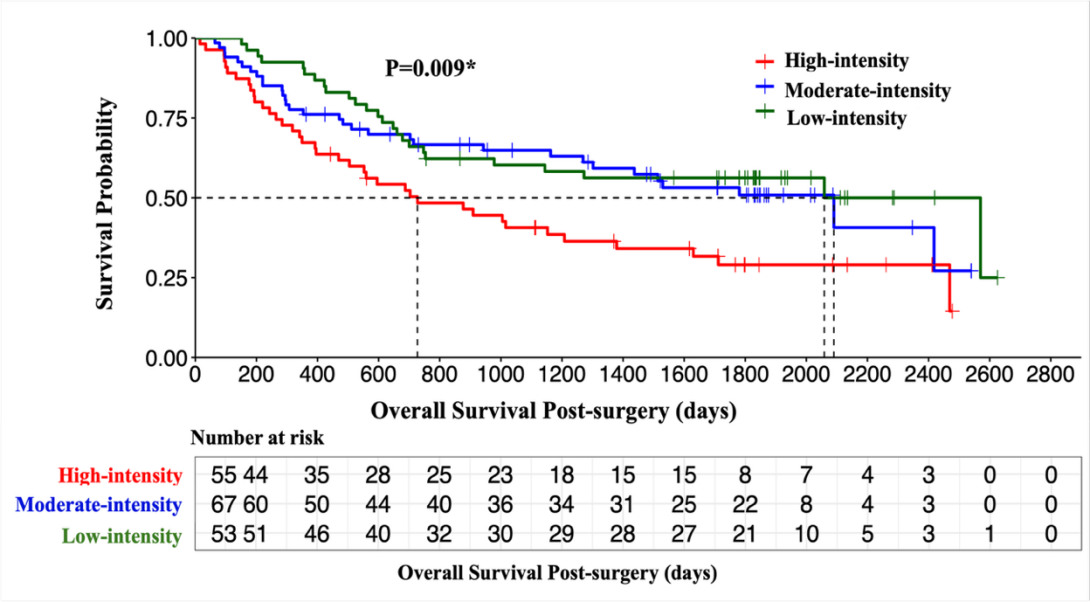


Fig. 5.6 Comparison of overall survival post-surgery across surveillance intensity groups.

Table 5.3 Multivariable analysis of surveillance intensity overall survival post-surgery

| Factor | Adjusted hazard ratio | 95%CI | Adjusted P-value |
|---|---|---|---|
| Age | 1.01 | 0.98–1.03 | 0.747 |
| Smoking Pack Years | 1.01 | 1–1.01 | 0.221 |
| Adjuvant Therapy | 0.92 | 0.55–1.54 | 0.747 |
| Histology | | | 0.039* |
| pTNM stage | | | 0.006* |
| Surveillance Intensity | | | 0.098 |

### 1.2.1 Early-stage tumours across high-, moderate-, and low-intensity surveillance groups

In the first two years after resection, the median surveillance durations were 269 days for stage I, 151 days for stage II, and 150 days for stage III patients, respectively (P<0.0001; *Appendix 3*, Fig. 1A–B). Before relapse, the median surveillance periods were 301 days for stage I, 170 days for stage II, and 150 days for stage III patients, respectively (P<0.0001). Not all stage I patients underwent low-frequency imaging; specifically, 8 of 60 (13%) received high-intensity surveillance. Meanwhile, 18 of 65 (28%) stage III patients received low-frequency follow-ups. Notably, 9 stage II patients relapsed within

6 months, suggesting that relying solely on TNM staging as a surveillance guideline is insufficient. Due to the fewer stage I patients in the high-intensity group, patients with stage I and II tumours were categorised as early-stage tumours. No significant differences in overall survival were observed among the three surveillance intensity groups in patients with early-stage tumours (Fig. 5.7). These findings suggest that high-frequency scans may not improve survival in early-stage tumours. However, given the limited cohort size and potential confounding factors, further validation in larger prospective studies is needed before altering clinical surveillance guidelines.

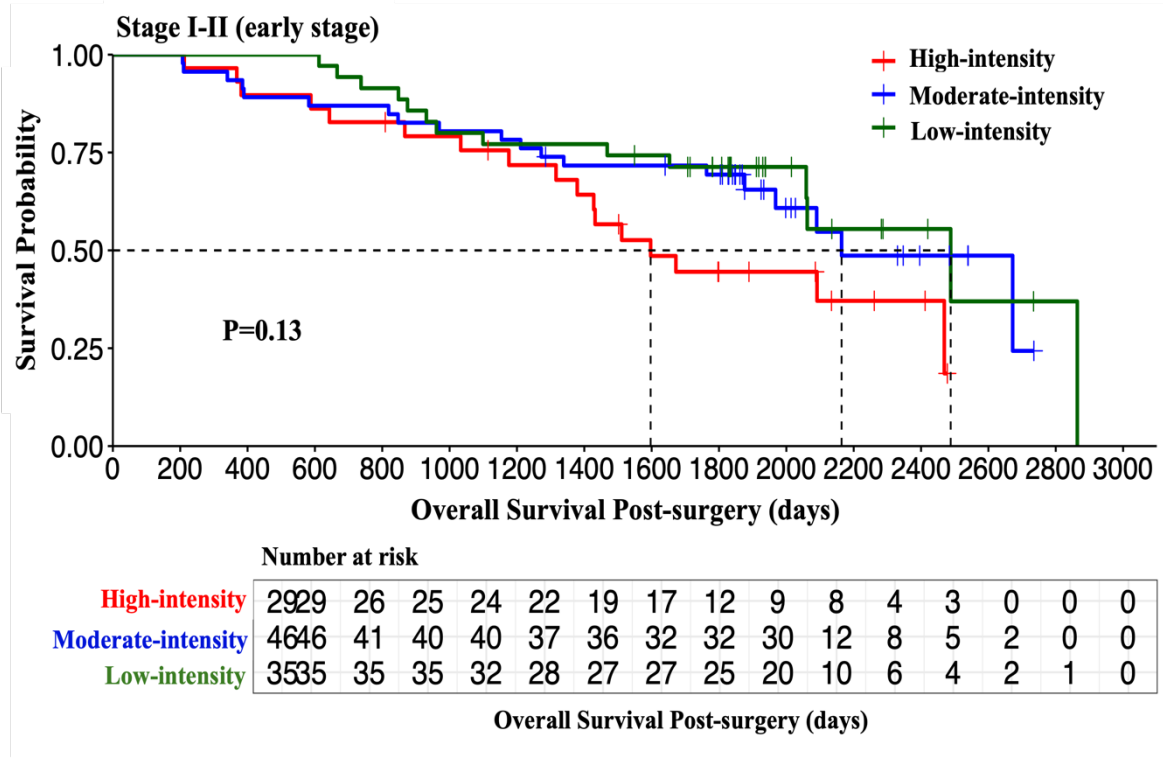


Fig. 5.7 Overall survival post-surgery stratified by three surveillance intensity groups in early-stage tumours.

### 1.2.2 Primary tumour volume and speed across high-, moderate-, and low-intensity surveillance groups

Given that previous results in this study demonstrated primary tumour volume as a stronger predictor of prognosis, it is important to investigate how surveillance frequency affects survival across volume-based patient subgroups. Among 175 patients, the median primary tumour volume was 19,680 $mm^3$. Patients with small tumours had significantly longer surveillance periods both before relapse or within the first two years

(median: 325 and 269 days, respectively) than those with median- and large-sized tumours (median: 196 and 180 days; 154 and 150 days, respectively) (Fig. 5.8A). While larger tumours were more frequently monitored through imaging, no significant size difference was found between the moderate- and low-intensity follow-up groups (Fig. 5.8B).

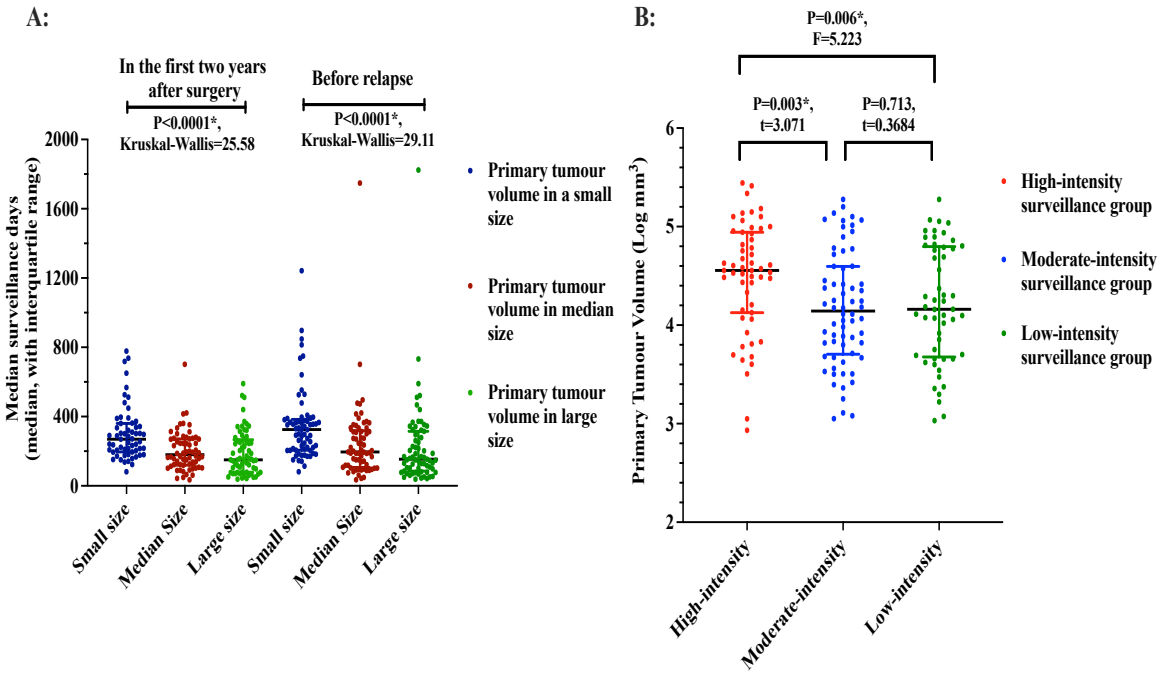


Fig. 5.8 Median surveillance duration across different primary tumour volume groups stratified by surveillance intensity. A: Median surveillance duration across different primary tumour volume groups stratified by surveillance intensity. Median surveillance days within the first two years or before relapse were more prolonged in small-sized primary tumours. B: Distributions of primary tumour volumes among surveillance intensity subgroups. Large-sized primary tumours were more likely to undergo frequent imaging follow-up checks.

High-frequency surveillance did not appear to improve post-surgical or post-recurrence survival in patients with small tumour volumes or varying tumour growth rates (Fig. 5.9). These findings are exploratory. They may be influenced by treatment heterogeneity, limited cohort size, and unmeasured confounding factors. Further validation in larger, standardised cohorts is necessary before clinical conclusions can be drawn.

**A:**

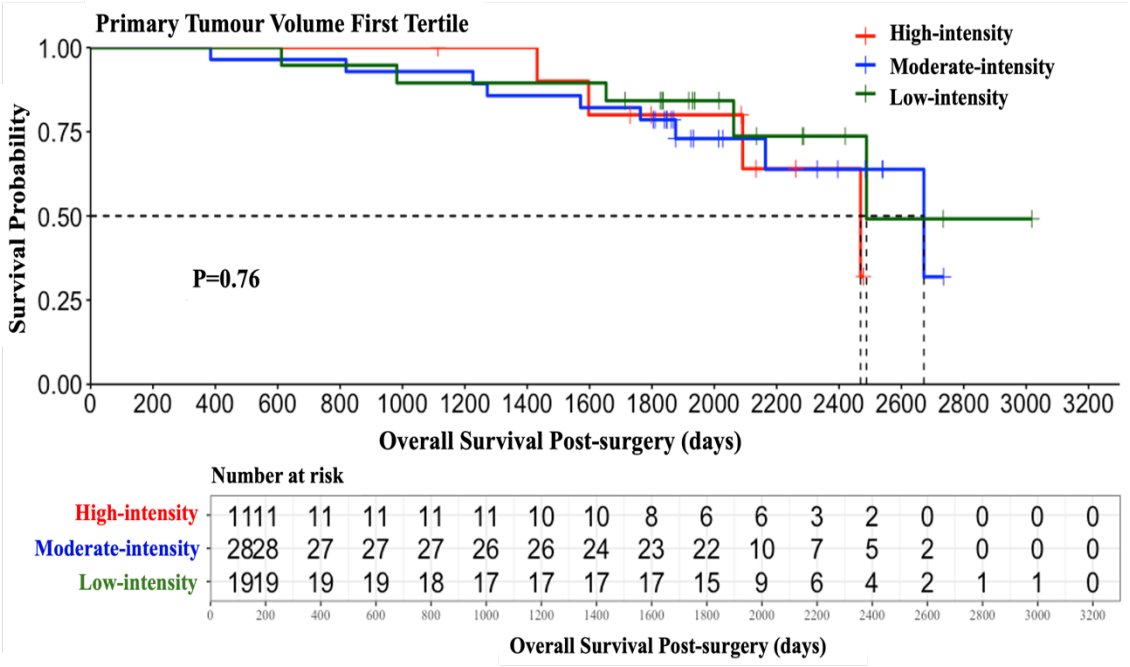
Primary Tumour Volume First Tertile
High-intensity
Moderate-intensity
Low-intensity
Survival Probability
1.00
0.75
0.50
0.25
0.00
P=0.76
0 200 400 600 800 1000 1200 1400 1600 1800 2000 2200 2400 2600 2800 3000 3200
Overall Survival Post-surgery (days)
Number at risk
High-intensity 1111 11 11 11 11 10 10 8 6 6 3 2 0 0 0 0
Moderate-intensity 2828 27 27 27 26 26 24 23 22 10 7 5 2 0 0 0
Low-intensity 1919 19 19 18 17 17 17 17 15 9 6 4 2 1 1 0
0 200 400 600 800 1000 1200 1400 1600 1800 2000 2200 2400 2600 2800 3000 3200
Overall Survival Post-surgery (days)

**B:**

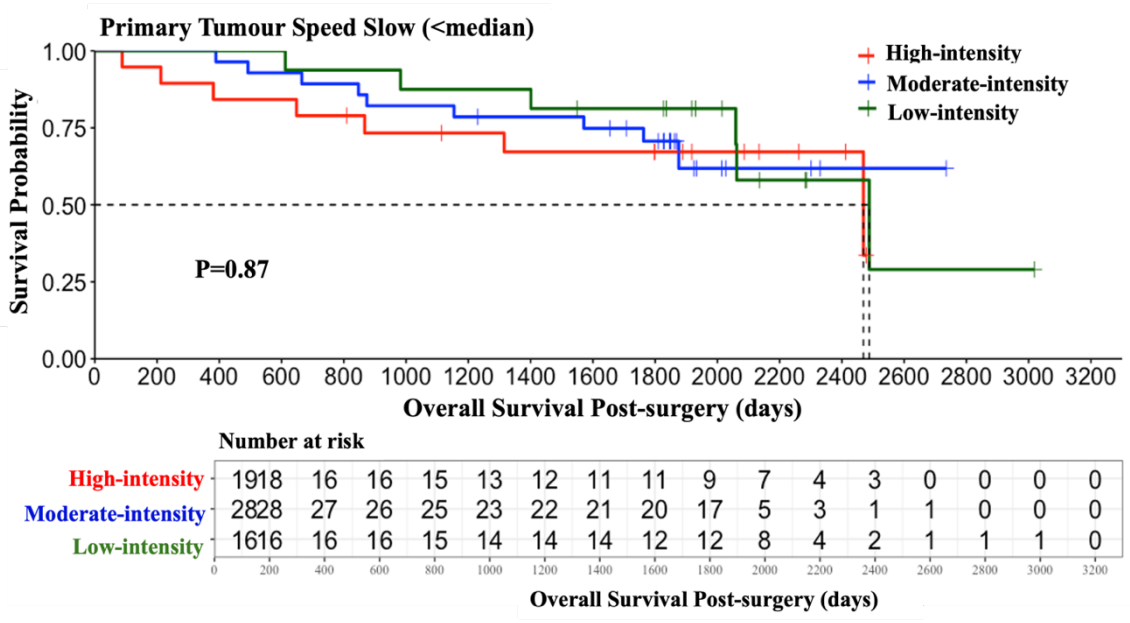
Primary Tumour Speed Slow (<median)
High-intensity
Moderate-intensity
Low-intensity
Survival Probability
1.00
0.75
0.50
0.25
0.00
P=0.87
0 200 400 600 800 1000 1200 1400 1600 1800 2000 2200 2400 2600 2800 3000 3200
Overall Survival Post-surgery (days)
Number at risk
High-intensity 1918 16 16 15 13 12 11 11 9 7 4 3 0 0 0 0
Moderate-intensity 2828 27 26 25 23 22 21 20 17 5 3 1 1 0 0 0
Low-intensity 1616 16 16 15 14 14 14 12 12 8 4 2 1 1 1 0
0 200 400 600 800 1000 1200 1400 1600 1800 2000 2200 2400 2600 2800 3000 3200
Overall Survival Post-surgery (days)

**C:**

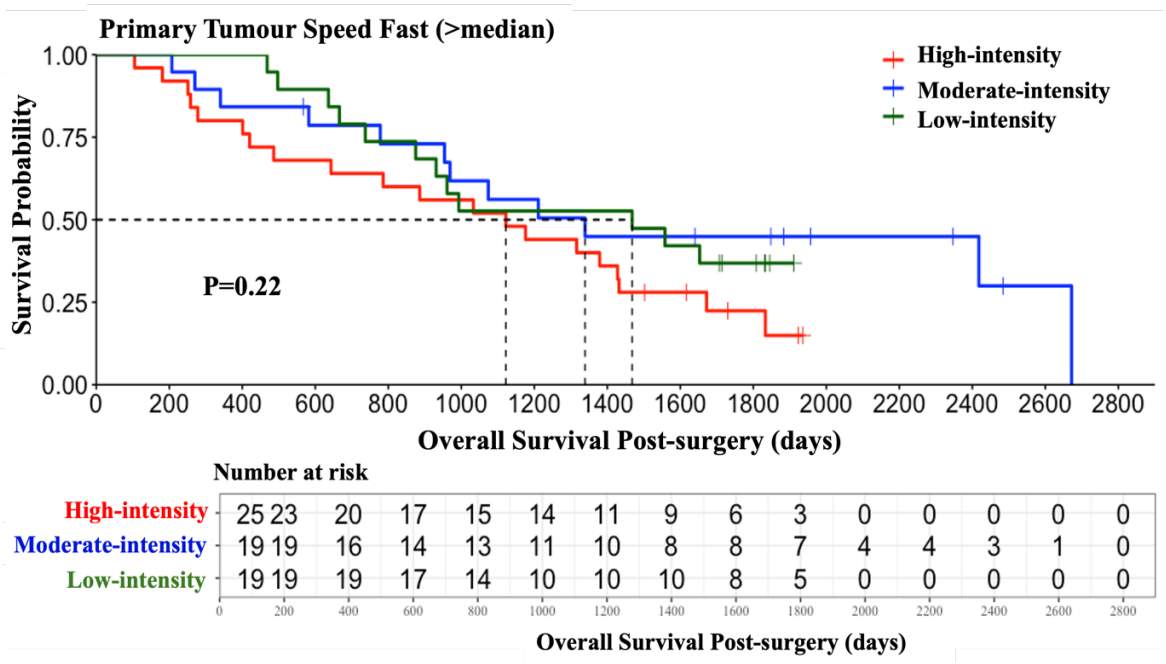


Fig. 5.9 Overall survival post-surgery in small tumours and across different primary tumour growth rates among three intensity surveillance groups. A: Overall survival post-surgery in small tumours stratified by high-, moderate- and low-intensity groups; B: Overall survival post-surgery in slow-speed tumours, stratified by surveillance intensity; C: Overall survival post-surgery in fast-speed tumours, stratified by surveillance intensity.

## 2. Relapse diversity among high-, moderate-, and low-intensity surveillance groups.

### 2.1 Diversity of relapse sites across surveillance intensity groups.

A lesion was classified as the dominant lesion if it comprised at least 50% of the total tumour volume at the time of relapse, and the organ containing this lesion was identified as the dominant organ. Patients whose lesions did not have a single lesion comprising ≥50% of the total volume were classified as having high relapse organ heterogeneity. In total, 111 patients had a dominant organ.

Given the limited presence and imbalanced distribution of lesions across three surveillance groups in the adrenals, bones, livers, extrathoracic soft tissues, and extrathoracic lymph nodes within this cohort, these sites were grouped under the category of ‘other extrathoracic organ’. The median percentage of total recurrence tumour volume

attributed to the dominant lesion was 100% for lung relapses (IQR: 81–100), 90% for intrathoracic lymph node relapses (IQR: 62–100), 100% for brain relapses (IQR: 94–100), and 88% for other extrathoracic relapses (IQR: 59–100). In contrast, patients classified as having heterogeneous relapse had a median dominant lesion contribution of only 43% (IQR: 35–45). No significant differences in disease-free survival (DFS) or overall survival (OS) following surgery were observed across the lung, brain, intrathoracic lymph node, or other extrathoracic relapse groups.

The lung emerged as the most affected organ for dominant recurrence in both the high- and moderate-surveillance intensity groups. With a decreased surveillance frequency, a noted reduction was observed in the detection of lung and brain relapses. Conversely, the incidence of intrathoracic lymph node involvement and high heterogeneity increased (as shown in Fig. 5.10). Among other extrathoracic recurrence sites, adrenal and extrathoracic soft tissue relapses were more frequently identified in the low-intensity surveillance group. Interestingly, 5 patients had new primary lung tumours: 4 out of 45 (9%) in the moderate-intensity group and 1 out of 29 (3%) in the low-intensity group. It appears that higher-frequency imaging checks may not improve the early detection of new primary lung cancers.

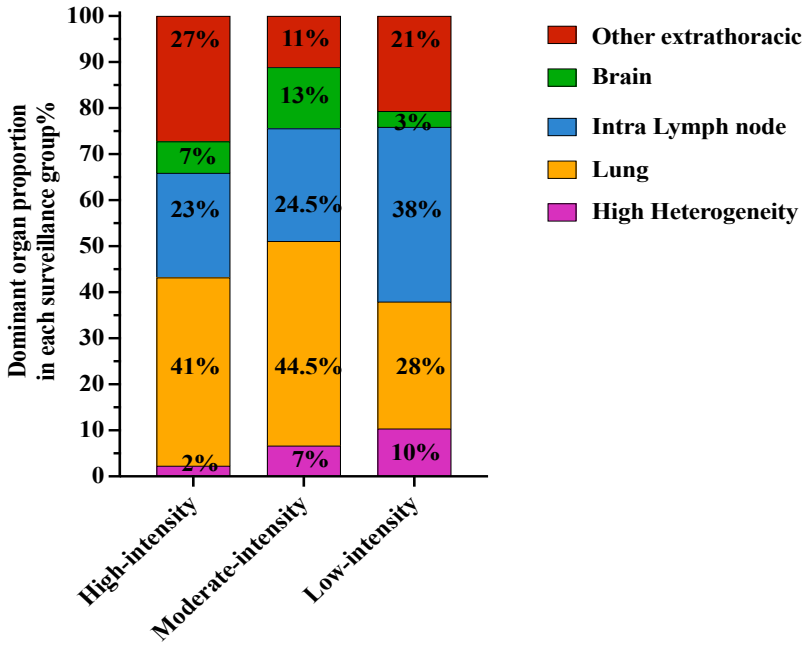


Fig. 5.10 Proportion of dominant relapse organs across surveillance intensity groups.

In clinical practice, the anatomical site of dominant relapse plays a critical role in guiding post-relapse treatment decisions and predicting survival. For example, patients with isolated brain relapse are typically treated with radiotherapy. Given this, it is essential to evaluate whether surveillance frequency impacts survival outcomes across various dominant relapse sites, thereby informing clinical decision-making. The median surveillance period prior to relapse in the high-intensity, moderate-intensity, and low-intensity groups was 81, 165, and 328 days, respectively, for other extrathoracic organ relapses; 95, 146, and 346 days for brain relapses; 88, 154, and 301 days for intrathoracic lymph node relapses; and 96, 185, and 330 days for lung relapses. A significant difference in the median surveillance period to relapse was observed among the high-, moderate-, and low-intensity surveillance groups across all dominant relapse organs (Fig. 5.11A). However, within each surveillance group, there were no significant differences in the median surveillance periods before relapse when stratified by dominant relapse organ (Fig. 5.11B). Furthermore, increased surveillance frequency did not significantly improve overall survival post-recurrence (Fig. 5.11C–F). However, these findings are subject to limitations, including a small sample size, treatment heterogeneity, and potential confounding factors. Further studies with larger cohorts are needed to confirm these observations.

**A:**

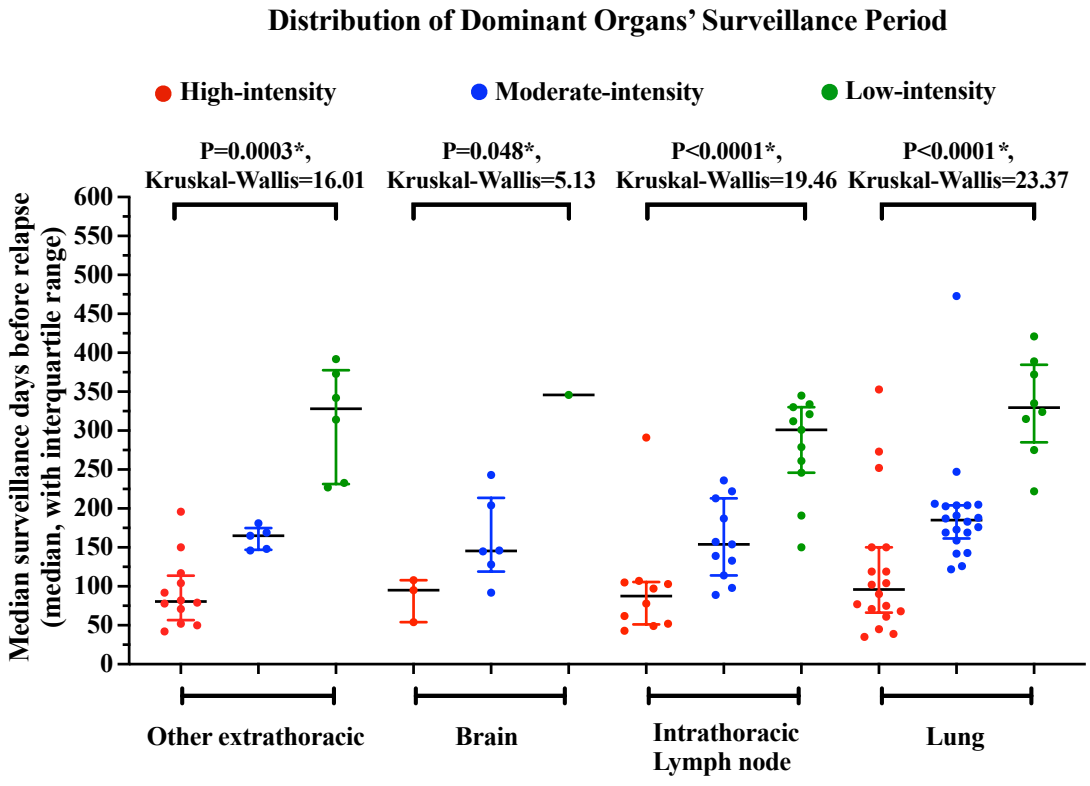

**B:**

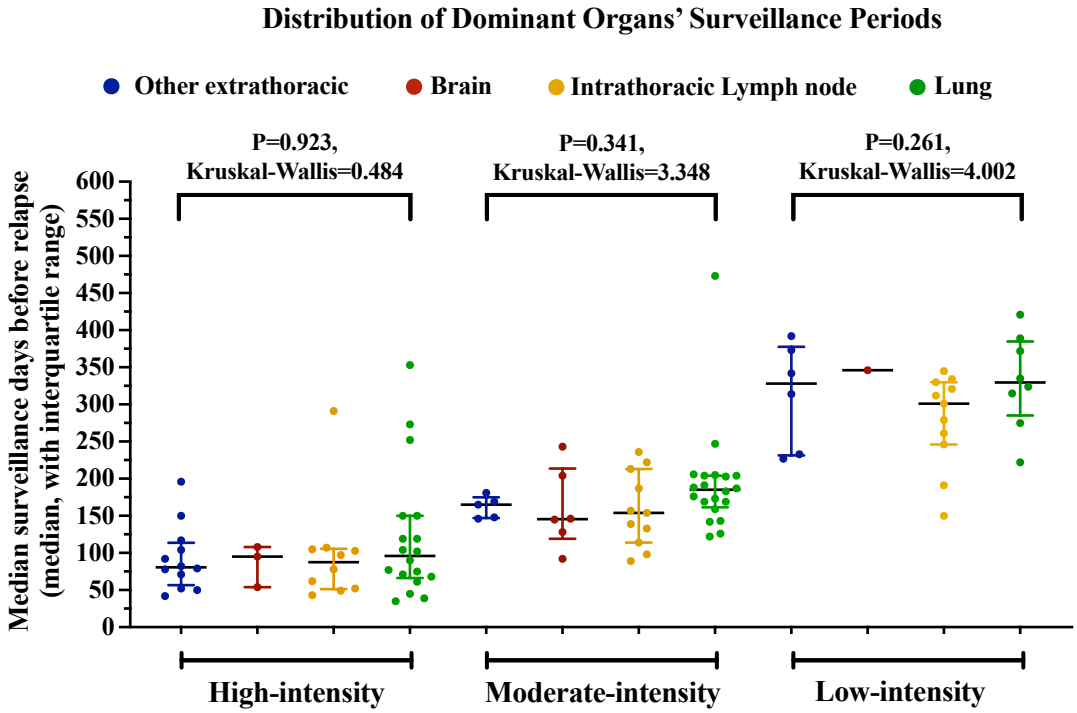
Distribution of Dominant Organs' Surveillance Periods
Other extrathoracic
Brain
Intrathoracic Lymph node
Lung
P=0.923,
Kruskal-Wallis=0.484
P=0.341,
Kruskal-Wallis=3.348
P=0.261,
Kruskal-Wallis=4.002
Median surveillance days before relapse
(median, with interquartile range)
600
550
500
450
400
350
300
250
200
150
100
50
0
High-intensity
Moderate-intensity
Low-intensity

**C:**

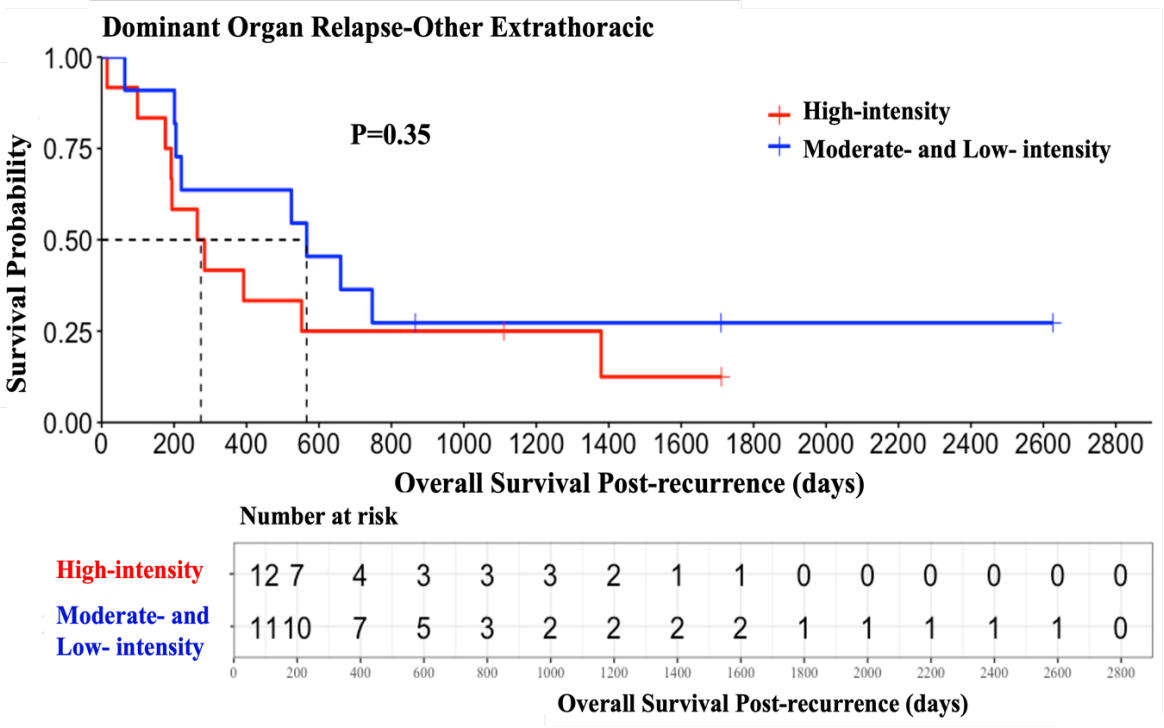
Dominant Organ Relapse-Other Extrathoracic
P=0.35
High-intensity
Moderate- and Low- intensity
Survival Probability
1.00
0.75
0.50
0.25
0.00
0
200
400
600
800
1000
1200
1400
1600
1800
2000
2200
2400
2600
2800
Overall Survival Post-recurrence (days)
Number at risk
High-intensity
12 7 4 3 3 3 2 1 1 0 0 0 0 0 0
Moderate- and Low- intensity
11 10 7 5 3 2 2 2 2 1 1 1 1 1 0
Overall Survival Post-recurrence (days)

**D:**

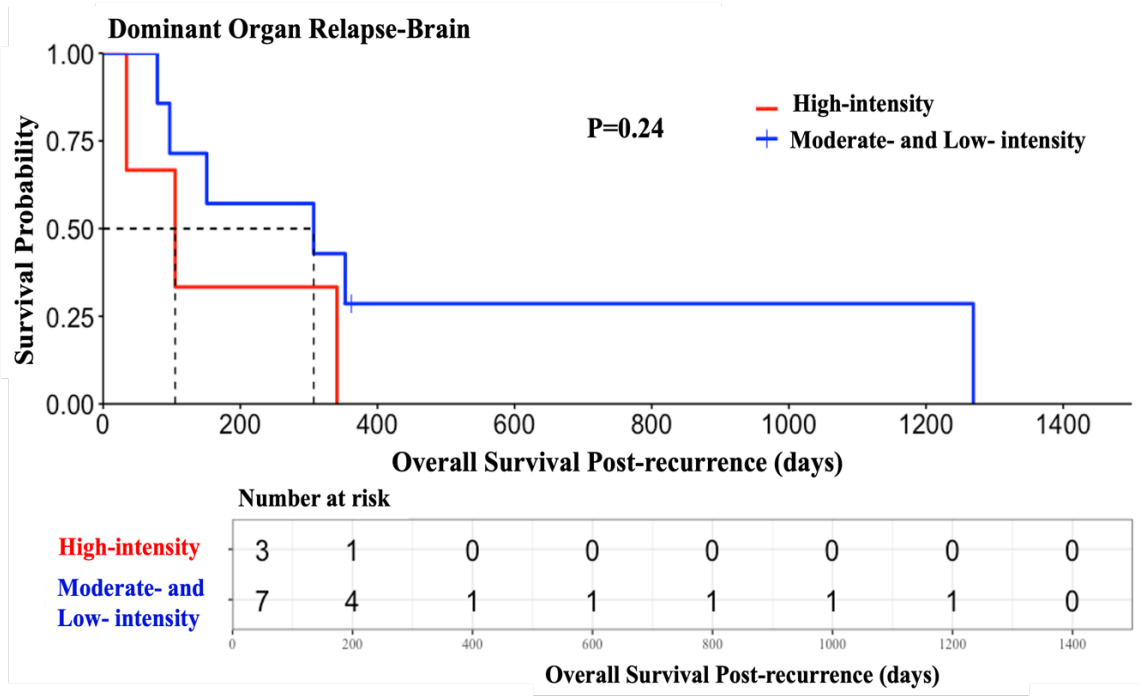
Dominant Organ Relapse-Brain
Survival Probability
1.00
0.75
0.50
0.25
0.00
P=0.24
High-intensity
Moderate- and Low- intensity
0
200
400
600
800
1000
1200
1400
Overall Survival Post-recurrence (days)
Number at risk
High-intensity
Moderate- and Low- intensity
3 1 0 0 0 0 0 0
7 4 1 1 1 1 1 0
Overall Survival Post-recurrence (days)

**E:**

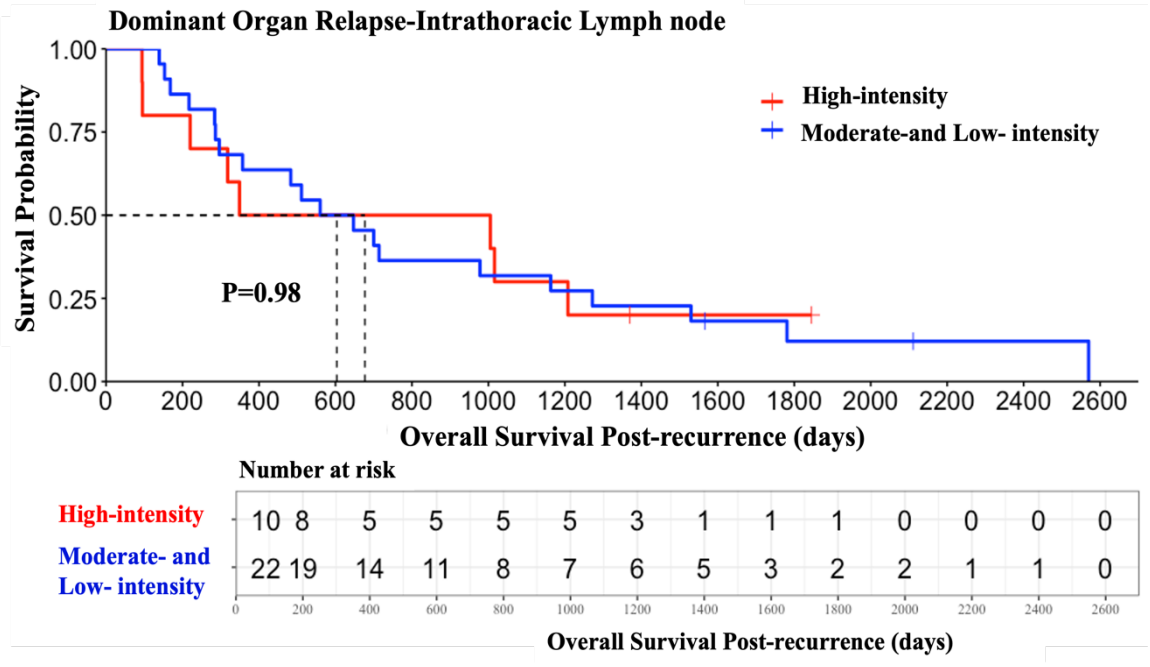
Dominant Organ Relapse-Intrathoracic Lymph node
Survival Probability
1.00
0.75
0.50
0.25
0.00
P=0.98
High-intensity
Moderate-and Low- intensity
0
200
400
600
800
1000
1200
1400
1600
1800
2000
2200
2400
2600
Overall Survival Post-recurrence (days)
Number at risk
High-intensity
Moderate- and Low- intensity
10 8 5 5 5 5 3 1 1 1 0 0 0 0
22 19 14 11 8 7 6 5 3 2 2 1 1 0
Overall Survival Post-recurrence (days)

**F:**

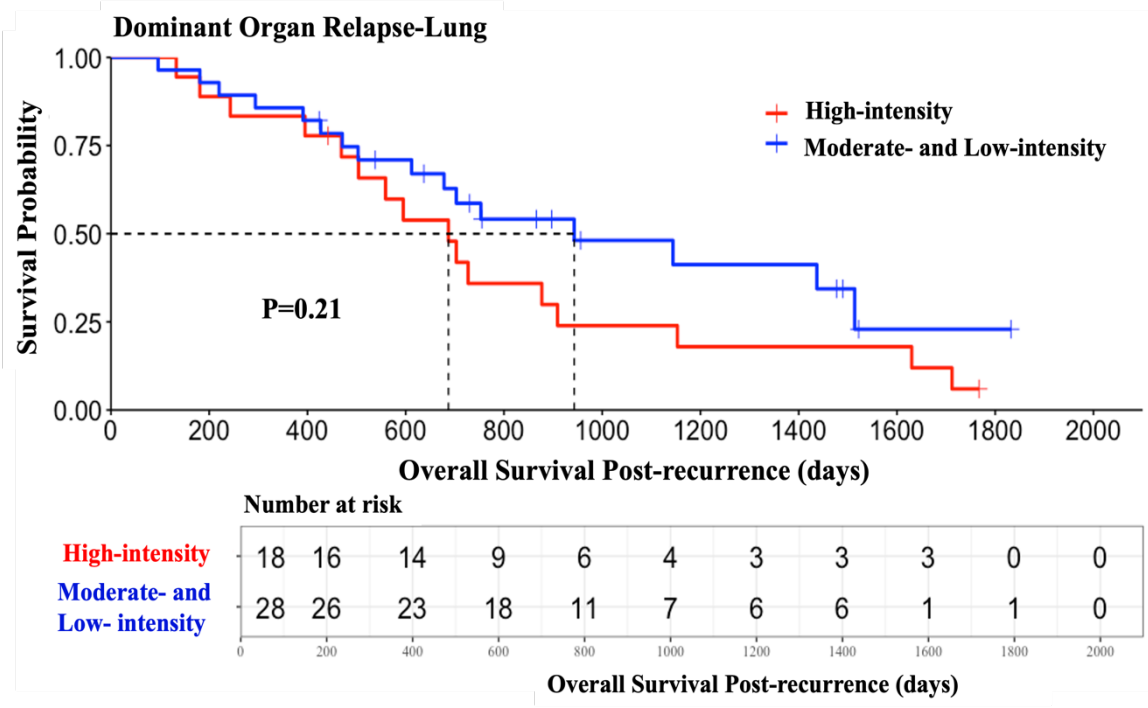


Fig. 5.11 Distribution of surveillance periods and post-recurrence survival (PRS) by dominant relapse site and surveillance intensity. A–B: Median surveillance duration prior to relapse for each dominant organ (lung, brain, lymph node, other extrathoracic) across high-intensity, moderate-intensity, and low-intensity surveillance groups; C: PRS comparisons of extrathoracic dominant relapses stratified by surveillance groups; D: PRS comparisons of brain dominant relapses stratified by surveillance groups; E: PRS comparisons of intrathoracic lymph node dominant relapses stratified by surveillance groups; F: PRS comparisons of lung dominant relapses stratified by surveillance groups. The plots demonstrate that high-frequency imaging did not significantly improve survival in patients with organ-dominant relapses.

### 2.2 Relapse volume and growth rate across surveillance groups.

Previous results from this study indicated that tumour volume and growth rate can impact patient outcomes. Some clinicians are concerned that delayed surveillance may result in late detection of relapse, potentially leading to a greater tumour burden at the time of detection. To investigate this hypothesis, further analysis was done to evaluate the relationship between surveillance frequency and relapse volume. In this study, 44 patients relapsed in the high-intensity group, 45 in the moderate-intensity group, and 29 in the

low-intensity group. No significant differences in relapse tumour volumes were observed among the groups. Additionally, no correlations were found between median surveillance days before relapse and relapse volume (P=0.239, r=0.1), no correlation between median surveillance durations and total volume (P=0.969, r=0.003), and no correlation between time to first surveillance scan and relapse volume (P=0.366, r=0.08). No significant difference in relapse tumour volume across imaging frequencies was observed (Fig. 5.12), although variability was high due to imbalanced scan intervals. These findings suggest that lower-frequency imaging does not necessarily lead to a larger tumour burden at the time of recurrence. However, this observation should be interpreted cautiously due to potential confounding factors, such as differences in tumour biology, treatment timing, and cohort size.

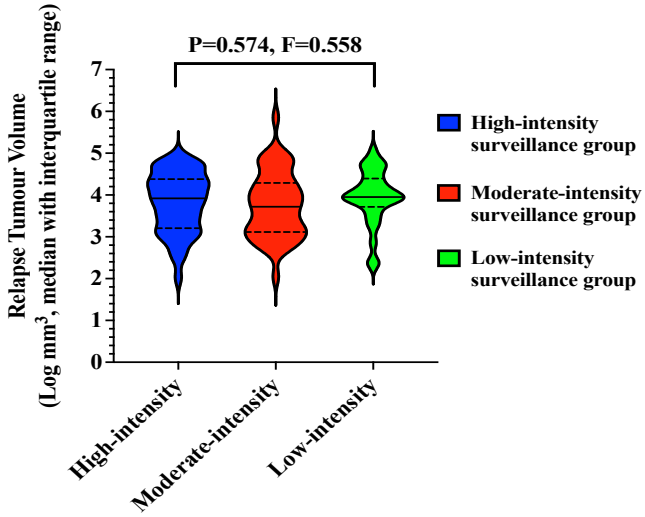


Fig. 5.12 Comparison of relapse tumour volumes across surveillance intensity groups.

## 3. Post-relapse surveillance considerations

### 3.1 First progression after relapse

**Grouping and Classification of Relapsed Patients:**

In this retrospective study, clinicians evaluated all 130 relapsed patients using the RECIST criteria to determine treatment delivery time and stop time. Therefore, I used the RECIST criteria to calculate the progression-free survival (PFS) here.

**Surveillance Considerations for Specific Dominant Organ:** Previous results demonstrated that different sites of dominant relapse were associated with distinct survival durations. To investigate surveillance periods, patients were stratified based on

the dominant site at relapse. Among patients who received treatment after relapse, the median PFS days for each dominant site were as follows: 201 days (IQR: 109–390) for lung, 121 days (IQR: 38–290) for intrathoracic lymph node, 89 days (IQR: 77–127) for brain, and 78 days (IQR: 37–201) for other extrathoracic sites. When further stratified by relapse speed (fast vs slow) within each group, the median PFS durations were:

- Lung dominant relapse: 289 days (IQR: 155–538) vs. 240 days (IQR: 79–736).
- Intrathoracic lymph node dominant relapse: 141 days (IQR: 40–374) vs. 153 days (IQR: 67–885).
- Brain dominant relapse: 98 days (IQR: 66–122) vs. 99 days (IQR: 79–658).
- Other Extrathoracic organs dominant relapse: 86 days (IQR: 36–212) vs. 65 days (IQR: 49–111).

Lung-dominant relapse was associated with longer PFS (P<0.0001, Fig. 5.13). The speed of relapse (fast vs slow) did not significantly affect PFS across relapse sites: lung (P=0.39), intrathoracic lymph node (P=0.068), brain (P=0.33), and other extrathoracic sites (P=0.9). These non-significant results are likely due to the limited cohort and the heterogeneity of treatment regimens. Nonetheless, these findings suggest that lung and intrathoracic-dominant relapses may be associated with more stable disease courses, whereas brain and other extrathoracic relapses may progress more aggressively. It highlights the biological differences in post-relapse behaviour by anatomical site. If confirmed in larger, prospective cohorts, such patterns could support the future development of relapse site-specific surveillance strategies.

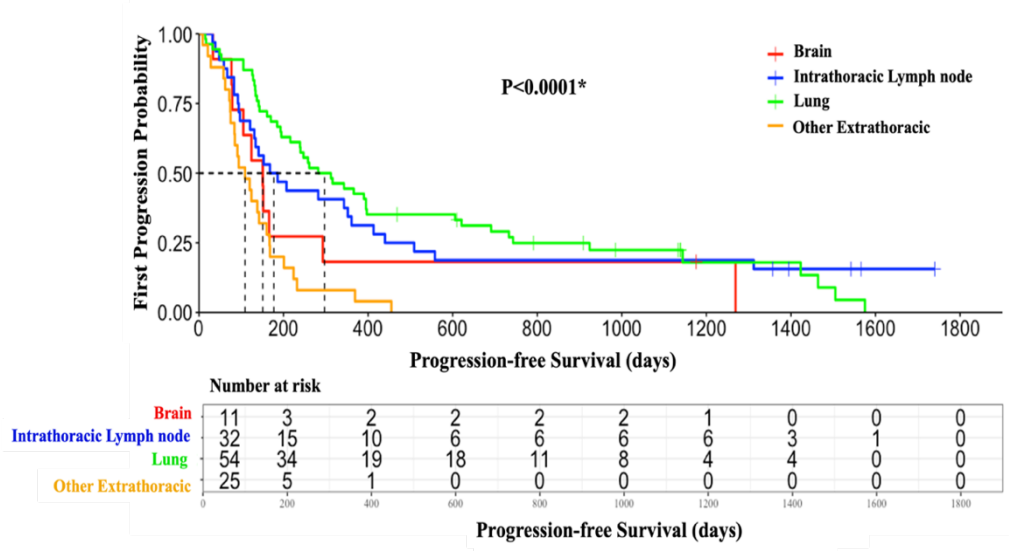


Fig. 5.13 Progression-free survival stratified by relapse location.

### 3.2 Surveillance and treatment management suggestions.

Previous sections demonstrated the prognostic importance of relapse rate and tumour volume. Further analysis is warranted to determine how post-treatment progression metrics can predict clinical outcomes. To support personalised post-relapse surveillance strategies, it is crucial to understand how treatment responses influence tumour dynamics and survival. Additionally, evaluating whether post-treatment tumour volume thresholds can serve as risk stratification tools may help guide clinical decision-making and improve outcomes for patients with relapsed disease.

**Post-Relapse Treatment Management:** The median progression-free survival (PFS) following treatment was 126 days for the entire cohort and 124 days among patients who experienced progression. The duration of PFS was predictive of overall survival after recurrence (Fig. 5.14). These findings underscore the importance of evaluating treatment efficacy to guide therapeutic decisions.

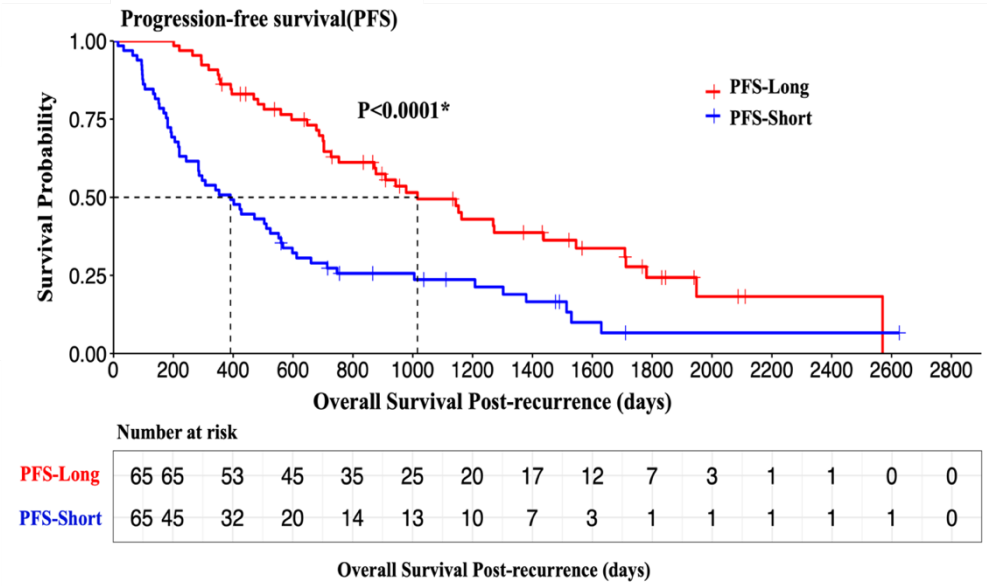


Fig. 5.14 Overall survival post-recurrence in 130 relapsed patients, categorised by length of progression-free survival.

Among 130 patients who relapsed, 115 received treatment. The median interval from relapse to the start of treatment was 73 days (IQR: 48–116 days). Table 5.4 details the first treatment methods for these 115 patients. The Volume-RECIST criteria were used to evaluate the best treatment response after the first therapy. Survival analysis revealed that patients who achieved a complete response (CR) following the first therapy had the best

overall survival. In contrast, patients who experienced progressive disease (PD) had the poorest clinical outcomes, as shown in Fig. 5.15.

Table 5.4 Summary of first-line post-relapse treatment strategies among relapsed patients.

| Best Treatment response | Radical Local (n=) | Palliative Radiotherapy or other (n=) | Systemic (n=) | Systemic and Local (n=) | Targeted (n=) |
|---|---|---|---|---|---|
| All | 38 | 18 | 35 | 13 | 11 |
| CR | 20 | 0 | 3 | 1 | 3 |
| PR | 12 | 3 | 11 | 5 | 2 |
| SD | 3 | 3 | 6 | 2 | 4 |
| PD | 3 | 11 | 15 | 5 | 2 |
| No scan | | 1 | | | |

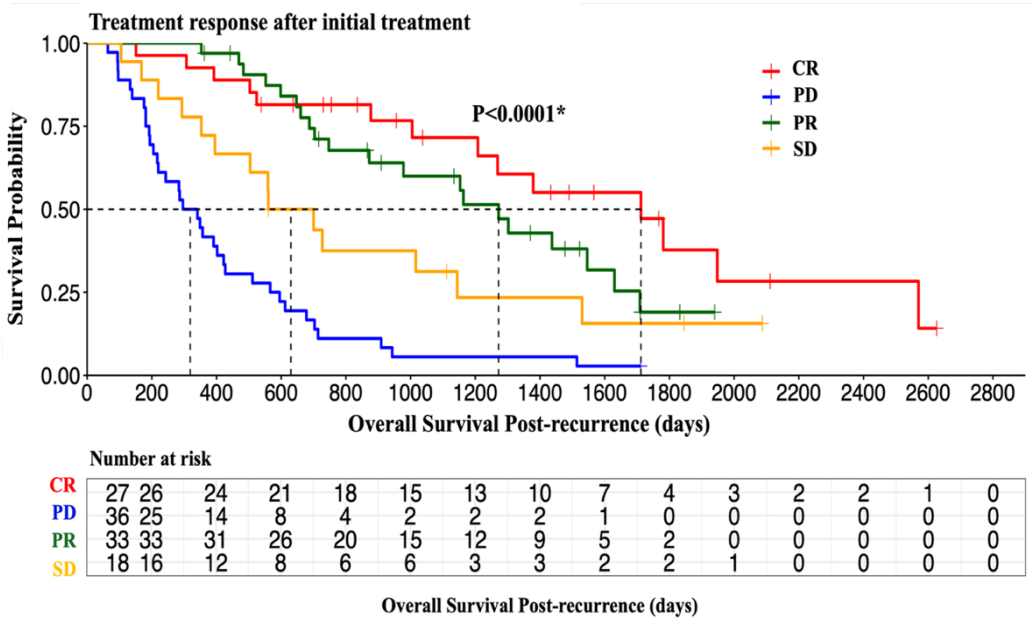


Fig. 5.15 Overall survival post-recurrence stratified by best treatment response after first-line therapy.

Standard RECIST criteria was used to define the first progression. Patients who died at the first progression and those who did not progress after the initial therapy were excluded. Different methods of therapy were associated with distinct progression-free survival (PFS) rates. Radical local treatment was shown to enhance survival across, notably among those

with a limited relapse burden (as shown in *Appendix 3, Table 1*). A total of 83 patients had their first progression tumour volumes measured from post-treatment imaging scans. Patients who achieved a complete response (CR) to the first therapy had the slowest growth rates and smallest tumour volumes at first progression. In contrast, tumour growth rates increased progressively among patients with partial response (PR), stable disease (SD), and progressive disease (PD), with the PD group showing the fastest growth and largest tumour volumes (Fig. 5.16 A–B). Hence, the best response status to the first-line therapy could be a predictive indicator of subsequent tumour progression speed and burden.

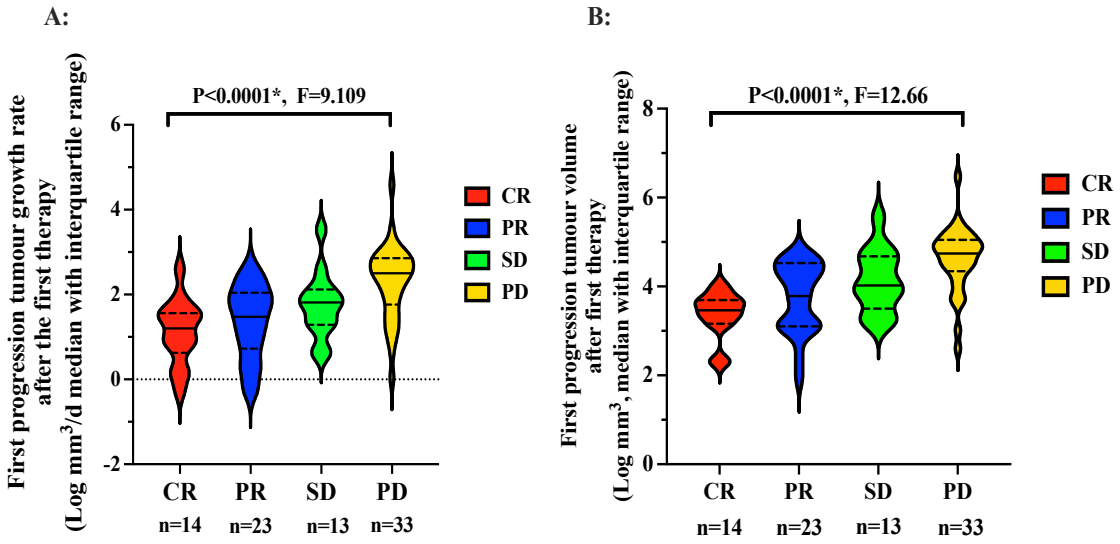


Fig. 5.16 Relationship between tumour volume, growth rate at first progression, and best response status to initial therapy. A: Relationship between tumour growth rate at first progression and best response status to initial therapy. These violin plots indicate an approximately normal distribution of the data; B: Relationship between tumour volume at first progression and best response status to initial therapy. These violin plots indicate an approximately normal distribution of the data.

A significant correlation was found between the tumour volume and the tumour growth rate at first progression (Fig. 5.17A). Specifically, patients with smaller tumour volumes at first progression exhibited better overall survival rates post-first progression than those with larger tumours (Fig. 5.17B). Similarly, patients with slower growth rates at first progression were associated with better overall survival rates post-first progression than those with faster tumour growth rates (Fig. 5.17C).

Therefore, the best response status to first-line therapy, along with tumour volume and growth rate at first progression, may serve as predictive indicators of subsequent progression dynamics and overall survival. Interestingly, the pre-treatment tumour growth rate showed only a weak correlation with the post-treatment growth rate (Spearman's r=0.38, P<0.0001), potentially reflecting the influence of different therapeutic modalities. The efficacy of distinct treatment types requires further investigation.

**A:**

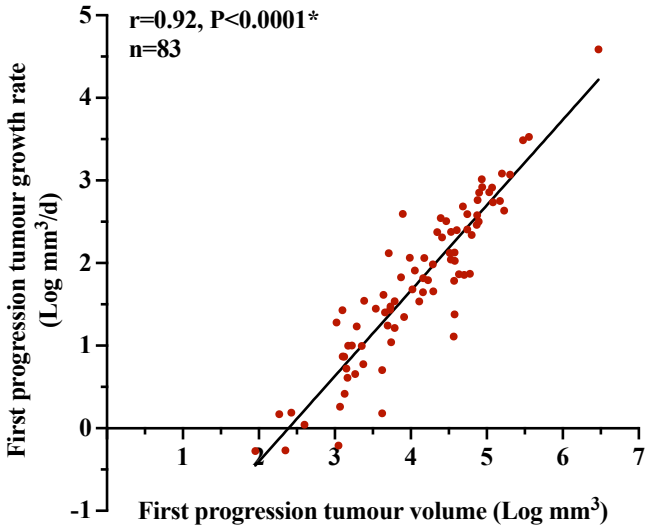


**B:**

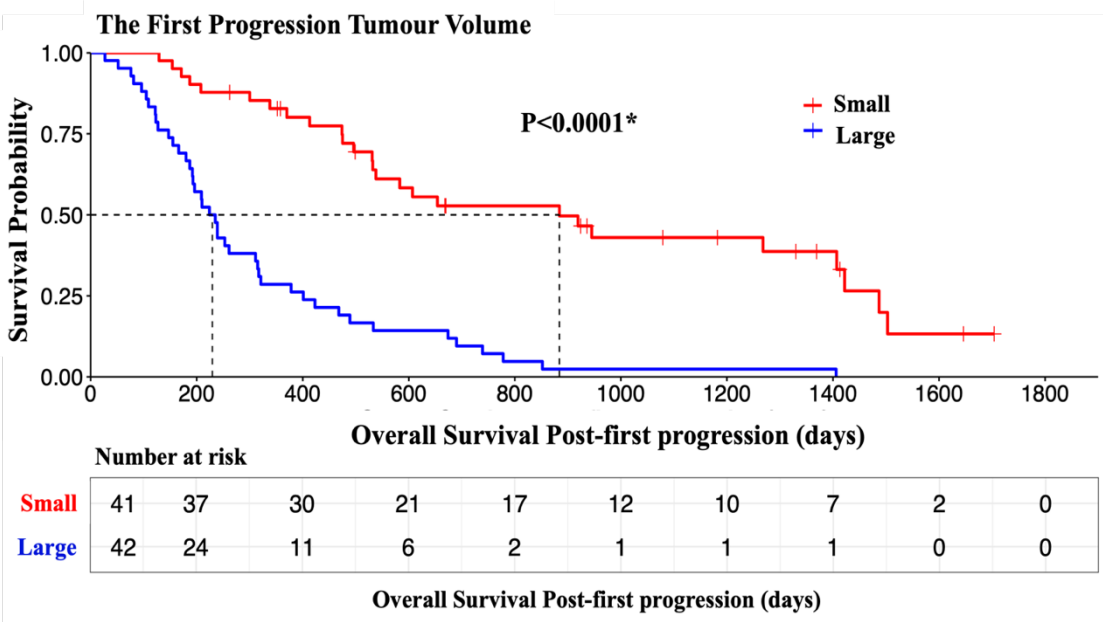

**C:**

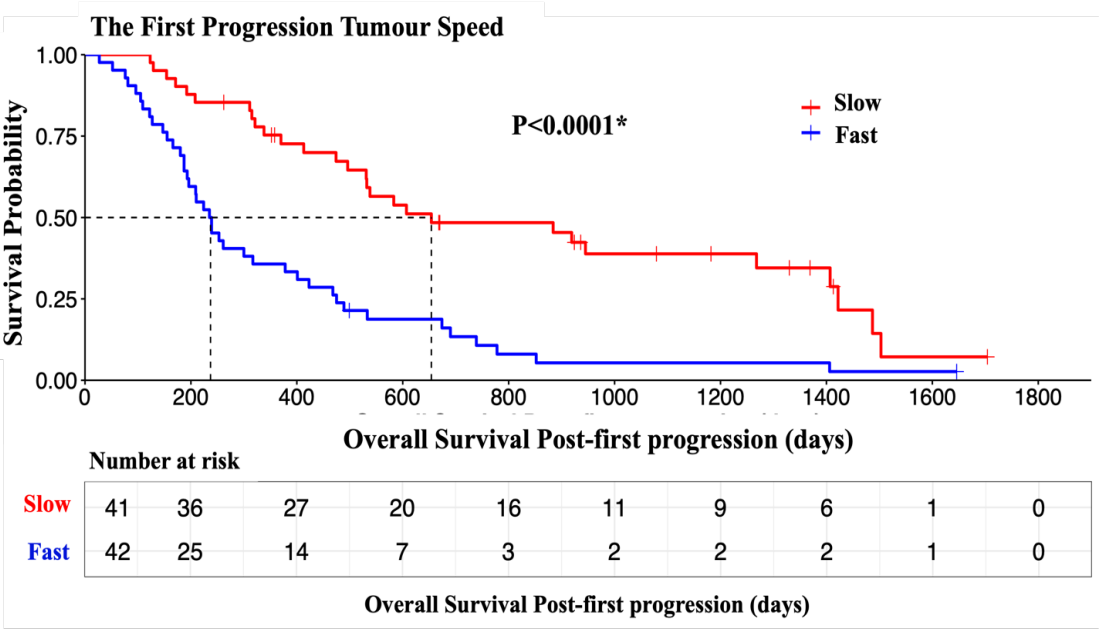


Fig. 5.17 Relationship between tumour volume and growth rate at first progression and their association with overall survival. A: Association between tumour volume and growth rate at first progression. A significant correlation was found between the tumour volume and the tumour growth rate at first progression; B: Comparison of overall survival post-first progression categorised by tumour volume; C: Comparison of overall survival post-first progression categorised by tumour speed. The plots demonstrated that patients with smaller volumes or slower progression rates at the first progression exhibited better overall survival rates after the first progression.

### 3.3 Optimal Volume Change Metrics for Assessing Treatment Efficacy and Predicting Prognosis.

**Optimal Volume Change Metrics for Assessing Treatment Efficacy:** There is limited literature defining optimal thresholds for volume change in assessing treatment response. This study identified several important findings. Among patients with dominant lesion relapse following initial therapy, the median progression-free survival (PFS) was 129 days. PFS durations below and above this value were categorised as short-PFS and long-PFS, respectively. To determine a volume change threshold as a predictor of PFS, a Receiver Operating Characteristic (ROC) curve analysis was conducted using the best volumetric response of the dominant lesion post-treatment. The analysis showed an area

under the curve (AUC) of 0.81, with an optimal cutoff value of –65% (Fig. 5.18). This result indicates that a tumour volume reduction of greater than 65% following therapy is associated with a more favourable prognosis.

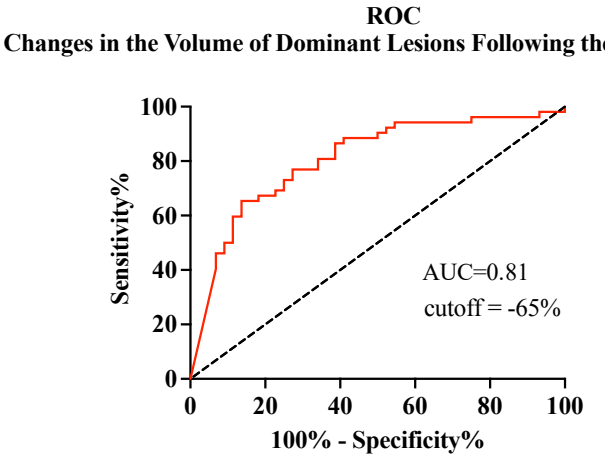


Fig. 5.18 The Receiver Operating Characteristic (ROC) curve assessing volume change in the dominant lesion after first-line therapy post-recurrence.

**4. Impact of maximum tumour volume occurrence timing on tumour heterogeneity.**

**Patient Categorizing Based on Volume Timing:** To gain a better understanding of tumour evolution, the patients were divided into two categories based on the timing of their maximum tumour volume: those whose maximum tumour occurred in the first half of the overall course, indicating rapid early progression, and those whose maximum tumour occurred in the second half of the overall course, suggesting late-phase acceleration.

Given that tumour evolution is accompanied by increasing heterogeneity [107,158,183,200,220,230], this classification aimed to preliminarily explore whether the temporal pattern of tumour burden correlates with growth dynamics, lesion counts, treatment resistance, intratumour heterogeneity, and survival outcomes. Patients in the latter category often experienced rapid acceleration and died shortly after reaching their maximum tumour volume (Fig. 5.19), suggesting a possible association with emerging resistant subclones.

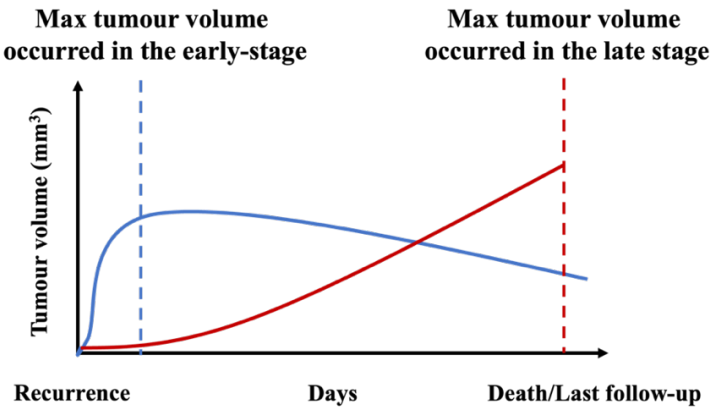


Fig. 5.19 Conceptual models illustrating two tumour growth patterns.

**Tumour Burden Comparison:** Regardless of whether progression events were defined using the RECIST criteria or the Volume-RECIST criteria, patients whose maximum tumour volume appeared before the halfway point (early phase) had a significantly smaller tumour burden than those whose maximum tumour volume appeared after the halfway point (late phase). This finding was consistent in both the group of 130 relapsed patients (P<0.0001, Fig. 5.20A) and the subgroup of 97 dead patients (P<0.0001, Fig. 5.20B). However, no significant difference in baseline tumour volume and tumour growth rate at relapse was found. This result suggests that tumour evolution is complicated; neither baseline nor relapse characteristics alone can fully explain the dynamics of the progression process.

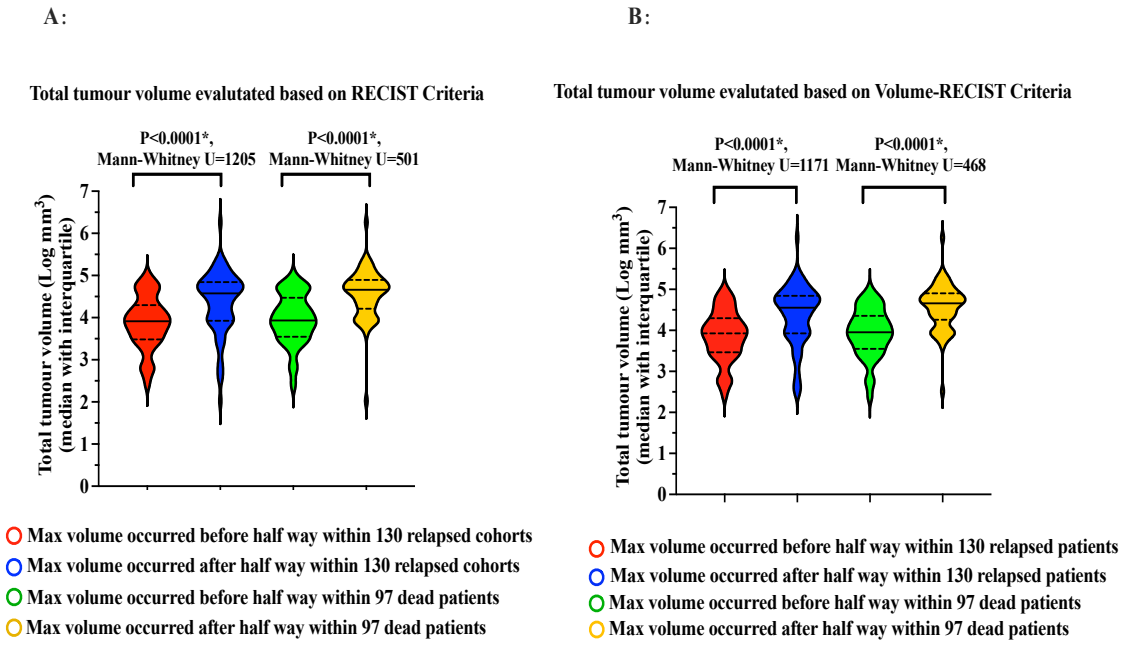

Fig. 5.20 Distribution of total tumour volume based on timing of peak tumour burden. A: Distribution of total tumour volume based on timing of peak tumour burden among 130 relapsed patients. The plots show slightly asymmetric patterns; B: Distribution of total tumour volume based on timing of peak tumour burden among a subgroup of 97 dead patients who experienced a relapse. The plots show slightly asymmetric patterns.

**Prognosis Based on Max Volume Occurrence:** Among all 130 patients who experienced a relapse, those whose maximum tumour volume occurred in the first half of the overall process, indicating rapid early growth, had a better prognosis than those whose maximum tumour volume happened in the second halfway, indicating rapid later growth (Fig. 5.21A, P<0.0001). The same result was found in a subgroup of 97 dead patients (Fig. 5.21B, P=0.016). Therefore, for patients with rapid early growth, especially with smaller tumour burdens, tumour monitoring intervals can be shortened in the early phase of the process. In comparison, frequent imaging tests should be conducted in the later phase for those with rapid growth and larger tumour burdens.

**A:**

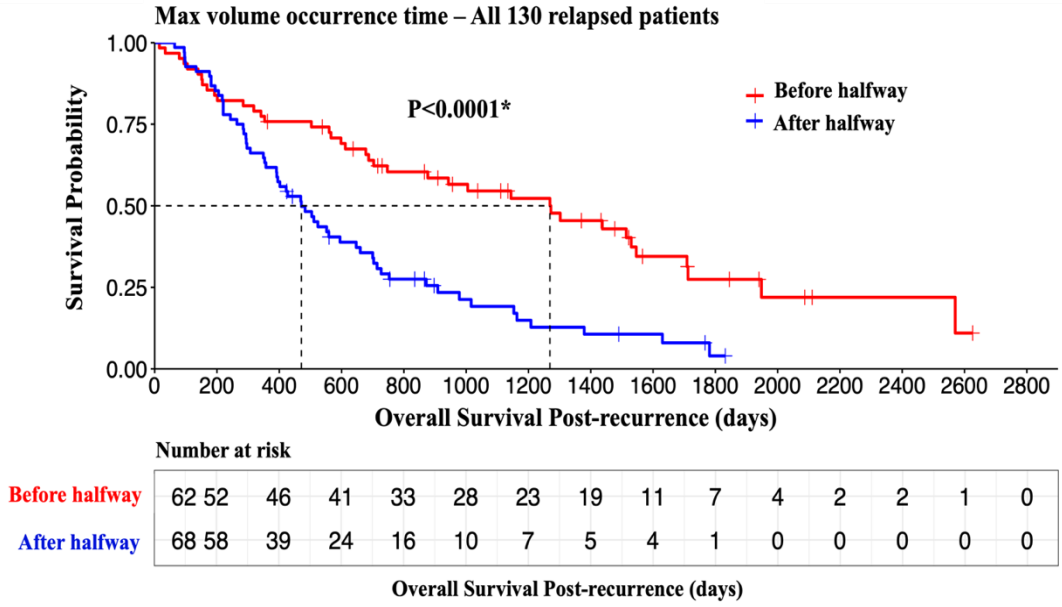

**B:**

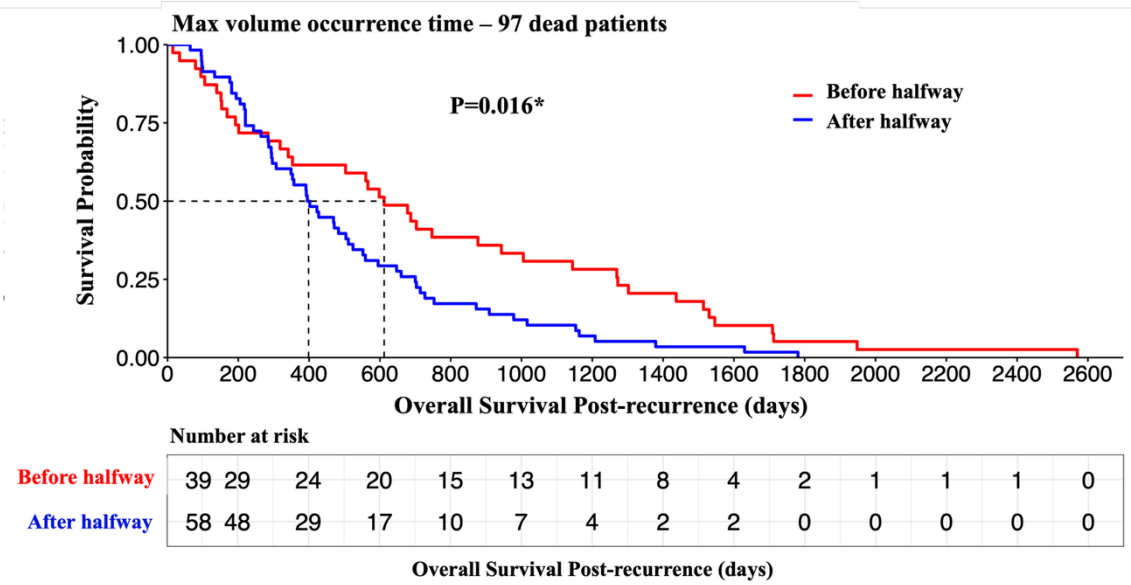


Fig. 5.21 Overall survival post-recurrence based on early versus late growth patterns. A: Overall survival post-recurrence based on early vs. late growth patterns among all 130 relapsed patients; B: Overall survival post-recurrence based on early vs late growth patterns among the 97 dead patients out of the 130 relapsed patients.

**Implications for Tumour Monitoring and Immunotherapy:** Patients peaking in tumour volume later were more likely to experience an increase in lesions ($P<0.0001$, $\chi^2 = 29.83$, Fig. 5.22) and exhibited high tumour heterogeneity. These individuals exhibited variable responses to immunotherapy, including therapy resistance, as illustrated by examples in Fig. 5.23. Immunotherapy responses varied not only within individuals but also across different patients.

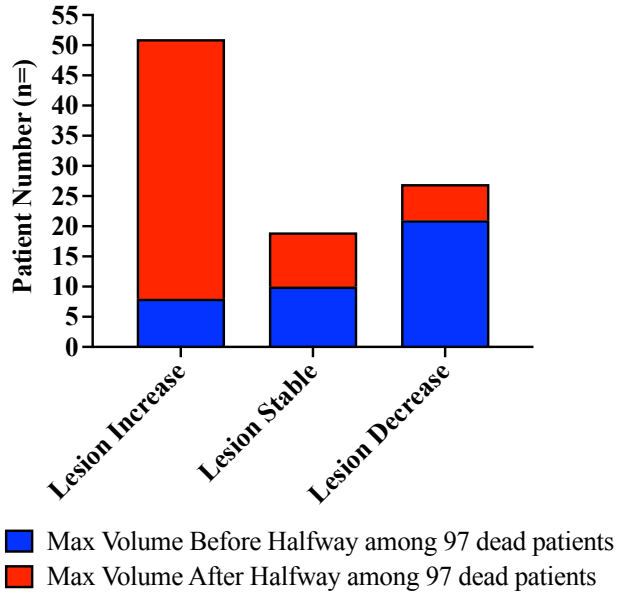


Fig. 5.22 Lesion status in relation to tumour growth timing among 97 dead patients.

**Example 1**

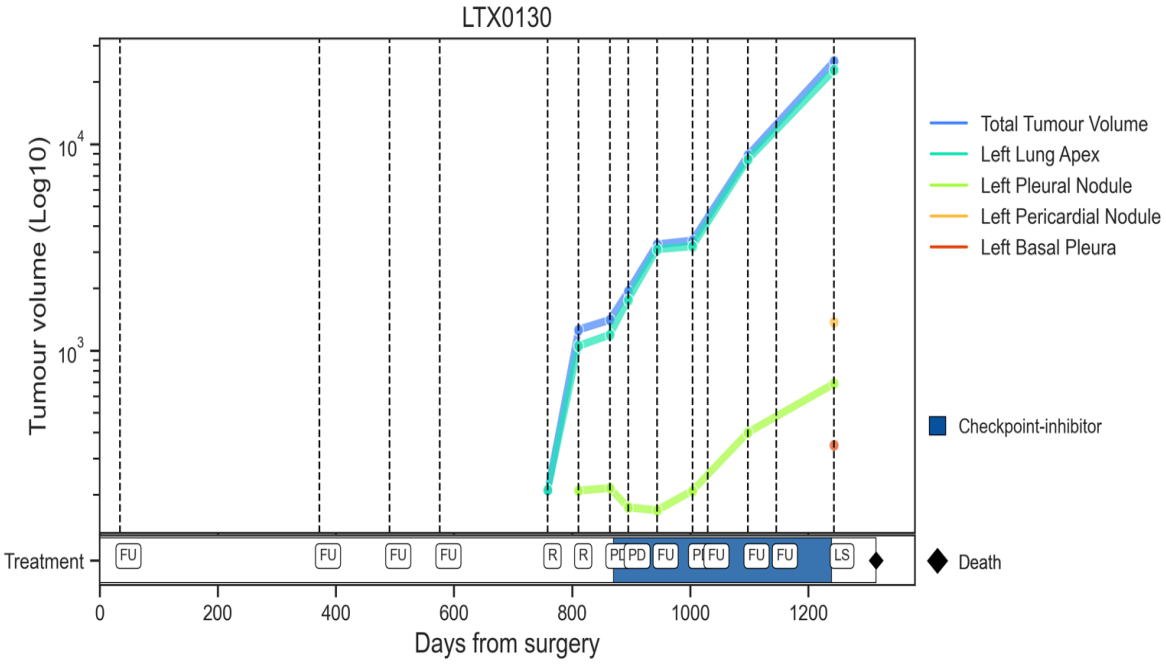

**Example 2**

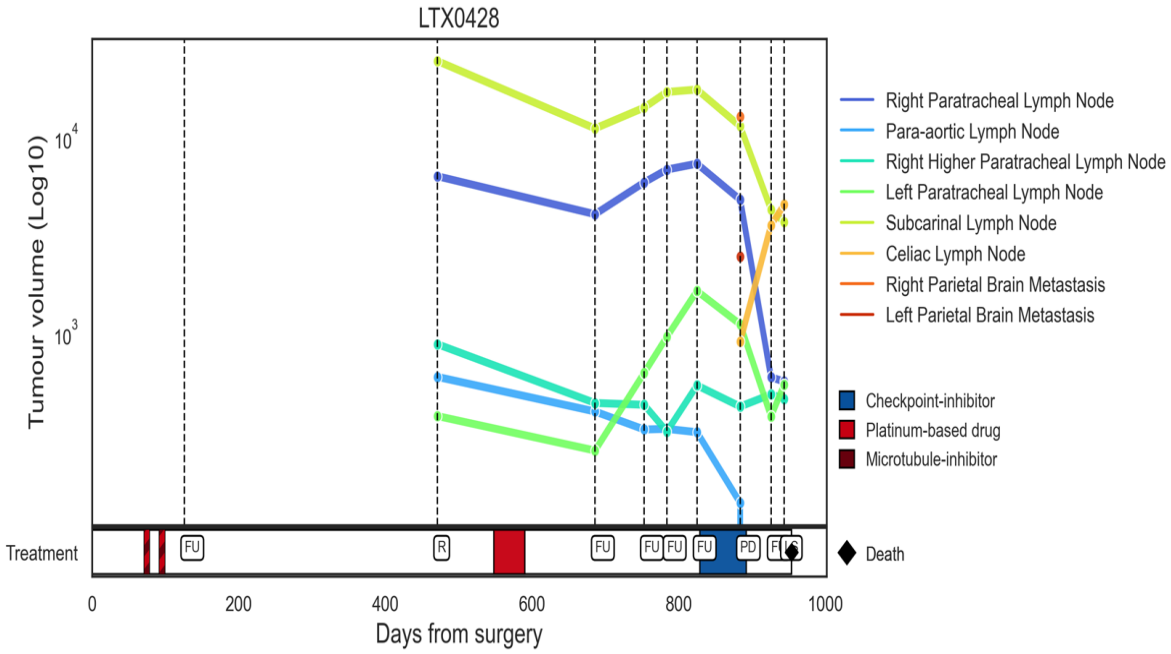


**Example 3**

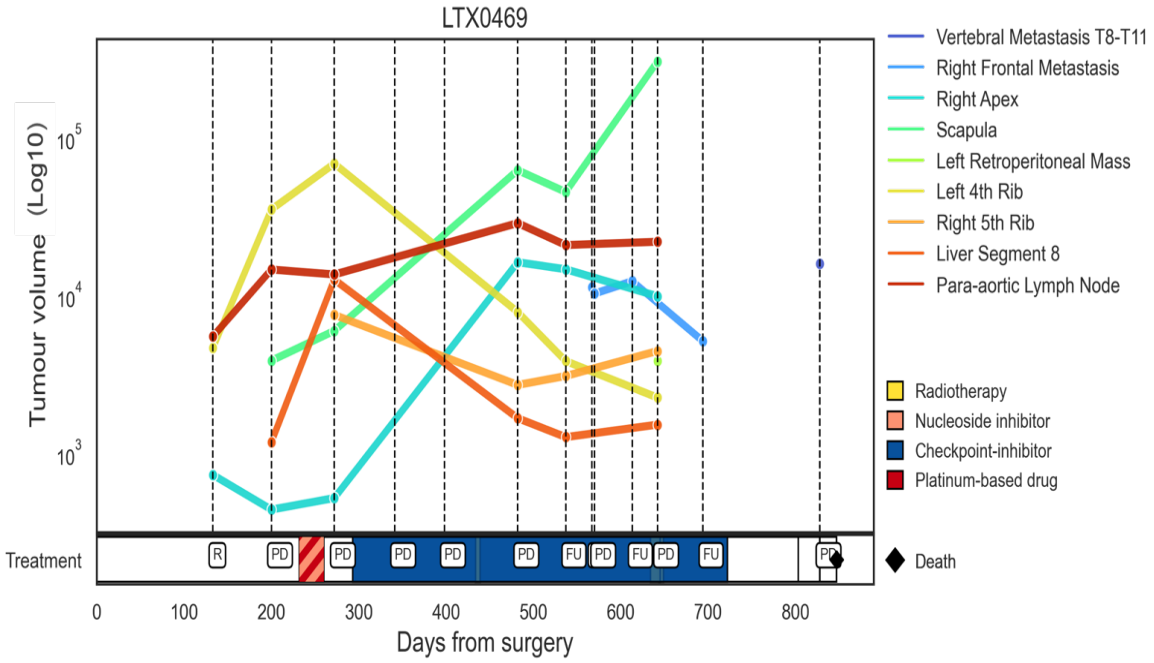

**Example 4**

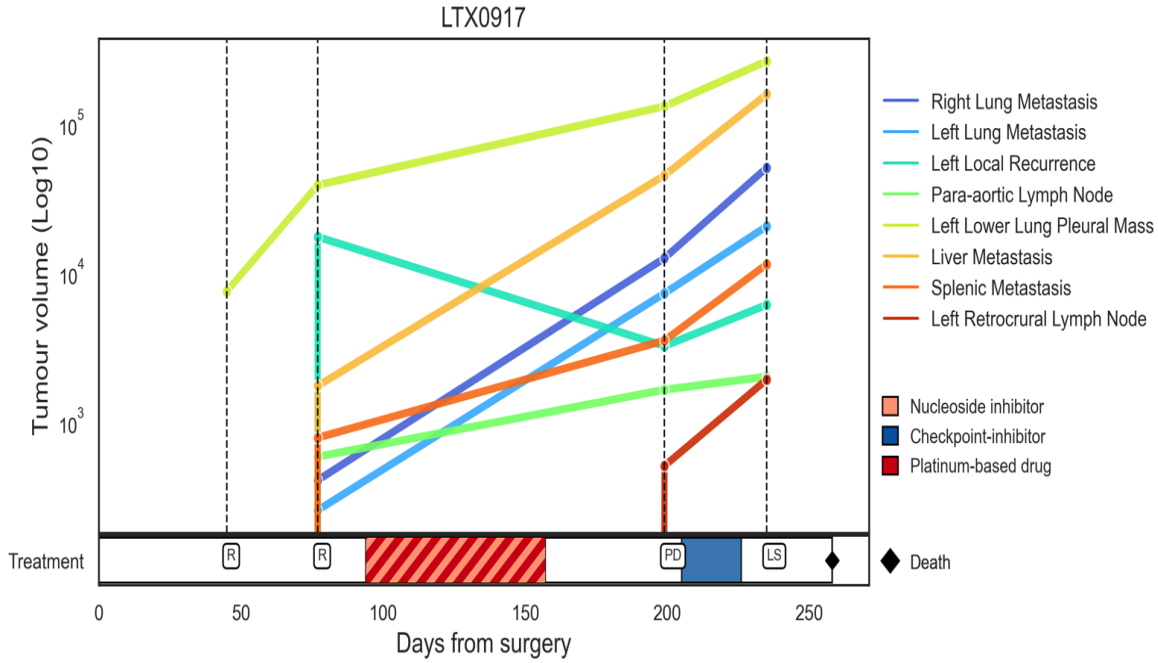


**Example 5**

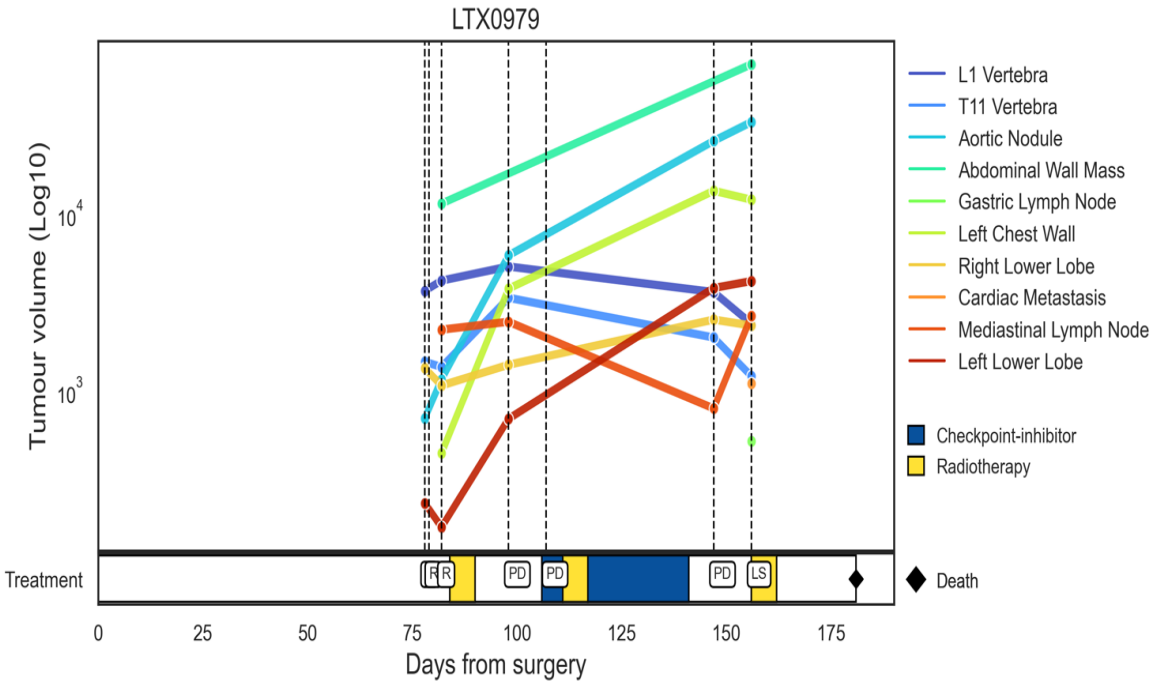


Fig. 5.23 Examples of patients with late-peaking tumour volume showing intrapatient and interpatient heterogeneity and resistance to immunotherapy.

## Results Summary

1. **Frequency of Scans and Prognosis:** 30% of patients presented with equivocal lesions post-surgery, with 68.9% later confirmed malignant. Frequent imaging follow-ups were more common in large-sized primary tumours. High frequency did not improve overall survival, especially in early-stage and smaller tumours, consistent with previous findings. Additionally, high-frequency imaging did not correlate with the earlier detection of smaller relapse volumes. These observations suggest a limited benefit from intensified surveillance; however, the findings should be interpreted cautiously due to the cohort size and potential confounders.
2. **Post-Relapse Treatment Timing Considerations:** The findings from this study primarily demonstrated that the speed of relapse did not significantly impact progression-free survival (PFS) across relapse sites. However, differences in post-relapse progression patterns were observed. Lung and intrathoracic-dominant relapses were generally associated with more stable disease courses, while brain and other extrathoracic relapses appeared to progress more rapidly. While no definitive surveillance interval can be proposed based on these data, the observed site-specific differences may have important implications for future research.
3. **Progression-free survival (PFS) and Tumour Burden as Predictive Factors:** The findings from this study primarily demonstrated that PFS, best response to initial therapy (as assessed by Volume-RECIST), tumour volume, and growth rate at first progression, were indicative factors of progression speed and volume, all of which influenced overall survival. Notably, a tumour volume reduction greater than 65% following initial treatment was associated with improved prognosis (AUC = 0.81).
4. **Maximum tumour burden related to Heterogeneity:** The findings from this study primarily demonstrated that patients reaching maximum tumour burden earlier in the disease course tended to have smaller tumour burden and better prognosis compared to those with later peak volumes. Later-peak tumours more frequently showed lesion increase and higher heterogeneity, potentially contributing to immunotherapy resistance.

# Discussion

CT imaging plays a vital role in detecting malignant lung lesions, with its sensitivity particularly pronounced in identifying nodules larger than 1 cm in their largest dimension, using thin transverse CT sections. The size threshold not only enhances the likelihood of identifying nonbenign lesions but also facilitates the feasibility of operation of transthoracic needle aspiration biopsies [231,232]. However, the task of confirming malignancy in lesions smaller than 1cm remains challenging due to the limitations of morphologic imaging characteristics [233,234]. Studies investigating the efficacy of postoperative CT in recurrence detection reported a high negative predictive value (95%) but a notably lower positive predictive value (53%), indicating a high sensitivity (94%) and specificity (87%) [235]. Conversely, PET/CT imaging, capable of detecting malignant lesions as small as 1cm [236], demonstrated a higher sensitivity than CT (96%, range: 83%–100%), but a variable specificity (52%–100%). This variability is largely due to differences in the cutoff values used for standardised uptake value (SUV), which range from ≥4.5 to ≥10 [170,237–239]. Despite PET/CT offering superior sensitivity, its clinical application remains challenging due to inconsistent SUV thresholds and reduced specificity.

Malignant nodules typically exhibited a volume doubling time ranging from approximately 30 days to 14 months [240,241]. Inflammatory or infectious diseases were more easily detected when the doubling time was less than 30 days. These studies illustrate the heterogeneity of lung lesions. However, there were few studies to explore the clinical characteristics related to equivocal lesions. In this cohort, 31 of 45 patients with equivocal lesions on surveillance CT were eventually diagnosed with malignancy, reflecting a specificity of 68.9% for positive predictive value, which is slightly higher than the 50% reported in the previous study [121]. Equivocal lesions within the intrathoracic region, particularly in the lungs, were found to be the most common, as also reported by other researchers [242]. CT surveillance frequency recommendations vary widely among health organisations. American physicians recommends that patients receive follow-up CT imaging every 6 months for the first two years, followed by annual imaging thereafter [131]. Similarly, the National Comprehensive Cancer Network (NCCN) recommends a frequency of every 6–12 months for the initial two years, followed by

annual scans [7]. The American Academy of Chest Physicians (AACP) recommends biannual chest CT scans for 2 years, followed by yearly scans, for patients with resected non-small cell lung cancer (NSCLC) [243]. The European Society of Medical Oncology recommends at least annual chest CT scans [244]. Despite these guidelines, adherence varies. A Surveillance, Epidemiology, and End Results (SEER) analysis of stage I NSCLCs showed that only 61.4% followed the surveillance guidelines in the initial two years [245].

Further studies have evaluated the effectiveness of different surveillance frequencies in improving early detection and clinical outcomes. A comparison between forty trial patients with locally advanced NSCLC undergoing routine CT imaging and thirty-five non-trial control patients receiving less intensive radiologic follow-up showed no survival rate differences [122]. McMurry analysed over 4000 NSCLC patients, and categorised them into high-intensity, moderate-intensity, and low-intensity surveillance groups, finding that increased CT imaging frequency did not enhance survival [125]. This finding is supported by another study, which found that high-intensity imaging did not benefit stage I NSCLC [123]. In contrast, an analysis of SEER-Medicare data [229] indicated that initiating surveillance scans between 4 and 8 months post-surgery could potentially extend survival rates for stage I NSCLC patients. However, these studies are limited by their retrospective nature and potential bias, especially the inclusion of many stage III patients in high-intensity imaging groups in McMurry's study. Moreover, a prospective study investigating the effects of intensified follow-up, defined as regular monthly phone contacts rather than increased imaging, showed no improvement in relapse detection rates, highlighting the complexity of surveillance strategies [213]. Still, this study was limited by its small sample size of only 88 patients. In this study cohort, massive volume cancers were subject to frequent imaging follow-ups. Due to clinician decisions regarding relapse risk, response to clinical symptoms and the impact of COVID-19 on hospital access, exploring the relationship between surveillance intensity and DFS is unrealistic and may introduce bias. Furthermore, the increased surveillance frequency did not improve overall survival, which may be due to the influence of post-relapse treatment strategies. These observations align with previous studies [118,122–124,229]. Some researchers have raised concerns that delayed CT follow-ups might not detect recurrences promptly, potentially leading to a significant burden of recurrence. However, based on the findings of this study, correlation between imaging frequency and increased relapse tumour volume was not

observed. Relapse volume was highly correlated with relapse speed, which can predict prognosis, explaining why earlier detection of recurrence does not prolong overall survival rates post-surgery in this cohort. In summary, any apparent relationship between scan frequency and survival is likely reflective of underlying tumour biology and stage at diagnosis rather than the surveillance schedule. Future prospective and randomised studies are needed to evaluate the actual relationship between surveillance intensity and survival, particularly in subgroups with varying risk profiles.

Progression-free survival (PFS) was strongly correlated with overall survival following recurrence. Lung and intrathoracic lymph node dominant relapses were generally associated with more stable disease courses, while brain and other extrathoracic relapses appeared to progress more rapidly. While no definitive surveillance interval can be proposed based on these data, the observed site-specific differences may have important implications for future research. If validated in larger, prospective cohorts, these patterns could support the development of stratified post-relapse monitoring strategies.

Interestingly, baseline tumour volume was strongly and positively correlated with baseline growth rate; similarly, relapse volume strongly and positively correlated with relapse growth rate, and progression volume correlated with progression growth rate. However, baseline growth rate showed only a weak correlation with relapse growth rate, and relapse growth rate was also weakly correlated with post-treatment growth rate, highlighting the complexity of cancer progression and underscoring the importance of treatment management. Patients whose best response after initial treatment was a complete response (CR) had smaller tumours and slower growth rates at the first progression compared to those with partial response (PR), stable disease (SD), or progressive disease (PD). The first progression dynamics were indicative of overall survival in this cohort. Nonetheless, standard criteria for evaluating treatment responses still need improvement. Evaluating the best response status by calculating the decreases and increases in total tumour volume can indicate the dynamics of tumour progression, as well as overall survival rates. Moreover, analysis using the ROC curve showed that the best response, a reduction of more than 65% following initial therapy, could predict prognosis, with an area under the curve (AUC) of 0.81.

Tumour mutation burden (TMB) has been identified as a significant factor influencing the effectiveness of immunotherapy [84]. However, there are limited studies using tumour volume to understand the patterns of tumour evolution and heterogeneity. Categorising patients by the timing of maximum tumour emergence into groups of early fast-growing and late fast-growing revealed a notable difference in overall survival. Those with later peak tumour volumes tended to develop more lesions over time, showed higher tumour heterogeneity and a greater resistance to immunotherapy. Such resistance, often acquired through PD-1 blockade, commonly occurs in lymph nodes and less frequently in the liver [246]. For example, patient LTX0469 showed expanded lymph node metastases post-immunotherapy while liver lesions decreased. The complexity of immunotherapy resistance is due to diverse metastatic immune evasion strategies, such as neoantigen depletion [247–249] and disrupted antigen presentation [157]. Furthermore, various metastases may originate from distinct subclone branches, leading to the heterogeneity of tumour evolution. The KEYNOTE-001 study has shown that advanced NSCLC patients benefit from radiotherapy followed by immunotherapy, as seen in patient LTX0169, whose PFS was prolonged by Atezolizumab treatment after radiation [250]. The results of this study highlight the potential benefits of integrating various treatment approaches to enhance patient outcomes. Further genomics studies, alongside tumour volume assessment, can be applied more tightly to fully understand tumour biology, enabling the selection of practical and cost-efficient treatment methods.

In summary, the role of high-intensity surveillance in detecting early relapse remains inconclusive. Despite several limitations—including a small cohort size, imbalance between relapsed and non-relapsed patients, overrepresentation of early-stage disease in the low-intensity group, incomplete documentation on whether the first scan was symptom-triggered or routine, limited hospital access during the COVID-19 pandemic, absence of genomic data, lack of response duration analysis, and the absence of a precise model for predicting tumour growth dynamics—the study offers meaningful insights. Notably, a reduction in tumour volume following initial treatment may serve as a predictive marker for survival. The strong correlation between progression-free survival (PFS) and overall survival post-recurrence underscores the clinical importance of timely therapeutic intervention. Additionally, site-specific relapse patterns may help inform tailored surveillance strategies. If validated in prospective studies, novel predictors such

as tumour volume, relapse speed, sites and early response to therapy could enhance personalised risk stratification and improve post-treatment monitoring strategies. Moreover, tumours with significant late-stage burdens exhibit a high degree of heterogeneity in response to immunotherapy, suggesting that the administration of immunotherapy should be further discussed and emphasising the importance of using genomic data, volumes, and anatomical data to explain metastasis seeding questions in the future.

## Conclusions

Current follow-up protocols, based solely on the TNM stage, may be insufficient for optimising surveillance. Site-specific relapse patterns may help to tailor follow-up intensity in the future. Key prognostic indicators include PFS, the best initial therapy response (particularly volume reduction of>65%), and tumour burden. Additionally, rapid tumour growth and high heterogeneity are associated with larger, more resistant relapses. These results support the potential value of personalised surveillance strategies in NSCLC.

# Chapter Six

## Summary and Future Work

**Aim One:**

Create the largest global imaging dataset to track tumour evolution from diagnosis to death by contouring individual malignant lesions and recording imaging factors. The goal is to better understand how recurrence rates vary across different subgroups of non-small cell lung cancer (NSCLC) patients, with particular emphasis on evaluating primary tumour volumes and growth rates as predictors of relapse.

**Answers:**

Manually contoured primary tumour volume is a stronger predictor of relapse than diameter-based calculation, pT stage and pTNM stage. Larger tumours are associated with earlier relapse, extrathoracic relapse and higher recurrence burden. In pT2N0M0 tumours, preliminary thresholds for tumour volume (>17,010 $mm^3$) and growth rate (>58 $mm^3$/day) are identified. While these metrics may help stratify adjuvant therapy, they are not clinically applicable without further prospective validation.

**Future works:** 1. Develop appropriate volume-based staging systems to enhance prognostic accuracy and improve patient stratification beyond conventional diameter-based metrics. 2. Expand the cohort size to further explore recurrence patterns in current smokers and nonsmokers. A specific focus should be given to right lung-predominant mutations observed in current smokers. Investigate the relationship between these mutations and tumour dynamics. 3. Construct tumour phylogenetic trees using volumetric data to elucidate evolutionary trajectories and better understand how tumour burden correlates with clonal expansion and resistance development over time.

**Aim Two:**

This study aims to explore and characterise the heterogeneity of relapse, progression, and prognosis across different tumour sites and growth patterns in non-small cell lung cancer. Specifically, it seeks to:

1. Investigate the temporal and spatial diversity of tumour relapse.
2. Examine the patterns of progression with an emphasis on tumour burden, anatomical location, and growth rate.

3. Assess the prognostic impact of site-specific recurrences on patient outcomes.

**Answers:**

This study identifies several novel findings: larger tumour volumes, faster progression, and extrathoracic involvement are associated with higher initial relapse rates and poorer outcomes, highlighting that volume and speed may serve as stronger prognostic indicators than lesion count alone. Relapse and progression patterns vary by timing, anatomical location, and growth characteristics, with intrathoracic recurrence—especially in the lung—being most common and generally associated with better outcomes. Poor prognosis is observed in patients with relapses involving multiple organs or the brain, consistent with previous research. Notably, intrathoracic relapses often present as new lesions or localised expansions, whereas extrathoracic relapses frequently involve both new and expanding lesions, indicating a more complex progression and poorer survival.

**Future works:** 1. Explore the characteristics of progression from intrathoracic to extrathoracic relapse: Investigate the subset of patients who initially relapse within the thorax and later progress to extrathoracic disease. Perform single-cell sequencing on paired pre-progression and post-progression samples to identify key subclones responsible for extrathoracic dissemination. Analyse whether accelerated relapse originates from early (truncal) or late (branch) evolutionary events by reconstructing phylogenetic trees. 2. Genomic comparison of relapse and autopsy samples: Conduct genomic profiling of relapse and autopsy samples to identify genetic differences between patients who developed lung or brain relapses and those who did not. This comparative analysis may uncover molecular signatures underlying site-specific relapse patterns and clarify their association with survival outcomes.

**Aim Three:**

To evaluate the role of surveillance frequency and identify key factors influencing progression-free survival (PFS) in non-small cell lung cancer (NSCLC). By analysing post-surgical and post-relapse tumour dynamics, this work proposes a framework to inform individualised surveillance and treatment strategies for improved patient outcomes.

1. Examine how frequent imaging follow-ups affect prognosis and surveillance considerations.
2. Investigate predictive factors of tumour progression and overall survival.
3. Investigate how tumour growth dynamics and treatment response influence post-relapse outcomes.

**Answers:**

Current follow-up protocols, based solely on the TNM stage, may be insufficient for optimising surveillance. Site-specific relapse patterns may help to tailor follow-up intensity in the future. Key prognostic indicators include PFS, the best initial therapy response (particularly volume reduction of>65%), and tumour burden. Additionally, rapid tumour growth and high heterogeneity are associated with larger, more resistant relapses. These results support the potential value of personalised surveillance strategies in NSCLC.

**Future works:** 1. The plan is to expand the cohort and explore tumour growth patterns more accurately by dividing the survival time of all patients into 25%, 50%, and 75% intervals. Then, plot the total tumour volume growth rate across these different life stages to analyse the pace of growth. Based on the results, patients can be grouped into three distinct growth models (see the illustration figure below). Further analysis will involve using volcano plots to explore resistance genes to immunotherapy across the different growth models. This approach will help determine a personalised surveillance frequency for each patient, thereby optimising treatment and monitoring strategies.

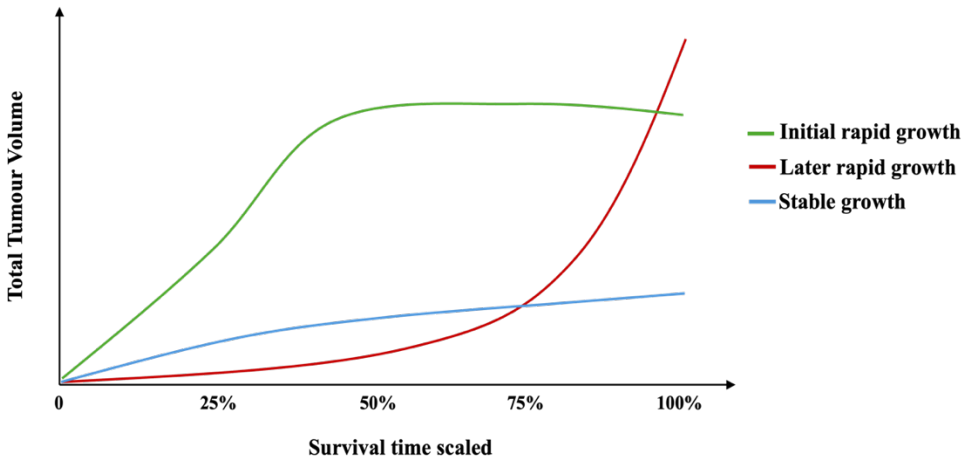

2. To determine the optimal time for assessing volume reduction after treatment in order to predict clinical outcomes.

3. During post-surgery follow-ups, use ctDNA levels to monitor tumour dynamics alongside imaging data. Plot the increase in equivocal lesion volume detected by imaging and the corresponding rise in ctDNA levels (illustration figure is listed below). Analyse the time gap between the rise in ctDNA and the appearance of lesions on imaging among different subgroups. This analysis will help assess the accuracy of ctDNA and imaging in detecting equivocal lesions and determining which of these ultimately develop into malignancies. The ultimate goal is to evaluate how to effectively combine ctDNA and imaging techniques as early indicators of malignant transformation, optimising early detection and intervention strategies.

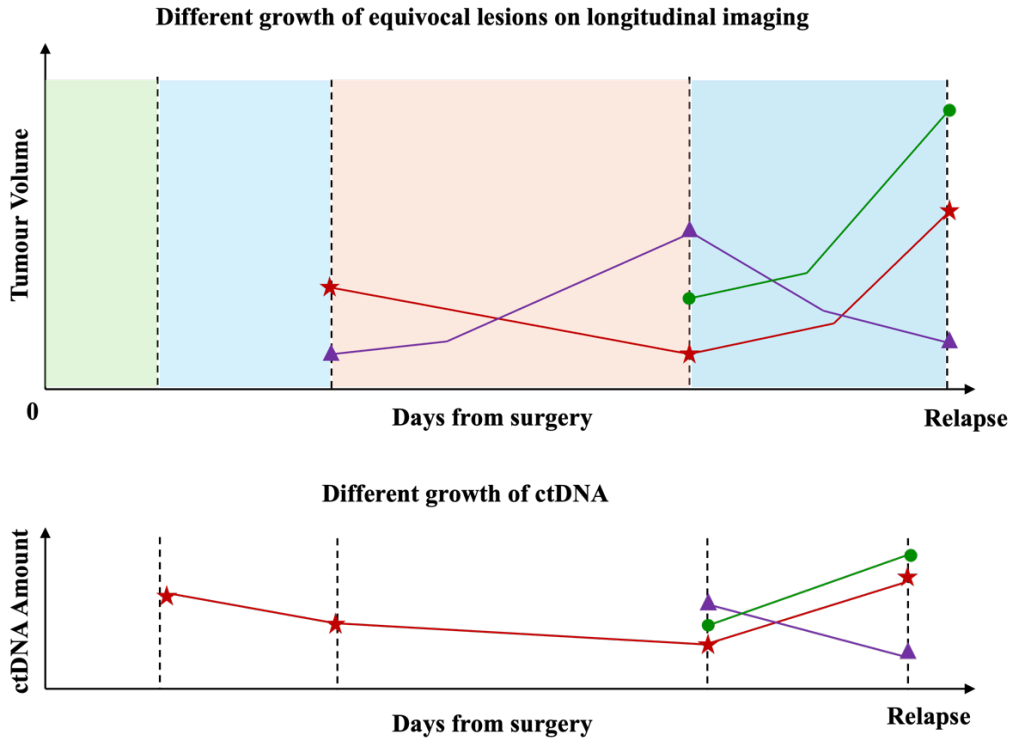

# Appendix 1

To assess contouring variations, 10 patients were randomly selected, and each lesion was contoured 3 times at each time point. The table below shows the details. The results showed a 95% confidence interval difference ranging from 0.54% to 42.6%, with 90.9% of the population under 20%. The coefficient of variation (CV) for each lesion ranged from 0.27% to 21.3%, with 90.9% of the population having a value under 10%, indicating that most contouring errors were less than 10%, thus confirming the reliability of manual contours.

Table 1 Tumour segmentation details for ten patients using ITK-SNAP

| Patient ID | Time point | Lesion | Standard Deviation | Standard Error Mean | CV% |
|---|---|---|---|---|---|
| LTX0012 | 1 | Right upper lung | 31.63 | 18.26 | 0.68 |
| LTX0012 | 2 | Lymph node | 209.84 | 121.15 | 1.90 |
| LTX0012 | 3 | Lymph node | 155.03 | 89.50 | 1.17 |
| LTX0012 | 4 | Lymph node | 1432.63 | 827.13 | 3.60 |
| LTX0012 | 4 | Right lung apex | 11.78 | 6.80 | 3.06 |
| LTX0012 | 5 | Lymph node | 842.85 | 486.62 | 1.67 |
| LTX0012 | 5 | Right lung apex | 29.38 | 16.96 | 8.76 |
| LTX0012 | 6 | Lymph node | 2081.44 | 1201.72 | 3.67 |
| LTX0012 | 6 | Right lung apex | 13.30 | 7.68 | 4.29 |
| LTX0012 | 7 | Lymph node | 1400.08 | 808.34 | 6.66 |
| LTX0012 | 7 | Right lung apex | 28.39 | 16.39 | 8.52 |
| LTX0012 | 8 | Lymph node | 1879.10 | 1084.90 | 4.66 |
| LTX0012 | 8 | Right lung apex | 15.75 | 9.1 | 4.71 |
| LTX0012 | 9 | Lymph node | 2560.43 | 1478.26 | 5.13 |
| LTX0012 | 9 | Right lung apex | 8.73 | 5.04 | 2.10 |
| LTX0012 | 10 | Lymph node | 1455.64 | 840.42 | 2.21 |
| LTX0012 | 10 | Right lung apex | 20.99 | 12.12 | 4.87 |
| LTX0012 | 11 | Lymph node | 3717.27 | 2146.17 | 4.11 |
| LTX0012 | 11 | Right lung apex | 18.99 | 10.96 | 3.39 |
| LTX0012 | 12 | Lymph node | 1650.01 | 952.63 | 8.08 |

| | | | | | |
|---|---|---|---|---|---|
| LTX0012 | 12 | Right lung apex | 71.04 | 41.01 | 6.82 |
| LTX0085 | 1 | Right upper lung | 533.51 | 308.02 | 4.04 |
| LTX0085 | 2 | Right pleura | 73.26 | 42.3 | 1.33 |
| LTX0097 | 1 | Right upper lung | 820.08 | 473.47 | 1.97 |
| LTX0097 | 1 | 4R lymph node | 215.00 | 124.13 | 9.59 |
| LTX0097 | 2 | Left brain | 1071.77 | 618.78 | 16.05 |
| LTX0097 | 3 | Left brain | 281.35 | 162.44 | 2.77 |
| LTX0103 | 1 | Right lower lung | 20.03 | 11.57 | 0.93 |
| LTX0103 | 2 | Liver1 | 3.64 | 2.1 | 0.86 |
| LTX0103 | 2 | Liver2 | 19.96 | 11.52 | 5.21 |
| LTX0103 | 2 | Left adrenal | 42.88 | 24.76 | 1.27 |
| LTX0103 | 3 | Left adrenal | 120.44 | 69.54 | 4.41 |
| LTX0103 | 4 | Liver2 | 3.18 | 1.84 | 3.26 |
| LTX0103 | 5 | Liver1 | 210.23 | 121.38 | 9.55 |
| LTX0103 | 6 | Liver1 | 235.10 | 135.74 | 9.35 |
| LTX0103 | 7 | Liver1 | 285.50 | 164.84 | 21.30 |
| LTX0271 | 1 | Left upper | 144.51 | 83.43 | 3.74 |
| LTX0271 | 2 | Left AP | 2085.72 | 1204.19 | 8.68 |
| LTX0271 | 3 | Left AP | 195.02 | 112.6 | 0.77 |
| LTX0271 | 4 | Left AP | 115.90 | 66.92 | 0.96 |
| LTX0287 | 1 | Left lower lung | 283.98 | 163.96 | 3.28 |
| LTX0287 | 2 | Lymph node | 1094.09 | 631.67 | 8.18 |
| LTX0287 | 2 | Diaphragm | 56.36 | 32.54 | 14.33 |
| LTX0474 | 1 | Right upper lung | 2502.15 | 1444.62 | 5.64 |
| LTX0474 | 2 | Left upper | 2738.80 | 1581.25 | 6.60 |
| LTX0474 | 2 | Right kidney | 31.43 | 18.15 | 1.81 |
| LTX0474 | 3 | Left upper | 2340.85 | 1351.49 | 7.07 |
| LTX0474 | 3 | Right kidney | 300.02 | 173.22 | 4.89 |
| LTX0474 | 4 | Left upper | 2406.69 | 1389.50 | 3.85 |
| LTX0474 | 4 | Right kidney | 251.82 | 145.39 | 4.79 |
| LTX0474 | 4 | Right gastric | 1.40 | 0.81 | 0.27 |
| LTX0474 | 5 | Left upper | 6246.57 | 3606.46 | 6.55 |
| LTX0474 | 5 | Right kidney | 2925.00 | 1688.75 | 11.88 |

| | | | | | |
|---|---|---|---|---|---|
| LTX0474 | 5 | Right lower | 59.52 | 34.36 | 4.09 |
| LTX0474 | 5 | Right retroperitoneal | 125.74 | 72.6 | 2.55 |
| LTX0474 | 5 | Right gastric | 109.23 | 63.07 | 4.97 |
| LTX0474 | 5 | celiac | 13.18 | 7.07 | 2.47 |
| LTX0582 | 1 | Right primary | 343.12 | 198.10 | 2.56 |
| LTX0582 | 1 | Left ground glass | 130.52 | 75.3 | 7.58 |
| LTX0582 | 1 | Right lower metastasis | 16.85 | 9.73 | 6.68 |
| LTX0582 | 2 | Left ground glass | 209.04 | 120.69 | 9.05 |
| LTX0582 | 2 | Right lower metastasis | 18.55 | 10.71 | 5.34 |
| LTX0582 | 3 | Left ground glass | 88.83 | 51.29 | 2.04 |
| LTX0582 | 3 | Right lower metastasis | 17.6 | 10.16 | 3.25 |
| LTX0582 | 4 | Right lower metastasis | 4.68 | 2.70 | 2.18 |
| LTX0582 | 5 | Right lower metastasis | 13.54 | 7.82 | 3.75 |
| LTX0817 | 1 | Right lower | 2443.87 | 1410.97 | 4.51 |
| LTX0817 | 2 | Right peri-esophageal | 190.62 | 110.05 | 3.01 |
| LTX0817 | 3 | Right peri-esophageal | 330.36 | 190.74 | 5.63 |
| LTX0817 | 4 | Right peri-esophageal | 379.24 | 218.95 | 11.08 |
| LTX0817 | 5 | Right peri-esophageal | 97.38 | 56.22 | 1.52 |
| LTX0817 | 6 | Right peri-esophageal | 64.81 | 37.42 | 1.07 |

| | | | | | |
|---|---|---|---|---|---|
| LTX0817 | 7 | Right peri-esophageal | 273.156 | 157.71 | 10.93 |
| LTX0862 | 1 | Left lower lung | 124.13 | 71.67 | 2.44 |
| LTX0862 | 2 | Right apical | 209.69 | 121.06 | 5.66 |
| LTX0862 | 3 | Right 5$^{th}$ rib | 338.58 | 195.48 | 2.05 |

UK radiation oncologists typically use Eclipse for tumour contouring and radiotherapy planning, but Eclipse only supports DICOM files, not NIfTI formats, which are less storage-intensive and faster to process. Given the impracticality of contouring thousands of images through Eclipse, 10 patients were randomly selected to compare contouring variation between ITK-SNAP and Eclipse, as detailed below.

Table 2 Comparison of tumour segmentation volumes at each time point for ten patients using ITK-SNAP and Eclipse.

| **Patient ID** | **Lesion** | **Mean Volume in ITK-SNAP ($mm^3$)** | **Volume in Eclipse ($cm^3$)** | **Range (%)** |
|---|---|---|---|---|
| LTX0012 | Right upper lung | 4653.333 | 4.3 | –7.593 |
| LTX0012 | Lymph node | 11053.333 | 13.5 | 22.14 |
| LTX0012 | Lymph node | 13286.667 | 15.2 | 14.4 |
| LTX0012 | Lymph node | 39816.667 | 41 | 2.972 |
| LTX0012 | Right lung apex | 384.5 | 0.4 | 4.031 |
| LTX0012 | Lymph node | 50620 | 50.8 | 0.356 |
| LTX0012 | Right lung apex | 335.467 | 0.3 | –10.57 |
| LTX0012 | Lymph node | 56660 | 54.2 | –4.342 |
| LTX0012 | Right lung apex | 310.367 | 0.3 | –3.34 |
| LTX0012 | Lymph node | 21033.333 | 23.8 | 13.15 |
| LTX0012 | Right lung apex | 333.133 | 0.4 | 20.07 |
| LTX0012 | Lymph node | 40366.667 | 37.6 | –6.854 |
| LTX0012 | Right lung apex | 334.467 | 0.3 | –10.3 |
| LTX0012 | Lymph node | 49866.667 | 49.6 | –0.535 |
| LTX0012 | Right lung apex | 416.2 | 0.5 | 20.13 |

| | | | | |
|---|---|---|---|---|
| LTX0012 | Lymph node | 65890 | 64.9 | –1.503 |
| LTX0012 | Right lung apex | 431.067 | 0.5 | 15.99 |
| LTX0012 | Lymph node | 90426.667 | 94 | 3.952 |
| LTX0012 | Right lung apex | 560.533 | 0.5 | –10.8 |
| LTX0012 | Lymph node | 20426.667 | 21.1 | 3.296 |
| LTX0012 | Right lung apex | 1040.867 | 1 | –3.926 |
| LTX0085 | Right upper lung | 13196.667 | 13.2 | 0.025 |
| LTX0085 | Right pleura | 5503 | 5.6 | 1.763 |
| LTX0097 | Right upper lung | 41603.333 | 38 | –8.661 |
| LTX0097 | 4R lymph node | 2241 | 2.5 | 11.56 |
| LTX0097 | Left brain | 6676 | 8 | 19.83 |
| LTX0097 | Left brain | 10147.667 | 9.6 | –5.397 |
| LTX0103 | Right lower lung | 2159.333 | 2.1 | –2.748 |
| LTX0103 | Liver1 | 423.33 | 0.5 | 18.11 |
| LTX0103 | Liver2 | 382.867 | 0.2 | –47.76 |
| LTX0103 | Left adrenal | 3365 | 3.1 | –7.875 |
| LTX0103 | Left adrenal | 2731.333 | 2.8 | 2.514 |
| LTX0103 | Liver2 | 97.56 | 0.1 | 2.501 |
| LTX0103 | Liver1 | 2202 | 1.8 | –18.26 |
| LTX0103 | Liver1 | 2514 | 2.7 | 7.399 |
| LTX0103 | Liver1 | 1340.333 | 1.5 | 11.91 |
| LTX0271 | Left upper | 3862.333 | 3.7 | –4.203 |
| LTX0271 | Left AP | 24033.333 | 24.6 | 2.358 |
| LTX0271 | Left AP | 25413.333 | 25 | –1.626 |
| LTX0271 | Left AP | 12073.333 | 10.7 | –11.37 |
| LTX0287 | Left lower lung | 8662.333 | 8.7 | 0.435 |
| LTX0287 | Lymph node | 13373.333 | 12 | –10.27 |
| LTX0287 | Diaphragm | 393.233 | 0.4 | 1.721 |
| LTX0474 | Right upper lung | 44332 | 47.1 | 6.244 |
| LTX0474 | Left upper | 41503.333 | 40.9 | –1.454 |
| LTX0474 | Right kidney | 1739 | 1.8 | 3.508 |
| LTX0474 | Left upper | 33130 | 30.4 | –8.24 |
| LTX0474 | Right kidney | 6131.667 | 7 | 14.16 |

| | | | | |
|---|---|---|---|---|
| LTX0474 | Left upper | 62456.667 | 64.9 | 3.912 |
| LTX0474 | Right kidney | 5255.333 | 5.5 | 4.656 |
| LTX0474 | Right gastric | 519.467 | 0.4 | –23 |
| LTX0474 | Left upper | 95393.333 | 100.1 | 4.934 |
| LTX0474 | Right kidney | 24626.667 | 28 | 13.7 |
| LTX0474 | Right lower | 1455.667 | 1.4 | –3.824 |
| LTX0474 | Right retroperitoneal | 4928.333 | 5 | 1.454 |
| LTX0474 | Right gastric | 2198 | 2.2 | 0.091 |
| LTX0474 | celiac | 534.367 | 0.5 | –6.431 |
| LTX0582 | Right primary | 13406.667 | 13.8 | 2.934 |
| LTX0582 | Left ground glass | 1721.667 | 1.7 | –1.258 |
| LTX0582 | Right lower metastasis | 252.333 | 0.3 | 18.89 |
| LTX0582 | Left ground glass | 2310.667 | 2.2 | –4.789 |
| LTX0582 | Right lower metastasis | 347.6 | 0.4 | 15.07 |
| LTX0582 | Left ground glass | 4347 | 4.3 | –1.081 |
| LTX0582 | Right lower metastasis | 542 | 0.6 | 10.7 |
| LTX0582 | Right lower metastasis | 214.4 | 0.2 | –6.716 |
| LTX0582 | Right lower metastasis | 360.967 | 0.3 | –16.89 |
| LTX0817 | Right lower | 54200 | 52.1 | –3.875 |
| LTX0817 | Right peri-esophageal | 6341.667 | 6.1 | –3.811 |
| LTX0817 | Right peri-esophageal | 5872.333 | 5.9 | 0.471 |
| LTX0817 | Right peri-esophageal | 3424 | 3.8 | 10.98 |
| LTX0817 | Right peri-esophageal | 6425.667 | 6.5 | 1.157 |

| | | | | |
|---|---|---|---|---|
| LTX0817 | Right peri-esophageal | 6076.333 | 6 | –1.256 |
| LTX0817 | Right peri-esophageal | 2499.667 | 2.2 | –11.99 |
| LTX0862 | Left lower lung | 5092.333 | 5.3 | 4.078 |
| LTX0862 | Right apical | 3705.667 | 3.7 | –0.153 |

I contoured each malignant lesion from follow-up scans post-surgery to the date of confirmed relapse. Below are examples illustrating how tumours relapse at different rates, making it unreasonable to use an exponential model or other single model to calculate growth speed. Current models built to predict relapse are limited due to an imbalance in scan frequency, significant heterogeneity in growth patterns within and between individuals, and the small cohort size. In the future, with an expanded cohort, deep learning algorithms can be developed and tested to improve prediction accuracy. (as shown in Fig. 1)

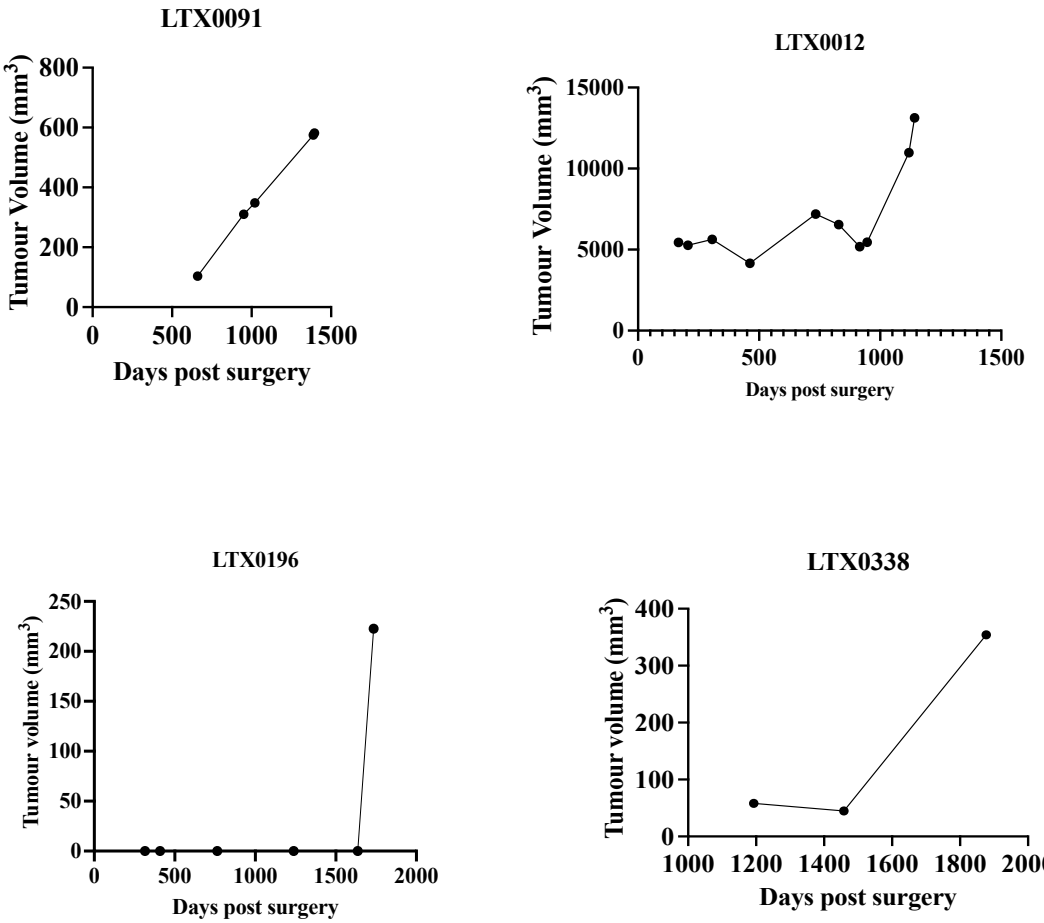

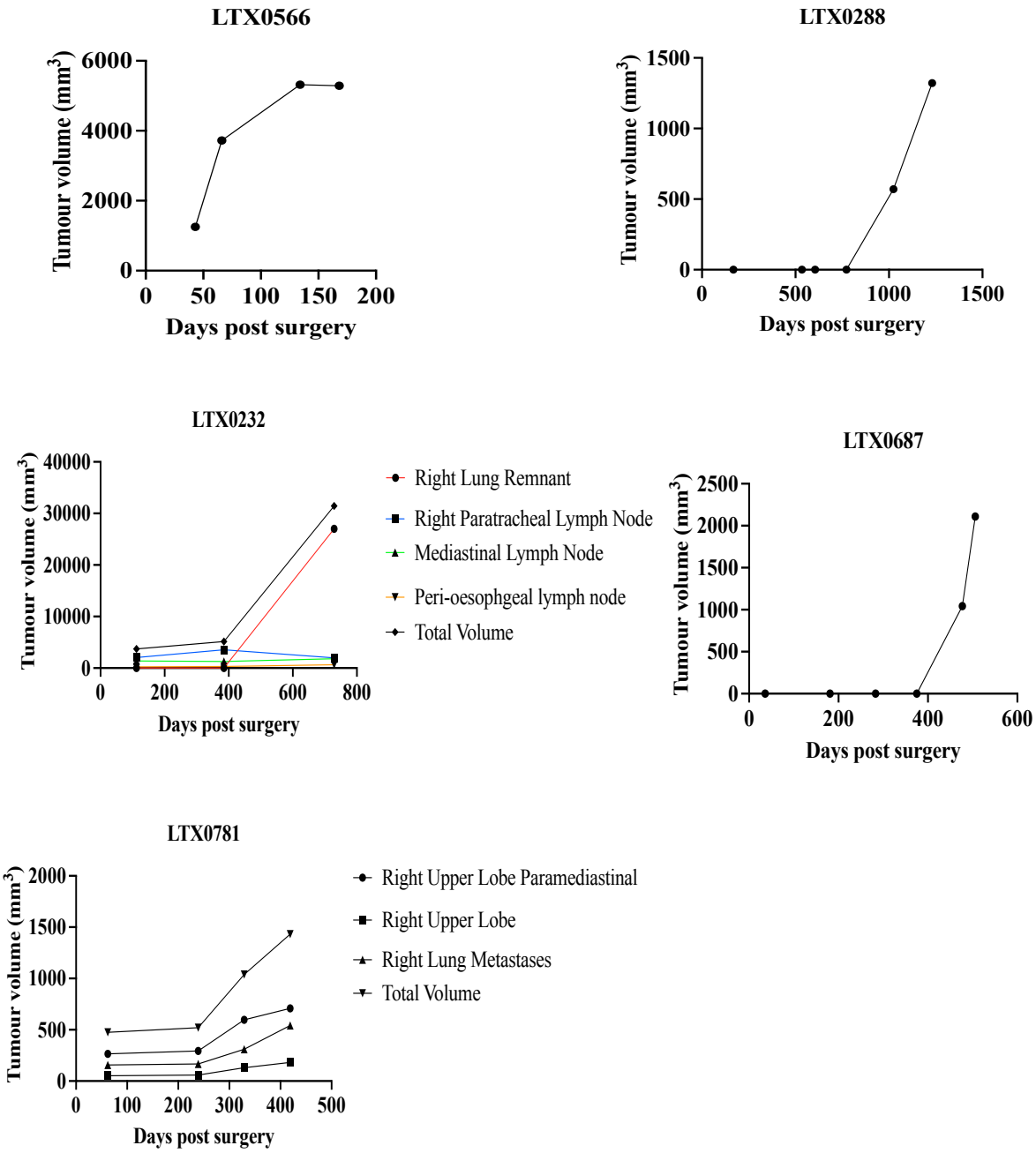


Fig. 1 Heterogeneity of tumour relapse speed both within and across individuals. These figures illustrate the variability in tumour growth dynamics from surveillance imaging post-surgery to confirmed relapse.

# Appendix 2

Different methods were used to define high-intensity, moderate-intensity, and low-intensity. Among 200 patients, approximately 90% underwent the first surveillance scan within 450 days. Firstly, 450 days were divided into three equal periods. Using 0–150 days (3 months, high-intensity), 151–300 days (6 months, moderate-intensity), and 301–405 days (1 year, low-intensity) to define surveillance periods. However, the number of patients in the three groups was found imbalanced; there were fewer low-intensity patients (Table 1). Besides, primary tumour volumes in the low-intensity group were significantly smaller than in the high-intensity group. In this situation, the high-intensity group showed a worse OS (Fig. 1).

Table 1 Patient Demographics for the 3 surveillance groupings based on the first definition version, presented as n (%) for categorical variables and median for continuous variables.

| **Characteristics (n=)** | **3-month (0–150)** | **6-month (151–300)** | **1-year (301–450)** | **Adjusted P-value** |
|---|---|---|---|---|
| N | 72 | 66 | 39 | |
| Relapse within period | 19 (26%) | 16 (24%) | 11 (28%) | 0.93 |
| 2-year relapse | 52 (72%) | 32 (48%) | 16 (41%) | 0.012* |
| Overall Relapse | 57 (79%) | 42 (64%) | 20 (51%) | 0.045* |
| Age (median) | 69 | 69 | 66 | 0.518 |
| Sex (male) | 40 (56%) | 38 (58%) | 21 (54%) | 0.93 |
| Smoking Status | | | | |
| *Current smoker* | 6 (8%) | 6 (9%) | 5 (13%) | 0.258 |
| *Ex-smoker* | 31 (44%) | 41 (62%) | 17 (43.5%) | |
| *Recent Ex-smoker* | 26 (36%) | 14 (21%) | 16 (41%) | |
| *Never smoker* | 9 (12%) | 5 (8%) | 1 (2.5%) | |
| Histology | | | | |
| *LUSC* | 21 (29%) | 20 (30%) | 11 (28%) | 0.869 |
| *LUAD* | 40 (56%) | 39 (59%) | 25 (64%) | |
| *Other* | 11 (15%) | 7 (11%) | 3 (8%) | |
| Pathologic stage | | | | 0.012* |

| | | | | |
|---|---|---|---|---|
| *I* | 12 (17%) | 30(45%) | 19 (49%) | |
| *II* | 28 (39%) | 13 (20%) | 10 (25.5%) | |
| *III* | 32 (44%) | 23 (35%) | 10 (25.5%) | |
| Adjuvant therapy | 31 (43%) | 25 (38%) | 14 (36%) | 0.837 |
| Surgery | | | | 0.518 |
| *Lobectomy* | 59 (82%) | 59 (89%) | 31 (79%) | |
| *Segmentectomy or wedge* | 5 (7%) | 5 (8%) | 3 (8%) | |
| *Bilobectomy or Pneumonectomy* | 8 (11%) | 2 (3%) | 5 (13%) | |
| Primary Tumour Volume ($mm^3$, median, IQR) | 35955 (12690.2–89457.1) | 14930 (4663–25990) | 12530 (4738–53510) | 0.012* |
| Primary Growth Rate ($mm^3$/d, median, IQR) | 62.24 (8.33–314.22) | 27 (6.79–103.81) | 41.67 (9.395–135.705) | 0.518 |
| Anatomical Location | | | | 0.2414 |
| *RU/ML* | 30 (42%) | 26 (39%) | 10 (26%) | |
| *RLL* | 16 (22%) | 17 (26%) | 13 (33%) | |
| *LUL* | 18 (25%) | 17 (26%) | 7 (18%) | |
| *LLL* | 8 (11%) | 6 (9%) | 9 (23%) | |
| Central Location | 29 (40%) | 19 (29%) | 10 (26%) | 0.398 |
| Pleural Attachment | 51 (71%) | 41 (62%) | 19 (49%) | 0.185 |
| Bronchial Attachment | 28 (39%) | 11 (17%) | 11 (28%) | 0.063 |
| Air Bronchogram | 29 (37%) | 22 (30%) | 19 (42.5%) | 0.44 |
| Atelectasis | 37 (48.7%) | 26 (37.7%) | 14 (35%) | 0.414 |
| Pleural Retraction | 34 (40%) | 32 (33%) | 12 (49%) | 0.398 |
| Relapse Site | | | | 0.15 |
| *Intrathoracic* | 27 (38%) | 27 (41%) | 10 (26%) | 0.15 |
| *Extrathoracic* | 13 (18%) | 7 (11%) | 4 (10%) | |
| *Both* | 17 (23%) | 8 (12%) | 6 (15%) | |
| *None* | 15 (21%) | 24 (36%) | 19 (49%) | |

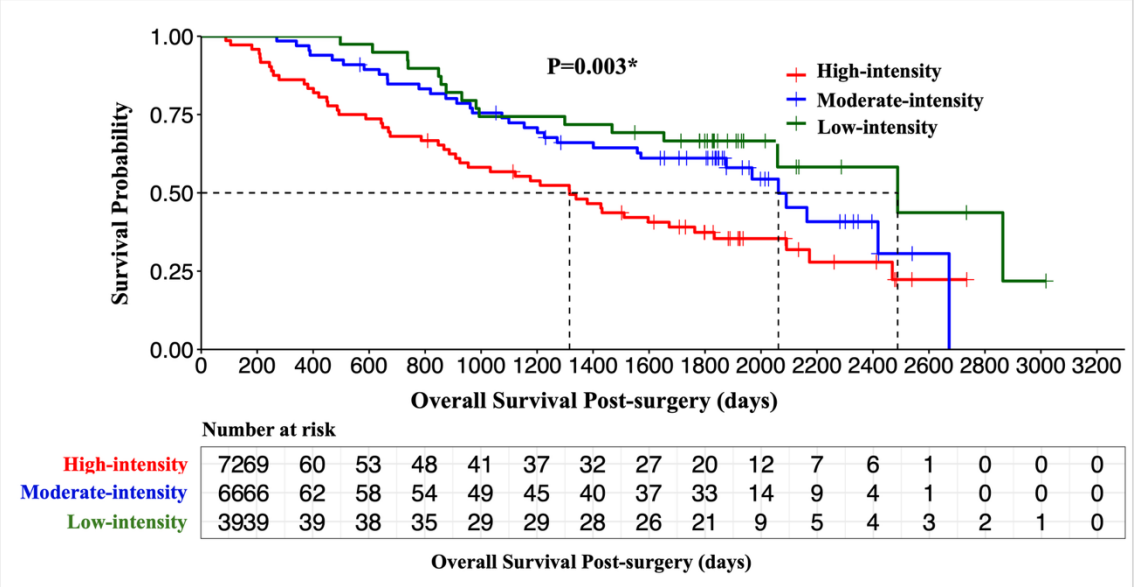


Fig. 1 Overall survival post-surgery among high-, moderate- and low-intensity surveillance groups.

Secondly, to balance the patient number among three groups, I found there were 59 patients whose first surveillance scan was undertaken within 0–130 days (3 months), 60 patients within 131–240 days (6 months), and 58 patients within 241–450 days (1 year), accordance with high, moderate and low-intensity surveillance. Using this definition, the results indicated that the high-intensity group had worse OS (Fig. 2). However, in the real world, clinicians usually follow up with patients using complete months, and 130 days does not constitute an entire month. It may not be a suitable choice for analysis and clinical practice suggestions (Table 2).

Table 2 Patient Demographics for the 3 surveillance groupings based on the second definition version, presented as n (%) for categorical variables and median for continuous variables.

| **Characteristics (n=)** | **3-month (0–130)** | **6-month (131–240)** | **1-year (241–450)** | **Adjusted P-value** |
|---|---|---|---|---|
| n | 59 | 60 | 58 | |
| Relapse within period | 15 (26%) | 15 (18%) | 17 (14.8%) | 0.889 |
| 2-year relapse | 44 (75%) | 30 (50%) | 26 (45%) | 0.048* |
| Overall Relapse | 48 (81%) | 39 (65%) | 32 (55%) | 0.063 |

| | | | | |
|---|---|---|---|---|
| Age (median) | 70 | 68 | 67 | 0.678 |
| Sex (male) | 31 (61%) | 36 (60%) | 32 (55%) | 0.884 |
| Smoking Status | | | | |
| *Current smoker* | 4 (7%) | 8 (13%) | 5 (9%) | 0.678 |
| *Ex-smoker* | 27 (46%) | 31 (52%) | 31 (53%) | |
| *Recent Ex-smoker* | 20 (34%) | 16 (27%) | 20 (35%) | |
| *Never smoker* | 8 (13%) | 5 (8%) | 2 (3%) | |
| Histology | | | | |
| *LUSC* | 18 (31%) | 17 (28%) | 17 (29%) | 0.884 |
| *LUAD* | 32 (54%) | 38 (63%) | 34 (59%) | |
| *Other* | 9 (15%) | 5 (9%) | 7 (12%) | |
| Pathologic stage | | | | |
| *I* | 10 (17%) | 26 (43%) | 25 (43%) | 0.084 |
| *II* | 22 (37%) | 15 (25%) | 14 (24%) | |
| *III* | 27 (46%) | 19 (32%) | 19 (33%) | |
| Adjuvant therapy | 25 (42%) | 21 (35%) | 24 (41%) | 0.884 |
| Surgery | | | | 0.898 |
| *Lobectomy* | 48 (82%) | 51 (85%) | 50 (86%) | |
| *Segmentectomy or wedge* | 5 (8%) | 5 (8%) | 3 (5%) | |
| *Bilobectomy or Pneumonectomy* | 6 (10%) | 4 (7%) | 5 (9%) | |
| Primary Tumour Volume ($mm^3$, median, IQR) | 35940 (12400.5–86370) | 12930 (4982–39540) | 15165(4954–59205) | 0.063 |
| Primary Growth Rate ($mm^3$/d, median, IQR) | 82.39 (9.11–318.23) | 19.31 (6.79–54.29) | 48.415 (9.973–133.167) | 0.2 |
| Anatomical Location | | | | 0.652 |
| *RU/ML* | 24 (40.5%) | 23 (38%) | 19 (33%) | |
| *RLL* | 13 (22%) | 15 (25%) | 18 (31%) | |
| *LUL* | 14 (24%) | 18 (30%) | 10 (17%) | |

| | | | | |
|---|---|---|---|---|
| *LLL* | 8 (13.5%) | 4 (7%) | 11 (19%) | |
| Central Location | 21 (36%) | 20 (33%) | 17 (29%) | 0.884 |
| Pleural Attachment | 42 (71%) | 38 (63%) | 31 (53%) | 0.347 |
| Bronchial Attachment | 22 (33%) | 12 (20%) | 16 (28%) | 0.316 |
| Air Bronchogram | 21(37%) | 25 (20%) | 20 (28%) | 0.815 |
| Atelectasis | 31 (53%) | 24 (40%) | 22 (38%) | 0.497 |
| Pleural Retraction | 26 (44%) | 26 (43%) | 19 (33%) | 0.678 |
| Relapse Site | | | | 0.215 |
| *Intrathoracic* | 25 (42%) | 25 (42%) | 14 (24%) | |
| *Extrathoracic* | 10 (17%) | 7 (11.5%) | 7 (12%) | |
| *Both* | 13 (22%) | 7 (11.5%) | 11 (19%) | |
| *None* | 11 (19%) | 21 (35%) | 26 (45%) | |

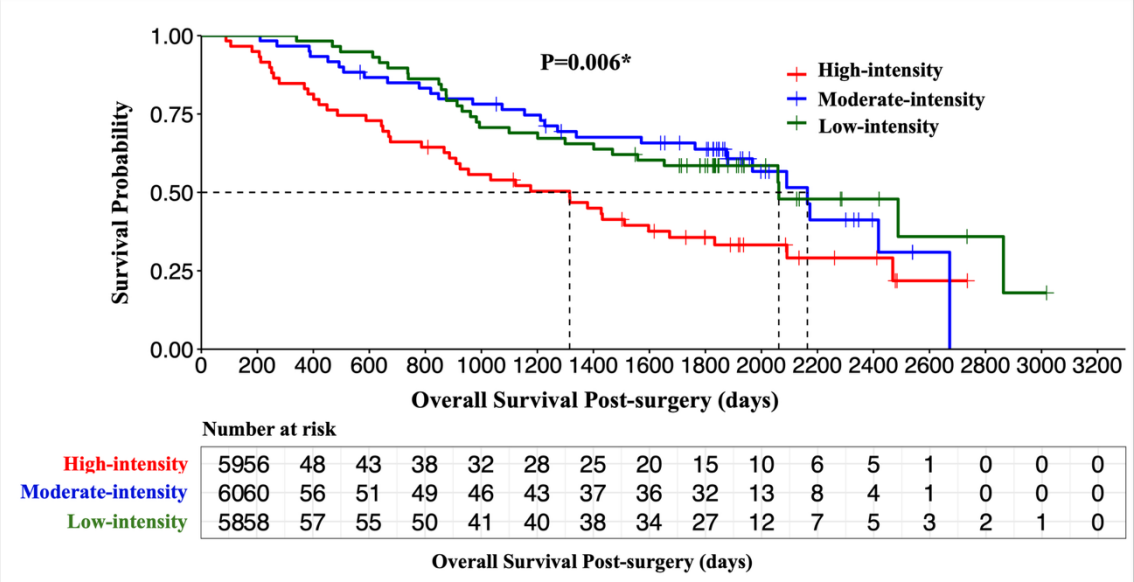


Fig. 2 Overall survival post-surgery among high-, moderate- and low-intensity surveillance groups.

# Appendix 3

The frequency of surveillance varied among TNM stages, with early-stage patients typically having longer intervals between surveillance days

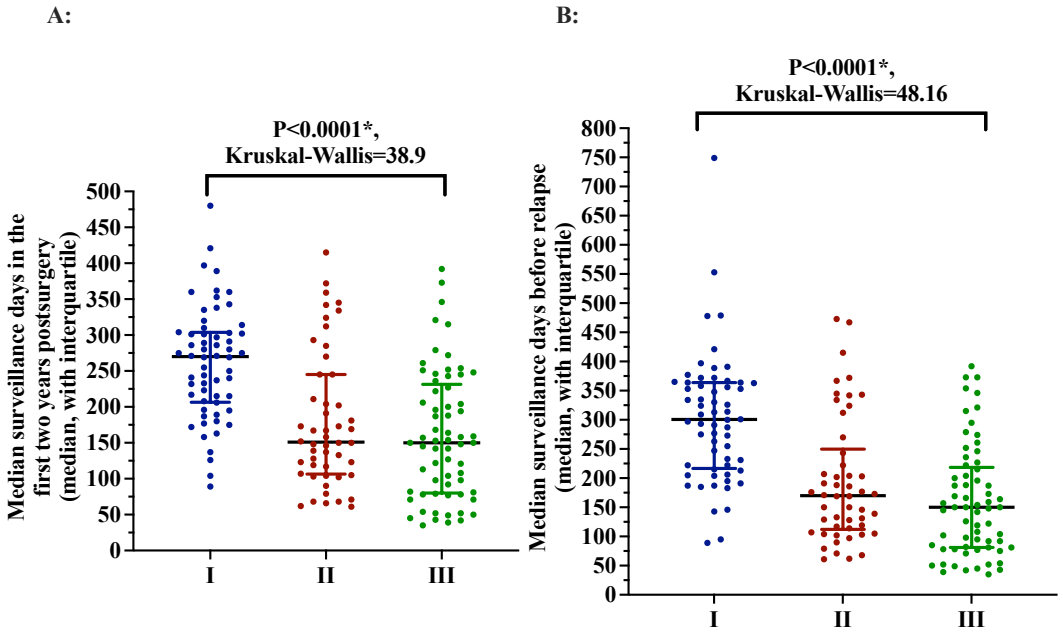


Fig. 1 Median surveillance days in the first two years after surgery and the median surveillance days until relapse across stages. A: Median surveillance days in the first two years after surgery across stages; B: Median surveillance days until relapse across stages.

Due to the limited number of stage I patients in the high-intensity group, I categorised patients with stage I and II primary tumours as having early-stage tumours, but also separately explored OS in stage II. No significant difference was observed in OS across the three intensity groups in stage II.

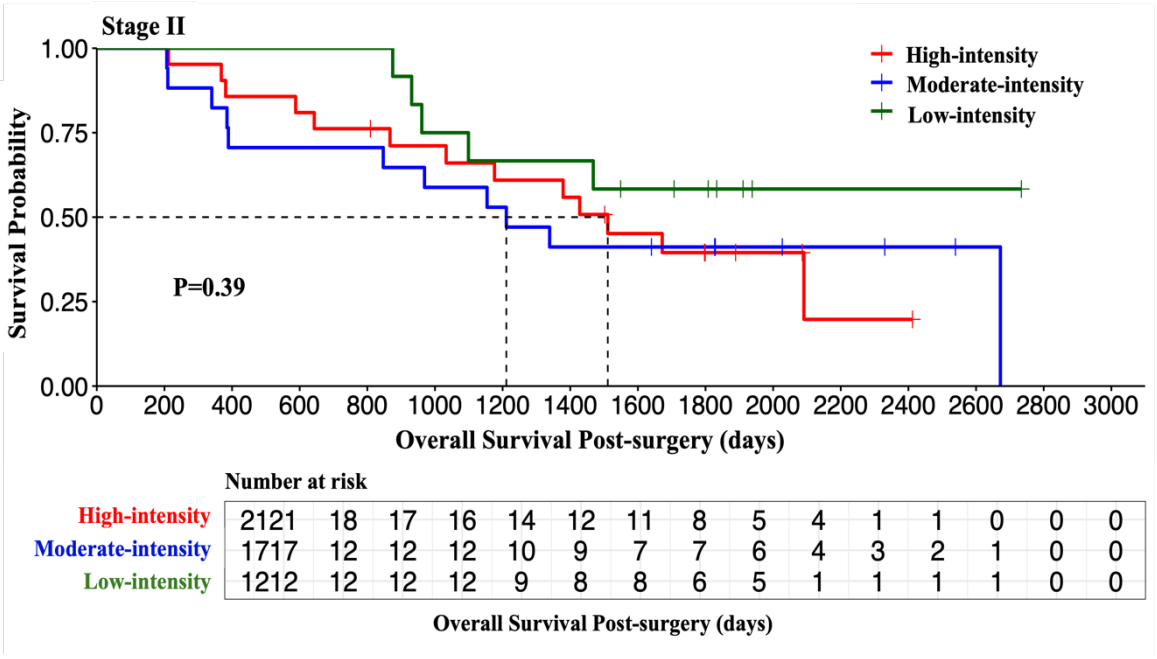


Fig. 2 Overall survival post-surgery by surveillance groups in Stage II tumours.

Different methods of therapy can have distinct progression-free survival (PFS) rates (as shown in Table 1). The median progression-free survival (PFS) for the various treatments was as follows: palliative therapies (73 days), systemic therapies (127 days), a combination of systemic and local therapies (208 days), local treatments (319 days), and targeted therapies (407 days).

Table 1 Post-recurrence survival in different types of the first treatment methods across dominant relapses.

| **Dominant relapse** | **Tumour burden** | **First line treatment** | | **Post-relapse survival (2 year%)** |
|---|---|---|---|---|
| 1. Lung | *All* | | n=49 | 59.2 |
| | *Oligo* | Radical Local | n=20 | 80 |
| | | Other | n=17 | 41.2 |
| | *Poly* | Radical Local | n=0 | |
| | | Other | n=12 | 41.7 |
| 2. Intrathoracic Lymph node | *All* | | n=28 | 46.4 |
| | *Oligo* | Radical Local | n=11 | 72.7 |
| | | Other | n=14 | 35.7 |
| | *Poly* | Radical Local | n=0 | |
| | | Other | n=3 | 0 |
| 3. Brain | *All* | | n=8 | 25 |
| | *Single* | Radical Local | n=3 | 66.7 |
| | | Other | n=1 | 0 |
| | *≥2lesions* | Radical Local | n=1 | 0 |
| | | Other | n=3 | 0 |
| 4. Other extrathoracic | *All* | | n=22 | 33.3 |
| | *Oligo* | Radical Local | n=5 | 40 |
| | | Other | n=9 | 44.4 |
| | *Poly* | Radical Local | n=1 | 100 |

# Bibliography


1. Siegel RL, Giaquinto AN, Jemal A. Cancer statistics, 2024. *CA Cancer J Clin*. 2024;74(1):12-49. doi:10.3322/caac.21820
2. Herbst RS, Heymach JV, Lippman SM. Lung cancer. *N Engl J Med*. 2008;359(13):1367-1380. doi:10.1056/NEJMra0802714
3. Bodalal Z, Trebeschi S, Nguyen-Kim TDL, Schats W, Beets-Tan R. Radiogenomics: bridging imaging and genomics. *Abdom Radiol (NY)*. 2019;44(6):1960-1984. doi:10.1007/s00261-019-02028-w
4. Jamal-Hanjani M, Wilson GA, McGranahan N, et al. Tracking the Evolution of Non-Small-Cell Lung Cancer. *N Engl J Med*. 2017;376(22):2109-2121. doi:10.1056/NEJMoa1616288
5. Nelson DA, Tan TT, Rabson AB, Anderson D, Degenhardt K, White E. Hypoxia and defective apoptosis drive genomic instability and tumorigenesis. *Genes Dev*. 2004;18(17):2095-2107. doi:10.1101/gad.1204904
6. Kang BJ, Ra SW, Lee K, et al. Circulating Tumor Cell Number Is Associated with Primary Tumor Volume in Patients with Lung Adenocarcinoma. *Tuberc Respir Dis (Seoul)*. 2020;83(1):61-70. doi:10.4046/trd.2019.0048
7. Ettinger DS, Wood DE, Aisner DL, et al. NCCN Guidelines® Insights: Non-Small Cell Lung Cancer, Version 2.2023. *J Natl Compr Canc Netw*. 2023;21(4):340-350. doi:10.6004/jnccn.2023.0020
8. Ashworth AB, Senan S, Palma DA, et al. An individual patient data metaanalysis of outcomes and prognostic factors after treatment of oligometastatic non-small-cell lung cancer. *Clin Lung Cancer*. 2014;15(5):346-355. doi:10.1016/j.cllc.2014.04.003
9. Hellman S, Weichselbaum RR. Oligometastases. *J Clin Oncol*. 1995;13(1):8-10. doi:10.1200/JCO.1995.13.1.8
10. Dingemans AC, Hendriks LEL, Berghmans T, et al. Definition of Synchronous Oligometastatic Non-Small Cell Lung Cancer-A Consensus Report. *J Thorac Oncol*. 2019;14(12):2109-2119. doi:10.1016/j.jtho.2019.07.025
11. Swanton C, Govindan R. Clinical Implications of Genomic Discoveries in Lung Cancer. *N Engl J Med*. 2016;374(19):1864-1873. doi:10.1056/NEJMra1504688
12. Doebele RC, Lu X, Sumey C, et al. Oncogene status predicts patterns of metastatic spread in treatment-naive nonsmall cell lung cancer. *Cancer*. 2012;118(18):4502-4511. doi:10.1002/cncr.27409
13. Kim S, Kim TM, Kim DW, et al. Heterogeneity of genetic changes associated with acquired crizotinib resistance in ALK-rearranged lung cancer. *J Thorac Oncol*. 2013;8(4):415-422. doi:10.1097/JTO.0b013e318283dcc0
14. Guo H, Xing Y, Liu R, et al. -216G/T (rs712829), a functional variant of the *EGFR* promoter, is associated with the pleural metastasis of lung adenocarcinoma. *Oncol Lett*. 2013;6(3):693-698. doi:10.3892/ol.2013.1442
15. Fan Y, Zhu X, Xu Y, et al. Cell-Cycle and DNA-Damage Response Pathway Is Involved in Leptomeningeal Metastasis of Non-Small Cell Lung Cancer. *Clin Cancer Res*. 2018;24(1):209-216. doi:10.1158/1078-0432.CCR-17-1582
16. Vignot S, Frampton GM, Soria JC, et al. Next-generation sequencing reveals high concordance of recurrent somatic alterations between primary tumor and metastases from patients with non-small-cell lung cancer. *J Clin Oncol*. 2013;31(17):2167-2172. doi:10.1200/JCO.2012.47.7737

17. Li YS, Jiang BY, Yang JJ, et al. Unique genetic profiles from cerebrospinal fluid cell-free DNA in leptomeningeal metastases of EGFR-mutant non-small-cell lung cancer: a new medium of liquid biopsy. *Ann Oncol*. 2018;29(4):945-952. doi:10.1093/annonc/mdy009
18. Lee HW, Seol HJ, Choi YL, et al. Genomic copy number alterations associated with the early brain metastasis of non-small cell lung cancer. *Int J Oncol*. 2012;41(6):2013-2020. doi:10.3892/ijo.2012.1663
19. Shih DJH, Nayyar N, Bihun I, et al. Genomic characterization of human brain metastases identifies drivers of metastatic lung adenocarcinoma. *Nat Genet*. 2020;52(4):371-377. doi:10.1038/s41588-020-0592-7
20. Boelens MC, Kok K, van der Vlies P, et al. Genomic aberrations in squamous cell lung carcinoma related to lymph node or distant metastasis. *Lung Cancer*. 2009;66(3):372-378. doi:10.1016/j.lungcan.2009.02.017
21. Marusyk A, Polyak K. Tumor heterogeneity: causes and consequences. *Biochim Biophys Acta*. 2010;1805(1):105-117. doi:10.1016/j.bbcan.2009.11.002
22. Li T, Kung HJ, Mack PC, Gandara DR. Genotyping and genomic profiling of non-small-cell lung cancer: implications for current and future therapies. *J Clin Oncol*. 2013;31(8):1039-1049. doi:10.1200/JCO.2012.45.3753
23. Pleasance E, Titmuss E, Williamson L, et al. Pan-cancer analysis of advanced patient tumors reveals interactions between therapy and genomic landscapes. *Nat Cancer*. 2020;1(4):452-468. doi:10.1038/s43018-020-0050-6
24. Hellmann MD, Nathanson T, Rizvi H, et al. Genomic Features of Response to Combination Immunotherapy in Patients with Advanced Non-Small-Cell Lung Cancer. *Cancer Cell*. 2018;33(5):843-852.e4. doi:10.1016/j.ccell.2018.03.018
25. Blakely CM, Watkins TBK, Wu W, et al. Evolution and clinical impact of co-occurring genetic alterations in advanced-stage EGFR-mutant lung cancers. *Nat Genet*. 2017;49(12):1693-1704. doi:10.1038/ng.3990
26. Hu Z, Li Z, Ma Z, Curtis C. Multi-cancer analysis of clonality and the timing of systemic spread in paired primary tumors and metastases. *Nat Genet*. 2020;52(7):701-708. doi:10.1038/s41588-020-0628-z
27. Burrell RA, Swanton C. Tumour heterogeneity and the evolution of polyclonal drug resistance. *Mol Oncol*. 2014;8(6):1095-1111. doi:10.1016/j.molonc.2014.06.005
28. Yang J, Zhang Y, Sun X, et al. The prognostic value of multiorgan metastases in patients with non-small cell lung cancer and its variants: a SEER-based study. *J Cancer Res Clin Oncol*. 2018;144(9):1835-1842. doi:10.1007/s00432-018-2702-9
29. Miettinen M, Lasota J. Gastrointestinal stromal tumors: pathology and prognosis at different sites. *Semin Diagn Pathol*. 2006;23(2):70-83. doi:10.1053/j.semdp.2006.09.001
30. Harun N, Nikfarjam M, Muralidharan V, Christophi C. Liver regeneration stimulates tumor metastases. *J Surg Res*. 2007;138(2):284-290. doi:10.1016/j.jss.2006.06.024
31. Wu J, Sun X, Wang J, et al. Identifying relations between imaging phenotypes and molecular subtypes of breast cancer: Model discovery and external validation. *J Magn Reson Imaging*. 2017;46(4):1017-1027. doi:10.1002/jmri.25661

32. Mendoza DP, Piotrowska Z, Lennerz JK, Digumarthy SR. Role of imaging biomarkers in mutation-driven non-small cell lung cancer. *World J Clin Oncol*. 2020;11(7):412-427. doi:10.5306/wjco.v11.i7.412
33. Garrana SH, Dagogo-Jack I, Cobb R, et al. Clinical and Imaging Features of Non-Small-Cell Lung Cancer in Young Patients. *Clin Lung Cancer*. 2021;22(1):23-31. doi:10.1016/j.cllc.2020.10.012
34. Digumarthy SR, Mendoza DP, Lin JJ, et al. Computed Tomography Imaging Features and Distribution of Metastases in ROS1-rearranged Non-Small-cell Lung Cancer. *Clin Lung Cancer*. 2020;21(2):153-159.e3. doi:10.1016/j.cllc.2019.10.006
35. van Griethuysen JJM, Fedorov A, Parmar C, et al. Computational Radiomics System to Decode the Radiographic Phenotype. *Cancer Res*. 2017;77(21):e104-e107. doi:10.1158/0008-5472.CAN-17-0339
36. Thawani R, McLane M, Beig N, et al. Radiomics and radiogenomics in lung cancer: A review for the clinician. *Lung Cancer*. 2018;115:34-41. doi:10.1016/j.lungcan.2017.10.015
37. Lee Y, Lee HJ, Kim YT, et al. Imaging characteristics of stage I non-small cell lung cancer on CT and FDG-PET: relationship with epidermal growth factor receptor protein expression status and survival. *Korean J Radiol*. 2013;14(2):375-383. doi:10.3348/kjr.2013.14.2.375
38. Hsu JS, Huang MS, Chen CY, et al. Correlation between EGFR mutation status and computed tomography features in patients with advanced pulmonary adenocarcinoma. *J Thorac Imaging*. 2014;29(6):357-363. doi:10.1097/RTI.0000000000000116
39. Rizzo S, Petrella F, Buscarino V, et al. CT Radiogenomic Characterization of EGFR, K-RAS, and ALK Mutations in Non-Small Cell Lung Cancer. *Eur Radiol*. 2016;26(1):32-42. doi:10.1007/s00330-015-3814-0
40. Zhou JY, Zheng J, Yu ZF, et al. Comparative analysis of clinicoradiologic characteristics of lung adenocarcinomas with ALK rearrangements or EGFR mutations. *Eur Radiol*. 2015;25(5):1257-1266. doi:10.1007/s00330-014-3516-z
41. Liu Y, Kim J, Balagurunathan Y, et al. Radiomic Features Are Associated With EGFR Mutation Status in Lung Adenocarcinomas. *Clin Lung Cancer*. 2016;17(5):441-448.e6. doi:10.1016/j.cllc.2016.02.001
42. Lee HJ, Kim YT, Kang CH, et al. Epidermal growth factor receptor mutation in lung adenocarcinomas: relationship with CT characteristics and histologic subtypes. *Radiology*. 2013;268(1):254-264. doi:10.1148/radiol.13112553
43. Digumarthy SR, Mendoza DP, Padole A, et al. Diffuse Lung Metastases in *EGFR*-Mutant Non-Small Cell Lung Cancer. *Cancers (Basel)*. 2019;11(9):1360. doi:10.3390/cancers11091360
44. Halpenny DF, Riely GJ, Hayes S, et al. Are there imaging characteristics associated with lung adenocarcinomas harboring ALK rearrangements?. *Lung Cancer*. 2014;86(2):190-194. doi:10.1016/j.lungcan.2014.09.007
45. Mendoza DP, Stowell J, Muzikansky A, Shepard JO, Shaw AT, Digumarthy SR. Computed Tomography Imaging Characteristics of Non-Small-Cell Lung Cancer With Anaplastic Lymphoma Kinase Rearrangements: A Systematic Review and Meta-Analysis. *Clin Lung Cancer*. 2019;20(5):339-349. doi:10.1016/j.cllc.2019.05.006

46. Mendoza DP, Lin JJ, Rooney MM, et al. Imaging Features and Metastatic Patterns of Advanced *ALK*-Rearranged Non-Small Cell Lung Cancer. *AJR Am J Roentgenol*. 2020;214(4):766-774. doi:10.2214/AJR.19.21982
47. Plodkowski AJ, Drilon A, Halpenny DF, et al. From genotype to phenotype: Are there imaging characteristics associated with lung adenocarcinomas harboring RET and ROS1 rearrangements?. *Lung Cancer*. 2015;90(2):321-325. doi:10.1016/j.lungcan.2015.09.018
48. Brose MS, Volpe P, Feldman M, et al. BRAF and RAS mutations in human lung cancer and melanoma. *Cancer Res*. 2002;62(23):6997-7000.
49. Gevaert O, Xu J, Hoang CD, et al. Non-small cell lung cancer: identifying prognostic imaging biomarkers by leveraging public gene expression microarray data--methods and preliminary results. *Radiology*. 2012;264(2):387-396. doi:10.1148/radiol.12111607
50. Horn L, Spigel DR, Vokes EE, et al. Nivolumab Versus Docetaxel in Previously Treated Patients With Advanced Non-Small-Cell Lung Cancer: Two-Year Outcomes From Two Randomized, Open-Label, Phase III Trials (CheckMate 017 and CheckMate 057). *J Clin Oncol*. 2017;35(35):3924-3933. doi:10.1200/JCO.2017.74.3062
51. Herbst RS, Baas P, Kim DW, et al. Pembrolizumab versus docetaxel for previously treated, PD-L1-positive, advanced non-small-cell lung cancer (KEYNOTE-010): a randomised controlled trial. *Lancet*. 2016;387(10027):1540-1550. doi:10.1016/S0140-6736(15)01281-7
52. Barlesi F, Garon EB, Kim DW, et al. Health-Related Quality of Life in KEYNOTE-010: a Phase II/III Study of Pembrolizumab Versus Docetaxel in Patients With Previously Treated Advanced, Programmed Death Ligand 1-Expressing NSCLC. *J Thorac Oncol*. 2019;14(5):793-801. doi:10.1016/j.jtho.2019.01.016
53. Antonia SJ, Villegas A, Daniel D, et al. Durvalumab after Chemoradiotherapy in Stage III Non-Small-Cell Lung Cancer. *N Engl J Med*. 2017;377(20):1919-1929. doi:10.1056/NEJMoa1709937
54. Jiang M, Sun D, Guo Y, et al. Assessing PD-L1 Expression Level by Radiomic Features From PET/CT in Nonsmall Cell Lung Cancer Patients: An Initial Result. *Acad Radiol*. 2020;27(2):171-179. doi:10.1016/j.acra.2019.04.016
55. Castaldo R, Pane K, Nicolai E, Salvatore M, Franzese M. The Impact of Normalization Approaches to Automatically Detect Radiogenomic Phenotypes Characterizing Breast Cancer Receptors Status. *Cancers (Basel)*. 2020;12(2):518. doi:10.3390/cancers12020518
56. Koukourakis MI, Manolas C, Minopoulos G, Giatromanolaki A, Sivridis E. Angiogenesis relates to estrogen receptor negativity, c-erbB-2 overexpression and early relapse in node-negative ductal carcinoma of the breast. *Int J Surg Pathol*. 2003;11(1):29-34. doi:10.1177/106689690301100107
57. Fuckar D, Dekanić A, Stifter S, et al. VEGF expression is associated with negative estrogen receptor status in patients with breast cancer. *Int J Surg Pathol*. 2006;14(1):49-55. doi:10.1177/106689690601400109
58. Li H, Zhu Y, Burnside ES, et al. Quantitative MRI radiomics in the prediction of molecular classifications of breast cancer subtypes in the TCGA/TCIA data set. *NPJ Breast Cancer*. 2016;2:16012. doi:10.1038/npjbcancer.2016.12
59. Thompson PM, Martin NG, Wright MJ. Imaging genomics. *Curr Opin Neurol*. 2010;23(4):368-373. doi:10.1097/WCO.0b013e32833b764c

60. Patel V, Chiang MC, Thompson PM, et al. Scalar connectivity measures from fast-marching tractography reveal heritability of white matter architecture. In: Proceedings of the 2010 IEEE International Conference on Biomedical Imaging: From Nano to Macro. 2010;1109-1112. doi.org/10.1109/ISBI.2010.5490187
61. Gutman DA, Dunn WD Jr, Grossmann P, et al. Somatic mutations associated with MRI-derived volumetric features in glioblastoma. *Neuroradiology*. 2015;57(12):1227-1237. doi:10.1007/s00234-015-1576-7
62. NSCLC Meta-analysis Collaborative Group. Preoperative chemotherapy for non-small-cell lung cancer: a systematic review and meta-analysis of individual participant data. *Lancet*. 2014;383(9928):1561-1571. doi:10.1016/S0140-6736(13)62159-5
63. Lopez Guerra JL, Gomez DR, Lin SH, et al. Risk factors for local and regional recurrence in patients with resected N0-N1 non-small-cell lung cancer, with implications for patient selection for adjuvant radiation therapy. *Ann Oncol*. 2013;24(1):67-74. doi:10.1093/annonc/mds274
64. Schuchert MJ, Normolle DP, Awais O, et al. Factors influencing recurrence following anatomic lung resection for clinical stage I non-small cell lung cancer. *Lung Cancer*. 2019;128:145-151. doi:10.1016/j.lungcan.2018.12.026
65. Bubb RS, Komaki R, Hachiya T, et al. Association of Ki-67, p53, and bcl-2 expression of the primary non-small-cell lung cancer lesion with brain metastatic lesion. *Int J Radiat Oncol Biol Phys*. 2002;53(5):1216-1224. doi:10.1016/s0360-3016(02)02861-4
66. Lou F, Sima CS, Rusch VW, Jones DR, Huang J. Differences in patterns of recurrence in early-stage versus locally advanced non-small cell lung cancer. *Ann Thorac Surg*. 2014;98(5):1755-1761. doi:10.1016/j.athoracsur.2014.05.070
67. Bae MK, Yu WS, Byun GE, et al. Prognostic factors for cases with no extracranial metastasis in whom brain metastasis is detected after resection of non-small cell lung cancer. *Lung Cancer*. 2015;88(2):195-200. doi:10.1016/j.lungcan.2015.02.013
68. O'Connor JPB. Cancer heterogeneity and imaging. *Semin Cell Dev Biol*. 2017;64:48-57. doi:10.1016/j.semcdb.2016.10.001
69. Yu W, Tang C, Hobbs BP, et al. Development and Validation of a Predictive Radiomics Model for Clinical Outcomes in Stage I Non-small Cell Lung Cancer. *Int J Radiat Oncol Biol Phys*. 2018;102(4):1090-1097. doi:10.1016/j.ijrobp.2017.10.046
70. van Timmeren JE, Leijenaar RTH, van Elmpt W, et al. Survival prediction of non-small cell lung cancer patients using radiomics analyses of cone-beam CT images. *Radiother Oncol*. 2017;123(3):363-369. doi:10.1016/j.radonc.2017.04.016
71. Coroller TP, Grossmann P, Hou Y, et al. CT-based radiomic signature predicts distant metastasis in lung adenocarcinoma. *Radiother Oncol*. 2015;114(3):345-350. doi:10.1016/j.radonc.2015.02.015
72. Nishino M, Dahlberg SE, Fulton LE, et al. Volumetric Tumor Response and Progression in EGFR-mutant NSCLC Patients Treated with Erlotinib or Gefitinib. *Acad Radiol*. 2016;23(3):329-336. doi:10.1016/j.acra.2015.11.005
73. Goldstraw P, Chansky K, Crowley J, et al. The IASLC Lung Cancer Staging Project: Proposals for Revision of the TNM Stage Groupings in the Forthcoming (Eighth) Edition of the TNM Classification for Lung Cancer. *J Thorac Oncol*. 2016;11(1):39-51. doi:10.1016/j.jtho.2015.09.009

74. Li H, Galperin-Aizenberg M, Pryma D, Simone CB 2nd, Fan Y. Unsupervised machine learning of radiomic features for predicting treatment response and overall survival of early stage non-small cell lung cancer patients treated with stereotactic body radiation therapy. *Radiother Oncol*. 2018;129(2):218-226. doi:10.1016/j.radonc.2018.06.025
75. Wu CF, Fu JY, Yeh CJ, et al. Recurrence Risk Factors Analysis for Stage I Non-small Cell Lung Cancer. *Medicine (Baltimore)*. 2015;94(32):e1337. doi:10.1097/MD.0000000000001337
76. Cruz C, Afonso M, Oliveiros B, Pêgo A. Recurrence and Risk Factors for Relapse in Patients with Non-Small Cell Lung Cancer Treated by Surgery with Curative Intent. *Oncology*. 2017;92(6):347-352. doi:10.1159/000458533
77. Eisenhauer EA, Therasse P, Bogaerts J, et al. New response evaluation criteria in solid tumours: revised RECIST guideline (version 1.1). *Eur J Cancer*. 2009;45(2):228-247. doi:10.1016/j.ejca.2008.10.026
78. Coroller TP, Agrawal V, Narayan V, et al. Radiomic phenotype features predict pathological response in non-small cell lung cancer. *Radiother Oncol*. 2016;119(3):480-486. doi:10.1016/j.radonc.2016.04.004
79. Jin C, Yu H, Ke J, et al. Predicting treatment response from longitudinal images using multi-task deep learning. *Nat Commun*. 2021;12(1):1851. doi:10.1038/s41467-021-22188-y
80. National Lung Screening Trial Research Team, Aberle DR, Adams AM, et al. Reduced lung-cancer mortality with low-dose computed tomographic screening. *N Engl J Med*. 2011;365(5):395-409. doi:10.1056/NEJMoa1102873
81. Ma J, Wang Q, Ren Y, Hu H, Zhao J. Automatic lung nodule classification with radiomics approach. In: Zhang J, Cook TS, eds. Medical Imaging 2016: PACS and Imaging Informatics: Next Generation and Innovations. Vol 9789. 2016:978906. doi:10.1117/12.2220768
82. Ardila D, Kiraly AP, Bharadwaj S, et al. End-to-end lung cancer screening with three-dimensional deep learning on low-dose chest computed tomography. *Nat Med*. 2019;25(6):954-961. doi:10.1038/s41591-019-0447-x
83. Bergamaschi A, Tagliabue E, Sørlie T, et al. Extracellular matrix signature identifies breast cancer subgroups with different clinical outcome. *J Pathol*. 2008;214(3):357-367. doi:10.1002/path.2278
84. Seo DC, Sung JM, Cho HJ, et al. Gene expression profiling of cancer stem cell in human lung adenocarcinoma A549 cells. *Mol Cancer*. 2007;6:75. doi:10.1186/1476-4598-6-75
85. Zhou M, Leung A, Echegaray S, et al. Non-Small Cell Lung Cancer Radiogenomics Map Identifies Relationships between Molecular and Imaging Phenotypes with Prognostic Implications. *Radiology*. 2018;286(1):307-315. doi:10.1148/radiol.2017161845
86. Miller AB, Hoogstraten B, Staquet M, Winkler A. Reporting results of cancer treatment. *Cancer*. 1981;47(1):207-214. doi:10.1002/1097-0142(19810101)47:1<207::aid-cncr2820470134>3.0.co;2-6
87. Baar J, Tannock I. Analyzing the same data in two ways: a demonstration model to illustrate the reporting and misreporting of clinical trials. *J Clin Oncol*. 1989;7(7):969-978. doi:10.1200/JCO.1989.7.7.969
88. Paesmans M, Sculier JP, Libert P, et al. Response to chemotherapy has predictive value for further survival of patients with advanced non-small cell lung cancer: 10 years experience of the European Lung Cancer Working

Party. *Eur J Cancer*. 1997;33(14):2326-2332. doi:10.1016/s0959-8049(97)00325-0
89. Jang GS, Kim MJ, Ha HI, et al. Comparison of RECIST version 1.0 and 1.1 in assessment of tumor response by computed tomography in advanced gastric cancer. *Chin J Cancer Res*. 2013;25(6):689-694. doi:10.3978/j.issn.1000-9604.2013.11.09
90. Slim A, Kamoun H, Hadidene Y, Smadhi H, Meddeb A, Megdiche ML. Postoperative recurrence of primary lung cancer: anatomo-clinical and therapeutic study. *Tunis Med*. 2021;99(5):560-568.
91. Cancer Imaging Program. Imaging Response Criteria. National Cancer Institute, Division of Cancer Treatment & Diagnosis. https://imaging.cancer.gov/clinical_trials/imaging_response_criteria.htm
92. Kim YJ, Lee SH, Park CM, Kim KG. Evaluation of Semi-automatic Segmentation Methods for Persistent Ground Glass Nodules on Thin-Section CT Scans. *Healthc Inform Res*. 2016;22(4):305-315. doi:10.4258/hir.2016.22.4.305
93. Mehnert A, Jackway P. An improved seeded region growing algorithm. *Pattern Recognit Lett*. 1997;18(10):1065-1071. doi:10.1016/S0167-8655(97)00131-1
94. Kim YJ, Lee SH, Lim KY, Kim KG. Development and Validation of Segmentation Method for Lung Cancer Volumetry on Chest CT. *J Digit Imaging*. 2018;31(4):505-512. doi:10.1007/s10278-018-0051-5
95. Wang Z, Liu YJ. Active contour model by combining edge and region information discrete dynamic systems. *Adv Mech Eng*. 2017;9(3). doi:10.1177/1687814017692947
96. Shyu KK, Pham VT, Tran TT, Lee PL. Global and local fuzzy energy-based active contours for image segmentation. *Nonlinear Dyn*. 2012;67(2):1559-1578. doi:10.1007/s11071-011-0088-1
97. Mingoti SA, Lima JO. Comparing SOM neural network with Fuzzy c-means, K-means and traditional hierarchical clustering algorithms. *Eur J Oper Res*. 2006;174(3):1742-1759. doi:10.1016/j.ejor.2005.03.039
98. Gong L, Jiang S, Yang Z, Zhang G, Wang L. Automated pulmonary nodule detection in CT images using 3D deep squeeze-and-excitation networks. *Int J Comput Assist Radiol Surg*. 2019;14(11):1969-1979. doi:10.1007/s11548-019-01979-1
99. Cui Y, Arimura H, Nakano R, Yoshitake T, Shioyama Y, Yabuuchi H. Automated approach for segmenting gross tumor volumes for lung cancer stereotactic body radiation therapy using CT-based dense V-networks. *J Radiat Res*. 2021;62(2):346-355. doi:10.1093/jrr/rraa132
100. Zhang F, Wang Q, Li H. Automatic Segmentation of the Gross Target Volume in Non-Small Cell Lung Cancer Using a Modified Version of ResNet. *Technol Cancer Res Treat*. 2020;19. doi:10.1177/1533033820947484
101. Yu H, Li J, Zhang L, Cao Y, Yu X, Sun J. Design of lung nodules segmentation and recognition algorithm based on deep learning. *BMC Bioinformatics*. 2021;22(Suppl 5):314. doi:10.1186/s12859-021-04234-0
102. Jiang J, Hu YC, Liu CJ, et al. Multiple Resolution Residually Connected Feature Streams for Automatic Lung Tumor Segmentation From CT Images. *IEEE Trans Med Imaging*. 2019;38(1):134-144. doi:10.1109/TMI.2018.2857800
103. Liu X, Li KW, Yang R, Geng LS. Review of Deep Learning Based Automatic Segmentation for Lung Cancer Radiotherapy. *Front Oncol*. 2021;11:717039. Published 2021 Jul 8. doi:10.3389/fonc.2021.717039

104. Rios Velazquez E, Aerts HJ, Gu Y, et al. A semiautomatic CT-based ensemble segmentation of lung tumors: comparison with oncologists' delineations and with the surgical specimen. *Radiother Oncol*. 2012;105(2):167-173. doi:10.1016/j.radonc.2012.09.023
105. Murphy H, Jaafari H, Dobrovolny HM. Differences in predictions of ODE models of tumor growth: a cautionary example. *BMC Cancer*. 2016;16:163. Published 2016 Feb 26. doi:10.1186/s12885-016-2164-x
106. Laird AK. Dynamics of Tumour Growth: Comparison of Growth Rates and Extrapolation of Growth Curve to One Cell. *Br J Cancer*. 1965;19(2):278-291. doi:10.1038/bjc.1965.32
107. Frankell AM, Dietzen M, Al Bakir M, et al. The evolution of lung cancer and impact of subclonal selection in TRACERx. *Nature*. 2023;616(7957):525-533. doi:10.1038/s41586-023-05783-5
108. Fu X, Zhao Y, Lopez JI, et al. Spatial patterns of tumour growth impact clonal diversification in a computational model and the TRACERx Renal study. *Nat Ecol Evol*. 2022;6(1):88-102. doi:10.1038/s41559-021-01586-x
109. Jamal-Hanjani M, Wilson GA, McGranahan N, et al. Tracking the Evolution of Non-Small-Cell Lung Cancer. *N Engl J Med*. 2017;376(22):2109-2121. doi:10.1056/NEJMoa1616288
110. Lugano R, Ramachandran M, Dimberg A. Tumor angiogenesis: causes, consequences, challenges and opportunities. *Cell Mol Life Sci*. 2020;77(9):1745-1770. doi:10.1007/s00018-019-03351-7
111. McGranahan N, Furness AJ, Rosenthal R, et al. Clonal neoantigens elicit T cell immunoreactivity and sensitivity to immune checkpoint blockade. *Science*. 2016;351(6280):1463-1469. doi:10.1126/science.aaf1490
112. Kraemer AI, Chong C, Huber F, et al. The immunopeptidome landscape associated with T cell infiltration, inflammation and immune editing in lung cancer. *Nat Cancer*. 2023;4(5):608-628. doi:10.1038/s43018-023-00548-5
113. Matin HN, Setayeshi S. A computational tumor growth model experience based on molecular dynamics point of view using deep cellular automata. *Artif Intell Med*. 2024;148:102752. doi:10.1016/j.artmed.2023.102752
114. Desharnais L, Sorin M, Rezanejad M, et al. Spatially mapping the tumour immune microenvironments of non-small cell lung cancer. *Nat Commun*. 2025;16(1):1345. Published 2025 Feb 4. doi:10.1038/s41467-025-56546-x
115. Al Bakir M, Huebner A, Martínez-Ruiz C, et al. The evolution of non-small cell lung cancer metastases in TRACERx. *Nature*. 2023;616(7957):534-542. doi:10.1038/s41586-023-05729-x
116. Abbosh C, Frankell AM, Harrison T, et al. Tracking early lung cancer metastatic dissemination in TRACERx using ctDNA. *Nature*. 2023;616(7957):553-562. doi:10.1038/s41586-023-05776-4
117. Isaka T, Adachi H, Murakami K, et al. Preoperative predictors for recurrence sites associated with poor post-recurrence survival after surgery of non-small cell lung cancer: a multicenter study. *BMC Cancer*. 2023;23(1):1064. Published 2023 Nov 6. doi:10.1186/s12885-023-11582-y
118. Nakamura R, Kurishima K, Kobayashi N, et al. Postoperative follow-up for patients with non-small cell lung cancer. *Onkologie*. 2010;33(1-2):14-18. doi:10.1159/000264623
119. Tjan-Heijnen VCG. Diagnosis and treatment of lung cancer: an evidence-based guide for the practicing clinician. *Lung Cancer*. 2001;35(2):219-220

120. Detterbeck FC, Mazzone PJ, Naidich DP, Bach PB. Screening for lung cancer: Diagnosis and management of lung cancer, 3rd ed: American College of Chest Physicians evidence-based clinical practice guidelines. *Chest*. 2013;143(5 Suppl):e78S-e92S. doi:10.1378/chest.12-2350
121. Korst RJ, Kansler AL, Port JL, Lee PC, Altorki NK. Accuracy of surveillance computed tomography in detecting recurrent or new primary lung cancer in patients with completely resected lung cancer. *Ann Thorac Surg*. 2006;82(3):1009-1015. doi:10.1016/j.athoracsur.2006.03.062
122. Benamore R, Shepherd FA, Leighl N, et al. Does intensive follow-up alter outcome in patients with advanced lung cancer?. *J Thorac Oncol*. 2007;2(4):273-281. doi:10.1097/01.JTO.0000263708.08332.76
123. Crabtree TD, Puri V, Chen SB, et al. Does the method of radiologic surveillance affect survival after resection of stage I non-small cell lung cancer?. *J Thorac Cardiovasc Surg*. 2015;149(1):45-53.e533. doi:10.1016/j.jtcvs.2014.07.095
124. Subramanian M, Liu J, Greenberg C, et al. Imaging Surveillance for Surgically Resected Stage I Non-Small Cell Lung Cancer: Is More Always Better?. *J Thorac Cardiovasc Surg*. 2019;157(3):1205-1217.e2. doi:10.1016/j.jtcvs.2018.09.119
125. McMurry TL, Stukenborg GJ, Kessler LG, et al. More Frequent Surveillance Following Lung Cancer Resection Is Not Associated With Improved Survival: A Nationally Representative Cohort Study. *Ann Surg*. 2018;268(4):632-639. doi:10.1097/SLA.0000000000002955
126. Nishino M, Jackman DM, DiPiro PJ, Hatabu H, Jänne PA, Johnson BE. Revisiting the relationship between tumour volume and diameter in advanced NSCLC patients: An exercise to maximize the utility of each measure to assess response to therapy. *Clin Radiol*. 2014;69(8):841-848. doi:10.1016/j.crad.2014.03.020
127. Mingoti SA LJ. Comparing SOM neural network with fuzzy C-means, k-means and traditional hierarchical clustering algorithms. *Eur J Oper Res*. 2006;174(3):1742–1759.
128. Kao YS, Yang J. Deep learning-based auto-segmentation of lung tumor PET/CT scans: a systematic review. *Clin Transl Imaging*. 2022;10(2):217-223. doi:10.1007/s40336-022-00482-z
129. Abbosh C, Birkbak NJ, Wilson GA, et al. Phylogenetic ctDNA analysis depicts early-stage lung cancer evolution. *Nature*. 2017;545(7655):446-451. doi:10.1038/nature22364
130. Walsh GL, O'Connor M, Willis KM, et al. Is follow-up of lung cancer patients after resection medically indicated and cost-effective?. *Ann Thorac Surg*. 1995;60(6):1563-1572. doi:10.1016/0003-4975(95)00893-4
131. Colt HG, Murgu SD, Korst RJ, Slatore CG, Unger M, Quadrelli S. Follow-up and surveillance of the patient with lung cancer after curative-intent therapy: Diagnosis and management of lung cancer, 3rd ed: American College of Chest Physicians evidence-based clinical practice guidelines. *Chest*. 2013;143(5 Suppl):e437S-e454S. doi:10.1378/chest.12-2365
132. Planchard D, Popat S, Kerr K, et al. Metastatic non-small cell lung cancer: ESMO Clinical Practice Guidelines for diagnosis, treatment and follow-up. *Ann Oncol*. 2018;29(Suppl 4):iv192-iv237. doi:10.1093/annonc/mdy275
133. Ettinger DS, Wood DE, Aisner DL, et al. Non-Small Cell Lung Cancer, Version 3.2022, NCCN Clinical Practice Guidelines in Oncology. *J Natl Compr Canc Netw*. 2022;20(5):497-530. doi:10.6004/jnccn.2022.0025

134. Schellinger PD, Meinck HM, Thron A. Diagnostic accuracy of MRI compared to CCT in patients with brain metastases. *J Neurooncol*. 1999;44(3):275-281. doi:10.1023/a:1006308808769
135. Gaspar LE, Scott C, Murray K, Curran W. Validation of the RTOG recursive partitioning analysis (RPA) classification for brain metastases. *Int J Radiat Oncol Biol Phys*. 2000;47(4):1001-1006. doi:10.1016/s0360-3016(00)00547-2
136. Stadnik TW, Chaskis C, Michotte A, et al. Diffusion-weighted MR imaging of intracerebral masses: comparison with conventional MR imaging and histologic findings. *AJNR Am J Neuroradiol*. 2001;22(5):969-976.
137. Freitas PS, Janicas C, Veiga J, Matos AP, Herédia V, Ramalho M. Imaging evaluation of the liver in oncology patients: A comparison of techniques. *World J Hepatol*. 2021;13(12):1936-1955. doi:10.4254/wjh.v13.i12.1936
138. Yin A, Moes DJAR, van Hasselt JGC, Swen JJ, Guchelaar HJ. A Review of Mathematical Models for Tumor Dynamics and Treatment Resistance Evolution of Solid Tumors. *CPT Pharmacometrics Syst Pharmacol*. 2019;8(10):720-737. doi:10.1002/psp4.12450
139. Fasano A, Bertuzzi A, Gandolfi A. Mathematical modelling of tumour growth and treatment. In: Complex Systems in Biomedicine. Milan, Italy: Springer; 2006:71–108. doi:10.1007/88-470-0396-2_3
140. Lindell RM, Hartman TE, Swensen SJ, Jett JR, Midthun DE, Mandrekar JN. 5-year lung cancer screening experience: growth curves of 18 lung cancers compared to histologic type, CT attenuation, stage, survival, and size. *Chest*. 2009;136(6):1586-1595. doi:10.1378/chest.09-0915
141. Hosmer, D.W., Lemeshow, S. and May, S. (2008) Applied Survival Analysis. Regression Modeling of Time-to-Event Data. 2nd Edition, Wiley, Hoboken. https://doi.org/10.1002/9780470258019
142. Bradburn MJ, Clark TG, Love SB, Altman DG. Survival analysis part II: multivariate data analysis--an introduction to concepts and methods. *Br J Cancer*. 2003;89(3):431-436. doi:10.1038/sj.bjc.6601119
143. Andrade C. Survival Analysis, Kaplan-Meier Curves, and Cox Regression: Basic Concepts. *Indian J Psychol Med*. 2023;45(4):434-435. doi:10.1177/02537176231176986
144. du Prel JB, Röhrig B, Hommel G, Blettner M. Choosing statistical tests: part 12 of a series on evaluation of scientific publications. *Dtsch Arztebl Int*. 2010;107(19):343-348. doi:10.3238/arztebl.2010.0343
145. Asano J, Hirakawa A, Hamada C. A stepwise variable selection for a Cox proportional hazards cure model with application to breast cancer data. *Jpn J Biometrics*. 2013;34(1):21-34. doi:10.5691/jjb.34.21
146. Karacz CM, Yan J, Zhu H, Gerber DE. Timing, Sites, and Correlates of Lung Cancer Recurrence. *Clin Lung Cancer*. 2020;21(2):127-135.e3. doi:10.1016/j.cllc.2019.12.001
147. Mandrekar JN. Receiver operating characteristic curve in diagnostic test assessment. *J Thorac Oncol*. 2010;5(9):1315-1316. doi:10.1097/JTO.0b013e3181ec173d
148. He Z, Zhang Q, Song M, Tan X, Wang W. Four overlooked errors in ROC analysis: how to prevent and avoid. *BMJ Evid Based Med*. 2025;30(3):208-211. doi:10.1136/bmjebm-2024-113078
149. Chen NB, Li QW, Zhu ZF, et al. Developing and validating an integrated gross tumor volume (GTV)-TNM stratification system for supplementing unresectable locally advanced non-small cell lung cancer treated with

concurrent chemoradiotherapy. *Radiat Oncol*. 2020;15(1):260. doi:10.1186/s13014-020-01704-2
150. Nahm FS. What the *P* values really tell us. *Korean J Pain*. 2017;30(4):241-242. doi:10.3344/kjp.2017.30.4.241
151. Noble WS. How does multiple testing correction work?. *Nat Biotechnol*. 2009;27(12):1135-1137. doi:10.1038/nbt1209-1135
152. Mountain CF. Revisions in the International System for Staging Lung Cancer. *Chest*. 1997;111(6):1710-1717. doi:10.1378/chest.111.6.1710
153. Zhu J, Yuan Y, Wan X, et al. Immunotherapy (excluding checkpoint inhibitors) for stage I to III non-small cell lung cancer treated with surgery or radiotherapy with curative intent. *Cochrane Database Syst Rev*. 2021;12(12):CD011300. doi:10.1002/14651858.CD011300.pub3
154. Endo C, Sakurada A, Notsuda H, et al. Results of long-term follow-up of patients with completely resected non-small cell lung cancer. *Ann Thorac Surg*. 2012;93(4):1061-1068. doi:10.1016/j.athoracsur.2012.01.004
155. Moskalenko Y, Smorodska O, Deineka V, Kravets O, Moskalenko R. Prognostic factors for recurrence in patients with surgically resected non-small cell lung cancer. *Contemp Oncol (Pozn)*. 2022;26(3):239-246. doi:10.5114/wo.2022.120638
156. Yun JK, Lee GD, Choi S, et al. Various recurrence dynamics for non-small cell lung cancer depending on pathological stage and histology after surgical resection. *Transl Lung Cancer Res*. 2022;11(7):1327-1336. doi:10.21037/tlcr-21-1028
157. McGranahan N, Rosenthal R, Hiley CT, et al. Allele-Specific HLA Loss and Immune Escape in Lung Cancer Evolution. *Cell*. 2017;171(6):1259-1271.e11. doi:10.1016/j.cell.2017.10.001
158. Negrao MV, Quek K, Zhang J, Sepesi B. TRACERx: Tracking tumor evolution to impact the course of lung cancer. *J Thorac Cardiovasc Surg*. 2018;155(3):1199-1202. doi:10.1016/j.jtcvs.2017.10.134
159. Kumar V, Abbas AK, Aster JC. Robbins Basic Pathology. 9th ed. Philadelphia, PA: Saunders; 2013.
160. Park HS, Harder EM, Mancini BR, Decker RH. Central versus Peripheral Tumor Location: Influence on Survival, Local Control, and Toxicity Following Stereotactic Body Radiotherapy for Primary Non-Small-Cell Lung Cancer. *J Thorac Oncol*. 2015;10(5):832-837. doi:10.1097/JTO.0000000000000484
161. Schanne DH, Nestle U, Allgäuer M, et al. Stereotactic body radiotherapy for centrally located stage I NSCLC: a multicenter analysis. *Strahlenther Onkol*. 2015;191(2):125-132. doi:10.1007/s00066-014-0739-5
162. Lee KY, Hsu CX. Adjuvant chemotherapy or immunotherapy for completely resected stage IB non-small cell lung cancer: still a grey zone?. *Transl Lung Cancer Res*. 2023;12(3):647-648. doi:10.21037/tlcr-22-897
163. Cheng YF, Chen YL, Liu CC, Lin CM, Tong SS, Wang BY. Adjuvant chemotherapy in pathological node-negative non-small cell lung cancer. *Sci Rep*. 2023;13(1):19137. doi:10.1038/s41598-023-46679-8
164. Detterbeck FC. The eighth edition TNM stage classification for lung cancer: What does it mean on main street?. *J Thorac Cardiovasc Surg*. 2018;155(1):356-359. doi:10.1016/j.jtcvs.2017.08.138
165. Chemotherapy in non-small cell lung cancer: a meta-analysis using updated data on individual patients from 52 randomised clinical trials. Non-small Cell Lung Cancer Collaborative Group. *BMJ*. 1995;311(7010):899-909.

166. Uramoto H, Tanaka F. Prediction of recurrence after complete resection in patients with NSCLC. *Anticancer Res*. 2012;32(9):3953-3960.
167. Kongsgaard A, Borgen E, Mælandsmo GM, et al. Clinical significance of disseminated tumour cells in non-small cell lung cancer. *Br J Cancer*. 2013;109(5):1264-1270. doi:10.1038/bjc.2013.450
168. Maeda R, Yoshida J, Hishida T, et al. Late recurrence of non-small cell lung cancer more than 5 years after complete resection: incidence and clinical implications in patient follow-up. *Chest*. 2010;138(1):145-150. doi:10.1378/chest.09-2361
169. Kelsey CR, Marks LB, Hollis D, et al. Local recurrence after surgery for early stage lung cancer: an 11-year experience with 975 patients. *Cancer*. 2009;115(22):5218-5227. doi:10.1002/cncr.24625
170. Subotic D, Van Schil P, Grigoriu B. Optimising treatment for post-operative lung cancer recurrence. *Eur Respir J*. 2016;47(2):374-378. doi:10.1183/13993003.01490-2015
171. Thomas PA Jr, Rubinstein L. Malignant disease appearing late after operation for T1 N0 non-small-cell lung cancer. The Lung Cancer Study Group. *J Thorac Cardiovasc Surg*. 1993;106(6):1053-1058.
172. al-Kattan K, Sepsas E, Fountain SW, Townsend ER. Disease recurrence after resection for stage I lung cancer. *Eur J Cardiothorac Surg*. 1997;12(3):380-384. doi:10.1016/s1010-7940(97)00198-x
173. Taylor MD, Nagji AS, Bhamidipati CM, et al. Tumor recurrence after complete resection for non-small cell lung cancer. *Ann Thorac Surg*. 2012;93(6):1813-1821. doi:10.1016/j.athoracsur.2012.03.031
174. Okada M, Nishio W, Sakamoto T, Harada H, Uchino K, Tsubota N. Long-term survival and prognostic factors of five-year survivors with complete resection of non-small cell lung carcinoma. *J Thorac Cardiovasc Surg*. 2003;126(2):558-562. doi:10.1016/s0022-5223(03)00360-x
175. Schwartz LH, Ginsberg MS, DeCorato D, et al. Evaluation of tumor measurements in oncology: use of film-based and electronic techniques. *J Clin Oncol*. 2000;18(10):2179-2184. doi:10.1200/JCO.2000.18.10.2179
176. Harris KM, Adams H, Lloyd DC, Harvey DJ. The effect on apparent size of simulated pulmonary nodules of using three standard CT window settings. *Clin Radiol*. 1993;47(4):241-244. doi:10.1016/s0009-9260(05)81130-4
177. Wormanns D, Diederich S, Lentschig MG, Winter F, Heindel W. Spiral CT of pulmonary nodules: interobserver variation in assessment of lesion size. *Eur Radiol*. 2000;10(5):710-713. doi:10.1007/s003300050990
178. Yankelevitz DF, Reeves AP, Kostis WJ, Zhao B, Henschke CI. Small pulmonary nodules: volumetrically determined growth rates based on CT evaluation. *Radiology*. 2000;217(1):251-256. doi:10.1148/radiology.217.1.r00oc33251
179. Yankelevitz DF, Gupta R, Zhao B, Henschke CI. Small pulmonary nodules: evaluation with repeat CT--preliminary experience. *Radiology*. 1999;212(2):561-566. doi:10.1148/radiology.212.2.r99au33561
180. Ko JP, Rusinek H, Jacobs EL, et al. Small pulmonary nodules: volume measurement at chest CT–phantom study. *Radiology*. 2003;228(3):864-870. doi:10.1148/radiol.2283020059
181. Velazquez ER, Parmar C, Jermoumi M, et al. Volumetric CT-based segmentation of NSCLC using 3D-Slicer. *Sci Rep*. 2013;3:3529. doi:10.1038/srep03529

182. Pignon JP, Tribodet H, Scagliotti GV, et al. Lung adjuvant cisplatin evaluation: a pooled analysis by the LACE Collaborative Group. *J Clin Oncol*. 2008;26(21):3552-3559. doi:10.1200/JCO.2007.13.9030
183. Mitchell TJ, Turajlic S, Rowan A, et al. Timing the Landmark Events in the Evolution of Clear Cell Renal Cell Cancer: TRACERx Renal. *Cell*. 2018;173(3):611-623.e17. doi:10.1016/j.cell.2018.02.020
184. Martínez-Ruiz C, Black JRM, Puttick C, et al. Genomic-transcriptomic evolution in lung cancer and metastasis. *Nature*. 2023;616(7957):543-552. doi:10.1038/s41586-023-05706-4
185. Maeda R, Yoshida J, Ishii G, Hishida T, Nishimura M, Nagai K. The prognostic impact of cigarette smoking on patients with non-small cell lung cancer. *J Thorac Oncol*. 2011;6(4):735-742. doi:10.1097/JTO.0b013e318208e963
186. Hendriksen BS, Rocco R, Blackmon SH, Tapias L. Risk factors and survival associated with lung cancer recurrence after curative-intent surgery: beyond TNM staging. Chest. 2023;164(4):A150. doi:10.1016/j.chest.2023.07.150
187. Kamran SC, Coroller T, Milani N, et al. The impact of quantitative CT-based tumor volumetric features on the outcomes of patients with limited stage small cell lung cancer. *Radiat Oncol*. 2020;15(1):14. doi:10.1186/s13014-020-1460-4
188. Taugner J, Käsmann L, Karin M, et al. Planning target volume as a predictor of disease progression in inoperable stage III non-small cell lung cancer patients treated with chemoradiotherapy and concurrent and/or sequential immune checkpoint inhibition. *Invest New Drugs*. 2022;40(1):163-171. doi:10.1007/s10637-021-01143-0
189. Nishino M, Dahlberg SE, Cardarella S, et al. Tumor volume decrease at 8 weeks is associated with longer survival in EGFR-mutant advanced non-small-cell lung cancer patients treated with EGFR TKI. *J Thorac Oncol*. 2013;8(8):1059-1068. doi:10.1097/JTO.0b013e318294c909
190. Tran HT, Heeke S, Sujit S, et al. Circulating tumor DNA and radiological tumor volume identify patients at risk for relapse with resected, early-stage non-small-cell lung cancer. *Ann Oncol*. 2024;35(2):183-189. doi:10.1016/j.annonc.2023.11.008
191. Mery CM, Pappas AN, Bueno R, et al. Similar long-term survival of elderly patients with non-small cell lung cancer treated with lobectomy or wedge resection within the surveillance, epidemiology, and end results database. *Chest*. 2005;128(1):237-245. doi:10.1378/chest.128.1.237
192. Agarwal M, Brahmanday G, Chmielewski GW, Welsh RJ, Ravikrishnan KP. Age, tumor size, type of surgery, and gender predict survival in early stage (stage I and II) non-small cell lung cancer after surgical resection. *Lung Cancer*. 2010;68(3):398-402. doi:10.1016/j.lungcan.2009.08.008
193. Goodgame B, Viswanathan A, Zoole J, et al. Risk of recurrence of resected stage I non-small cell lung cancer in elderly patients as compared with younger patients. *J Thorac Oncol*. 2009;4(11):1370-1374. doi:10.1097/JTO.0b013e3181b6bc1b
194. Zhu JF, Feng XY, Zhang XW, et al. Time-varying pattern of postoperative recurrence risk of early-stage (T1a-T2bN0M0) non-small cell lung cancer (NSCLC): results of a single-center study of 994 Chinese patients. *PLoS One*. 2014;9(9):e106668. Published 2014 Sep 9. doi:10.1371/journal.pone.0106668
195. Yamamoto K, Padilla Alarcón J, Calvo Medina V, et al. Surgical results of stage I non-small cell lung cancer: comparison between elderly and younger

patients. *Eur J Cardiothorac Surg*. 2003;23(1):21-25. doi:10.1016/s1010-7940(02)00661-9
196. Watanabe K, Sakamaki K, Nishii T, et al. Gender Differences in the Recurrence Timing of Patients Undergoing Resection for Non-Small Cell Lung Cancer. *Asian Pac J Cancer Prev*. 2018;19(3):719-724. Published 2018 Mar 27. doi:10.22034/APJCP.2018.19.3.719
197. Howlader N, Noone A, Krapcho M, et al. SEER Cancer Statistics Review. Bethesda, MD: National Cancer Institute; Published 2022. https://seer.cancer.gov/csr/
198. Wang M, Wu Q, Zhang J, et al. Prognostic impacts of extracranial metastasis on non-small cell lung cancer with brain metastasis: A retrospective study based on surveillance, epidemiology, and end results database. *Cancer Med*. 2021;10(2):471-482. doi:10.1002/cam4.3562
199. Yang J, Zhang Y, Sun X, et al. The prognostic value of multiorgan metastases in patients with non-small cell lung cancer and its variants: a SEER-based study. *J Cancer Res Clin Oncol*. 2018;144(9):1835-1842. doi:10.1007/s00432-018-2702-9
200. Al Bakir M, Huebner A, Martínez-Ruiz C, et al. The evolution of non-small cell lung cancer metastases in TRACERx. *Nature*. 2023;616(7957):534-542. doi:10.1038/s41586-023-05729-x
201. Aerts HJ, Velazquez ER, Leijenaar RT, et al. Decoding tumour phenotype by noninvasive imaging using a quantitative radiomics approach. *Nat Commun*. 2014;5:4006. doi:10.1038/ncomms5006
202. Martínez-Jiménez F, Movasati A, Brunner SR, et al. Pan-cancer whole-genome comparison of primary and metastatic solid tumours. *Nature*. 2023;618(7964):333-341. doi:10.1038/s41586-023-06054-z
203. Sugimura H, Nichols FC, Yang P, et al. Survival after recurrent nonsmall-cell lung cancer after complete pulmonary resection. *Ann Thorac Surg*. 2007;83(2):409-418. doi:10.1016/j.athoracsur.2006.08.046
204. Hardenberg MC, Patel B, Matthews C, et al. The value of disease-free survival (DFS) and osimertinib in adjuvant non-small-cell lung cancer (NSCLC): an international Delphi consensus report. *ESMO Open*. 2022;7(5):100572. doi:10.1016/j.esmoop.2022.100572
205. Stirling RG, Chau C, Shareh A, Zalcberg J, Fischer BM. Effect of Follow-Up Surveillance After Curative-Intent Treatment of NSCLC on Detection of New and Recurrent Disease, Retreatment, and Survival: A Systematic Review and Meta-Analysis. *J Thorac Oncol*. 2021;16(5):784-797. doi:10.1016/j.jtho.2021.01.1622
206. Westeel V, Choma D, Clément F, et al. Relevance of an intensive postoperative follow-up after surgery for non-small cell lung cancer. *Ann Thorac Surg*. 2000;70(4):1185-1190. doi:10.1016/s0003-4975(00)01731-8
207. Lou F, Sima CS, Rusch VW, Jones DR, Huang J. Differences in patterns of recurrence in early-stage versus locally advanced non-small cell lung cancer. *Ann Thorac Surg*. 2014;98(5):1755-1761. doi:10.1016/j.athoracsur.2014.05.070
208. O'Brien M, Paz-Ares L, Marreaud S, et al. Pembrolizumab versus placebo as adjuvant therapy for completely resected stage IB-IIIA non-small-cell lung cancer (PEARLS/KEYNOTE-091): an interim analysis of a randomised, triple-blind, phase 3 trial. *Lancet Oncol*. 2022;23(10):1274-1286. doi:10.1016/S1470-2045(22)00518-6

209. Shah A, Apple J, Belli AJ, et al. Real-world study of disease-free survival & patient characteristics associated with disease-free survival in early-stage non-small cell lung cancer: A retrospective observational study. *Cancer Treat Res Commun*. 2023;36:100742. doi:10.1016/j.ctarc.2023.100742
210. Ortuzar W, Hanna N, Pennella E, et al. Brain metastases as the primary site of relapse in two randomized phase III pemetrexed trials in advanced non-small-cell lung cancer. *Clin Lung Cancer*. 2012;13(1):24-30. doi:10.1016/j.cllc.2011.05.007
211. Gauger J, Patz EF Jr, Coleman RE, Herndon JE 2nd. Clinical stage I non-small cell lung cancer including FDG-PET Imaging: sites and time to recurrence. *J Thorac Oncol*. 2007;2(6):499-505. doi:10.1097/JTO.0b013e3180600990
212. Ni J, Guo T, Li Y, et al. Patterns and risks of postoperative recurrence in completely resected EGFR-mutant non-small cell lung cancer: prognostic significance of routine immunohistochemical markers. *Transl Lung Cancer Res*. 2019;8(6):967-978. doi:10.21037/tlcr.2019.12.02
213. Subotic D, Mandaric D, Radosavljevic G, Stojsic J, Gajic M, Ercegovac M. Relapse in resected lung cancer revisited: does intensified follow up really matter? A prospective study. *World J Surg Oncol*. 2009;7:87. doi:10.1186/1477-7819-7-87
214. Curran WJ Jr, Herbert SH, Stafford PM, et al. Should patients with post-resection locoregional recurrence of lung cancer receive aggressive therapy?. *Int J Radiat Oncol Biol Phys*. 1992;24(1):25-30. doi:10.1016/0360-3016(92)91016-g
215. Yang W, Fu Z, Yu J, et al. Value of PET/CT versus enhanced CT for locoregional lymph nodes in non-small cell lung cancer. *Lung Cancer*. 2008;61(1):35-43. doi:10.1016/j.lungcan.2007.11.007
216. Wang Y, Jing L, Wang G. Risk factors for lymph node metastasis and surgical methods in patients with early-stage peripheral lung adenocarcinoma presenting as ground glass opacity. *J Cardiothorac Surg*. 2020;15(1):121. doi:10.1186/s13019-020-01167-2
217. Chiappetta M, Leuzzi G, Sperduti I, et al. Mediastinal Up-Staging During Surgery in Non-Small-Cell Lung Cancer: Which Mediastinal Lymph Node Metastasis Patterns Better Predict The Outcome? A Multicenter Analysis. *Clin Lung Cancer*. 2020;21(5):464-471.e1. doi:10.1016/j.cllc.2020.03.004
218. Kotoulas CS, Foroulis CN, Kostikas K, et al. Involvement of lymphatic metastatic spread in non-small cell lung cancer accordingly to the primary cancer location. *Lung Cancer*. 2004;44(2):183-191. doi:10.1016/j.lungcan.2003.10.012
219. Wang X, Wang Z, Pan J, et al. Patterns of Extrathoracic Metastases in Different Histological Types of Lung Cancer. *Front Oncol*. 2020;10:715. doi:10.3389/fonc.2020.0071
220. Liu WK, Ding B, Hessey S, Kittel J. Mapping the pattern and pace of tumour dissemination using longitudinal imaging and ctDNA in the TRACERx lung study. *Ann Oncol*. 2022;33:S1387. doi:10.1016/j.annonc.2022.09.012
221. Ng WL, Huang Q, Liu X, Zimmerman M, Li F, Li CY. Molecular mechanisms involved in tumor repopulation after radiotherapy. *Transl Cancer Res*. 2013;2(5):442-448. doi:10.3978/j.issn.2218-676X.2013.10.03
222. Marusyk A, Janiszewska M, Polyak K. Intratumor Heterogeneity: The Rosetta Stone of Therapy Resistance. *Cancer Cell*. 2020;37(4):471-484. doi:10.1016/j.ccell.2020.03.007

223. Li Y, Liu L, You R, et al. Effect of initial recurrence site on the prognosis of different tissue types of non-small cell lung cancer: a retrospective cohort study. *World J Surg Oncol*. 2023;21(1):360. doi:10.1186/s12957-023-03252-x
224. Mujoomdar A, Austin JH, Malhotra R, et al. Clinical predictors of metastatic disease to the brain from non-small cell lung carcinoma: primary tumor size, cell type, and lymph node metastases. *Radiology*. 2007;242(3):882-888. doi:10.1148/radiol.2423051707
225. Long KJ, Pitcher T, Kurman JS, Pritchett MA, Silvestri GA. Using a Blood Biomarker to Distinguish Benign From Malignant Pulmonary Nodules: A Subgroup Analysis Comparing Screen Detection, Sex, Smoking History, and Nodule Size. *Chest*. 2023;164(6):1572-1575. doi:10.1016/j.chest.2023.06.037
226. Varlotto JM, Recht A, Flickinger JC, Medford-Davis LN, Dyer AM, DeCamp MM. Varying recurrence rates and risk factors associated with different definitions of local recurrence in patients with surgically resected, stage I nonsmall cell lung cancer. *Cancer*. 2010;116(10):2390-2400. doi:10.1002/cncr.25047
227. Pepek JM, Chino JP, Marks LB, et al. How well does the new lung cancer staging system predict for local/regional recurrence after surgery?: A comparison of the TNM 6 and 7 systems. *J Thorac Oncol*. 2011;6(4):757-761. doi:10.1097/JTO.0b013e31821038c0
228. Subotic D, Mandaric D, Radosavljevic G, Stojsic J, Gajic M, Ercegovac M. Relapse in resected lung cancer revisited: does intensified follow up really matter? A prospective study. *World J Surg Oncol*. 2009;7:87. doi:10.1186/1477-7819-7-87
229. Backhus LM, Farjah F, Liang CK, et al. Imaging surveillance and survival for surgically resected non-small-cell lung cancer. *J Surg Res*. 2016;200(1):171-176. doi:10.1016/j.jss.2015.06.048
230. Turajlic S, Xu H, Litchfield K, et al. Tracking Cancer Evolution Reveals Constrained Routes to Metastases: TRACERx Renal. *Cell*. 2018;173(3):581-594.e12. doi:10.1016/j.cell.2018.03.057
231. Zerhouni EA, Stitik FP, Siegelman SS, et al. CT of the pulmonary nodule: a cooperative study. *Radiology*. 1986;160(2):319-327. doi:10.1148/radiology.160.2.3726107
232. Klein JS, Salomon G, Stewart EA. Transthoracic needle biopsy with a coaxially placed 20-gauge automated cutting needle: results in 122 patients. *Radiology*. 1996;198(3):715-720. doi:10.1148/radiology.198.3.8628859
233. Siegelman SS, Khouri NF, Leo FP, Fishman EK, Braverman RM, Zerhouni EA. Solitary pulmonary nodules: CT assessment. *Radiology*. 1986;160(2):307-312. doi:10.1148/radiology.160.2.3726105
234. Zwirewich CV, Vedal S, Miller RR, Müller NL. Solitary pulmonary nodule: high-resolution CT and radiologic-pathologic correlation. *Radiology*. 1991;179(2):469-476. doi:10.1148/radiology.179.2.2014294
235. Korst RJ, Kansler AL, Port JL, Lee PC, Altorki NK. Accuracy of surveillance computed tomography in detecting recurrent or new primary lung cancer in patients with completely resected lung cancer. *Ann Thorac Surg*. 2006;82(3):1009-1015. doi:10.1016/j.athoracsur.2006.03.062
236. Marom EM, Sarvis S, Herndon JE 2nd, Patz EF Jr. T1 lung cancers: sensitivity of diagnosis with fluorodeoxyglucose PET. *Radiology*. 2002;223(2):453-459. doi:10.1148/radiol.2232011131

237. Vansteenkiste JF, Stroobants SG. The role of positron emission tomography with 18F-fluoro-2-deoxy-D-glucose in respiratory oncology. *Eur Respir J*. 2001;17(4):802-820. doi:10.1183/09031936.01.17408020
238. Gould MK, Maclean CC, Kuschner WG, Rydzak CE, Owens DK. Accuracy of positron emission tomography for diagnosis of pulmonary nodules and mass lesions: a meta-analysis. *JAMA*. 2001;285(7):914-924. doi:10.1001/jama.285.7.914
239. Fischer BM, Mortensen J, Højgaard L. Positron emission tomography in the diagnosis and staging of lung cancer: a systematic, quantitative review. *Lancet Oncol*. 2001;2(11):659-666. doi:10.1016/S1470-2045(01)00555-1
240. Nathan MH, Collins VP, Adams RA. Differentiation of benign and malignant pulmonary nodules by growth rate. *Radiology*. 1962;79:221-232. doi:10.1148/79.2.221
241. Weiss W. Peripheral measurable bronchogenic carcinoma. Growth rate and period of risk after therapy. *Am Rev Respir Dis*. 1971;103(2):198-208. doi:10.1164/arrd.1971.103.2.198
242. Lee JI, Lee YJ, Park KY, et al. Fate of newly detected lesions during postoperative surveillance for non-small cell lung cancer. *Ann Thorac Surg*. 2013;95(6):1867-1871. doi:10.1016/j.athoracsur.2013.03.084
243. Colt HG, Murgu SD, Korst RJ, Slatore CG, Unger M, Quadrelli S. Follow-up and surveillance of the patient with lung cancer after curative-intent therapy: Diagnosis and management of lung cancer, 3rd ed: American College of Chest Physicians evidence-based clinical practice guidelines. *Chest*. 2013;143(5 Suppl):e437S-e454S. doi:10.1378/chest.12-2365
244. Postmus PE, Kerr KM, Oudkerk M, et al. Early and locally advanced non-small-cell lung cancer (NSCLC): ESMO Clinical Practice Guidelines for diagnosis, treatment and follow-up. *Ann Oncol*. 2017;28(suppl_4):iv1-iv21. doi:10.1093/annonc/mdx222
245. Erb CT, Su KW, Soulos PR, Tanoue LT, Gross CP. Surveillance Practice Patterns after Curative Intent Therapy for Stage I Non-Small-Cell Lung Cancer in the Medicare Population. *Lung Cancer*. 2016;99:200-207. doi:10.1016/j.lungcan.2016.07.017
246. Schoenfeld AJ, Rizvi H, Memon D, et al. Acquired resistance to PD-1 blockade in NSCLC. *J Clin Oncol*. 2020;38(15_suppl):9621. doi:10.1200/JCO.2020.38.15_suppl.9621
247. Rooney MS, Shukla SA, Wu CJ, Getz G, Hacohen N. Molecular and genetic properties of tumors associated with local immune cytolytic activity. *Cell*. 2015;160(1-2):48-61. doi:10.1016/j.cell.2014.12.033
248. O'Donnell TJ, Rubinsteyn A, Laserson U. MHCflurry 2.0: Improved Pan-Allele Prediction of MHC Class I-Presented Peptides by Incorporating Antigen Processing. *Cell Syst*. 2020;11(1):42-48.e7. doi:10.1016/j.cels.2020.06.010
249. Shukla SA, Rooney MS, Rajasagi M, et al. Comprehensive analysis of cancer-associated somatic mutations in class I HLA genes. *Nat Biotechnol*. 2015;33(11):1152-1158. doi:10.1038/nbt.3344
250. Leighl NB, Hellmann MD, Hui R, et al. Pembrolizumab in patients with advanced non-small-cell lung cancer (KEYNOTE-001): 3-year results from an open-label, phase 1 study. *Lancet Respir Med*. 2019;7(4):347-357. doi:10.1016/S2213-2600(18)30500-9